

**NONLINEAR OPTICAL, FLUORESCENCE AND LIQUID
CRYSTALLINE PROPERTIES OF NOVEL
AZOBENZENE POLYMERS AND THEIR OLIGOMERS**

THESIS SUBMITTED TO
THE UNIVERSITY OF KERALA
FOR THE DEGREE OF
DOCTOR OF PHILOSOPHY
IN CHEMISTRY
UNDER THE FACULTY OF SCIENCE



By

SMITHA P

**CHEMICAL SCIENCES & TECHNOLOGY DIVISION
NATIONAL INSTITUTE FOR INTERDISCIPLINARY SCIENCE &
TECHNOLOGY - CSIR**
Formerly: REGIONAL RESEARCH LABORATORY
THIRUVANANTHAPURAM-695019
KERALA, INDIA

APRIL 2008

Dedicated to My Dear Ones.....

DECLARATION

I hereby declare that the matter embodied in the thesis entitled “**Nonlinear Optical, Fluorescence and Liquid Crystalline Properties of Novel Azobenzene Polymers and Their Oligomers**” are the results of investigations carried out by me at the Chemical Sciences and Technology Division, National Institute for Interdisciplinary Science and Technology, Thiruvananthapuram, under the supervision of Dr. C. K. S. Pillai and Dr. S. K. Asha and the same has not been submitted elsewhere for any other degree.

Smitha P

Thiruvananthapuram
April 2008

राष्ट्रीय अंतर्विषयी विज्ञान तथा प्रौद्योगिकी संस्थान

(वैज्ञानिक एवं प्रौद्योगिकी अनुसंधान परिषद्)

(पहले क्षेत्रीय अनुसंधान प्रयोगशाला)

NATIONAL INSTITUTE FOR INTERDISCIPLINARY SCIENCE AND TECHNOLOGY

(Council of Scientific & Industrial Research)

(formerly Regional Research laboratory)



इन्डस्ट्रियल इस्टेट डाक घर, तिरुवनन्तपुरम 695 019, भारत
Industrial Estate P.O., Thiruvananthapuram 695 019, India

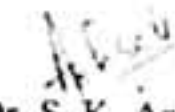
भारत सरकार में प्रमाणित
ISO 9001 CERTIFIED



CERTIFICATE

This is to certify that the work embodied in the thesis entitled "**Nonlinear Optical, Fluorescence and Liquid Crystalline Properties of Novel Azobenzene Polymers and Their Oligomers**" has been carried out by Mrs. Smitha. P under our supervision at the Inorganic and Polymeric Materials Group of National Institute for Interdisciplinary Science and Technology (Formerly Regional Research Laboratory) (CSIR), Thiruvananthapuram and the same has not been submitted elsewhere for any other degree.


D. C. K. S. Pillai
Thesis Supervisor


Dr. S. K. Asha
Thesis Supervisor

ACKNOWLEDGEMENTS

It is with great pleasure that I place on record my deep sense of gratitude to Dr. C.K.S. Pillai for suggesting the research problem and for inspiring me throughout the tenure of my work, I am indebted to Dr. S. K. Asha for her constant guidance, discussions and support for the successful completion of this work.

I would like to acknowledge the support and motivation given by Prof. T. K. Chandrashekar, Director, National Institute for Interdisciplinary Science and Technology (Formerly Regional Research Laboratory), Thiruvananthapuram.

I am obliged to Dr. M. Jayakannan for his help and support. I thank him for inspiring me throughout the tenure of this work.

I have great pleasure in thanking Dr. C. Pavitran, Dr. Emilia Abraham, Dr. V. S. Prasad, Dr. J. D. Sudha, Dr. A. R. R. Menon, Mr. Brahmakumar and Mr. Anandan for their valuable suggestions and support.

I gratefully acknowledge Dr. Suresh Das, Head of the Division. I also thank Dr. K. R. Gopidas, Dr. Ajayghosh.A and Dr. George Thomas for their useful discussions.

I thank Dr. M. L. P.Reddy and Dr. T. Prasad Rao and Dr. A. Srinivasan for their suggestions and help.

I always remember the help rendered by the following people for the successful completion of my work;

*Prof. S. Ramakrishnan and Prof. P. K. Das, Indian Institute of Science,
Bangalore for NLO measurements.*

*Dr. C. P. Sharma and Mr. Willi Paul, SCTIMST, Thiruvananthapuram, for DLS
measurements*

*Dr. Suparna Sen Gupta and Mr. Sanjay RGCB, Thiruvananthapuram for TEM
analysis*

Dr. Peter Koshy and Mr. M. R. Chandran (SEM analysis),

*Mr. Robert Philip and Mr. Narendran (TEM analysis), Dr. Syamaprasad
and Mr. Gurusamy (XRD measurements), Mrs. Soumini Mathew (NMR
spectra), Mrs S. Viji (HRMS, Elemental Analysis)*

*Dr. Sandhya. K. Y, Dr. Neethu Sundaresan, Dr. Gisha Elizabeth Luckachen,
Ms. Sangeetha. K, Ms. Deepa. P, Ms. Amrutha. S. Rajan, Mrs. Jancy Baby,
Mr. Deepak Vishnu D, Dr. Bakare. I. O, Mr. Anilkumar. P, Mr. Jinish
Antony, Mr. Anish Cyriac, Ms. Swathy S. L, Ms. Rekhia Narayan,
Mr. A. Balamurugan and Ms. Resmi Raveendran of Polymer Research Group, NIIST,
Thiruvananthapuram*

*Dr. Smitha. M. Nair and Dr. Kishore Mohanan, Organic Chemistry Division
Ms. Bindu. P. Nair, Ms. Reena. V. L, Ms. Sasiqala. T. S, Ms. Sivakala.S and Ms.
Chameswary. J, Material Science Division, NIIST, Thiruvananthapuram*

Ms. Priya Carol and Mr. Kabeer, VSSC, Thiruvananthapuram

Ms Sonia. T. A, Ms. Viola.B. Morris, SCTIMST, Thiruvananthapuram

*All members of Photonics and Photosciences, Inorganic Chemistry and Organic Chemistry
Groups.*

*I thank all the staffs of administration, finance, accounts, stores section, library and the IT
lab of NIIST who helped my research to move along swiftly and smoothly.*

*I express my sincere thanks to all my teachers especially to Dr. Maria Starwin for the
motivation and encouragement at different stages of my academic career.*

*I wish to express my deepest gratitude to my parents, husband, Rajesh Viswanath, my sister
Anu and all family members for their constant encouragement, prayer and love throughout
my life.*

Financial assistance from CSIR is gratefully acknowledged.

Thiruvananthapuram

April 2008

Smitha P

CONTENTS

	Page
Declaration	i
Certificate	ii
Acknowledgements	iii
Preface	viii
List of Publications	x
CHAPTER 1. Azobenzene Molecules and Polymers: Nonlinear Optical, Photoluminescence and Liquid Crystalline Properties	1-42
1.1 Introduction	2
1.2 Structural Chemistry of Azo Compounds	2
1.3 Photochemistry of Azo Compounds	3
1.4 Photoisomerization	4
1.4.1 Mechanism of Isomerization	4
1.5 Color of Azo Compounds	5
1.6 Application of Azo Based Molecules and Polymers	5
1.7 Nonlinear Optics	6
1.8 Basic Principles of Nonlinear Optics	7
1.9 Measurement Techniques for Second–order Nonlinear Optical Effect	8
1.10 Materials for Nonlinear Optics	10
1.11 Azobenzene Based Nonlinear Optical Materials	12
1.12 Fluorescence	15
1.13 Fluorescence in Azo Compounds	18
1.14 Liquid Crystallinity	26
1.15 Classification of Liquid Crystals	26

1.16	Azobenzene Liquid Crystals	28
1.17	Origin and Objectives of the Present Investigation	34
1.18	References	35
CHAPTER 2. Synthesis, Characterization and Hyperpolarizability Measurements of Main Chain Azobenzene Monomers and Their Polymers		43-74
2.1	Abstract	44
2.2	Introduction	44
2.3	Experimental Section	48
2.4.	Synthesis of Monomers	49
2.5	Synthesis of Polymers	51
2.6	Results and Discussion	52
2.7	UV-Visible Spectra	55
2.8	Nonlinear Optical Properties	60
2.9	Thermal Properties of Monomers	64
2.10	Polymer Synthesis and Characterization	66
2.11	Thermal Properties of Polymers	69
2.12	Conclusion	71
2.13	References	72
CHAPTER 3. Synthesis, Characterization and Photophysical Properties of Highly Fluorescent Soluble Side Chain		75-122
3.1	Abstract	76
3.2	Introduction	77
3.3	Experimental Section	79
3.4	Results and Discussion	87
3.5	Photophysical Properties	94
3.6	Variable Concentration Fluorescence Measurements	102
3.7	Photoisomerization Studies	105
3.8	Morphological Studies	111

3.9	Solid State Luminescence Studies	117
3.10	Thermal Properties	118
3.11	Conclusions	119
3.12	References	120

**CHAPTER 4. Synthesis, Characterization and Photophysical Properties of
Liquid Crystalline Azobenzene Oligomers 123-183**

4.1	Abstract	124
4.2	Introduction	125
4.3	Excimer Formation in Naphthyl Derivatives	128
4.4	Experimental Section	131
4.5	Results and Discussion	139
4.6	Photophysical Properties	147
4.7	Emission Properties	149
4.8	Variable Solvent Fluorescence Measurements	158
4.9	Variable Concentration Fluorescence Measurements	158
4.10	Photoisomerization Studies	163
4.11	Thermal Properties	168
4.12	SEM Analysis	177
4.13	DLS Measurement	178
4.14	Conclusion	179
4.15	Reference	180
5.	Summary and Conclusion	185

PREFACE

Design and synthesis of azobenzene molecules and polymers with better optical and electronic properties are of great importance in the area of advanced material research. One of the major goals of these studies is the fundamental understanding of the structure-property relationship that might form the basis for the design of novel materials with tailored properties. Molecules and polymers containing azo chromophore have great significance due to their application in various fields such as nonlinear optics, electro-optics, telecommunication, data storage, liquid crystal display etc. The design strategy for second order nonlinear optically active materials involve a donor and acceptor connected by π -conjugated system. In most of the reports, the connecting bridge between the donor and acceptor is azo linkage because of the superior properties of this connector group like rigidity and planarity of the azo group. Also majority of the liquid crystalline materials so far reported are based on azo mesogen. In this context, the development of azo-based systems with multiple properties is of great significance. The main objective of the present study is the designing of multifunctional azobenzene molecules and polymers and the investigation of their optical, electronic and morphological properties.

Each chapter of the thesis is presented as an independent unit and therefore the structural formulae, schemes, figures and references are numbered chapter wise. The main findings of each chapter are given in the abstract.

In the first chapter of the thesis, a brief introduction about the properties of azo functionality, its photoisomerization and the general applications of azobenzene compounds is given. The basic principles of nonlinear optics, various measurement techniques and materials for nonlinear optics followed by an overview of literature of azo based nonlinear optical materials are described. The fundamentals of fluorescence emission, the significance of azobenzene fluorescence and an overview of literature of fluorescent azo systems are given.

Attention has been paid to discuss the basic concepts of liquid crystallinity and the brief overview of the literature.

The second chapter describes the design of a series of NLO active AB type azobenzene monomers having the same donor and acceptor group, but different conjugation length. The effect of substituents and the effect of conjugation length on NLO property are described. The increased conjugation length is found to have a positive influence on the second harmonic generation coefficient. The phenyl phenol based dye as well as the naphthol based dye possessed highest NLO activity which could be accounted on the basis of the increased conjugation length. The AB type monomers were polymerized to obtain main chain polymers, but the rigid nature of the polymers resulted in poor solubility which limited the characterization and further studies.

The third chapter deals with a series of highly fluorescent azobenzene side chain polymers which exhibited honeycomb morphology. The phenyl phenol based dye azobenzene ester and its polymer possessed high quantum yield value which could be accounted on the basis of the more planar geometry in the excited state. Eventhough the biphenyl unit is having a twisted geometry in the ground state, the incorporation into an azo chromophore makes it more planar. Porous honeycomb morphology is formed by phenol and phenyl phenol based side chain polymers and the driving force is the hydrophilic-hydrophobic interaction between the ethyleneoxy spacer and the methacrylate backbone.

The fourth chapter describes the synthesis, photophysical and optical properties of bichromophoric molecules and its model compounds. The bichromophores are dimeric twin molecules designed in the fashion 'chromophore-spacer-chromophore' in which the spacer is oligoethyleneoxy units of varying length. Naphthol derivatives were found to form static excimers. The phenyl phenol and naphthol based bichromophores were found to be highly fluorescent. Some of the molecules formed liquid crystalline patterns which were confirmed by DSC and PLM measurements.

The last chapter summarizes the outcome of the research work carried out in this Ph.D. thesis and the scope of future directions in related area of research.

The results of the present investigation are published/presented as described below:

List of Publications:

1. **P. Smitha**, C. K. S. Pillai and S. K. Asha, *J. Polym. Sci. Part A: Polym. Chem.* **2005**, 43, 19, 4455, *Synthesis, Characterization and Hyperpolarizability Measurements of Main Chain Azobenzene Molecules.*
2. **P. Smitha**, S. K. Asha. *J. Phys. Chem. B* **2007**, 111, 6364, *Structure Control for Fine tuning Fluorescence Emission from Side Chain Azobenzene Polymers.*
3. **P. Smitha**, S. K. Asha. *Observation of Excimer and Aggregate Emission from Naphthyl Azobenzene Bichromophores* (submitted for publication).

Papers presented at conference:

1. *Azobenzene Chromophore Monomers for Main Chain NLO Polymers*, International Conference on Polymers, **P. Smitha**, S. K. Asha, C. K. S. Pillai, **MACRO 2004**, Thiruvananthapuram
2. *A Series of Azobenzene NLO Chromophores in Main-chain and Side-chain Polymers*, **P. Smitha**, S. K. Asha, C. K. S. Pillai, International Conference on Ionic Polymerization, **IP 2005**, Goa.
3. *Highly Luminescent and Liquid Crystalline Azobenzene Materials*, **P. Smitha**, S. K. Asha. 9th National Conference on Polymers for Advanced Technologies, **MACRO 2006**, National Chemical Laboratory, Pune.
4. *Fluorescent Azobenzene Side Chain Polymers*, **P. Smitha**, S. K. Asha. International Conference on Advanced Materials and Composites, **ICAMC 2007**, Thiruvananthapuram **2007**.

Chapter 1

***Azobenzene Molecules and Polymers: Nonlinear Optical,
Photoluminescence and Liquid Crystalline Properties***

1.1 Introduction

Azobenzene is a well known mesogen as well as photoresponsive chromophore that can undergo geometrical isomerization under photoirradiation.¹ Azobenzene is one of the functional groups that exhibit a range of thermal, chemical, photochemical and biological properties and each of these properties form the basis for distinct class of functional molecules in the vast world of chemistry.² Azo compounds are organo-nitrogen derivatives with the characteristic double bonded -N=N- functionality with the general formula R-N=N-R' where R and R' can be the same or different groups.³⁻⁵ The moiety flanking the azo group is most commonly alkyl or aryl groups. Azobenzene can exist in two different geometrical isomeric forms, the cis form and the trans form. The cis form is termed as Z-isomer and the trans as E-isomer. The presence of a double bond generally has profound consequences on the stereochemistry; it gives the molecule more rigidity and restricts the number of possible forms. The main feature is the coplanarity of all atoms adjacent to a double bond as well as of the double bonded nitrogen atoms themselves.⁵ The aromatic azo compounds are highly colored explaining the wide spread utilization in the dye industry.⁶

1.2 Structural Chemistry of Azo Compounds

Azo compounds are relatively stable compounds and therefore a good number of different structures of azo compounds have been determined.⁷⁻⁸ Most of the molecules are planar with respect to the nitrogen atoms in the trans form. Bond lengths of 1.22-1.25 Å are found for aliphatic compounds whereas simple aromatic compounds or compounds with conjugated carbonyl groups (with -N=N-) have slightly longer N=N bonds of 1.24-1.26 Å. This indicates some resonance stabilization occurring in aromatic compounds. For molecules with several azo groups, the -N=N- bond length increases. The N-N-C bond angles for aromatic compounds are about 113° and for aliphatic ones about 115°.⁹

Aromatic azo compounds are resonance stabilized. Evidence for this comes from the shortening of the carbon-nitrogen bond in the trans azo benzene

from its usual value of 1.47Å to 1.41Å as a result of conjugation. Trans form is known to be considerably more stable than cis form which is directly related to the resonance stabilization in the almost coplanar structure of the former¹⁰ while in the cis isomer, the phenyl rings are rotated out of the plane containing nitrogen atoms by about 50°. Eventhough cis form is thermodynamically less stable than trans, the cis form can also be isolated.^{11, 12}

1.3 Photochemistry of Azo Compounds

Aliphatic azo compound usually undergo thermal/photo dissociation to give free radicals and nitrogen, whereas aromatic azo compounds are stable towards C-N bond scission. Azo compounds used commercially as free radical initiators contain at least one tertiary carbon atom attached to the azo nitrogen atom. Such azo compounds when appropriately substituted decompose upon heating by homolytic cleavage of two carbon-nitrogen bonds to generate two free radicals and nitrogen. For example, azo bisisobutyronitrile (AIBN) which is an aliphatic azo derivative is used as initiator for free radical polymerization as it undergoes dissociation at 80 °C. Azo compounds of azobenzene type generally are yellow to red in color. The main feature of their absorption spectra is a relatively weak long wavelength band well separated from the shorter wavelength band.¹³⁻¹⁵ Thus the azobenzene type is characterized by a low lying $^1(n-\pi^*)$ state and a large band gap between this and the next higher $^1(\pi-\pi^*)$ state. In most of the cases, the $n-\pi^*$ band is without vibrational structure. The low intensity of $n-\pi^*$ band when compared to the $\pi-\pi^*$ band is due to the selection rules, in the planar C_{2h} and C_{2v} symmetries, the $n-\pi^*$ transition is forbidden for trans compound but allowed for the cis form. Hence the intensity of the $\pi-\pi^*$ band in the spectrum of the trans form is very high. This has been attributed to the nonplanar distortions of the molecule and to the vibrational coupling.¹⁶ In the spectra of trans-azobenzene, these bands are nearly without vibrational structure at room temperature but shows fine structures in a rigid solvent matrix at 77K. In the spectra of cis-azobenzenes, the $\pi-\pi^*$ bands generally do not show any vibrational features.

1.4 Photoisomerization

Azobenzene and its derivatives are characterized by reversible transformations from the generally more stable trans form to the unstable cis form upon irradiation with ultraviolet (UV) or visible light to yield a photostationary composition that is both temperature and wavelength dependant.¹⁰ The intense absorption due to the trans isomer decreases when irradiated with light of wavelength around 360 nm whereas absorption due to the cis isomer increases. Thermal isomerization from photogenerated cis form to trans form can be easily followed by UV spectroscopy. Quantum yields are generally high for isomerization of azobenzene. Photoisomerization proceeds with a large structural change as reflected in the dipole moment and change in geometry. The process involves a decrease in the distance between para carbons in azobenzene from about 9.0 Å in trans form to 5.5 Å in the cis form.¹⁷ For the planar trans isomer, the dipole moment is zero, whereas for the bent nonplanar cis isomer, it is 3 Debye.

1.4.1 Mechanism of Isomerization

It has been proposed that the photoisomerization of azobenzene depends on the excitation wavelength.^{16, 18} The trans-cis isomerization proceeds through an inversion mechanism under $n-\pi^*$ excitation, whereas the rotational mechanism operates under $\pi-\pi^*$ excitation similar to the isomerization of stilbene. In the inversion mechanism, a linear geometry in the transition state is not involved because it is higher in energy than in a semilinear geometry. The quantum yields of the trans-cis isomerization of restricted azobenzene such as azobenzenophanes were examined under $n-\pi^*$ and $\pi-\pi^*$ excitation conditions.¹⁹ Only inversion mechanism can be expected in azobenzenophanes because of steric hindrance. The quantum yield of trans-cis isomerization was found to be 0.24 and 0.21 for $n-\pi^*$ and $\pi-\pi^*$ excitations respectively which are similar to that of azobenzene (0.23) for $n-\pi^*$ excitation. This suggests that the isomerization of trans azobenzene under $n-\pi^*$ excitation proceeds via an inversion mechanism as azobenzenophanes do. In trans azobenzene and its derivatives without any

restrictions, the quantum yields of trans-cis isomerization for π - π^* excitations are always smaller by a factor of 2.¹⁹⁻²² This may be an indication of rotational mechanism operating for trans-cis isomerization of azobenzene for π - π^* excitation, which is also supported by molecular orbital calculations.²³

1.5 Color of Azo Compounds

The azo dyes are very important coloring materials and in addition to finding wide spread use in the coloration of all types of fibers, they provide many useful pigments, historical stains and analytical colorimetric reagents. The versatility of azo dyes stems from their ease of synthesis and almost many diazotized aromatic amines can be coupled with any stable nucleophilic unsaturated system to give colored azo product. In the absence of electron donor groups, azo dyes are weakly colored and the visible absorption band corresponds to the low intensity n- π^* transition of azo group. By introducing electron withdrawing substituents to the second phenyl ring, the polarity and thus the absorption wavelength can be increased.

1.6 Application of Azo based Molecules and Polymers

The most important property of azobenzene compounds which is exploited in a large number of applications is its photochromic behavior. As previously discussed, they can exist in two different forms, the E (trans) and Z (cis) form, which can be recognized by their differences in UV spectra. In principle, azobenzene can function as molecular switches by applying light of different wavelengths to obtain varying amounts of cis and trans isomers, where the excess of one of the two isomers may be detected by a change in the absorption spectra. Photoanisotropic materials are widely investigated for optical data storage and processing applications. The most promising among them seem to be the azo systems because of the large value of the photoinduced birefringence in them. These systems possess advantages for high optical nonlinearities due to photoinduced trans-cis isomerization, molecular reorientation and nonlinear absorption. Among the potential materials for reversible optical data storage, liquid crystalline azobenzene side chain polymers

are especially promising due to their unique optical properties. Holograms of very high diffraction efficiency and exceptional stability can be written by laser illumination in this material. Azobenzene polymers are interesting because they combine the properties of anisotropy with photoresponsive behavior that give rise to applications in areas such as LC displays, NLO materials, holographic surface gratings and information storage.²⁴⁻²⁶

Azobenzene based amphiphilic molecules and block copolymers are of considerable interest for various applications in which the combination of hydrophilic and hydrophobic properties of these materials can be used; such as emulsifiers, dispersion stabilizers and compatibilizers. Also amphiphilic block copolymers and molecules can self assemble into a variety of micellar aggregates. Colloidal particles, which have at least one dimension within the nanometer to micrometer range, have been widely applied in many industrial products such as inks, paints, coating, cosmetics and photographic films. Incorporating azo systems into colloidal particles can further enhance those interesting properties like photoinduced shape deformation, photoinduced dichroism etc and lead to new applications in various photodriven devices.²⁷⁻²⁹ The majority of reports on light-sensitive surfactant systems make use of the azobenzene group although other moieties such as stilbene and spiropyran have also been used.³⁰⁻⁴⁹ Azobenzene based molecules are also used to construct nano-organized self assembled systems which are photoresponsive.⁵⁰⁻⁵³ Most of the light-switchable molecular shuttles are based on arylazo-cyclodextrin supramolecular chemistry.⁵⁴⁻⁵⁶ Thus azobenzene is a system with enormous potentials that can find application in numerous fields. A few important properties of azobenzene systems like their nonlinear optical property, liquid crystalline property and fluorescence behavior will be discussed in detail in the coming sections as they are of utmost relevance to the present study undertaken.

1.7 Nonlinear Optics

Nonlinear optics is one of the modern scientific frontiers of immense interest because of its technological applications. This newly emerging

technology utilizes photons instead of electrons to acquire, store, transmit and process information. Concepts of optical computing, optical signal processing and image analysis have been developed which utilize nonlinear optical processes to perform functions of frequency conversion, light modulation, optical switching, optical logic, optical memory stage and optical limiter function. Organic polymers containing electron donor (push) and acceptor (pull) groups, especially polymers or copolymers based on azobenzenic structures are currently being studied as systems with good non-linear optical behavior.

1.8 Basic Principles of Nonlinear Optics

Nonlinear optics (NLO) is the study of the interaction of electromagnetic radiation with matter to produce new fields altered in phase, frequency, amplitude and other propagation characteristics different from the incident light. In a nonlinear optical material, the refractive index is not a constant but a function of the intensity of the incident light striking the material and there is interaction between light and material. To observe a nonlinear optical phenomenon, the light used should be coherent and of very high intensity such as lasers.

When a beam of light is launched into a linear optical material, the photons will interact with material and the electric component of light will distort the electron cloud and displaces it. The amount of charge displacement is proportional to the instantaneous magnitude of electric field. The charges oscillate at the same frequency as the frequency of the incident light. The oscillating charges either radiate light at that frequency or the energy is transferred into non-radiative modes that result in material heating or other energy transfer mechanisms. The displacement of electron cloud will lead to charge separation between nucleus and electron cloud and results in a dipole moment.

The dipole moment per unit volume is called polarization which is given by the equation

$$\mu_{\text{ind}} = -er$$

where e is the electronic charge and r is the displacement of electrons from the equilibrium position induced by the applied electric field. When the strength of the applied electric field is small, of the order of 10^4 V/cm, the polarization induced in the molecule is proportional to the strength of the applied electric field and is given by the equation,

$$P = \alpha E$$

where P is the polarization induced in the molecule, α is the linear polarizability, mathematically a second rank tensor and E is the electric field.

When a laser beam passes through a nonlinear optical material, it interacts with matter and the polarization is nonlinear in behavior.

The polarization is expressed in a power series of the field strength E .

$$P = \chi^{(1)} \cdot E + \chi^{(2)} \cdot E \cdot E + \chi^{(3)} \cdot E \cdot E \cdot E + \dots$$

where P is the bulk polarization and $\chi^{(1)}$, $\chi^{(2)}$ and $\chi^{(3)}$ are the 1st, 2nd and 3rd order susceptibilities and E is the field strength. For most materials, the higher order effects $\chi^{(n)}$ ($n = 4$) are extremely difficult to observe.

At the molecular level, the polarization is given as

$$p = \alpha E + \beta E \cdot E + \gamma E \cdot E \cdot E + \dots$$

where α is the molecular polarizability, β is the first hyperpolarizability, γ is the second hyperpolarizability.

A lot of work has been done in the field of nonlinear optics, especially on the frequency doubling phenomenon ie, second harmonic generation. The most promising of them seem to be azobenzene based molecules and polymers because they possess the advantages for high nonlinear optical activity in addition to photoinduced trans-cis isomerization, molecular reorientation and nonlinear absorption.

1.9 Measurement Techniques for Second-order Nonlinear Optical Effect

Several methods have been employed for NLO measurements.

1) Kurtz-Perry Powder Technique

The method was developed by Kurtz and Perry in 1968.⁵⁷ This technique

gives information concerning angular averages of second order nonlinear tensor component, coherence length and phase matching behavior. In this method, the sample is powdered and particles of known size distribution are packed into a thin cell, which is irradiated with a fundamental beam. The second harmonic intensity in the forward direction is measured with a photomultiplier tube and compared with a signal from a reference sample such as quartz or urea.

2) Electric Field Induced Second Harmonic Generation (EFISHG)

This technique was developed in 1975 by Levine and Bethea to determine the value of β of molecules which are in liquid state or in solution.⁵⁸ In this method, a strong dc electric field is applied to a liquid or solution causing a bias on the average orientation of the molecules. The partial removal of orientational average reduces the symmetry of the medium, allowing the second harmonic field to propagate with the nonlinear polarization from the fundamental over some distance in the medium. The limitations of this method are that (i) the molecules must possess a permanent dipole moment and (ii) they must not ionize in solution.

3) Hyper Rayleigh Scattering (HRS)

HRS is the scattering of light at frequency 2ω when a liquid sample is irradiated by light at frequency ω . This is a parametric frequency conversion and does not involve two-photon fluorescence. The first reported use of HRS to accurately measure NLO coefficients of solvent and solute molecules was by Clays et al. in 1991.⁵⁹ The objective of HRS method is to determine the first hyperpolarizability β of molecules in solution by measuring the second harmonic scattered light as a function of concentration. The advantages of this technique are (i) it does not require a DC applied field (ii) it offers a means of measuring the nonvector part of β (i.e. where μ and the vector part of β make an arbitrary angle) (iii) it does not require measuring γ or μ as the second harmonic scattered light is proportional to β^2 and (iv) it can use an internal solvent for calibration. Since this method does not require an external field it can be used to characterize nonpolar (e.g. octupolar) and ionic samples. It also has several disadvantages.

1) The scattered second harmonic is weak and requires sensitive detection. 2) It requires high fundamental intensity. 3) The high intensity used must not be so high that it introduces complications such as stimulated Raman or Brillouin scattering, self-focusing or dielectric breakdown in the liquid.

4) Maker Fringe Technique

This technique was developed by Maker et al.⁶⁰ The measurements were performed on polymer films after poling and were made relative to a Y-cut quartz plate ($d_{11}=1.2 \times 10^{-9}$ esu=0.5pm/v). In this technique, a plane parallel sample of the nonlinear optical material is rotated in the path of a fundamental beam of wavelength 1.064 μm from a Q-switched Nd:YAG laser. For samples with thickness of millimeters, the power of the 532 nm radiation produced by optical frequency doubling in the film is found to oscillate in a periodic fashion as the incidence angle is varied. Analysis of the periodicity and intensity of these fringes provides information on the coherence length of the radiation within the sample and also on the value and tensorial nature of the second harmonic coefficients.

1.10 Materials for Nonlinear Optics

The basic conditions for a material to exhibit second order NLO property are as follows:

- (1) the material should be polarizable (the electrons should be greatly perturbed from their equilibrium position)
- (2) there should be asymmetric charge distribution
- (3) there should be an extended π -conjugation allowing for the polarization of electrons
- (4) there should be acentric crystal packing.

A typical SHG active molecule can be represented schematically as given in figure 1.

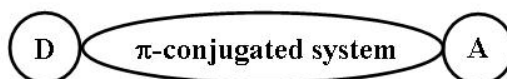
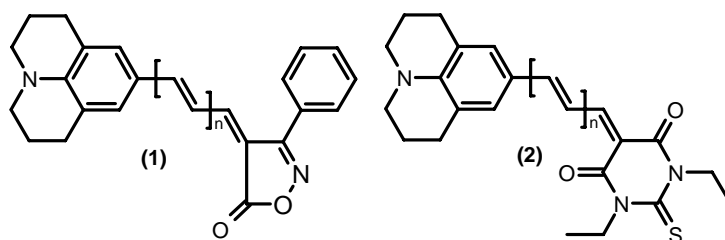


Figure 1

In the beginning, studies were concentrated mainly on inorganic materials such as quartz, potassium dihydrogen phosphate (KDP), lithium niobate etc. In 1970, Davidov et al. reported a strong SHG in organic molecules having electron donor and acceptor groups connected with a benzene ring.⁶¹ This discovery led to an entirely new concept of molecular engineering to synthesis new organic materials for SHG studies. In 1980s tremendous growth occurred in the design and development of organic materials for second order nonlinear optics. Organic materials that have been investigated for second order nonlinear optics falls into several categories such as single crystals, Langmuir-Blodgett (LB) films, poled polymers, guest (NLO dye)-host (polymer matrix) systems, NLO chromophore functionalized polymers, self assembled systems and liquid crystals.

Because of their very high efficiency, inorganic crystals were the first choice for device applications. But recent reports reveal that organic molecules also can be used instead of inorganic materials. SHG was first observed in quartz crystal by Franken and co-workers in 1961.⁶² When they irradiated the quartz crystal with a ruby laser of wavelength 694.3 nm, they observed that the emitted light contained light of double frequency at 347.15 nm which is in the ultraviolet region and the conversion efficiency was 10^{-4} percent. The first observation of SHG in an organic material (benzpyrene) was made by Rentzepis and Pao in 1965.⁶³ Thereafter tremendous advancement in the field of organic nonlinear optical materials has been made during the last few decades.

Marder has reported two molecules with highest first order hyperpolarizability reported so far.^{64, 65} The structures of the molecules are given below. Julolidinyl-6-isoxazolone with $n=6$ (1) and julolidinyl-6-N, N'-diethylthiobarbituric acid (2) possessed $\mu\beta(0) = 13600 \times 10^{-48}$ and 14290×10^{-48} esu respectively (Scheme 1).



Scheme 1

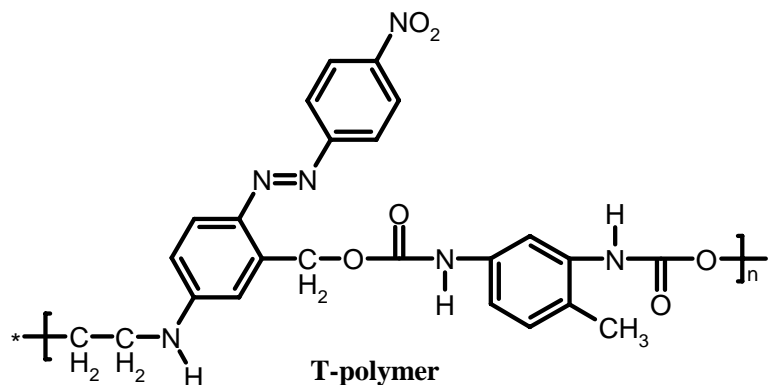
Polymeric materials are attractive NLO materials because they are compatible with manufacturing methods practiced in industry and they can provide durability, environmental protection and packaging advantages, often not provided by crystalline materials. There are two ways of incorporating the NLO chromophore in polymer matrix.

- (1) Guest/Host systems wherein NLO chromophores are dispersed in the amorphous polymers
- (2) NLO chromophores are covalently linked to the polymer backbone.

1.11 Azobenzene based Nonlinear Optical Materials

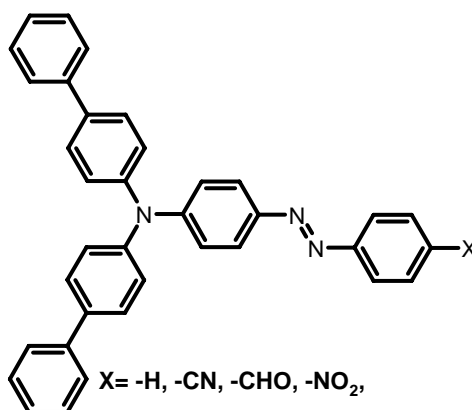
Organic nonlinear optical materials have been extensively studied because of their potential applications in integrated optical signal processing, optical switching etc. One of the features of the organic and polymeric nonlinear optical materials is the large electro-optic coefficients due to large second order nonlinearity. Recently, large numbers of azobenzene containing molecules and polymers possessing nonlinear optical property have been reported.⁶⁶⁻⁷⁷ Tsutsumi et al. reported linear polyurethane of T-polymer (Scheme 2) based on an azodiol and aromatic diisocyanate, in which the NLO dipole moment is aligned transverse to the main chain.^{78, 79} Azobenzene dendrons (Scheme 3) with 15 chromophoric units having first hyperpolarizability value 3010×10^{-30} esu have been reported by Yokoyama et al.⁸⁰ They found that the level of molecular hyperpolarizability was much higher than that for an azobenzene monomer and the polarized nonlinear optical measurement provided structural information on the dendrons and indicated that each chromophore was oriented

noncentrosymmetrically along the molecular axis to become a cone shaped rather than a spherical shape.



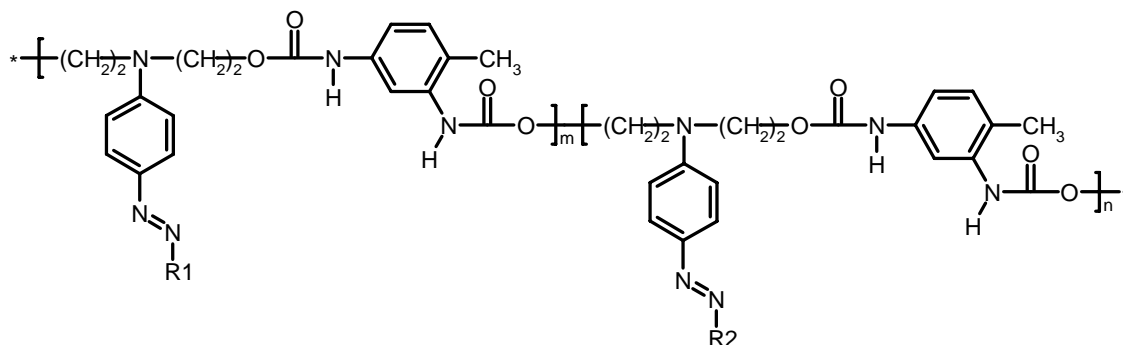
Scheme 2

Ishow et al. reported for the first time a series of push-pull azo systems comprising of a bulky electron-donating triaryl amino group linked to various electron withdrawing groups like cyano, nitro, dicyanovinylene etc forming amorphous materials with spontaneous NLO activity without requiring any external poling process.⁸¹



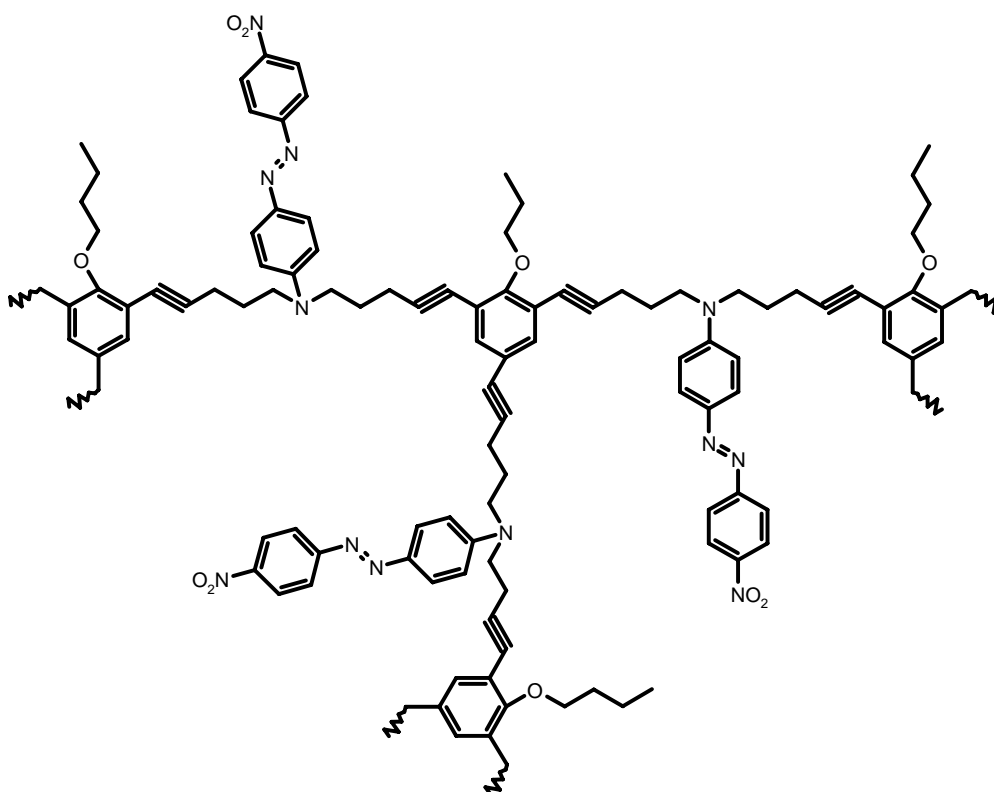
Scheme 3

Gopalan et al. reported star shaped azo-based dipolar chromophores with dendritic architecture having highest electro-optic coefficient 22-25 pm/V at 1550 nm wavelength.⁸² Roviello et al. reported a series of side chain polyurethanes (Scheme 4) based on azo-bridged push-pull chromophores with second harmonic generation coefficient in the range of 20-30 pm/V.^{83, 84}



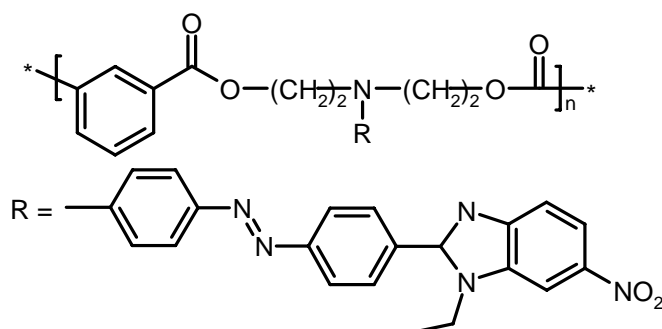
Scheme 4

Azo-functionalized hyperbranched poly(aryleneethynylene)s (Scheme 5) with second harmonic generation coefficients upto 77 pm/V have been reported by Tang et al.⁸⁵



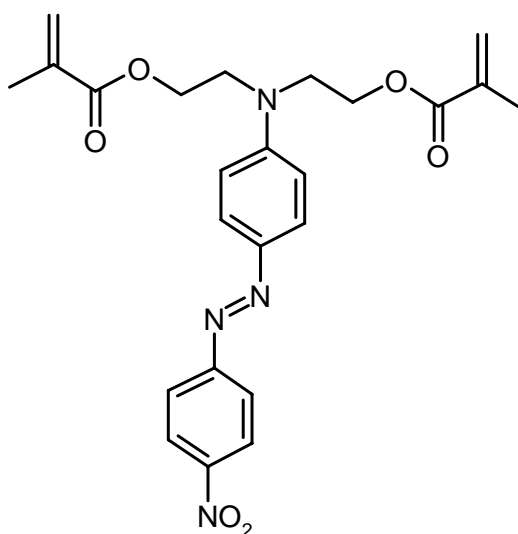
Scheme 5

Polyurethanes and polyesters with high thermal stability and Tg based on NLO active azo-benzimidazole chromophores (Scheme 6) have been reported by Carella et al.⁸⁶



Scheme 6

Carella et al. also reported pure azo-benzimidazole based dimethacrylic push-pull chromophores (Scheme 7) with quadratic nonlinear optical properties having SHG coefficient of 14 pm/V.⁸⁷



Scheme 7

This recent examples show the significance and the current development in the field of azobenzene based NLO materials.

1.12 Fluorescence

Luminescence is the emission of light from any substance and occurs from electronically excited states. Luminescence is divided into two categories, fluorescence and phosphorescence, depending on the nature of excited states. In the excited singlet state, the electron in the excited orbital is paired to the second

electron in the ground-state orbital. Consequently, return to the ground state is spin allowed and occurs rapidly by the emission of a photon.

The emission rates of fluorescence are typically 10^8 s^{-1} , so that a typical fluorescence lifetime is near 10 ns. Phosphorescence is the emission of light from the triplet state, in which the electron in the excited state has the same spin orientation as the ground state electron. Transitions to the ground state are forbidden and the emission rates are slow, so that the phosphorescence lifetimes are typically of the order of milliseconds to seconds.

The processes which occur between the absorption and emission of light are usually illustrated by the Jablonski diagram.⁸⁸ A typical Jablonski diagram is shown in figure 2.

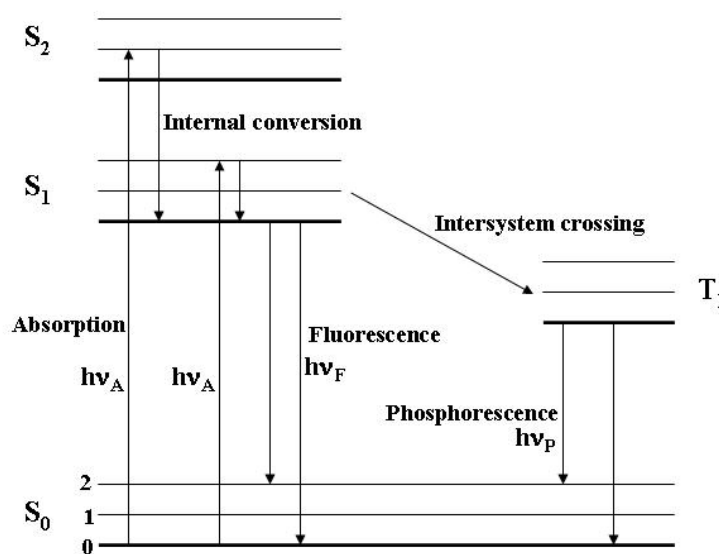


Figure 2

The singlet ground, first and second electronic states are depicted as S₀, S₁ and S₂ respectively. At each of these electronic energy levels, the fluorophores can exist in a number of vibrational energy levels denoted by 0, 1, 2 etc. The transitions between states are depicted as vertical lines to illustrate the instantaneous nature of light absorption. Transitions occur in about 10^{-15} s , a time too short for significant displacement of nuclei. This is the Franck-Condon principle.⁸⁸ Absorption typically occurs from molecules with lowest vibrational

energy. The energy difference between the S_0 and S_1 states is too large for thermal population of S_1 and it is for this reason, light and not heat is used to induce fluorescence. Following the light absorption, several processes can occur. A fluorophore is usually excited to some higher vibrational level of either S_1 or S_2 . With a few rare exceptions, molecules in condensed phases rapidly relax to the lowest vibrational level of S_1 . This process is called internal conversion and generally occurs in 10^{-12} s or less. Since fluorescence lifetimes are typically 10^{-8} s, internal conversion is complete prior to emission. Hence, fluorescence emission generally results from a thermally equilibrated excited state, that is, the lowest-energy vibrational state of S_1 .

Return to the ground state typically occurs to a higher excited vibrational level, which then quickly reaches thermal equilibrium. An interesting consequence of emission to higher vibrational ground states is that emission spectrum is typically a mirror image of the absorption spectrum of S_0 to S_1 transition. This similarity occurs because electronic excitation does not greatly alter the nuclear geometry. Hence, the spacing of the vibrational energy levels of the excited states is similar to that of ground states. As a result, the vibrational structures seen in the absorption and emission spectra are similar. Molecules in the S_1 state can undergo a spin conversion to the first triplet state, T_1 . Emission from T_1 is termed as phosphorescence and is generally shifted to longer wavelengths relative to fluorescence. Conversions of S_1 to T_1 is called intersystem crossing. Transition from T_1 to the singlet state is forbidden and as a result, rate constants for triplet emission are several orders of magnitude smaller than those for fluorescence.

From the Jablonski diagram we can see that the energy of emission is typically less than that of absorption. Hence, fluorescence typically occurs at lower energies or longer wavelengths. This difference in wavelength between the absorption and emission is termed as Stokes' shift.⁸⁸ Energy losses between excitation and emission are observed for fluorescent molecules in solution. One common cause of the Stokes' shift is the rapid decay to the lowest vibrational

level of S_1 . Furthermore, fluorophores generally decay to higher vibrational levels of S_0 , resulting in further loss of excitation energy by thermalization of the excess vibrational energy. In addition to these effects, fluorophores can display further Stokes' shift due to solvent effects, excited-state reactions, complex formation or energy transfer.

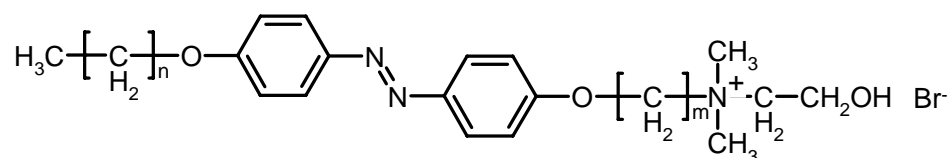
Another general property of fluorescence is that the same fluorescence emission spectrum is generally observed irrespective of the excitation wavelength. This is known as Kasha's rule.⁸⁸ Upon excitation into higher electronic and vibrational levels, the excess energy is quickly dissipated, leaving the fluorophore in the lowest vibrational level of S_1 . This relaxation occurs in about 10^{-12} s and is presumably a result of strong overlap among numerous states of nearly equal energy. Because of this rapid relaxation, emission spectra are usually independent of the excitation wavelength. Exceptions exist, such as fluorophores which exist in two ionization states, each of which displays distinct absorption and emission spectra. The intensity of fluorescence can be decreased by a wide variety of processes. Such decrease in intensity is called quenching. A variety of molecular interactions can result in quenching. These include excited-state reactions, molecular rearrangements, energy transfer, ground-state complex formation and collisional quenching.

1.13 Fluorescence in Azo Compounds

Generally azobenzene systems in solution do not fluoresce with appreciable quantum yield since the photoisomerization process is very efficient in photoexcited azobenzenes compared to the radiative deactivation processes, which are slower and not competitive.⁸⁹

There have been only limited exceptional azobenzene derivatives that show fluorescence, however, most of them fluoresce only in a rigid matrix at low temperature and their fluorescence quantum yields are very low.⁹⁰⁻⁹⁴ Ortho-metallated azobenzene complexes and self assembled aggregates of azobenzene derivatives have also been reported as emissive azobenzene derivatives and most of their fluorescence quantum yields at ambient temperature in the solution state

are about 10^{-3} . The first observation of $n-\pi^*$ (S_1 state) luminescence of trans azobenzene was by Struve in 1977 in the 600-800 nm region when excited at 531 nm and the lifetime determined was 25 picosecond.⁹⁵ Later Morgante and Struve studied the fluorescence of trans azobenzene derivatives from the $\pi-\pi^*$ (S_2) state by picosecond laser and the quantum yield was found to be 10^{-5} .⁹⁶ Shimomura and Kunitake reported fluorescence emission from bilayer aggregates of azobenzene containing amphiphiles (Scheme 8) and they observed that in their case, fluorescence intensity decreased as the chromophore orientation changed from tilted head to tail to the parallel type.⁹⁷



Scheme 8

They studied two different molecules with formulae $C_8AzoC_{10}N^+$ and $C_{12}AzoC_5N^+$ and they irradiated the aqueous dispersion of azobenzene bilayer with 360 nm light. As a result of irradiation, the trans isomer was converted to the cis form and fluorescence was observed for $C_{12}AzoC_5N^+$ at 600nm whereas $C_8AzoC_{10}N^+$ remained nonfluorescent. This difference in behavior was explained in terms of the difference in the orientation of the amphiphiles in the bilayer structure as shown below (Figure 3). The efficiency of trans–cis isomerization is related to the chromophore orientation. The $C_8AzoC_{10}N^+$ bilayers which possess the head-to-tail chromophore orientation (Figure 3a) isomerize faster than the $C_{12}AzoC_5N^+$ bilayer which possesses the parallel chromophore orientation (Figure 3b).

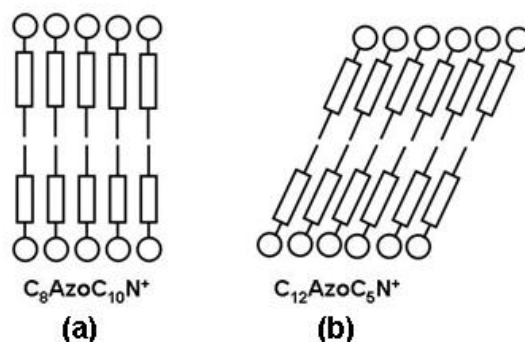
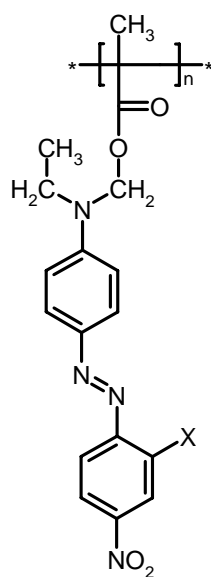


Figure 3

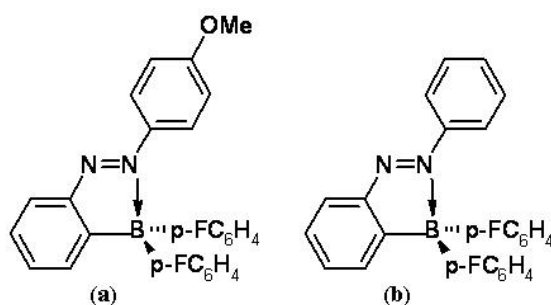
The mobility of the chromophores is crucial for efficient isomerization. The molecular reorganization accompanying photoisomerization proceeds more readily in the tilted packing of the half-bilayer in $C_{12}AzoC_5N^+$ than in the parallel, interdigitated structure of the $C_8AzoC_{10}N^+$ bilayer. Aroca et al. reported emission from Langmuir-Blodgett (LB) films of homopolymer of methacrylate derivative of red-13 (HPDR13) (Scheme 9) at 680 and 750 nm when excited at 633 and 514 nm respectively.⁹⁸ The mixed LB film technique whereby HPDR13 is co-deposited with cadmium stearate (StCd) was applied to achieve good quality multilayer LB films. In this case, even though the photoisomerization occurs, which lead to the surface relief gratings, a part of the azobenzene moieties in the polymer chains are restrained and do not undergo photoisomerization and hence fluorescence could be detected.



Scheme 9

In addition to the room temperature fluorescence of dendrimers, they could observe emission from the azo monomer at temperature closer to its melting point.

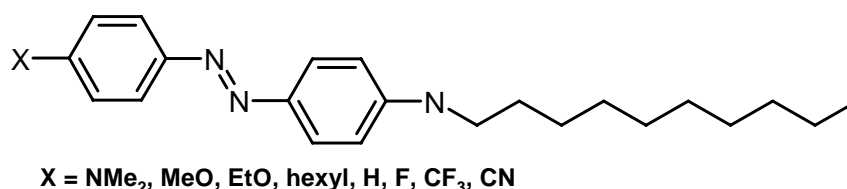
Recently Jayakannan et al. reported a new fluorescent amphiphilic azobenzene sulphonic acid dopant based on the renewable resource cardanol which was used as a fluorescent dopant for polyaniline nanofiber synthesis.¹⁰¹ There are also reports of metallation of azo group in the trans configuration which showed weak luminescence of the order of 10^{-4} in contrast to the uncomplexed azobenzene reference which was non luminescent. Ghedini et al. have reported luminescent organometallic azobenzene Pd (II) complexes¹⁰² where they studied the spectroscopic properties of 4, 4'-bis-hexyloxyazobenzene, chloro-bridged cyclopalladated dimer and the mononuclear derivatives containing acetylacetonate, tropolonate and cyclopentadienyl monoanionic ligands. With palladium (II) species, azobenzenes underwent cyclopalladation and a five membered ring containing both the palladium center and azo linkage was formed. In such an arrangement the $-N=N-$ fragment was trans blocked as a consequence of which the typical photochromic behavior was suppressed and luminescent products were formed. A highly intense fluorescence with quantum yield in the range of 0.2 to 0.7 (highest known so far) was reported very recently by Kawashima et al. where boron substituted azobenzene (Scheme 11) showed strong green fluorescence upon irradiation by 360 nm light.¹⁰³



Scheme 11

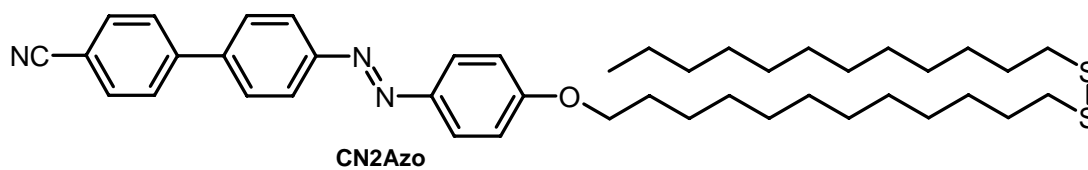
Irradiation with light of wavelength 360 nm in C_6D_6 at room temperature did not cause their photoisomerization, but caused strong green fluorescence in contrast

to the behavior of most azobenzene derivatives. The molecule **a** showed emission maxima at 503 nm with a quantum yield of $\phi_{\text{FL}}=0.23$ when excited at 386 nm and the molecule **b** at 524 nm when excited at 439 nm with $\phi_{\text{FL}} = 0.76$. The mechanism responsible for the very efficient radiationless deactivation and the high fluorescence quantum yield in **a** and **b** was attributed to the enhanced rigidity of the structure around the azo group which suppresses any conformation and thus locks the photoisomerization around N=N. Han et al. reported light driven self assembly and the resulting fluorescence enhancement of azobenzene molecules para substituted with electron donating or electron withdrawing groups (Scheme 12).¹⁰⁴



Scheme 12

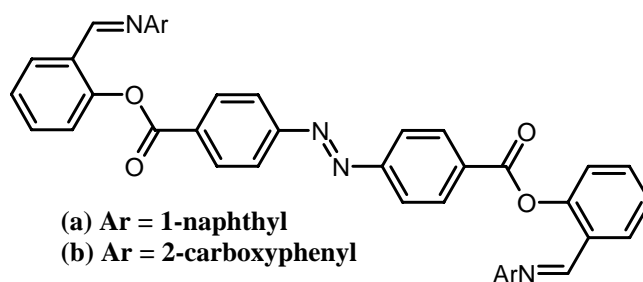
When the dichloromethane solution of the azo compound was excited at 365 nm, no fluorescence was observed. However, continuous exposure of the solution to 365 nm resulted in blue fluorescence. The spontaneous formation of spherical aggregates by cis isomer was responsible for the emission observed. It was also found that as the substituents become more electron donating, the azobenzene seemed to assemble more efficiently into spherical aggregates with diameter ranging from 10 to 200 nm. Therefore, the unusual fluorescence enhancement upon UV exposure was attributed to the light driven self assembly of the cis form showing sufficient lifetime and a larger dipole moment. The same group also reported intense fluorescence from light-driven self assembled aggregates of nonionic azobenzene derivative (Scheme 13) upon irradiation with 365 nm.¹⁰⁵



Scheme 13

When CN2Azo solution ($4 \times 10^{-5} \text{M}$) was excited at 325 nm, very weak fluorescence was observed centered at 417 nm. Upon irradiation with light of 365 nm for 390 min, a 1000 times enhancement in fluorescence was observed. SEM images confirmed the formation of spherical aggregates of diameter 10-120 nm when exposed to UV light up to 120 min. Concentration and time of irradiation were found to have strong influence on the size of the aggregate. The hydrophilic-hydrophobic interaction was responsible for the spontaneous self assembly of the azobenzene molecules into spherical aggregates. Also the bulky and polar cyano group could play an important role in the head to tail intermolecular interactions of azobenzene aromatic units forming J-aggregates.

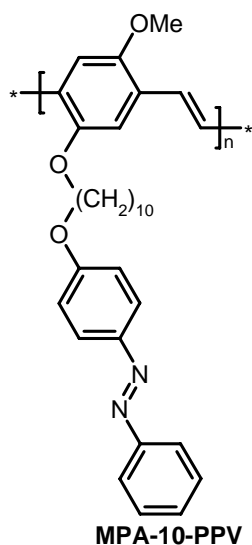
Azobenzene systems have also been made fluorescent by attaching fluorophores like 1-aminonaphthalene and 2-aminobenzoic acid to it and the reversible trans-cis isomerization was shown to induce changes in the fluorescence properties of the fluorophores. Zacharias et al. exploited this concept to obtain fluorescence from azobenzene derivatives (Scheme 14).¹⁰⁶ The molecules **a** and **b** were excited at ~ 330 nm and monomer like emission was observed at 406 and 400 nm for **a** and **b** respectively. On irradiation, there was a 13 fold and 6 fold enhancement in the fluorescence intensity for **a** and **b** respectively. The emission observed in **a** and **b** originated from the fluorophores that are coupled to azobenzene.



Scheme 14

But the enhanced emission upon irradiation was attributed to the inhibition of photoinduced electron transfer (PET) mechanism by the cis isomer. The cis isomer formed is nonplanar and therefore the lone pair of electrons on nitrogen atom can no longer effectively conjugate with the π -electrons of the fluorophore, thereby inhibiting PET mechanism.

There are no reports in the literature of intense fluorescence exhibited by azobenzene based polymers – main chain or side chain – at room temperature in the trans state. There are reports of fluorescence from poly (p-phenylenevinylene) (PPV) derivatives substituted with azobenzene side chains, but the emission in these cases is entirely due to the PPV backbone.^{107, 108} Harbron et al. studied the fluorescence modulation of PPV derivative (Scheme 15) with alkyl tethered azobenzene side chains.¹⁰⁷



Scheme 15

Here, the emission was entirely due to the PPV backbone as the azobenzene side chains do not emit. The emission intensity of MPA-10-PPV was partially quenched when azobenzene side chain was attached to the PPV backbone. They found that the emission of MPA-10-PPV was dependent on the isomeric form of the azobenzene side chain. The quenching of fluorescence is due to the nonradiative energy transfer from PPV backbone to the side chain and the transfer is more efficient to the cis isomer than to the trans isomer which is

attributed to the improved spectral overlap between the absorption of the cis isomer and the PPV emission. This differential can be used for the reversible modulation of emission intensity by controlling the isomeric form of the azobenzene side chain with light. There is also one report of poly (p-phenylene) (PPP) unit in conjugation with azobenzene units in the main chain which showed weak fluorescence expected to be originating from the terphenyl units in the main chain.¹⁰⁹

1.14 Liquid Crystallinity

The liquid crystal state is the fourth state of matter, represents a number of different states whose degree of order lies between perfect crystals and isotropic liquids. Crystalline, amorphous and liquid are the three conventional limiting states of condensed phase. Crystals have long range order and positional order, whereas the amorphous solids have only a short range order. In a normal melting process of a solid, the degree of freedom of the molecules increases in three dimensions. Thus those molecules which are ordered in the solid state tumble freely in the liquid. However, in the melting process mediated by mesophase behavior, there is a stepwise breakdown of the order and a concomitant selective increase in the number and type of degree of freedom. Each step in the breakdown of the order coincides with the formation of a thermodynamically stable mesophase. The molecules with sufficient rigidity and flexibility form LC phase.

The asymmetry in the molecular shape allows the thermodynamically stable orientational order in the preferred direction of molecular long axis. These orientationally ordered liquids or positionally disordered solids are widely known as liquid crystals. The liquid crystal glasses are obtained by quenching the LC phases where the LC phase exists as frozen-in state. This is possible only when the glass transition is lower than the decomposition temperature.

1.15 Classification of Liquid Crystals

Liquid crystals can be classified into four classes based on their formation.

1. Thermotropic systems: In this class, LC formation is induced purely by thermal effect. Thermotropic LC which is stable at a temperature above melting point is termed as enantiotropic. The liquid crystalline state that is stable only at temperature below the melting point and can be obtained only with decreasing temperature is called monotropic.
2. Lyotropic systems: Here LC phase arise from the action of a solvent. There are three important variables to be optimized and they are solvent strength, concentration of the solution and temperature.
3. Amphotropic systems: These are compounds that are able to form thermotropic as well as lyotropic liquid crystalline states. Alkali salts of long chain aliphatic acids are good examples of this category.
4. Barotropic systems: Pressure is the factor that generates LC phase.

Based on the macroscopic structure formed, there are four structural classes of LC.

1. Smectic LC: The structure of this phase may be described as an orientationally ordered fluid which is superimposed on a one dimensional density wave. The layers are liquid like with molecules upright on the average and negligible in-plane and inter layer correlations. Smectic LCs are one dimensional crystals and two dimensional fluids. This LCs show polymorphism in which the layer structure is the common feature. Due to the layered structure, the large scale movement in any direction other than tangential to the surface is rather difficult (Figure 4b). Therefore, smectic phases are quite viscous and solid like.
2. Nematic LC : These are three dimensional fluids with a high degree of long range orientational order of the molecules approximately parallel to the long molecular axis (Figure 4a). Among the known LC phases, nematic LCs are the least ordered mesophase. Thus, specific heat, volume expansion and compressibility in nematic LCs are similar to those of normal liquid.

Linear discontinuities and twisted like thread are the optical features characteristic of this type of LCs.

3. Cholesteric or chiral nematic liquid crystals: The unique optical properties of the cholesteric phase were recognized by both Reinitzer and Lehmann at the time of their investigations which culminated in the discovery of liquid crystalline state. Locally cholesteric is very similar to nematic material with a spontaneous twist about an axis perpendicular to the molecular axis or the director, \mathbf{n} . The director is not constant in space, so that in each layer \mathbf{n} is displaced to a constant angle with the precession of the director about the helical axis (Figure 4c). Hence the structure is helicoidal with the pitch of the helix much larger than the molecular dimensions.

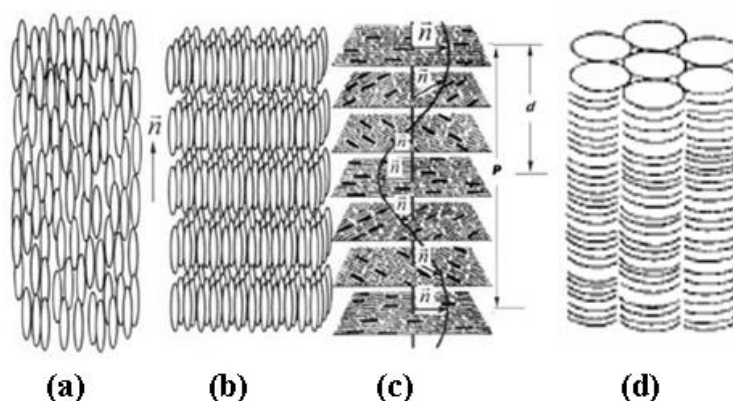


Figure 4

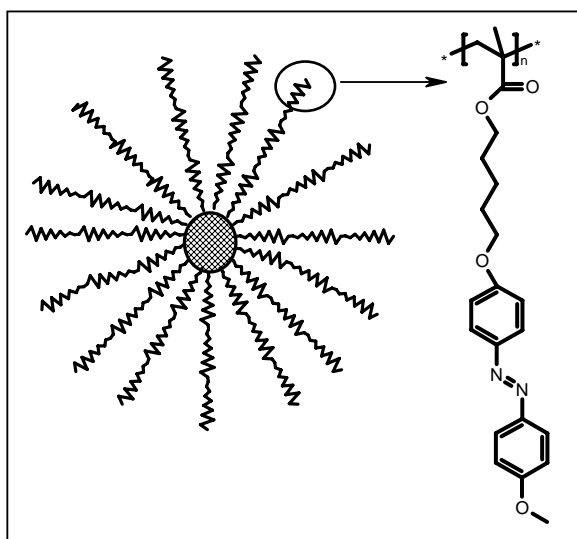
4. Discotic liquid crystals: Discotic LCs are formed by disc like molecules or nearly so with flexibilizers of at least five carbon atoms and four or more lateral substituents normally alkoxy and ester groups. The structures are based on the tendency of the discs to align with their short axis parallel. (Figure 4d)

1.16 Azobenzene Liquid Crystals

Azobenzene group is the most common rigid unit used in the design of liquid crystals because it offers the structural rigidity imparted by the coplanarity of all atoms adjacent to a double bond as well as the double bonded nitrogen

atom itself. Also azo group is a good electronic bridging group with aromatic rings on either side. There are a large number of reports on azobenzene based liquid crystals which fall into different categories like polymeric material, both main chain and side chain, achiral bent core mesogens, dendrimeric LCs etc.

Yan et al. reported liquid crystalline multiarm star-shaped azo-dendrimers (Scheme 16) and the effect of irradiation of nanosecond pulsed laser on the orientation of azo group which affects the LC alignment.¹¹⁰ They found that the pulsed irradiation led to the anisotropic orientation of azo groups and the thermal effect accompanied by this procedure strongly affected the distribution of azo groups due to change in aggregated state of azo groups. Both the orientation of azo moieties and laser induced periodic surface structure showed a decisive effect on LC alignment and the preferred direction of LC alignment can be altered via annealing.

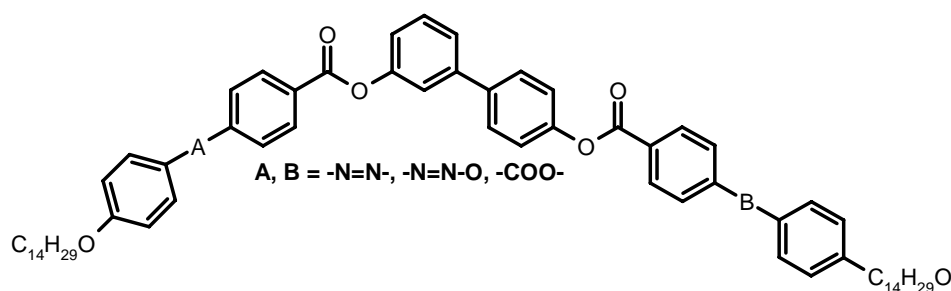


Scheme 16

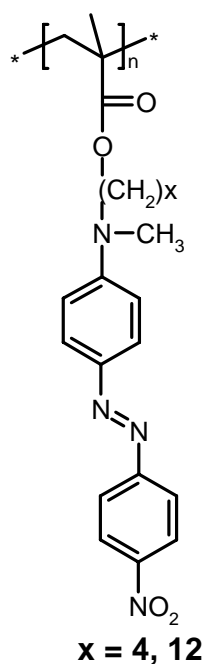
Ortega et al. reported bent core mesogens (Scheme 17) possessing photoactive azo linkage which gave columnar and smectic phases which were NLO active also.¹¹¹ They selected azobenzene systems for two reasons. The first point was that these systems allowed delocalized electronic charge distribution between donor and acceptor at both sides of the π -system. This possibility is interesting for the design of materials with good nonlinear optical properties. In particular,

azobenzene seems to be good candidate to be incorporated in the lateral cores of the bent-shaped molecules. Second factor was the ability of azo systems to undergo trans-cis isomerization by light absorption. In the field of liquid crystals this property gives rise to a new added value to the materials, which can be used for photoalignment.

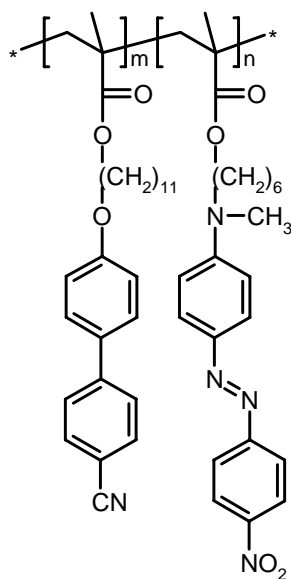
Natansohn et al. reported azobenzene containing side chain polymers (Scheme 18) with different number of methylene groups in the spacer.¹¹² They studied the effect of the photoisomerization and reorientation processes on the observed mesophases and physical properties of the polymer. They found that annealing of polymers with short spacers induced a hypsochromic shift while for the long spacer, it induced a bathochromic shift in the absorption spectra. These effects were attributed to the strong dipolar interaction and the interdigitation of the side chain chromophores in an antiparallel orientation. The irradiation of such organized films with either circularly or linearly polarized light induced a bathochromic shift in breaking the antiparallel organization that is a consequence of the angular reorientation of the azobenzene moieties as a result of trans-cis isomerization.



Scheme 17



Scheme 18

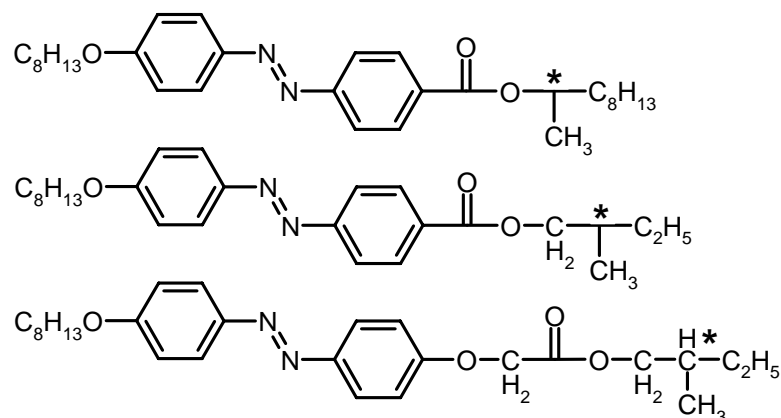


Scheme 19

Rochon et al. reported the photo induced chirality in thin films of liquid crystalline copolymers (Scheme 19) with a low content of azobenzene units.¹¹³ They investigated the co-operative motion of the nonmesogens on irradiation of circularly polarized light (CPL). CPL with opposite handedness produced enantiomeric structures and a chiro optical switch could be achieved by alternating irradiation with left and right CPL. The level of photo induced

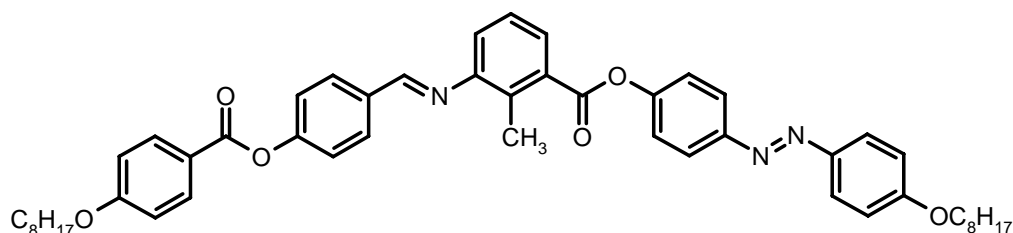
chirality depended on the amount of azobenzene units and the sample temperature. The photoinduced circular dichroism could be erased by heating the films above clearing temperature or by annealing the films in the liquid crystalline phase.

Kurihara et al. reported the photochemical reversible phase transition between nematic and cholesteric phases achieved by trans-cis isomerization of azobenzene molecules (Scheme 20).¹¹⁴ They found that the photochemical change in helical pitch was due to the perturbation effect of the trans-cis photoisomerization on the molecular reorientation and the photochemical change in an intermolecular interaction between the trans or cis chiral azobenzene molecule and the host LC molecule. The higher twisting power of the trans azobenzene molecule than that of cis one was interpreted in terms of intermolecular interaction between guest azo molecule and the host LC molecule. The intermolecular interaction between the chiral trans azo molecule and the LC host molecule was higher than that in the chiral cis one and the host LC molecule because of the similarity in their molecular shape.



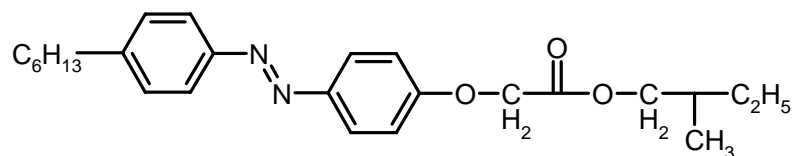
Scheme 20

Kang et al. reported azo substituted achiral bent core mesogens (Scheme 21) exhibiting uniaxial and biaxial nematic and three smectic phases at different temperatures in a single component small molecule system.¹¹⁵



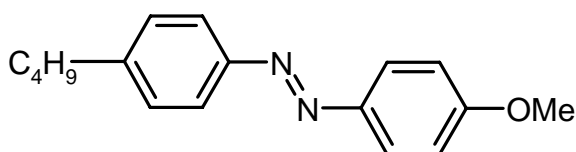
Scheme 21

Bunning et al. reported a photoresponsive holographically patterned Bragg reflector in a polymer-stabilized azo liquid crystal by the incorporation of a photoresponsive azobenzene derived liquid crystal.¹¹⁶ The device was optically clear in the unexposed state and the exposure to UV light developed an index profile within the material according to the holographic pattern. The profile was developed through disruption of local order within the LC structure which selectively affected the areas within the structure with little polymer content. The diffraction efficiency of the Bragg reflector increased depending on the exposure dose and reached a stationary value that depended on the intensity. This was correlated with the production of cis-Azo LC population within the material. Ikeda et al. reported photochemical modulation of color and transmittance in chiral nematic liquid crystal containing photosensitive azobenzene chromophore (Scheme 22).¹¹⁷ Photoirradiation at 366 nm which causes the efficient trans-cis isomerization of azo led to color change of cholesteric LC towards shorter wavelength region with concomitant lowering of phase transition temperature from a cholesteric to an isotropic phase. Reversible change in color was induced all optically by irradiating alternatively at effective wavelengths for reversible isomerization of azo group. A remarkable change in transmittance was also observed when the photoinduced change in colors was measured by a probe light with the same handedness as the sense of the cholesteric LCs.



Scheme 22

Ikeda et al. also reported the dynamics of the photochemical phase transition process of guest-host liquid crystals containing photosensitive azobenzene chromophore (Scheme 23).¹¹⁸ Because the photochemical phase transition of the LCs results in a change in the refractive indices and birefringence of materials, it is possible to switch the transmittance of the light with another light. Thus the guest-host LCs can have applications as optical-switching materials.



Scheme 23

These examples throw light on the significance of azo based liquid crystals and its advanced modification and application in various optical materials. Researchers are making use of the LC behavior as well as the isomerization and the tuning of various properties like transmittance, reflectance etc with respect to isomerization to find applications in a wide variety of fields. Azo based LCs are widely used in the preparation of optical shutters, optical displays, photocontrollable coatings etc

1.17 Origin and Objectives of the Present Investigation

Azobenzene systems are very promising because they combine the properties of anisotropy with photoresponsive behavior that give rise to applications in areas such as NLO materials, LC displays, information storage etc. There are a number of reports in recent literature exploring these properties. Azobenzene molecules and polymers are found to have high nonlinearities due to photoinduced trans-cis isomerization, molecular reorientation and nonlinear

absorption. One of the most common mesogenic group used in liquid crystalline materials is the azo group. It was found that liquid crystallinity can enhance the NLO property. One of the consequences of the very efficient photoisomerization in azobenzene systems is that, they do not fluoresce. However there are few reports in literature on fluorescent azobenzenes. With this aim in view, a few novel azobenzene based polymers and oligomers were designed and various properties like NLO activity, liquid crystallinity and fluorescence was explored. The design strategy for second order NLO active material is to have a donor and acceptor system separated by π -conjugation unit. Increase in the donor-acceptor strength and conjugation length increases the NLO property. Therefore the azobenzene monomers in the present work was designed as NLO chromophores with a strong electron withdrawing group like the $-\text{COOH}$ and $-\text{OH}$ as the acceptor group with various substituents connected to the aromatic ring and also varying the conjugation length by the use of extended and fused ring systems. Thus the effect of substituents and conjugation length on NLO property could be addressed. Polymerization of these AB type chromophores results in main chain polymers with better NLO property. The second objective was to develop soluble azo side chain polymers where the azo chromophore was attached as pendant to a flexible backbone and to study the photoisomerization of the azo unit and its influence on fluorescence behavior. The final objective was to develop fluorescent liquid crystalline twin molecules where the aromatic rigid segments were sandwiched between flexible ethyleneoxy spacers of varying length. The present thesis describes a systematic investigation on the design, synthesis and study of various properties of azobenzene molecules and polymers including their morphology.

1.18 References

1. Griffiths, J. *Chem. Soc. Rev.* **1972**, 1, 481.
2. Sudesh Kumar, *Azo Functional Polymers: Functional Group Approach in Macromolecular Design*, Lancaster, Pennsylvania, U. S. A, **1992**.
3. Zollinger, H. *Azo and Diazo Chemistry*, **1961**. New York, NY, Wiley p1

4. Engel, P.S. *Chem. Rev.* **1980**, 80, 99.
5. Patai, S. *The Chemistry of the Hydrazo, Azo and Azoxy groups*, Part I & II, **1975**, New York, NY, Wiley.
6. Zollinger, H. *Color Chemistry: Synthesis, Properties and Application of Organic Dyes*, **1987**, Weinheim: VCH.
7. Allmann, R.; Patai, S. In *The Chemistry of the Hydrazo, Azo and Azoxy groups*, Part I. **1975**. New York, NY, Wiley.
8. Mostad, H.; Ronming, C. *Acta.Chem. Scandina*, **1971**, 25, 3561.
9. Hope, H.; Victor, D. *Acta. Cryst.* **1969**, B25, 1849.
10. Happer, D. A. R.; Vaughan, J. In *The Chemistry of the Hydrazo, Azo and Azoxy groups*, Part I. **1975**. New York, NY, Wiley p-225.
11. Hampson, C. C.; Robertson, J. M. *J. Chem. Soc.* **1941** p-409.
12. Lange, J. J.; Robertson, J. M. *Proc. Roy. Soc.* **1939**, A171, 398.
13. Suzuki, H. *Electronic Absorption Spectra and Geometry of Organic Molecules*, New York, NY: Academic Press, **1967**.
14. Jaffe, H. H.; Orchin, M. *Theory and Application of Ultraviolet Spectroscopy*, New York, NY: Academic Press. **1962**.
15. Birnbaum, P. P.; Linford, J. H.; Style, D .W. G. *Trans. Far. Soc.* **1953**, 49, 735
16. Rau, H. In *Photochromism Molecules and Systems*, Durr, H.; Bouas L. H. Eds. Elsevier: Amsterdam, **1990**, p165.
17. Kumar, G. S.; Neckers, D. C. *Chem. Rev.* **1989**, 89, 1915.
18. Rau, H. *J. Photochem.* **1984**, 26, 221.
19. Bortolus, P.; Monti, S. *J. Phys. Chem.* **1979**, 83, 648.
20. Rau, H.; Luddecke, E.; *J. Am. Chem. Soc.* **1982**, 104, 1616.
21. Zimmermann, A.; Chow, L. Y.; Paik, U.I. *J. Am. Chem. Soc.* **1958**, 80, 3528.
22. (a) Gegiou, D.; Muszkat, K. A.; Fischer, E. *J. Am. Chem. Soc.* **1968**, 90, 3907.
(b) Malkin, S.; Fischer, E. *J. Phys. Chem.* **1962**, 66, 2482.
23. Dugave, C.; Demange, L. *Chem. Rev.* **2003**, 103, 2475.

24. (a) Delaire, J. A.; Natakani, K. *Chem. Rev.* **2000**, 100, 1817.
(b) Ichimura, K. *Chem. Rev.* **2000**, 100, 1847.
(c) Tamai, N.; Miyasaka, H. *Chem. Rev.* **2000**, 100, 1875.
25. (a) Singh H. N, *Handbook of Advanced Electronic and Photonic Materials and Devices: Nonlinear Optical Materials*, Volume 9; Academic Press: San Diego, California, **2001**.
(b) Sutherland R. L, *Handbook of Nonlinear Optics*; Marcel Dekker, Inc.: New York, Basel, Hong Kong, **1996**.
26. Prasad P. N., Williams D. J. *Introduction to Nonlinear Optical Effects in Molecules and Polymers*, Wiley, New York, **1991**.
27. Li, Y. B.; He, Y. N.; Tong, X. L.; Wang, X. G. *J. Am. Chem. Soc.* **2005**, 127, 2402.
28. Li, Y. B.; Deng, Y. H.; Tong, X. L.; Wang, X. G. *Langmuir* **2005**, 21, 6567.
29. Li, Y. B.; Deng, Y. H.; Tong, X. L.; Wang, X. G. *Macromolecules* **2006**, 39,1108.
30. Hubbard, Jr., F. P.; Santonicola, G.; Kaler, E. W.; Abott, N. L. *Langmuir* **2005**, 21, 6131.
31. Sakai, H.; Matsumura, A.; Yokoyama, S.; Saji, T.; Abe, M. *J. Phys. Chem. B* **1999**, 103, 10737.
32. Shin, J. y.; Abbott, N. L. *Langmuir* **1999**, 15, 4404.
33. Kang, H. C.; Lee, B. M.; Yoon, M. *J. Colloid. Interface Sci.* **2000**, 231, 255.
34. Orihara, Y.; Matsumura, A.; Saito, Y.; Ogawa, N.; Saji, T.; Yamaguchi, A.; Sakai, H.; Abe, K. *Langmuir* **2001**, 17, 6072.
35. Buwalda, R. T.; Stuart, M. C. A.; Engberts, J. B. F. N. *Langmuir* **2002**, 18, 6507.
36. Zou, B.; Qiu, D.; Hou, X.; Wu, L.; Zhang, X.; Chi, L.; Fuchs, H. *Langmuir* **2002**, 18, 8006.
37. Eastoe, J.; Dominguez, M. S.; Cumber, H.; Burnett, G.; Wyatt, P.; Heenan, R. K. *Langmuir* **2003**, 19, 6579.
38. Shang, T.; Smith, K. A.; Hatton. T. A. *Langmuir* **2003**, 19, 10764.

39. Eastoe, J.; Dominguez, M. S.; Cumber, H.; Burnett, G.; Wyatt, P.; Heenan, R.K. *Langmuir* **2004**, 20, 1120.
40. Lee, C. T.; Smith, K. A.; Hatton, T. A. *Macromolecules* **2004**, 37, 5397.
41. Bonini, M.; Berti, D.; Di, Meglio, J. M.; Almgren, M.; Teixeira, J.; Baglioni, P. *Soft. Matter*. **2005**, 1, 444.
42. Faure, D.; Gravier, J.; Labrot, T.; Desbat, B.; Oda, R.; Bassani, D. M. *Chem. Commun.* **2005**, 9, 1167.
43. Lee, C. T.; Smith, K. A.; Hatton, T. A. *Biochemistry* **2005**, 44, 524.
44. Sakai, H.; Orihara, Y.; Kodashima, H.; Matsumara, A.; Ohkubo, T.; Tsuchiya, K.; Abe, M. *J. Am. Chem. Soc.* **2005**, 127, 13454.
45. Bradley, M.; Vincent, B.; Warren, N. *Langmuir* **2006**, 22, 101.
46. Eastoe, J.; Vesperinas, A.; Donnewirth, A. C.; Wyatt, P.; Grillo, I.; Heenan, R. K.; Davis, S. *Langmuir* **2006**, 22, 851.
47. Shang, T.; Smith, K. A.; Hatton, T. A. *Langmuir* **2006**, 22, 1436.
48. Hubbard, Jr., F. P.; Abbott, N. L. *Langmuir* **2007**, 23, 4819.
49. Yoshida, T.; Kanaoka, S.; Aoshima, S. *J. Polym. Sci. Part A: Polym. Chem.* **2005**, 43, 5337.
50. Mamiya, J.; Kanie, K.; Hiyama, T.; Ikeda, T.; Kato, T. *Chem. Commun.* **2002**, 1870.
51. Moriyama, M.; Mizoshita, N.; Yokota, T.; Kishimoto, K.; Kato, T. *Adv. Mater.* **2003**, 15, 1335.
52. Matsubara, K.; Watanabe, M.; Takeoka, Y. *Angew. Chem. Int. Ed.* **2007**, 46, 1688.
53. Kawaguchi, Y.; Harada, A. *Org. Lett.* **2000**, 2, 1353.
54. Kawaguchi, Y.; Harada, A. *J. Am. Chem. Soc.* **2000**, 122, 3797.
55. Ballardini, R.; Balzani, V.; Credi, A.; Gandlofi, M. T.; Venturi, M. *Acc. Chem. Res.* **2001**, 34, 445.
56. Murakami, H.; Kawabuchi, A.; Kotoo, K.; Kunitake, M.; Nakashima, N. *J. Am. Chem. Soc.* **1997**, 119, 7605.
57. Kurtz, S.K.; Perry, T.T. *Appl. Phys.* **1968**, 39, 3798.

58. Levine, B. F.; Bethea, C. G. *Appl. Phys. Lett.* **1974**, 24, 445.
59. Clays, K.; Persoons, A. *Phys. Rev. Lett.* **1991**, 66, 2980.
60. Maker, P. W.; Terhune, R.W.; Nisenoff, M.; Savage, C. M. *Phys. Rev. Lett.* **1962**, 21.
61. Davydov, B. L.; Derkacheva, L. D.; Dunina, V. V.; Zhabotinskei, M. E.; Zolin, V. K.; Kreneva, L. G.; Samokhina, M. A. *JEPT. Lett.* **1970**, 12, 16.
62. Franken, P. A.; Hill, A. E.; Peters, C. W.; Weinrich, G. *Phys. Rev. Lett.* **1961**, 7, 118.
63. Rentzepis, P. M.; Pao, Y. H. *Appl. Phys. Lett.* **1964**, 5, 156, 58.
64. Marder, S. R. *Science* **1994**, 263, 511.
65. Lu, D.; Marten, B.; Cao, Y.; Ringnalda, M. N.; Friesner, R. A.; Goddard III, W. A. *Chem. Phys. Lett.* **1995**, 242, 543.
66. Meredith, G.; Vandusen, J.; Williams, D. *Macromolecules* **1982**, 15, 1385.
67. Hampsch, H. L.; Yang, J.; Wong, G. K.; Torkelson, J. M. *Macromolecules*, **1988**, 21, 526.
68. Singer, K. D.; Sohn, J. E.; Lalama, S. J. *Appl. Phys. Lett.* **1986**, 49, 248.
69. Wang, C. H.; Guan, H.W. *J. Polym. Sci. Part B: Polym. Phys.* **1993**, 31, 1983.
70. Hagen, R.; Zobel, O.; Sah,r O.; Biber, M.; Eckel, M.; Strohriegl, P.; Eisenbach, C.D.; Haarer, D. *J. Appl. Phys.* **1996**, 80, 3162.
71. Delaire, J. A.; Natakani, K. *Chem. Rev.* **2000**, 100, 1817.
72. Yesodha, S. K.; Pillai, C. K. S.; Tsutsumi, N. *Prog. Polym. Sci.* **2004**, 29, 45.
73. Natansohn, A.; Rochon, P. *Chem. Rev.* **2002**, 102, 4139.
74. Zhang, W.; Xie, J.; Shi, W.; Deng, X.; Cao, Z.; Shen, Q. *Eur. Polym. J.* **2008**, 44, 872.
75. Yu, X.; Luo, Y.; Deng, Y.; Yan, Q.; Zou, G.; Zhang, Q. *Eur. Polym. J.* **2008**, 44, 881.
76. Li, Z.; Zeng, Q.; Yu, G.; Li, Z.; Ye, C.; Liu, Y.; Qin, J. *Macromol. Rapid Commun.* **2008**, 29, 136.
77. Chen, X.; Zhang, J.; Zhang, H.; Jiang, Z.; Shi, G.; Li, Y.; Song, Y. *Dyes and*

- Pigments*, **2008**, 77, 223.
78. Tsutsumi, N.; Matsumoto, O.; Sakai, W. *Macromolecules* **1997**, 30, 4584.
79. Tsutsumi, N.; Matsumoto, O.; Sakai, W.; Kiyotsukuri, T. *Macromolecules* **1996**, 29, 592.
80. Yokoyama, S.; Nakahama, T.; Otomo, A.; Mashiko, S. *J. Am. Chem. Soc.* **2000**, 122, 3174.
81. Ishow, E.; Bellaiche, C.; Bouteiller, L.; Natakani, K.; Delaire, J. A. *J. Am. Chem. Soc.* **2003**, 125, 15744.
82. Gopalan, P.; Katz, H. E.; McGee, D. J.; Erben, C.; Zielinski, T.; Bousquet, D.; Muller, D.; Grazul, J.; Olsson, Y. *J. Am. Chem. Soc.* **2004**, 126, 1741.
83. Caruso, U.; Casalboni, M.; Fort, A.; Fusco, M.; Panunzi, B.; Quatela, A.; Roviello, A.; Sarcinelli, F. *Opt. Mat.* **2005**, 27, 1800.
84. Casalboni, M.; Caruso, U.; Maria, D.; Fusco, M.; Panunzi, B.; Quatela, A.; Roviello, A.; Sarcinelli, F.; Sirigu, A. *J. Polym. Sci. Part A : Polym. Chem.* **2004**, 42, 3013.
85. Li, Zhen.; Qin, A.; Lam, W. Y.; Dong, Y.; Dong, Y.; Ye, C.; Williams, I. D.; Tang, B. Z. *Macromolecules* **2006**, 39, 1436.
86. Carella, A.; Casalboni, M.; Centore, R.; Fusco, S.; Noce, C.; Quatela, A.; Peluso, A.; Sirigu, A. *Opt. Mat.* **2007**, doi: 10.1016.
87. Carella, A.; Centore, R.; Mager, L.; Barsella, A.; Fort, A. *J. Orgel.* **2007**, 8, 57
88. Lakowicz, J. R. *Principles of Fluorescence Spectroscopy*, Plenum, New York, 2nd edn., **1999**.
89. Rau, H. *Angew. Chem., Int. Ed. Engl.* **1973**, 12, 224.
90. Rau, H. *Ber. Bunsen-Ges. Phys. Chem.* **1967**, 71, 48.
91. Rau, H. *Ber. Bunsen-Ges. Phys. Chem.* **1968**, 72, 637.
92. Rau, H. *Ber. Bunsen-Ges. Phys. Chem.* **1971**, 75, 1343.
93. Bisle, H.; Romer, M.; Rau, H. *Ber. Bunsen-Ges. Phys. Chem.* **1976**, 80, 301.
94. Nepra, M.; Lunak, Jr, S.; Hrdina, R.; Fabian, J.; *Chem. Phys. Lett.* **1989**, 159,

- 366.
95. Struve, W. S. *Chem. Phys. Lett.* **1977**, 46, 15
96. Morgante, C. G.; Struve, W. S. *Chem. Phys. Lett.* **1979**, 68, 267.
97. Shimomura, M.; Kunitake, T. *J. Am. Chem. Soc.* **1987**, 109, 5175.
98. Constantino, C. J. L.; Aroca, R. F.; Mendonca, C. R.; Mello, S. V.; Balogh, D. T.; Oliveira, O. N. *Spectrochim. Acta. Part: A.* **2001**, 57, 281.
99. Tsuda, K.; Dol, G. C.; Gensch, T.; Hofkens, J.; Latterini, L.; Weener, J. W.; Meijer, E. W.; De Schryver, F. C. *J. Am. Chem. Soc.* **2000**, 122, 3445.
100. Nithyanandhan, J.; Jayaraman, N.; Davis, R.; Das, S. *Chem. Eur. J.* **2004**, 10, 689.
101. Anilkumar, P.; Jayakannan, M. *J. Phys. Chem. C.* **2007**, 111, 3591.
102. Ghedini, M.; Pucci, D.; Calogero, G.; Barigelletti, F. *Chem. Phys. Lett.* **1997**, 267, 341.
103. Yoshino, J.; Kano, N.; Kawashima, T. *Chem. Comm.* **2007**, 6, 559.
104. Han, M. R.; Hirayama, Y.; Hara, M. *Chem. Mater.* **2006**, 18, 2784.
105. Han, M. R.; Hara, M. *J. Am. Chem. Soc.* **2005**, 127, 10951.
106. Zacharias, P. S.; Ameerunisha, S.; Korupoju, S. R. *J. Chem. Soc. Perkin Trans.* **1998**, 2, 2055.
107. Harbron, E. J.; Vicente, D. A.; Hoyt, M. T. *J. Phys. Chem. B.* **2004**, 108, 18789.
108. Grimes, A. F.; Call, S. E.; Vicente, D. A.; English, D. S.; Harbron, E. J. *J. Phys. Chem. B.* **2006**, 110, 19183.
109. Izumi, A.; Teraguchi, M.; Nomura, R.; Masuda, T. *Macromolecules* **2000**, 33, 5347.
110. Li, X.; Lu, X.; Lu, Q.; Yan, D. *Macromolecules* **2007**, 40, 3306.
111. Folcia, C. L.; Alonso, I.; Ortega, J.; Etxebarria, J.; Pintre, I.; Ros, M. B. *Chem. Mater.* **2006**, 18, 4617.
112. Labarthe, F. L.; Freiberg, S.; Pellerin, C.; Pezolet, M.; Natansohn, A.; Rochon, P. *Macromolecules* **2000**, 33, 6815.
113. Wu, Yiliang.; Natansohn, A.; Rochon, P. *Macromolecules* **2004**, 37, 6801.

114. Kurihara, S.; Nomiya, S.; Nonaka, T. *Chem. Mater.* **2000**, 12, 9.
115. Prasad, V.; Kang, S. W.; Suresh, K. A.; Joshi, L.; Wang, Qingbing.; Kumar, S. *J. Am. Chem. Soc.* **2005**, 127, 17224.
116. Urbas, A.; Tondiglia, V, Natarajan, L.; Sutherland, R.; Yu, Haiping.; Li, J. H.; Bunning, T. *J. Am. Chem. Soc.* **2004**, 126, 13580.
117. Lee, H. K.; Doi, K.; Harada, H.; Tsutsumi, O.; Kanazawa, A.; Shiono, T.; Ikeda, Tomiki. *J. Phys. Chem. B.* **2000**, 104, 7023.
118. Sung, J. H.; Hirano, S.; Tsutsumi, O.; Kanazawa, A.; Shiono, T.; Ikeda, T. *Chem. Mater.* **2002**, 14, 385.

Chapter 2

***Synthesis, Characterization and Hyperpolarizability
Measurements of Main Chain Azobenzene Monomers and their
Polymers***

2.1 Abstract

A series of NLO active AB type azobenzene based monomers and their polymers were synthesized. Keeping the donor (-OH) and acceptor (-COOH) groups constant, the conjugation length was varied using extended and fused ring systems besides varying the substituents attached to the phenolic ring. The effect of various substituents and change in conjugation length on the NLO property was studied. Hyper Rayleigh scattering technique was used to measure the first hyperpolarizability tensor β and the value varied from 15×10^{-30} esu to 42×10^{-30} esu for the simplest phenolic derivative to the highly conjugated naphthol derivative respectively. The β -value was in the following order of phenolic derivative: α -naphthol > phenyl phenol > 2, 6-dimethyl phenol > o-cresol > cardanol > phenol > β -naphthol. Even though the conjugation length of α -naphthol and β -naphthol was the same, there was an unusually low value for the first hyperpolarizability tensor for the latter azo derivative. This could be attributed to the presence of hydrogen bonding between the o-hydroxyl group and the β nitrogen of the azo bridge in the latter which is absent in the former azobenzene derivative. The extent of conjugation was higher in phenyl phenol derivative also, but the first hyperpolarizability tensor β was not so high as expected. This was accounted on the basis of the torsional twisting of the one of the phenyl rings of the phenyl phenol unit. All these NLO active monomers were polymerized to obtain main chain polymers with head to tail structure. Although the main chain polymers possessed high thermal stability, their insolubility in common organic solvents made it impossible to carry out structural characterization and further studies.

2.2 Introduction

Second order nonlinear optical materials are at the heart of telecommunication devices such as electro-optic modulators and optical switches and in lasers such as high power green and blue solid-state lasers and optical parametric amplifiers. Conventional NLO materials generally consist of inorganic crystals such as KTP, LiTaO₃ and LiNbO₃.¹ While they are quite

efficient, high quality crystals of sufficient size are expensive and difficult to manufacture. Organic NLO materials provide an alternative with the potential to provide high nonlinear susceptibilities in an economical fabrication process.² Organic molecules and polymers containing covalently attached chromophores are currently investigated for applications in second order nonlinear optics.³ In contrast with the traditional NLO materials, organic systems have many attractive properties including fast response times, lower dielectric constants, improved processability, facile three dimensional design capabilities and greatly enhanced NLO responses.⁴

There are several methods to measure the second harmonic generation coefficient, that is the first hyperpolarizability tensor β . They are Kurtz-Perry powder technique, electric field induced second harmonic generation method (EFISHG), Hyper Rayleigh scattering method and the Maker fringe technique. One of the main tools for NLO measurements has been the determination of β values by Hyper Rayleigh scattering (HRS).⁵ Hyper Rayleigh scattering is the scattering of light at frequency 2ω when a liquid sample is irradiated by light at frequency ω .

Typical NLO chromophores studied previously for application in optoelectronics and photonics are elongated conjugated systems with strong donor and acceptor groups as terminal substituents and a great deal of effort has been devoted to the synthesis of such organic molecules in the search of new materials exhibiting second order NLO property. This approach however dictates that noncentrosymmetric organization of dipolar NLO-phores is achieved at the molecular level. Dipolar push-pull molecules constitute the widest class of compounds investigated for their NLO properties and it is well known that the first molecular hyperpolarizability (β) depends not only on the strength of the donor and acceptor groups, but also on the nature of the π -conjugated spacer through which they interact. Use of the aromatic rings bonded by azo bridges to connect the donor and electron withdrawing group is usually adopted to obtain

chemically and thermally stable NLO-phores with good efficiency. Among the many molecular designs that are used for introducing NLO behavior, those involving the azo containing systems have a special significance. They exhibit photoswitching properties, which make it suitable for various kind of applications. Azobenzene can function as molecular switches by going from the cis to the trans state upon application of light of varying wavelength.^{6,7} The rigidity and planarity of the azo benzene group also can result in liquid crystalline property for the resulting material.^{8,9} There are a number of references for azo containing side chain as well as main chain polymers in the literature.¹⁰⁻¹⁴ For main chain polymers, the chromophores can be linked in a head to tail (isoregic), head to head (syndioregic) or random distribution of head to tail and head to head configuration (aregic). NLO polyesters having azobenzene mesogens in the main chain based on derivatives of phenyl azo benzoic acid have exhibited high stability of NLO response.¹⁵ Organic chromophores with large and stable NLO response are very important for the development of devices. Sandhya et al. and Saminathan et al. have reported the synthesis of azo containing AB type monomers prepared by the diazo coupling reaction between p-amino benzoic acid and alkyl substituted phenols.¹⁵⁻²⁰ These azobenzene chromophores were incorporated as side chain as well as main chain units in polymers and their liquid crystalline properties were studied. Yokoyama et al. reported nonlinear optical azobenzene dendrons which were modified by introducing varying numbers of azobenzene branching units as nonlinear optical chromophore and by placing aliphatic chains at the end of the dendritic chains.²¹ They observed that the first order molecular hyperpolarizability of the azobenzene dendrons having 15 chromophoric units was 3010×10^{-30} esu whereas for the azobenzene monomer, the value was 150×10^{-30} esu. Ishow et al. reported second order NLO active push-pull compounds comprising of a bulky electron donating triaryl amino group and linked to various electron withdrawing groups such as nitro, cyano, dicyano vinylene etc.²² These were the first examples of compounds forming amorphous materials with spontaneous NLO activity

without requiring any external poling process. The highest β value was obtained for the strongest electron withdrawing group dicyanovinylene. They also observed that the introduction of dicyanovinylene group substantially raised the NLO activity and glass transition temperature without generating lower thermal stability. There are also reports of NLO materials based on conjugated polymers like polyanilines, poly pyrroles and poly (3-alkyl) thiophenes (PATs). Among these materials, PATs have been widely used because of their good combined properties of stability, processability and functionalizability.²³ Efforts to increase β have mostly concentrated on varying the donor or acceptor strength, with less attention being paid to the molecular structure of the bridge connecting the two. Theoretical work by Rissler and coworkers based on the 4-level-model have shown that β can be enhanced with an asymmetric bridge, where the asymmetry could arise from relatively simple substitution of atoms or appended side chains without affecting the aromaticity of the bridge.^{24,25} Asha et al. reported that the addition of just one methylene unit to a central methylene spacer connecting two NLO chromophores in twin NLO systems has the ability to enhance the NLO property.²⁶ These NLO twins which can be considered as ideal models for main chain NLO polymers proved that non-conjugated spacer segments also play a dominant role in governing the NLO property of the final material.

The present study describes the synthesis of second order NLO active azobenzene monomers with the traditional design strategy, electron donor and acceptor separated by a π -conjugated system. The donor selected was hydroxyl group and acceptor was carboxylic acid functionality which was kept constant and the effective conjugation length was varied by varying the number and position of substituents as well as the number of aromatic rings with the aim to see if there is a clear structure/property relation, concerning their NLO outputs. All these monomers were polymerized to obtain the corresponding main chain polymers. Detailed studies on the synthesis and characterization of a series of azobenzene monomers and their polymers and the role of substituents and

change in π -conjugation in determining the optical and electronic properties are described.

2.3 Experimental Section

4-Amino benzoic acid and 4-phenyl phenol were purchased from Aldrich Chemicals and were used as such. Sodium nitrite, potassium hydroxide, phenol, o-cresol, 2,6-dimethyl phenol, α -naphthol and β -naphthol were purchased from S.D Fine Chemicals Ltd. Cardanol was obtained from the distillation of cashew nut shell liquid (CNSL obtained from Cashew Export Promotion Council, Cochin), 228-235 °C at 3.5mm of Hg.

^1H and ^{13}C -NMR spectra of monomers and polymers were recorded using 300-MHz Bruker NMR spectrophotometer in a mixture of trifluoroacetic acid and deuterated chloroform containing small amount of TMS as internal standard. For ^{13}C NMR experiments, the carbon atom in CDCl_3 was taken as 77 ppm and all other peaks were assigned with respect to it. The purity of the compounds was determined by JEOL JSM600 fast atom bombardment (FAB) high-resolution mass spectrometry. Infrared spectra of the monomers and the polymers were recorded using an Impact 400 D Nicolet FT-IR spectrophotometer. UV – Vis spectra were recorded using Perkin Elmer Lambda 35 UV-Vis Spectrometer. Thermogravimetric analysis (TGA) was performed using a TGA-50 Shimadzu Thermogravimetric Analyzer. Samples were run from 30 to 600 °C in the case of monomers and upto 800 °C in the case of polymers with a heating rate of 10 °C/min under nitrogen atmosphere. The thermal and phase behavior of the polymers were analyzed using a hot stage polarized light microscope (Leitz-1350 heating stage coupled with PLM) as well as a DSC-Perkin Elmer Pyris 6 Differential Scanning Calorimeter (DSC) at a heating rate of 10°C/min under nitrogen atmosphere. Elemental analysis was performed using Perkin Elmer Series II CHNS/O Analyzer 2400.

Quadratic hyperpolarizability β values were measured in methanol by the Hyper Rayleigh scattering (HRS) technique. The fundamental of a Q-switched Nd:YAG laser (Spectra Physics, 8 ns) was focused onto a glass cell containing

the solute in solution. The second harmonic scattered light was collected by an efficient condenser system at the photocathode of a photomultiplier tube. Other harmonics were eliminated first by low-pass optical filters and finally by a 4nm band width interference filter. A small fraction of the 1064 nm fundamental light was directed towards IR sensitive photomultiplier tube (PMT) for monitoring the incident light intensity. Signals from both PMTs were fed into a gated Boxcar averager (SRS 250) to record the intensities of the incident and second order scattered light pulses after averaging over 1000 shots. All data were collected at laser powers (≤ 12 mJ/pulse) well below the threshold for stimulated Raman and Brillouin scattering, self focusing or self-defocusing and dielectric breakdown.

2.4 Synthesis of Monomers

Synthesis of 4-[(4-hydroxyphenyl)azo]benzoic acid (S1): 4-aminobenzoic acid (6.85 g, 50 mmol) was dissolved in 10 % HCl (100 mL) and diazotized with aqueous sodium nitrite (3.45 g, 50 mmol) at 0 °C with stirring. The solution was further diluted with 200 mL of ice cold water. Phenol was dissolved in 5.4 g KOH (96 mmol) in 10 mL water and then added drop wise to the diazonium salt solution with stirring. The red dye formed was stirred for 3h and then neutralized with dilute HCl solution with stirring. The dye separated was filtered, washed thoroughly with water and dried in the vacuum oven for 12h. The dye was then purified by column chromatography on silica gel (60-120 mesh) using ethyl acetate-hexane mixture (80/20 v/v). Yield: 9.1 g (75 %) m.p: 274 °C. ^1H NMR (CDCl_3) δ ppm: 8.41 (2H, d, Ar), 8.32 (2H, d, Ar), 8.11 (2H, d, Ar), 7.32 (2H, d, Ar). ^{13}C NMR (CDCl_3) δ ppm: 120.39, 120.56, 120.84, 131.39, 132.43, 132.56, 134.28, 134.74, 140.22, 144.82, 170.85, 173.25. FTIR (KBr) (cm^{-1}): 3240, 1692, 1599, 1495, 1446, 1429, 1405, 1385, 1283, 1254, 1185, 1141, 1106, 1023, 944, 866, 839, 820, 776, 724, 697, 549.

The same procedure was adopted for the synthesis of **S2**, **S3**, **S4**, **S5**, **S6** and **S7** using 4-aminobenzoic acid and cardanol, o-cresol, 2,6-dimethyl phenol, phenyl phenol, α -naphthol and β -naphthol respectively. **S2** was prepared using 5 g (36 mmol) of 4-aminobenzoic acid and 11.1 g (36 mmol) of saturated cardanol and

S3 by using 5 g (36 mmol) of 4-aminobenzoic acid) and 3.9 g (36 mmol). In the case of the **S4**, 5 g (36 mmol) of 4-aminobenzoic acid and 4.4 g (36 mmol) of 2,6-dimethyl phenol was used whereas for the synthesis of **S5**, 5 g (36 mmol) of 4-aminobenzoic acid and 6.1 g (36 mmol) was used. **S6** and **S7** were prepared by coupling 5 g (36 mmol) of 4-aminobenzoic acid) with 5.2 g of α -naphthol and β -naphthol respectively.

4-[(4-hydroxy-2-pentadecylphenyl)azo]benzoic acid (S2) :Yield: 13.2 g (80 %). m.p: 151 °C. ^1H NMR (CDCl_3) δ ppm: 8.38 (2H, d, Ar), 8.20 (H, d, Ar) , 8.01 (2H, d, Ar) , 7.26 (2H, m, Ar), 3.20-0.88 (31H, m, $-\text{CH}_2-$). ^{13}C NMR (CDCl_3) δ ppm: 13.83, 22.72, 29.44, 29.75, 32.002, 32.71, 119.21, 120.03, 124.42, 130.96, 132.78, 138.19, 144.59, 170.54, 175.23. FTIR (KBr) (cm^{-1}): 3241, 1692, 1599, 1520, 1482, 1457, 1429, 1278, 1169, 1114, 1015, 963, 861, 831, 758, 689, 562.

4-[(4-hydroxy-3-methylphenyl)azo]benzoic acid (S3): Yield: 7.34 g (79 %), m.p: 245 °C. ^1H NMR (CDCl_3) δ ppm: 8.33 (2H, d, Ar), 8.26 – 8.14 (3H, m, Ar), 7.24 (2H, m, Ar), 2.37 (3H, d, CH_3). ^{13}C NMR (CDCl_3) δ ppm: 15.18, 120.34, 120.54, 131.38, 132.43, 132.78, 140.18, 144.27, 171.22, 173.88. FTIR (KBr) (cm^{-1}): 3070, 1685, 1597, 1580, 1509, 1465, 1390, 1432, 1320, 1277, 1248, 1190, 1141, 1094, 1037, 1018, 861, 812, 757, 694, 578.

4-[(4-hydroxy-3,5-dimethylphenyl)azo]benzoic acid (S4): Yield: 6.5 g (66 %), m.p: 202 °C. ^1H NMR (CDCl_3) δ ppm: 8.39 (2H, d, Ar), 8.22 (4H, m, Ar) , 2.30 (6H, s, CH_3). ^{13}C NMR (CDCl_3) δ ppm: 15.25, 120.28, 120.67, 130.44, 131.49, 132.82, 140.19, 144.31, 171.32, 171.69. FTIR (KBr) (cm^{-1}): 3341 , 1689, 1599, 1501, 1451, 1404, 1270, 1254, 1141, 1023, 861, 834, 773, 694, 543 .

4-[(4-hydroxybiphenyl-4yl)azo]benzoic acid (S5): Yield: 4.3 g (37 %), m.p: 305 °C. ^1H NMR (CDCl_3) δ ppm: 8.32 (2H, d, Ar), 8.20 (H, s, Ar), 8.05 (2H, d, Ar), 7.93 (H, d, Ar), 7.65 (2H, d, Ar), 7.54 (3H, m, Ar), 7.26 (H, m, Ar). ^{13}C NMR (CDCl_3) δ ppm: 107.96, 121.86, 126.35, 128.74, 130.84, 132.51, 177.12. FTIR (KBr) (cm^{-1}): 3061, 1684, 1599, 1577, 1509, 1465, 1435, 1391, 1322, 1248, 1276, 1193, 1135, 1094, 1039, 1018, 905, 858, 809, 760, 694.

4-[(4-hydroxynaphthen-1-yl)azo]benzoic acid (S6) : Yield: 2.9 g (28 %), m.p: 283 °C. ¹H NMR (CDCl₃) δ ppm: 8.82 (H, d, Ar), 8.64 (H, d, Ar), 8.49 (H, d, Ar), 8.36 (3H, t, Ar), 8.02 (3H, m, Ar), 7.84 (H, t, Ar). ¹³C NMR (CDCl₃) δ ppm: 120.34, 122.34, 127.77, 128.31, 132.91, 133.50, 146.26, 149.05, 171.52. FTIR (KBr) (cm⁻¹): 3244, 1683, 1599, 1498, 1451, 1404, 1273, 1254, 1163, 1138, 1106, 1026, 861, 837, 774, 694, 540.

4-[(2-hydroxynaphthen-1-yl)azo]benzoic acid (S7): Yield: 4.4 g (41 %) m.p: 311 °C ¹H NMR (CDCl₃) δ ppm: 8.55 (H, d, Ar), 8.30 (2H, d, Ar), 8.07 (H, d, Ar), 7.89 (2H, d, Ar), 7.73 (2H, m, Ar), 7.69 (H, t, Ar), 7.08 (H, d, Ar). ¹³C NMR (CDCl₃) δ ppm: 120.35, 122.34, 122.63, 127.77, 128.31, 129.05, 130.28, 131.1, 131.97, 132.91, 133.51, 146.26, 149.05, 172.53. FTIR (KBr) (cm⁻¹): 3034, 1689, 1681, 1602, 1577, 1459, 1388, 1316, 1275, 1245, 1092, 1018, 765, 690, 541.

2.5 Synthesis of Polymers

Synthesis of Poly4-[(4- hydroxyphenyl)azo]benzoic acid (MCP1)

0.5 mL (6.8 mmol) thionyl chloride was taken in a 3 necked 50 mL round bottomed flask and cooled in an ice bath. 1mL pyridine (12 mmol) was added drop wise with stirring to the ice cold solution under continuous nitrogen purge. 0.40 g (1.6 mmol) of dye **S1** was dissolved in 4 mL pyridine (49 mmol) and added drop wise to the ice cold solution. The temperature was then slowly increased to 80 °C and stirred for 8 hours. The polymer was precipitated into methanol, washed with acetone and dried in vacuum at 60 °C for 24 h. Yield: 0.3 g (88%). ¹H NMR (CDCl₃) δ ppm: 8.67-7.44 (m, Ar). FTIR (KBr) (cm⁻¹): 1737, 1597, 1560, 1494, 1407, 1262, 1197, 1140, 1065, 758, 672, 615 .

The same procedure was adopted for the polymerization of **S2**, **S3**, **S4**, **S5**, **S6** and **S7** using the respective azobenzene monomers.

Poly[4-(4-hydroxy-2-pentadecylphenyl)azo]benzoic acid (MCP2): Yield: 0.3 g (88 %) ¹H NMR (CDCl₃) δ ppm: 8.36-6.74 (m, Ar), 3.16-0.86 (aliphatic) FTIR (KBr) (cm⁻¹): 2924, 2851, 1727, 1602, 1620, 1553, 1537, 1513, 1501, 1483, 1468, 1215, 1106, 1055, 764, 676, 618.

Poly[4-(4-hydroxy-3-methylphenyl)azo]benzoic acid (MCP3): Yield: 0.3 g (78 %) ^1H NMR (CDCl_3) δ ppm: 8.52-6.99 (m, Ar), 2.42-2.21 (aliphatic). FTIR (KBr) (cm^{-1}): 2924, 1735, 1602, 1560, 1541, 1508, 1489, 1458, 1261, 1234, 1178, 1099, 1063, 1010, 862, 768, 497.

Poly[4-(4-hydroxy-3,5-dimethylphenyl)azo]benzoic acid (MCP4): Yield: 0.1 g (29 %) ^1H NMR (CDCl_3) δ ppm: 8.63-7.97 (m, Ar), 2.45-2.27 (aliphatic). FTIR (KBr) (cm^{-1}): 2925, 1737, 1605, 1599, 1468, 1262, 1175, 1114, 1068, 896, 769.

Poly[4-(4-hydroxybiphenyl-4-yl)azo]benzoic acid (MCP5): Yield: 0.3 g (82 %) ^1H NMR (CDCl_3) δ ppm: 8.41-7.53 (m, Ar). FTIR (KBr) (cm^{-1}): 1736, 1601, 1480, 1047, 1257, 1203, 1140, 1114, 1063, 858, 761, 686.

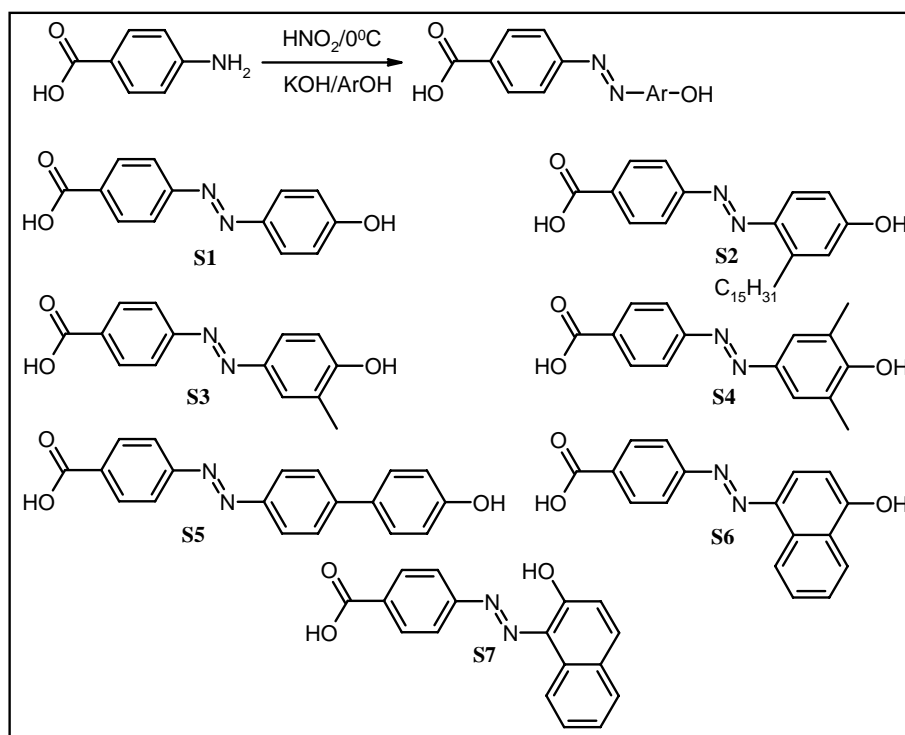
Poly[4-(4-hydroxynaphthalen-1-yl)azo]benzoic acid (MCP6): Yield: 0.3 g (75 %) ^1H NMR (CDCl_3) δ ppm: 8.78-7.84 (m, Ar). FTIR (KBr) (cm^{-1}): 1739, 1598, 1511, 1463, 1385, 1315, 1255, 1222, 1154, 1077, 1011, 859, 758, 685, 620

Poly[4-(2-hydroxynaphthalen-1-yl)azo]benzoic acid (MCP7): Yield: 0.1 g (27 %) ^1H NMR (CDCl_3) δ ppm: 8.53-6.89 (m, Ar). FTIR (KBr) (cm^{-1}): 1734, 1717, 1698, 1654, 1648, 1602, 1559, 1541, 1522, 1508, 1474, 1457, 1258, 1202, 1113, 1061, 1008, 854, 758, 686, 516

2.6 Results and Discussion

The monomers were synthesized by diazotization of 4-amino benzoic acid followed by coupling with various aromatic alcohols like phenol, penta decylphenol, o-cresol, 2, 6-dimethyl phenol, 4-phenyl phenol, α -naphthol and β -naphthol. The synthesis and structures of all the azobenzene monomers is shown in scheme 1. The yield, melting point and elemental analysis data are given in table 1. The azo dyes did not have very high solubility in chloroform and hence structural characterization using NMR spectroscopy was carried out in a mixture of trifluoroacetic acid and deuterated chloroform. The trifluoroacetic acid peak which appears downfield at around 11 ppm does not interfere with the aromatic peaks of the samples. ^1H NMR and high resolution mass spectral analysis were

in agreement with their structures. ^1H NMR spectra of monomers are shown in figure 1 and 2.

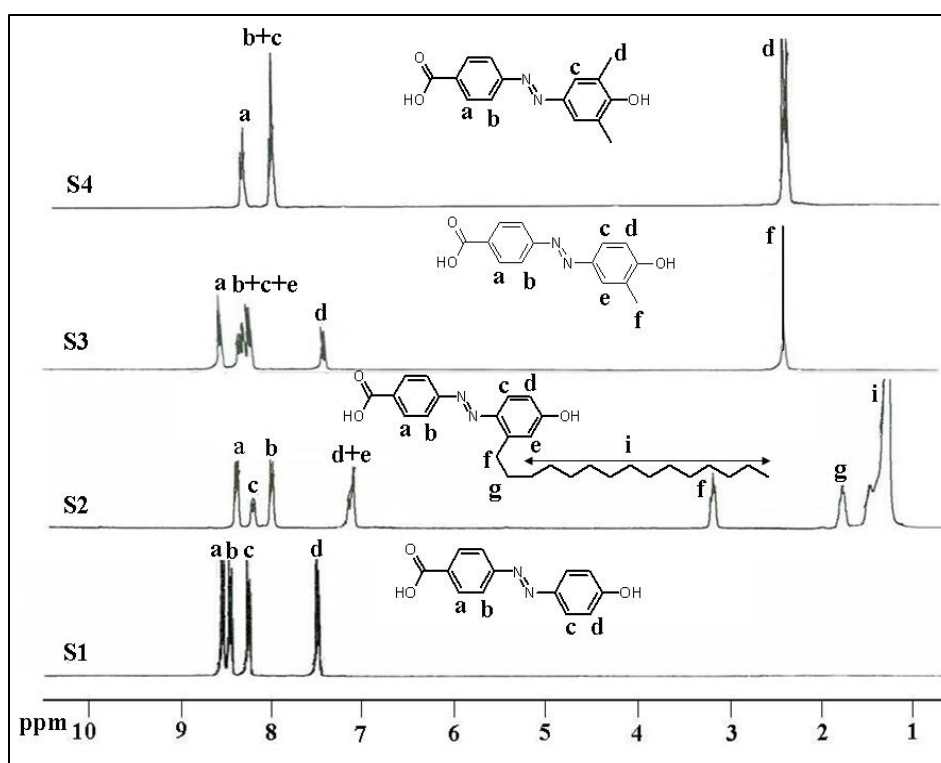


Scheme 1 Scheme of synthesis of monomers

The phenol based azo dye **S1**, had the simplest proton NMR spectra with a set of four doublets corresponding to the protons of the two aromatic rings. The two protons next to the carboxyl group, labeled a, were the most downfield with the doublet at 8.41 and 8.37 ppm respectively. On the other hand, the two protons next to the hydroxyl group, labeled c, were the most upfield with its doublet appearing at 7.32 and 7.29 ppm respectively. The four protons nearer to the azo linkage, labeled b, appeared as two sets of doublets at 8.32, 8.28 and 8.11, 8.08 ppm respectively. **S5**, **S6** and **S7** the phenyl phenol, α -naphthol and β -naphthol based azo dyes had peaks only in the aromatic region which corresponded very well with the number of protons. Saturated cardanol based azo dye **S2**, had peaks corresponding to the aliphatic protons at 0.88 to 3.20 ppm which matched in intensity with the seven aromatic protons.

Table 1 Yield and elemental analysis

Sample	Yield (%)	Meltin g point (°C)	Formula	Elemental Analysis	
				Calculated (%)	Found (%)
S1	75	274	C ₁₃ H ₁₀ N ₂ O ₃	C-64.46;H-4.13;N-11.57	C-65.12;H-4.3;N-10.95
S2	80	151	C ₂₈ H ₄₀ N ₂ O ₃	C-74.34;H-8.85;N-6.19	C-73.68;H-9.58;N-5.78
S3	79	245	C ₁₄ H ₁₂ N ₂ O ₃	C-65.62;H-4.68;N-10.93	C-65.62;H-4.3;N-10.95
S4	66	202	C ₁₅ H ₁₄ N ₂ O ₃	C-66.66;H-5.22;N-10.36	C-67.09;H-4.97;N-9.76
S5	37	305	C ₁₉ H ₁₄ N ₂ O ₃	C-71.69;H-4.43;N-8.83	C-8.80;H-4.04;N-8.78
S6	28	284	C ₁₇ H ₁₂ N ₂ O ₃	C-69.86;H-4.14;N-9.18	C-70.33;H-4.40;N-9.66
S7	41	311	C ₁₇ H ₁₂ N ₂ O ₃	C-69.86;H-4.14;N-9.18	C-72.22;H-5.48;N-7.96

Figure 1 ¹H NMR spectra of monomers **S1**, **S2**, **S3** and **S4**

Similarly **S3** and **S4** the cresol and 2,6-dimethyl phenol based azo dyes also had peaks corresponding to the CH₃ group in the aliphatic region, which matched

perfectly in intensity with the rest of the aromatic protons. In the ^{13}C NMR spectra, the resonances around 173-170 ppm represented the carbonyl carbon.

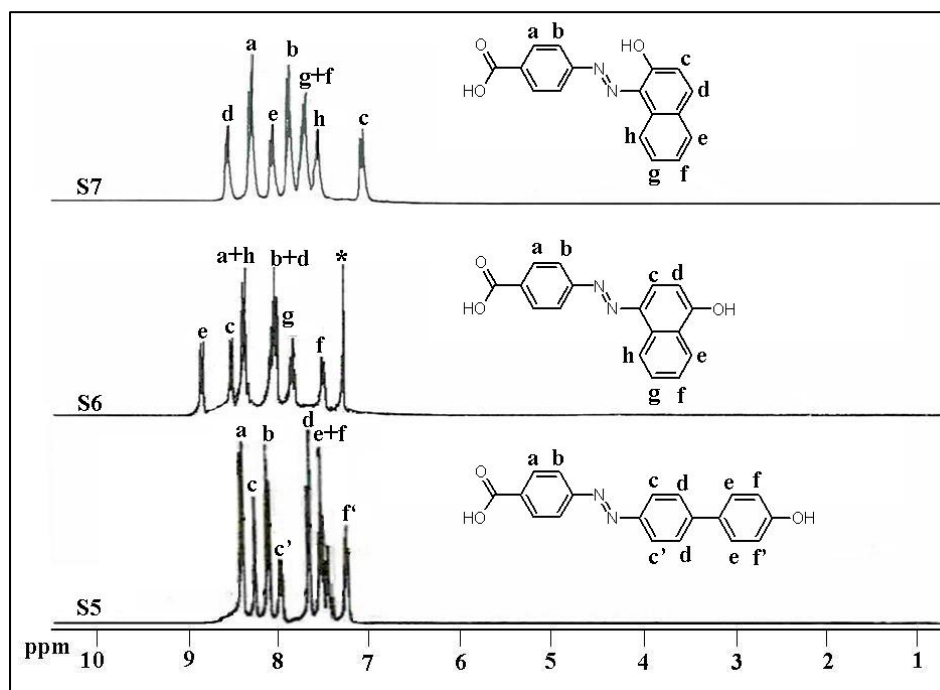


Figure 2 ^1H NMR spectra of monomers S5, S6 and S7

2.7 UV-Visible Spectra

Azobenzene monomers contain intramolecular charge-transfer chromophores and therefore, their UV-Vis absorption bands depend on the combination of electron-donating and withdrawing moieties in the molecules. Absorption spectra can give a good account of how the electronic properties can be modified by the effect of varying donor and acceptor strength or by varying the co planarity by means of substitution even though it is known that extending a system of conjugated double bonds need not bear a direct relation with the position of the absorption band. Coplanarity of the units play an important role in the electronic communication since it favors π overlap facilitating the conjugation to be more effective.

The absorption spectra of azobenzene derivatives in solution usually have two featureless absorption bands centered around 350 and 450 nm attributed to π - π^* and n - π^* transitions respectively. The n - π^* transition gives a weak band in the visible region and π - π^* transition gives an intense band in the

UV spectral region. The peak absorption values and the absorption coefficient for the monomers in methanol are reported in table 2 and their UV-Vis spectra in methanol are shown in figure 3. The simplest donor-acceptor substituted azo dye was **S1** and the band corresponding to the π - π^* transition appeared at 356 nm whereas the n - π^* band appears at 431 nm. The meta substituted dye **S2**, the ortho substituted one **S3** and the dimethyl substituted dye, **S4** had a slight redshift for both π - π^* and n - π^* transitions. **S5** which was based on phenyl phenol showed a blue shift in absorption maxima eventhough the conjugation length was more than in simple phenol dye.^{27, 28} The absorption maximum (λ_{\max}) for benzene molecule was 258 nm whereas for biphenyl it was 246 nm.

Table 2 UV-Vis data

Sample	First Absorption band		Second Absorption band	
	λ_{\max} (nm)	ϵ	λ_{\max} (nm)	ϵ
S1	356	19884	431	700
S2	367	21485	466	1674
S3	362	20437	466	1526
S4	363	34984	454	2900
S5	330	23978	406	8321
S6	278	13375	469	17128
S7	418	13212	484	19305

The torsional twisting of one of the phenyl ring of biphenyl unit lowers the coplanarity of the system which is responsible for the blue shifted absorption maxima. In the case of phenyl phenol the torsional angle is $\sim 54^\circ$. In fact, this

blue shift in UV absorption brought about by the presence of a biphenyl moiety in comparison with its polyenic analogue is seen as a means to solve the so-called nonlinearity-transparency tradeoff, which is a crucial factor as far as device applications are concerned.^{29, 30} **S6** and **S7** which were based on fused ring systems had increased conjugation length when compared with simple phenol based systems. This increased effective conjugation length was reflected in their redshifted absorption maxima. The band corresponding to the π - π^* transition appeared at 469 nm for **S6** and at 484 nm for **S7**. Comparing **S6** and **S7**, the latter showed a 15 nm red shift even though the extent of conjugation was the same in both the dyes. This redshift is a consequence of the hydrogen bonding between the phenolic oxygen and the β -hydrogen of the azo bridge.

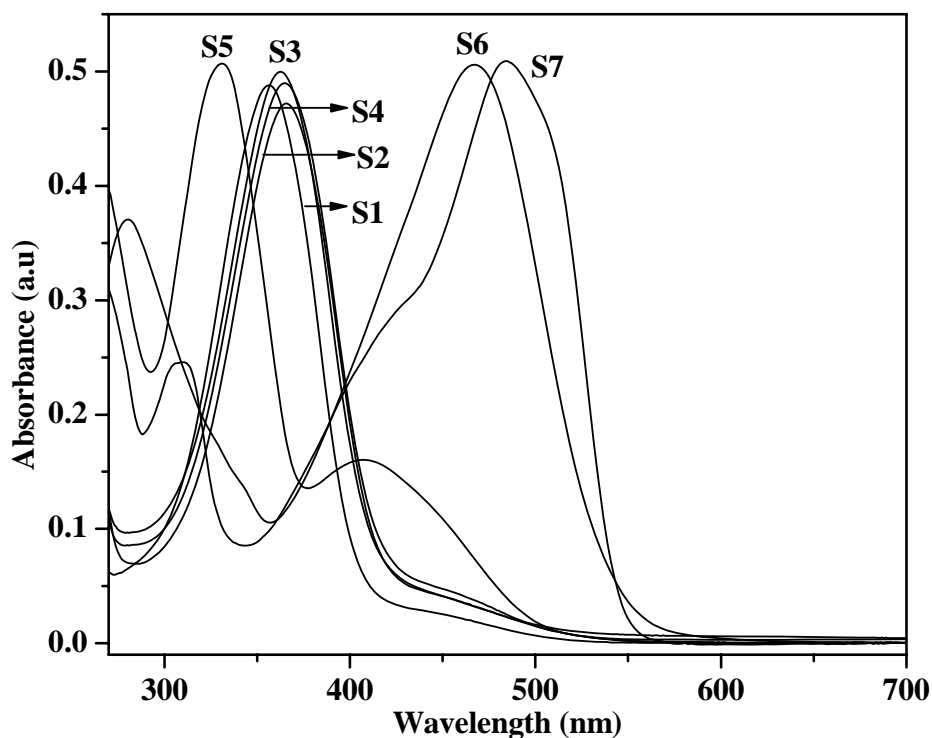
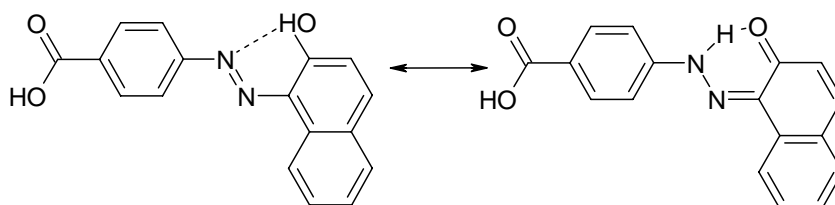


Figure 3 UV-Vis spectra of the chromophores in methanol

It is known that molecules of the type of **S7** can exist in tautomeric form, ie hydroxy azo form and hydrazone form. This is schematically represented in scheme 2 which shows the quinonoid structure of 4-[(2-hydroxynaphthen-1-yl)azo]benzoic acid. The presence of these forms is clearly indicated in the

absorption spectra. A weak band at ~ 420 nm in the absorption spectra corresponded to the hydroxy azo form whereas the one at 484 nm corresponded to the hydrazone form.³¹



Scheme 2 Tautomerism in S7

Solvatochromic effects can give an idea about the magnitude of the expected NLO properties, since they reflect the polarizabilities of a chromophore. High extent of solvatochromic response in solution is an indication of their high molecular polarizabilities. Generally, neutral azo dyes are known to show positive solvatochromism.³²⁻³⁶ Figure 3 shows the solvatochromic shift experienced by the monomers in solvents of varying polarity like dioxane, ethyl acetate, tetrahydrofuran (THF), dichloromethane (DCM), acetone, methanol, acetonitrile, dimethylformamide (DMF) and dimethyl sulfoxide (DMSO). The λ_{\max} values are the first (higher energy) absorption band for **S1** to **S5** and the high intense lower energy band beyond 450 nm for **S6** and **S7**. As can be seen from the figure, the azo dyes showed a positive solvatochromism, with **S6** showing the most prominent shift. Such a solvatochromic behavior is characteristic of the charge-transfer transitions with an increase of dipole moment upon excitation. Figure 4 shows the solvatochromic shift of **S6** in a few selective solvents. As can be seen from figures 4 & 5, **S6** has the maximum solvatochromic shift in methanol indicating higher polarizability in methanol. In the naphthol based dyes (**S6** and **S7**) the $n-\pi^*$ band is almost wholly overlain by the batho and hyper-chromically displaced $\pi-\pi^*$ band.³¹ The main transition at 469 or 484 nm in the **S6** and **S7** could be assigned to the $\pi-\pi^*$ band based on their bathochromic shift in solvents of increasing polarity. However, unlike the simple phenol based dyes, the naphthol based dyes have a tendency to exist in the hydroxyazo-quinonehydrazone

tautomeric forms as well as a tendency to associate. In figure 5, it can be seen that **S6** has an additional fine structure in solvents like DMSO and DMF. This may be due to the $-M$ effect of the hydroxyl group causing the acid even in concentrations of 1×10^{-6} M to exist mainly as aggregates, probably dimeric, in these solvents. Concentration as well as temperature dependent absorption studies were carried out for **S6** in the range of dye concentration 1×10^{-6} to 1×10^{-3} mol/L in methanol and no change in shape was found for the absorption band. These studies confirmed that no aggregation of dye took place in methanol.

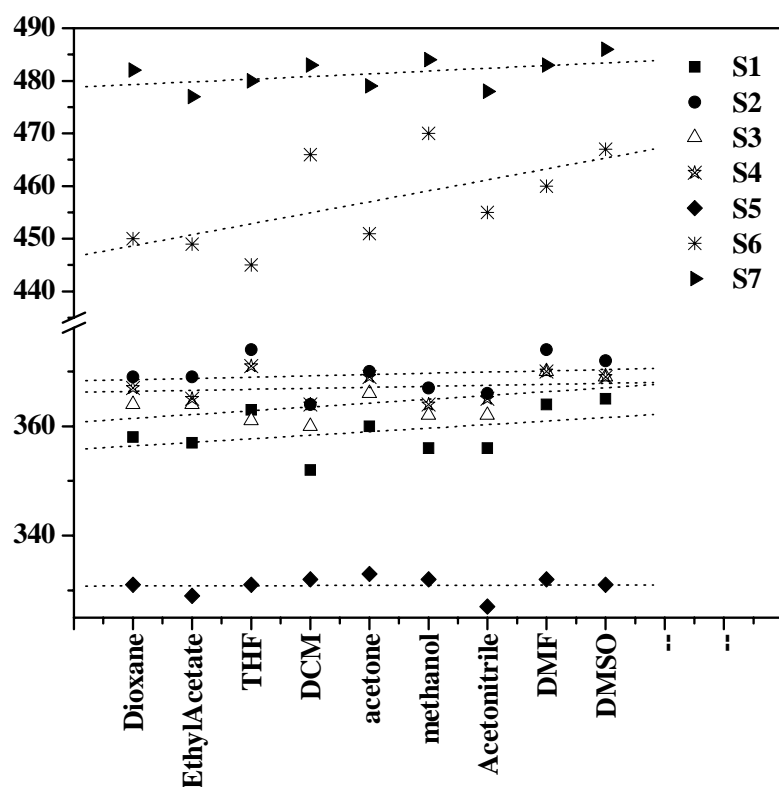


Figure 4 Solvatochromic shift shown by monomers in various solvents

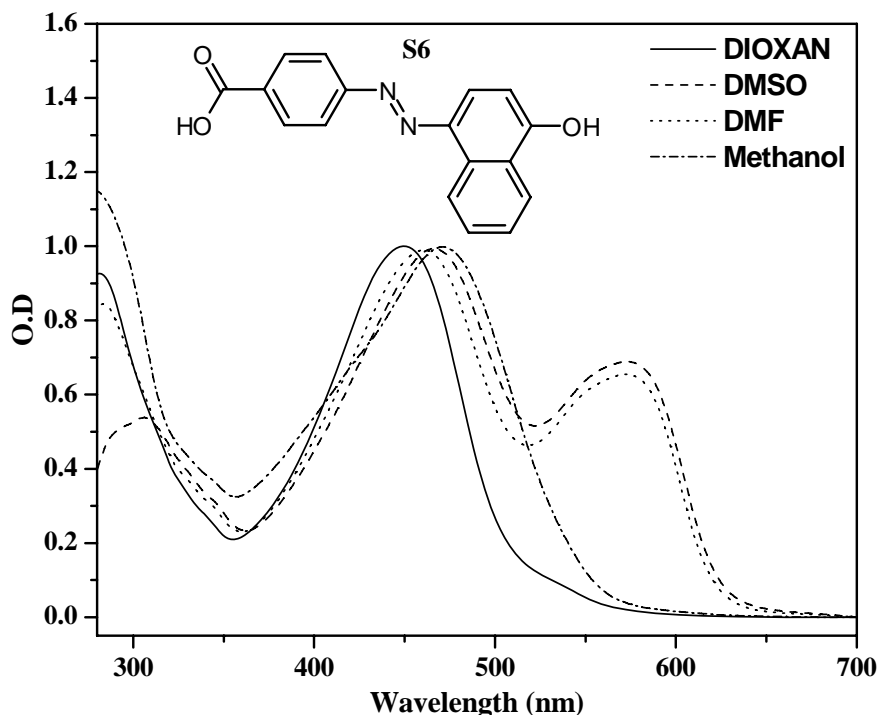


Figure 5 Absorption spectra of **S6** in various solvents

2.8 Nonlinear Optical Properties

The first order molecular hyperpolarizability (β) values of the monomers were measured by HRS technique in methanol using the fundamental excitation wavelength of 1064 nm. The known β value for p-NA in methanol (23×10^{-30} esu) was used as the external reference. The quadratic dependence of the HRS intensity on the incident intensity was checked for all the samples to make sure that the scattering intensity was indeed due to the second-order optical process. The plot of $I_{2\omega}/I_{\omega}^2$ vs. the number density showed a linear dependence of the HRS intensity on the chromophore number density indicating that the chromophore concentration was in the dilute solution limit. From the slope of the plot, the hyperpolarizability can be extracted after comparison with the external reference. Except for **S6** and **S7**, the azo chromophores did not have any appreciable absorption at 532 nm. The possibility of two-photon absorption-induced fluorescence (TPF) that may interfere with the HRS signal was ruled out for **S6** and **S7** by scanning through a range of wavelengths using TRIAX monochromator. A sharp response was obtained only at 532 nm and no signal at

all at any other wavelength. Fluorescence at 532 nm is known to artificially enhance the retrieved value for the first hyperpolarizability measured by HRS. All compounds were tested for fluorescence at this wavelength and no significant fluorescence was observed at this wavelength for any of the compounds. Table 3 gives a summary of the HRS data at 1064 nm for the chromophores measured in methanol. The second-order nonlinearity was evaluated by calculating the $\mu_g\beta$ value of the molecules, where μ_g and β represent the calculated dipole moment (using Titan Version 1 from Wavefunction, Inc.; 18401, Vonkarman, Suite 370, Irvine CA 92612 programme) and second-order hyperpolarizability, respectively. Figure 6 shows a plot of β and $\mu_g\beta$ for the different monomers.

Table 3 Nonlinear Optical Properties

Sample	μ_g (D)	$\beta_{\text{HRS } 1064 \text{ nm}}$ (10^{-30} esu)	$\mu_g\beta$ (10^{-30})
S1	2.850	17.16	48.906
S2	2.578	22.16	57.13
S3	3.661	28.91	105.84
S4	3.702	29.10	107.73
S5	3.548	33.31	118.18
S6	2.835	42.00	119.07
S7	2.289	15.0	34.335

From the table we can see that **S6** which is based on α -naphthol had the highest β -value of 42×10^{-30} esu and the least was for **S7** which is the β -naphthol based dye. **S7** had better effective conjugation length than the other dye molecules except **S6**, but its nonlinear optical activity is lower than even simple phenol

based dye **S1**. The optical nonlinearity was in the following order of phenolic component, α -naphthol > phenyl phenol > 2,6-dimethyl phenol > o-cresol > cardanol > phenol > β -naphthol. The unusually low value of β for **S7** - the β -naphthol based chromophore, could be explained based on the hydrogen bond between the phenolic oxygen and the β -hydrogen of the azo bridge as shown in scheme 3 which shows the quinonoid structure of 4-[(2-hydroxynaphthen-1-yl)azo]benzoic acid. Absorption spectra also support the existence of two different tautomeric forms in the case of **S7**. The FT-IR spectroscopy is the best method of detecting hydrogen bonding in a system. Figure 7 is the expanded region of the infra red spectra of **S1**, **S6** and **S7** showing the carbonyl and azo stretching vibrations.

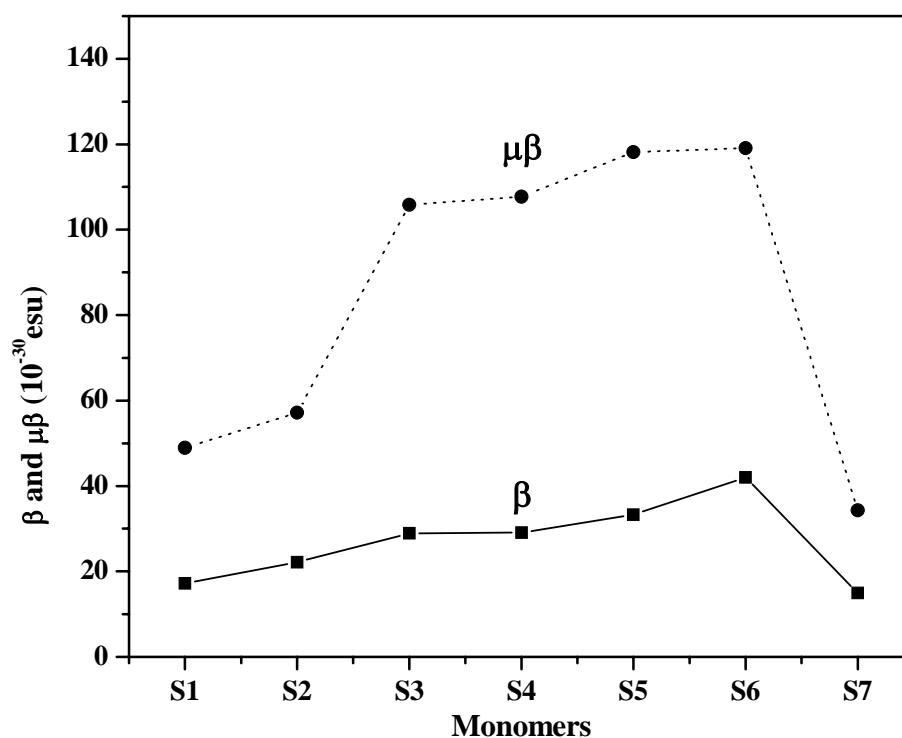


Figure 6 Plot of β and $\mu\beta$ for the different monomers

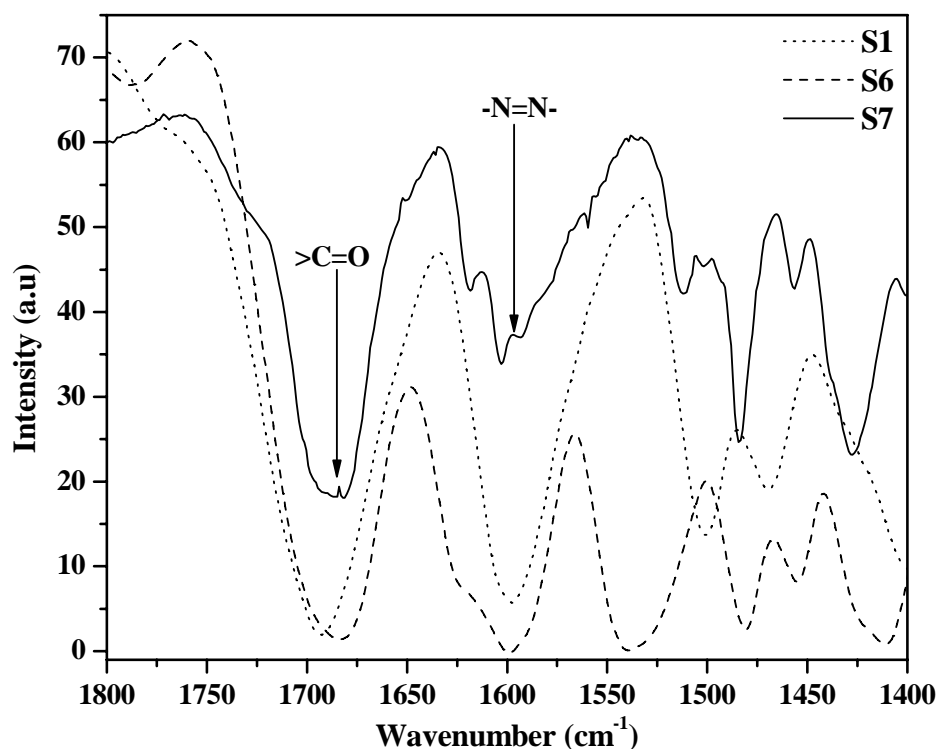


Figure 7 Expanded region of FT-IR spectra of **S1**, **S6** and **S7**

It can be seen that the $>\text{C}=\text{O}$ stretching vibration in **S7** exhibits a split, albeit small, indicating two different types of $>\text{C}=\text{O}$ stretch, which is absent in **S1** and **S6**. Additionally, the azo stretching vibration of **S7** is not so sharp and well-defined as in **S1** or **S6**. All these information point out the possibility of **S7** existing mostly as the hydrazone form, which is aided by the hydrogen bond between the hydroxyl group and the beta azo nitrogen. Even in the 1-naphthol derivative, i.e. **S6**, the tendency to exhibit tautomerism and to exist in the hydrazone form is higher compared with its simple phenyl analogue. It is a known fact that the tautomeric equilibrium increasingly favors the hydrazone as the number of rings becomes greater in going from derivatives of phenol to those of 1-naphthol.³⁷⁻³⁹ Confirmation of this fact comes from Hadzi's evaluation of the infra red spectra of 4-phenylazophenol exhibiting an OH band, but 4-phenylazo-1-naphthol exhibiting $>\text{C}=\text{O}$ and NH bands.⁴⁰ However, in comparison with **S7**, the tendency of **S6** to exist as the hydrazone tautomer is less. It has been shown that lengthening the polyenic chain linking the donor and

acceptor end groups lead to enhancement of both the transition dipole and the excited-state dipole, which in turn has a positive effect on the observed first hyperpolarizability. However, the introduction of a biphenyl moiety in place of its polyenic analogue displays slightly smaller ground state and transition dipoles and a significant decrease of the excited state dipole moment. Thus incorporation of the biphenyl moiety in the polyenic chain results in a significant reduction of the photo-induced ICT efficiency, stressing that the nature of the π -conjugated system of push-pull molecules is crucial in determining the NLO characteristics. This could well explain the increase in β being not so high for **S5** to **S7** members compared with that of **S1**, as one would have otherwise expected assuming an increase in conjugation length by way of increase in ring size. The higher solvatochromic shift of **S6** in methanol, the solvent in which the HRS measurement was carried out, could also explain its highest beta value in comparison with the others. In general, electronic properties give a good idea of the trends in NLO behavior in a series of similar azo systems.

2.9 Thermal Properties of Monomers

Thermal properties of the monomers were examined by thermogravimetric analysis (TGA) (figure 8) and the 10 and 50 % weight loss temperature values are summarized in table 4. The monomers showed good resistance to thermal decomposition at temperatures under 300°C. **S5** had the highest thermal stability and **S2**, the cardanol based monomer with the long alkyl side chain had the lowest thermal stability.

Table 4 Thermal data of monomers

Sample	10 % Wt loss temp (TGA) ($^{\circ}\text{C}$)	50 % Wt loss temp (TGA) ($^{\circ}\text{C}$)
S1	275	428
S2	227	435
S3	246	330
S4	237	514
S5	304	344
S6	272	541
S7	293	315

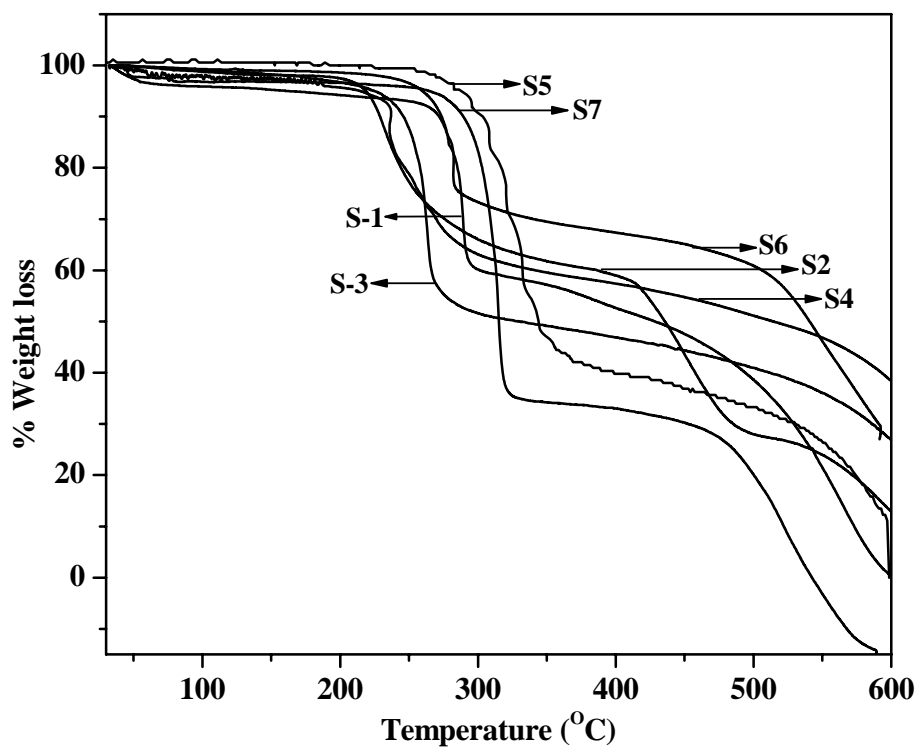


Figure 8 TG thermograms of monomers

2.10 Polymer Synthesis and Characterization

The most widely used reactions for the preparation of polyesters are direct esterification, usually performed at high temperature in the melt and by transesterification process or by interfacial methods.⁴¹ The direct esterification and transesterification methods for polymerization were ruled out in our case since the degradation temperatures of the monomers are much lower compared to the melt or high temperature conditions that are required and interfacial method also could not be used due to problems related to solubility. Reactions of monomers bearing acyl chloride groups with phenolic groups at low or medium temperature also provide a useful method for polyester synthesis. These reactions also do not suffer from the reversibility found for the other types of polyesterifications. Therefore, the polymerizations were carried out by directly condensing the AB type monomer in the presence of a condensing agent composed of pyridine and thionyl chloride under inert conditions.⁴² Optimization of the polymerization temperature is an important issue to address, since at high temperature, side reactions can occur that seriously limits the attainment of high molecular weight. The polymerizations were carried out at 30 °C as well as 80 °C and it was found that higher yield was obtained at higher temperature. As the polymers were insoluble in tetrahydrofuran, gel permeation chromatography could not be used to determine the molecular weight. Scheme 3 shows the polymerization conditions and the structure of the various polymers (**MCP1** to **MCP7**) obtained and table 5 gives the yield, inherent viscosity as well as the thermal analysis data. Due to poor solubility, the inherent viscosities could be recorded only for the soluble portions of **MCP2**, **MCP4** and **MCP6** in a solvent combination of phenol and tetrachloroethane. Therefore, the rather low solution viscosity value does not necessarily mean that the molecular weights are not very high since it only represents the soluble portion of the samples.

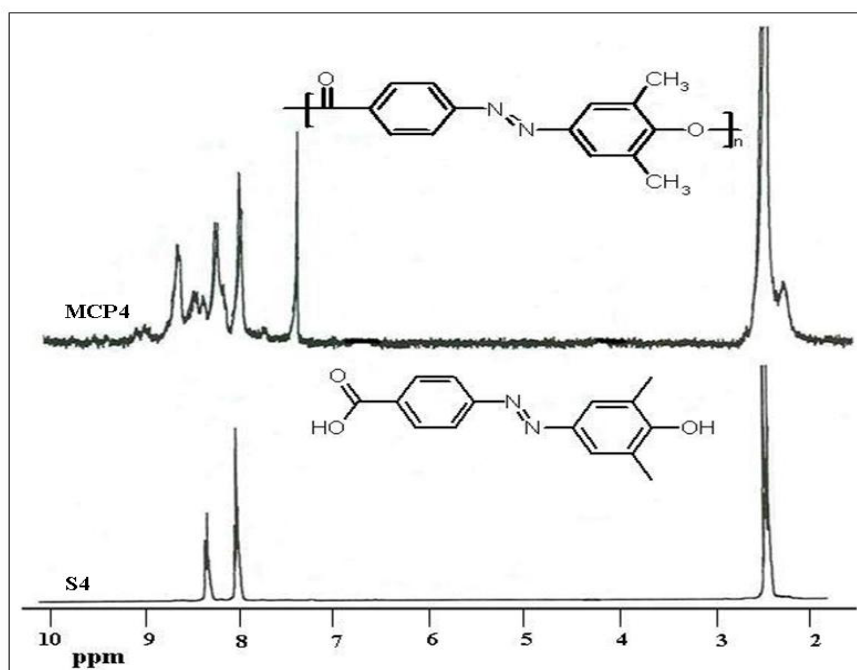


Figure 9 ^1H NMR spectra of **MCP4** with **S4**

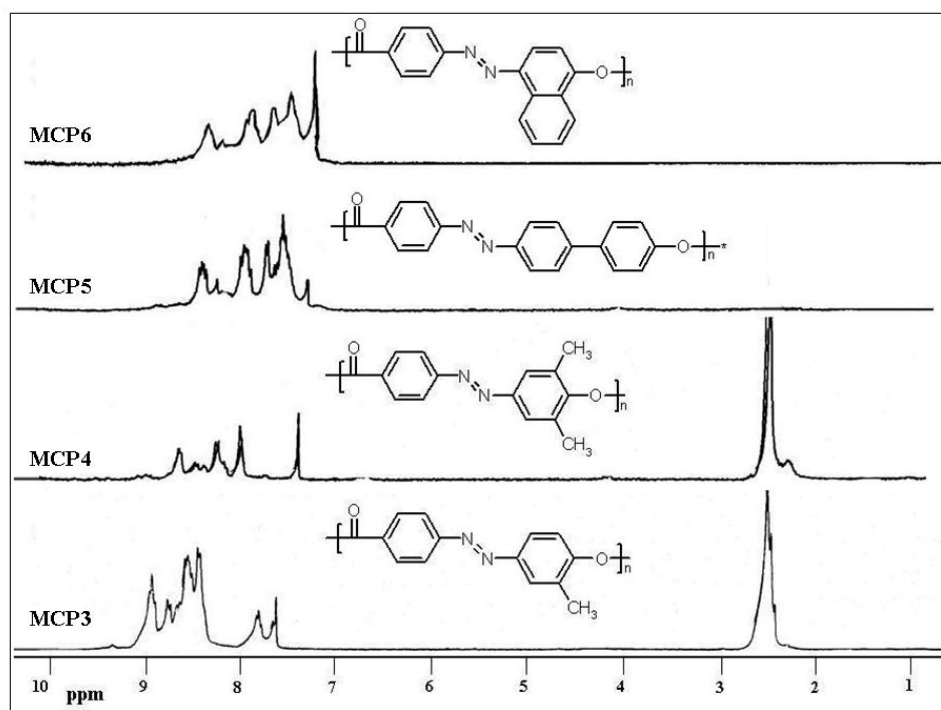


Figure 10 ^1H NMR spectra of **MCP3**, **MCP4**, **MCP5** and **MCP6**

The FTIR spectra of all the polymers showed characteristic peak of azo linkage around $1594\text{--}1600\text{ cm}^{-1}$ and the $>\text{C}=\text{O}$ peak of the ester group around

1740 cm^{-1} . IR data supports the formation of polymers as evidenced from the shift in the carbonyl stretching frequency of the carboxylic group of the monomer from around 1690 cm^{-1} to 1740 cm^{-1} which corresponds to the ester carbonyl stretching frequency of the polymer.⁴² The absence of hydroxyl peaks and the carbonyl peak of monomers in the range of 3550-3300 cm^{-1} also indicated the absence of monomer. Figure 11 shows the FTIR spectra of all the polymers.

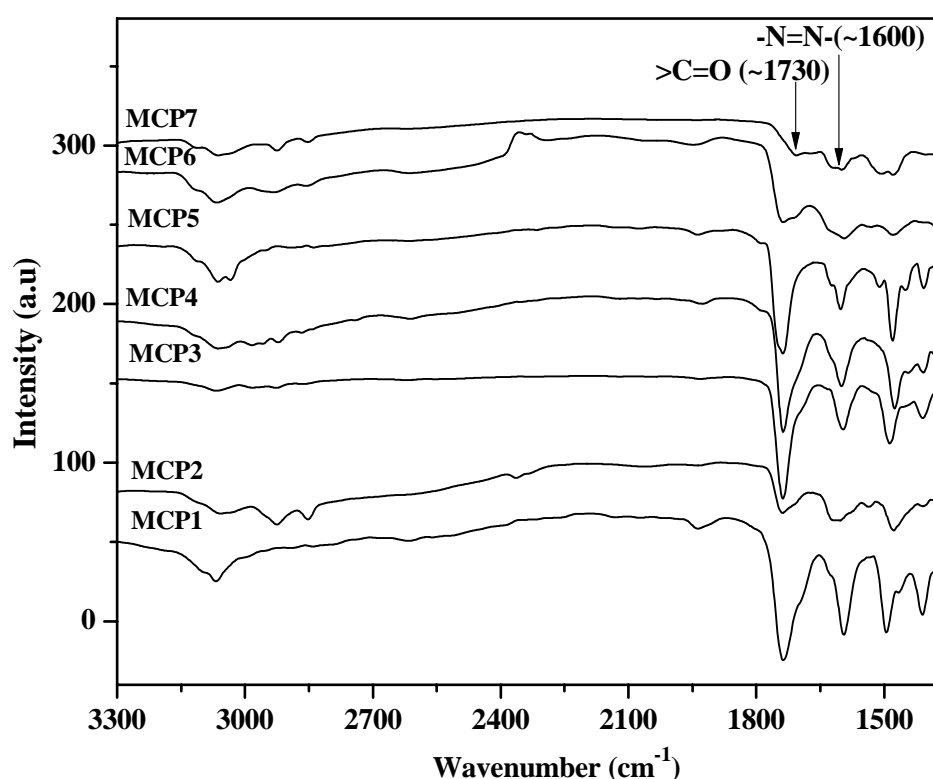


Figure 11 FTIR spectra of polymers

2.11 Thermal Properties of Polymers

Generally for azobenzenic structures, a thermal stability limit around 250°C is observed. Figure 12 shows the thermogravimetric analysis (TGA) of the polymers and the 10 and 50 wt % loss temperatures are given in table 5. As can be seen from table 3, **MCP5** has the highest thermal stability which could be attributed to the increased rigidity associated with the biphenyl system. The liquid crystalline behavior of the polymers was investigated using the differential scanning calorimetry (DSC) and polarized light microscopy (PLM). None of the

samples were liquid crystalline. Probably, the flexibility was insufficient for these highly rigid systems and the mesogenic units cannot organize themselves sufficiently to form the LC phase. Since the polymers were insoluble in most of the common organic solvents, attempts were made to measure the NLO property in the solid state. Unfortunately, the powder method did not give any measurable signal.

Table 5 Yield, thermal and viscosity data

Sample code	Yield (%)	TGA temperature (°C)		Viscosity data
		10 Wt % Loss	50 Wt% Loss	
MCP1	88	259	500	-
MCP2	88	180	400	0.13
MCP3	78	347	480	-
MCP4	29	278	480	0.19
MCP5	82	326	572	-
MCP6	75	262	480	0.21
MCP7	27	187	330	-

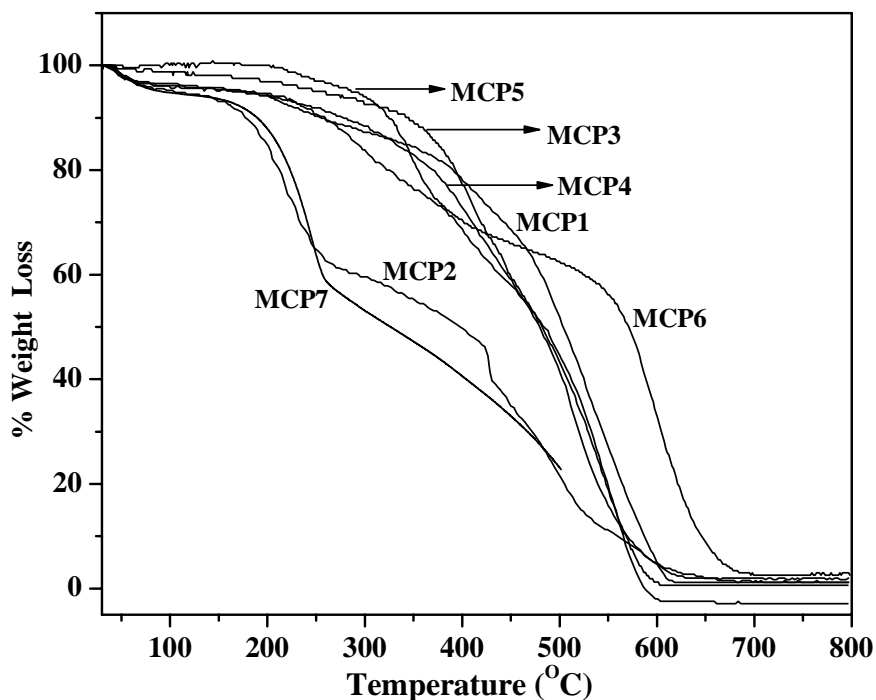


Figure 12 TG thermograms of polymers

2.12 Conclusion

This chapter describes the design strategy that was adopted to develop a series of NLO active azobenzene dyes. The donor (-OH) and acceptor (-COOH) groups were kept constant but the conjugation length and substituents were varied. An increase in the conjugation length between the donor and acceptor is known to improve the NLO property. However, in our studies we have shown that a simple increase in conjugation length by way of increase in the number of aromatic rings is not sufficient to improve the β value, since other parameters like geometry of the aromatic ring in the ground state, presence of hydrogen bonding etc also plays a prominent role in deciding the final NLO property. The naphthol and phenyl phenol based azobenzene monomers showed the highest β values in comparison with the simple phenol based monomer. This study revealed the effect of minor structural variations on molecular property like the hyperpolarizability tensor. Although main chain NLO polyesters based on these azobenzene monomers were synthesized, they had the problem of insolubility which prevented further studies of the polymers in solution.

2.13 References

1. Mizuuchi, K.; Yamamoto, K.; Kato, M.; Sato, H. *IEEE J. Quantum Electron*, **1994**, 30, 1596.
2. Endo, T.; Sueoka, K.; Mukasa, K. *Jpn. J. Appl. Phy: Part 1*, **2000**, 39, 397.
3. Dalton, L.R. *Adv. Polym. Sci.* **2002**, 158, 1.
4. Blau, W. *Phys. Technol.* **1987**, 18, 250.
5. Ray, P. C. *Chem. Phys. Lett.* **1996**, 248, 27.
6. Durr, H.; Laurent, H. B. In *Photochromism: Molecules and Systems in Studies in Organic Chemistry*, 40 Amsterdam, Elsevier, **1990**.
7. Zhang, C.; Du, M. H.; Cheng, H. P.; Zhang, X. G.; Roitberg, A. E.; Krause, J. *L. Phy. Rev. Lett.* **2004**, 92, 158301.
8. Sutherland, R. L, *Handbook of Nonlinear Optics*; Marcel Dekker, Inc.: New York, Basel, Hong Kong, **1996**.
9. Sekkat, S.; Knoll, W. In *Photoreactive Organic Thin Films*, Academic Press: Amsterdam, **2002**.
10. Tsutsumi, N.; Matsumoto, O.; Sakai, W.; Kiyotsukuri, T. *Macromolecules* **1996**, 29, 592.
11. Tsutsumi, N.; Morishima, M.; Sakai, W. *Macromolecules* **1998**, 31, 7764.
12. Bahulayan, D.; Sreekumar, K. *J. Mater. Chem.* **1999**, 7, 1425.
13. Kim, D, Y.; Li, L.; Jimg, X. L.; Shivshankar, V.; Kumar, J.; Tripathy, S. K. *Macromolecules* **1995**, 28, 8835.
14. Singer, K.D.; Kuzyk, M, G.; Holland, W. R.; Sohn, R. J.; Lalama, S. J.; Comizzoli, R. B.; Katz, H. E.; Schilling, M. L. *Appl. Phys. Lett.* **1988**, 53, 1800.
15. Sandhya, K. Y.; Pillai, C. K. S.; Sato, M.; Tsutsumi, N. *J. Polym. Sci. Part A: Polym. Chem.* **2003**, 41, 1527.
16. Saminathan, M.; Pillai, C. K. S.; Pavithran, C. *Macromolecules* **1993**, 26, 7103.
17. Sandhya, K. Y.; Pillai, C. K. S.; Sato, M.; Tsutsumi, N. *Macromol. Chem. Phys.* **2002**, 203, 1126.

18. Saminathan, M.; Pillai, C. K. S. *J. Polym. Mater.* **2000**, 18, 83.
19. Saminathan, M.; Pillai, C. K. S. *Polymer* **2000**, 41, 3103.
20. Saminathan, M.; Pillai, C. K. S. *Macromol. Chem. Phys.* **2000**, 201, 2475.
21. Yokoyama, S.; Nakahama, T.; Otomo, A.; Mashiko, S. *J. Am. Chem. Soc.* **2000**, 122, 3174.
22. Ishow, E.; Bellaiche, C.; Bouteiller, L.; Natakani, K.; Delaire, J. A. *J. Am. Chem. Soc.* **2003**, 125, 15744.
23. Casa, C. D.; Morgera, A. F.; Lanzi, M.; Bizzarri, P. C.; Paganin, L.; Bertinelli, F.; Luisa, S.; Mucci, A.; Mauro, C.; Sarcinelli, F.; Quatela, A. *Eur. Polym. J.* **2005**, 41, 2360.
24. Risser, S. M.; Beratan, D. N.; Marder, S. R. *J. Am. Chem. Soc.* **1993**, 115, 7719.
25. Marder, S. R.; Perry, J. W.; Bourhill, G.; Gorman, C. B.; Tiemann, B. G.; Mansour, K. *Science* **1993**, 261, 186.
26. Asha, S. K.; Kavita, K.; Das, P. K.; Ramakrishnan, S. *Chem. Mater.* **1999**, 11, 3352.
27. Sarker, A. M.; Ding, L.; Lahti, P. M.; Karasz, F. E. *Macromolecules* **2002**, 35, 223.
28. Bhowmik, P. K.; Han, H.; Cebe, J. J.; Burchett, R. A. *J. Polym. Sci. Part: A. Polym. Chem.* **2002**, 40, 141.
29. Luo, J.; Hua, J.; Qin, J.; Cheng, J.; Shen, Y.; Lu, Z.; Wang, P.; Ye, C. *Chem. Commun.* **2001**, 2, 171.
30. Alain, V.; Redoglia, S.; Blanchard-Desce, M.; Lebus, S.; Lukaszuk, K.; Wortmann, R.; Gubler, U.; Bosshard, C.; Gunter, P. *Chem. Phys.* **1999**, 245, 51.
31. Zollinger, H. In *Azo and Diazo Chemistry. Aliphatic and Aromatic Compounds*. Interscience Publishers, Inc: New York, **1961**.
32. Kim, J. J.; Funabiki, K.; Muramatsu, H.; Shibata, K.; Kim, S. H.; Shiozaki, H.; Hartmann, H.; Matsui, M. *Chem. Commun.* **2000**, 9, 753.
33. Hutchings, M. G.; Gregory, P.; Campbell, J. S.; Strong, A.; Zamy, J. P.;

- Lepre, A.; Mills, A. *Chem. Eur. J.* **1997**, 3, 1719.
34. Shin, D. M.; Schanze, K. S.; Whitten, D. G. *J. Am. Chem. Soc.* **1989**, 111, 8494.
35. Shin, D. M.; Whitten, D. G. *J. Am. Chem. Soc.* **1988**, 110, 5206.
36. Kobayashi, S.; Yokoyama, H.; Kamei, H. *Chem. Phys. Lett.* **1987**, 138, 333.
37. Burawoy, A.; Markowitsch, I. *Ann*, **1933**, 180, 503.
38. Burawoy, A.; Markowitsch, I. *Ann*, **1933**, 71, 504.
39. Burawoy, A.; Salem, A. G.; Thompson, A. R. *J. Chem. Soc.* **1952**, 4793
40. Hadzi, D. *J. Chem. Soc.* **1956**, 2143.
41. Allen, G.; Bevington, J. C.; Eastmond, G. C.; Ledwith, A.; Russo, S.; Sigwalt, P. *Comprehensive Polymer Science: The Synthesis, Characterization, Reactions & Applications of Polymers*, Volume 5, Step Polymerization; Pergamon Press plc: England, **1989**.
42. Higashi, F.; Mashino, T.; Takahashi, I. *J. Polym. Sci. Polym. Chem. Ed.* **1986**, 24, 97.

Chapter 3

Synthesis, Characterization and Photophysical Properties of Highly Fluorescent Soluble Side Chain Azobenzene Polymers

3.1 Abstract

A series of fluorescent azobenzene dyes and side chain polymers have been synthesized, characterized and photophysical properties studied. Azobenzene dyes having different fluorophores like phenol (**DE1**), phenyl phenol (**DE2**) and naphthol (**DE3**) incorporated in them were synthesized. **DE2** had unusually high fluorescence with a quantum yield of $\phi_{\text{FL}} = 0.2$ recorded in dichloromethane (DCM), whereas, **DE1** and **DE3** were found to be weakly fluorescent. The azobenzene dyes were converted into methacrylate monomers having short ethyleneoxy spacer and then free radically polymerized. Phenyl phenol based azobenzene polymer (**P2**) continued to show fluorescence whereas fluorescence was completely quenched in the case of phenol (**P1**) and naphthol (**P3**) based polymers. Phenyl phenol, though twisted in the ground state is known to have a more planar geometry in the excited state – a factor that enables it to retain its fluorescence behavior even when it is incorporated as part of an azobenzene unit. In contrast, naphthol which is a better fluorophore compared to phenyl phenol loses much of its emissive behavior upon coupling to the azobenzene unit. The extent of trans to cis photoisomerization in solution was very low (~17 %) for **P2** after 30 minutes of continuous irradiation using 360 nm light, in contrast to ~ 40 % for **P1** under identical conditions. This is attributed to the steric repulsion brought about by the bulky phenyl phenol unit that restricts rotation. A two fold enhancement in fluorescence emission was observed for **P2** upon irradiation by UV light at 365 nm, which relaxed to the original intensity in about 7 day's time. The higher emission of the cis azobenzenes is generally attributed to an inhibition of photoinduced electron transfer (PET) mechanism. The emission of **P2** showed a concentration dependence which increased initially and then decreased in intensity with the formation of a new red shifted peak at higher concentration due to aggregation. Irradiation of the fluorescence quenched highly concentrated (1×10^{-3} M) sample of **P2** showed an enhancement in emission from aggregates at 532 nm.

3.2 Introduction

Azobenzene and its derivatives are typical molecules showing cis-trans photoisomerization and they have attracted much interest for their high potential in industrial applications like liquid crystals, light-driven switches, image storage devices etc. Generally the trans isomer of an azo compound is the more stable form. The trans form can be converted into the cis form by UV illumination and this change in molecular structure can be used for memory write and read. The cis form can be converted into the trans state either by dark incubation or by illumination with visible light. Through this trans-cis isomerization of azobenzene, the physicochemical properties such as the absorption spectrum, dipole moment, refractive index and molecular conformation can be reversibly changed. Since the photoisomerization is a very efficient process in the excited state, their radiative deactivation processes which are slower are not competitive. Therefore azobenzenes do not emit light. But there are few exceptional reports of fluorescence from self assembled bilayer aggregates of azobenzene containing aggregates and azobenzene functionalized dendrimers. This emission is attributed to the densely packed arrangement of azobenzene chromophores in the bilayer structure.¹⁻⁵ Blocking of isomerization by metallation can result in fluorescence and there are a few reports based on this approach. Ghedini et al. reported that with palladium (II) species azobenzenes undergo cyclopalladation to form a five membered ring containing both palladium center and the azo linkage.⁶ In this arrangement the -N=N- fragment is trans blocked. The highest azo fluorescence so far reported is also based on metallation approach. Complexation with boron blocked the isomerization and irradiation with UV light resulted in green fluorescence with a quantum yield $\phi = 0.7$.⁷ Han et al. showed the photoinduced formation of blue fluorescent aggregates in the 460-500 nm region for simple azobenzene derivatives with different alkyl chain lengths whose isolated molecules in solution are non fluorescent at ambient temperature.^{8,9} This photoinduced fluorescence enhancement has been attributed to light driven self assembly of

cis azobenzenes. In contrast to the above reports, Zacharias et al. showed that coupling fluorophores such as 1-aminonaphthalene and 2-amino benzoic acid to azobenzene systems can induce fluorescence in the 400 nm region which showed a 6 fold enhancement in luminescence upon irradiation.¹⁰ The origin of this enhanced luminescence was explained as the result of non planar geometry in the cis isomer which obstructs effective conjugation of the lone pair of electrons on the nitrogen with the π electrons of the fluorophore, thereby inhibiting photoinduced electron transfer (PET).

The versatility of azobenzene derivatives as promising systems for various applications could be further extended if they emitted fluorescence. Attempts to fine tune the fluorescence properties of azobenzene derivatives in the literature have mostly concentrated on small molecules only. There are no reports in the literature of intense fluorescence exhibited by azobenzene based polymers – main chain or side chain – at room temperature in the trans state. There are reports of fluorescence from poly(p-phenylenevinylene) (PPV) derivatives substituted with azobenzene side chains, but the emission in these cases is entirely due to the PPV backbone.^{11,12} There is also one report of poly(p-phenylene) (PPP) unit in conjugation with azobenzene units in the main chain which showed weak fluorescence expected to be originating from the terphenyl units in the main chain.¹³ Fluorescence in polymers is an important tool that can be used to study molecular dynamics as it reflects the energy levels of the microstructure of the polymers. The development of freely soluble azobenzene polymers that can show room temperature fluorescence is interesting not only as new materials of fundamental scientific interest but also as potential candidates for sensor and other similar applications.

The present study describes the synthesis and photophysical properties of a series of azobenzene based side chain polymers. In the initial attempt to develop NLO active main chain polymers, solubility was the key problem which limited the characterization and further studies.¹⁴ In order to induce solubility, there are two main approaches, either by the introduction of flexible spacers like

ethyleneoxy or methylene units to the backbone or by the attachment of chromophores as pendants to a flexible backbone. In this study, the second approach was made use of and the backbone selected was poly (methacrylate). The azobenzene dyes based on naphthol and phenyl phenol having high β values along with the simple phenol based one were introduced as side chains in a methacrylate polymer which made them completely soluble in most of the common organic solvents. The morphology of these polymers was also analyzed using SEM and TEM measurements.

3.3 Experimental Section

4-Amino benzoic acid, 4-phenyl phenol and methacryloyl chloride were purchased from Aldrich Chemicals and were used as such. Phenol, α -naphthol, sodium nitrite, potassium hydroxide, potassium carbonate and potassium iodide were purchase from S.D Fine Chemicals Ltd. Dimethyl formamide (DMF), methanol, tetrahydrofuran, triethyl amine, 2-chloroethanol, and AIBN, were purchased locally and purified using standard procedures.

^1H and ^{13}C -NMR spectra of intermediates, monomers, and polymers were recorded using 300-MHz Bruker NMR spectrophotometer in deuterated chloroform containing small amount of TMS as internal standard. For ^{13}C NMR experiments, the carbon atom in CDCl_3 was taken as 77 ppm and all other peaks were assigned with respect to it. The purity of the compounds was determined by JEOL JSM600 fast atom bombardment (FAB) high-resolution mass spectrometry. The purity of the monomers and intermediate compounds were further confirmed by SEC in THF using polystyrene standards. The molecular weights of the polymers were determined by GPC in THF using polystyrene standards for the calibration. Waters 515 Pump connected through three series of Styragel HR columns (HR-3, HR-4E and HR-5E) and Waters Model 2487 Dual Wavelength UV-vis Detector and Waters 2414 Differential Refractometer was used for analyzing the samples. The flow rate of the THF was maintained as 1 mL throughout the experiments and 1 wt % of (2 mg in 1 mL) the polymer was

filtered and injected for recording the GPC chromatograms at 30 °C. Infrared spectra of the polymers were recorded using a Perkin Elmer, Spectrum one spectrophotometer in the range of 4000 to 400 cm^{-1} . UV-Vis spectra were recorded using Perkin Elmer Lambda 35 UV-Vis Spectrometer. The emission studies were performed by a SPEX Fluorolog F112X spectrofluorimeter. For recording solid-state photo physical properties, thin films were cast from dichloromethane (DCM) solution on a glass plate and allowed to dry for 24 h prior to measurements. The film thicknesses were varied by changing the concentration of the solution. The fluorescence quantum yields of the azobenzene derivatives and polymers were determined in DCM using quinine sulfate in 0.1M H_2SO_4 ($\phi = 0.546$) as the standard. The optical density at λ_{max} was maintained at 0.1 ± 0.05 to avoid reabsorption artifacts.

The quantum yield was calculated using the equation.

$$\phi_s = \phi_r [F_s A_r / F_r A_s] (n_r/n_s)^2$$

where ϕ_s is the fluorescence quantum yield of the sample, F is the area of the emission peak, n is the refractive index of solution and A is the absorbance of the solution at the exciting wavelength. The subscripts r and s denote reference and sample respectively.

Thermogravimetric analysis (TGA) was performed using a TGA-50 Shimadzu Thermogravimetric Analyzer. Samples were run from 40 to 400 °C with a heating rate of 10 °C/min under nitrogen. The thermal and phase behavior of the polymers were analyzed using a hot stage polarized light microscope (Leitz-1350 heating stage coupled with PLM) as well as a DSC-Perkin Elmer Pyris 6 Differential Scanning Calorimeter (DSC) at a heating rate of 10 °C/min under nitrogen atmosphere. Typically, 2-3 mg of samples was placed in an aluminium pan, sealed properly and scanned from 10-250 °C. The instrument was calibrated with indium standards before measurements. Irradiation measurements were carried out in dichloromethane with a 200 W high-pressure mercury lamp in combination with a 360 nm (8 mW/cm^{-2}) Oriel bandpass filter. The samples

were subsequently irradiated and the absorbance as well as fluorescence was monitored. The backward transition from cis to trans was followed after keeping the sample in dark for different periods of time and monitoring their UV absorption as well as fluorescence. Energy minimized conformations in the ground state were obtained by AM1 calculations carried out using Titan Version 1 from Wavefunction Inc; 18401, Von Karman Suite 370, Irvine, CA 92612. For scanning electron microscope (SEM) measurements, polymer samples were provided with a thin gold coating using JEOL JFC-1200 fine coater. The probing side was inserted into JEOL JSM-5600 LV scanning electron microscope for taking photographs. The sample preparation method adopted was as follows. The polymer solution of concentration 10^{-3} M in tetrahydrofuran was prepared and a drop of this solution was placed on a clean glass slide and was allowed to evaporate slowly in air. Transmission electron microscope (TEM) images were recorded using FEI Tecnai 30G² S Twin HRTEM instrument at 100KV. For TEM measurements, a drop of the polymer solution (10^{-6} M) in tetrahydrofuran was deposited directly on a formvar coated copper grid.

Synthesis of 4-(4-Hydroxy-phenylazo)-benzoic acid methyl ester (DE1): The hydroxy azobenzoic acids were synthesized as described in the previous chapter.¹⁴ Esterification of the azobenzoic acid was carried out using standard procedure.

4-[(4-Hydroxyphenyl)azo]benzoic acid (10 g, 41 mmol) was dissolved in 100 mL methanol with catalytic amount of concentrated sulphuric acid and refluxed for 3 h. After distilling off the excess solvent, the crude product was poured into water and neutralized with base. The precipitate was then filtered and dried. The crude dye was further purified by column chromatography on silica gel (60-120 mesh) using hexane-ethyl acetate mixture (v/v 70/30). Yield: 8.7 g (87 %), mp: 159 °C. ¹H NMR (CDCl₃) δ ppm: 8.19 (2H, d, Ar), 7.98 (4H, m, Ar), 7.05 (2H, d, Ar), 3.95 (3H, s, -C(O)OCH₃). ¹³C NMR (CDCl₃) δ ppm: 52.26, 115.95, 122.35, 125.19, 130.57, 131.22, 146.99, 155.34, 162.67, 166.65. FTIR (KBr)

(cm^{-1}): 3401, 1716, 1599, 1498, 1402, 1238, 1254, 1188, 1139, 1106, 859, 839, 820, 776, 724, 697, 669, 625, 549. FAB- HRMS $m+1$: 257.08

Similarly, (10 g, 31 mmol) of 4-[(4-Hydroxybiphenyl-4-yl)azo]benzoic acid and (10 g, 34 mmol) of 4-[(4-Hydroxynaphthen-1-yl)azo]benzoic acid were used to obtain the esters 4-(4'-Hydroxy-biphenyl-4-ylazo)-benzoic acid methyl ester (**DE2**) and 4-(4-Hydroxy-naphthalen-1-ylazo) benzoic acid methyl ester (**DE3**) respectively.

4-(4'-Hydroxy-biphenyl-4-ylazo)-benzoic acid methyl ester (DE2): Yield: 8.1 g (78 %) mp: 135 °C. ^1H NMR (CDCl_3) δ ppm: 8.22 (2H, d, Ar), 7.94 (2H, m, Ar), 7.65 (2H, d, Ar), 7.47-6.85 (6H, m, Ar), 3.89 (3H, s, $-\text{C}(\text{O})\text{OCH}_3$). ^{13}C NMR (CDCl_3) δ ppm: 52.44, 115.65, 122.09, 126.58, 128.27, 128.89, 129.82, 130.85, 132.88, 140.76, 151.62, 155.34, 157.41, 166.02. FTIR (KBr) (cm^{-1}): 3368, 1720, 1597, 1427, 1273, 1112, 1015, 963, 861, 831, 689, 635, 593, 562. FAB- HRMS m : 332.31

4-(4-Hydroxy-naphthalen-1-ylazo) benzoic acid methyl ester (DE3): Yield: 8.7 g (83 %) mp: 192 °C. ^1H NMR (CDCl_3) δ ppm: 8.89 (H, d, Ar), 8.27 (H, d, Ar), 8.15 (2H, d, Ar), 8.07 (3H, m, Ar), 7.66 (H, t, Ar), 7.55 (H, t, Ar), 6.89 (H, d, Ar), 3.85 (3H, s, $-\text{C}(\text{O})\text{OCH}_3$). ^{13}C NMR (CDCl_3) δ ppm: 52.28, 108.55, 116.28, 121.63, 122.17, 125.06, 125.96, 126.29, 127.57, 130.61, 131.29, 132.85, 141.67, 155.74, 159.25, 166.69. FTIR (KBr) (cm^{-1}): 3407, 1717, 1597, 1575, 1506, 1429, 1390, 1319, 1276, 1248, 1092, 1018, 862, 812, 757, 694, 579. FAB- HRMS $m+1$: 307.01

Synthesis of 4-[(2-Hydroxy-ethoxy)-phenylazo]-benzoic acid methyl ester (ACE1): 4-(4-Hydroxy-phenylazo)-benzoic acid methyl ester (**DE1**) (2.50 g, 9.70 mmol), anhydrous potassium carbonate (2.02 g, 14.6 mmol), catalytic amount of KI and 2-chloroethanol (0.79 g, 9.7 mmol) were dissolved in 10 mL DMF. The mixture was heated at 80 °C for 48 h under nitrogen. The resulting solution was cooled to room temperature and poured into water. The product was filtered, washed with water and dried and purified by column chromatography using hexane-ethyl acetate mixture (v/v 90/10).

Yield: 2.5 g (86 %) mp: 104 °C. ^1H NMR (CDCl_3) δ ppm: 8.21 (2H, d, Ar), 7.97 (4H, m, Ar), 7.04 (2H, d, Ar), 4.52 (2H, t, $-\text{OCH}_2\text{-CH}_2-$), 4.01 (2H, t, $-\text{OCH}_2\text{-CH}_2-$), 3.91 (3H, s, $-\text{C}(\text{O})\text{OCH}_3$). ^{13}C NMR (CDCl_3) δ ppm: 55.63, 61.41, 66.86, 114.34, 122.39, 125.23, 130.71, 131.22, 144.3, 155.33, 159.71, 166.64. FTIR (KBr) (cm^{-1}): 3396, 1714, 1687, 1604, 1583, 1498, 1454, 1402, 1270, 1144, 1026, 861, 837, 774, 694, 543. FAB- HRMS $m+1$: 301.40

Similarly, (2 g, 5.40 mmol) of **DE2** and (2 g, 5.80 mmol) of **DE3** were used to obtain the esters 4-[-(2-Hydroxy-ethoxy)-biphenylazo]-benzoic acid methyl ester (**ACE2**) and 4-[-(2-Hydroxy-ethoxy)-naphthalen-1-ylazo]-benzoic acid methyl ester (**ACE3**) respectively.

4-[-(2-Hydroxy-ethoxy)-biphenylazo]-benzoic acid methyl ester (ACE2).

Yield: 1.6 g (70 %) mp: 140 °C. ^1H NMR (CDCl_3) δ ppm: 8.23 (2H, d, Ar), 7.95-7.91 (4H, m, Ar), 7.63 (2H, d, Ar), 7.50 (2H, m, Ar), 7.33 (2H, m, Ar), 4.38 (2H, t, $-\text{OCH}_2\text{-CH}_2-$), 4.03 (2H, t, $-\text{OCH}_2\text{-CH}_2-$), 3.96 (3H, s, $-\text{C}(\text{O})\text{OCH}_3$). ^{13}C NMR (CDCl_3) δ ppm: 51.53, 61.01, 71.92, 115.64, 122.12, 126.67, 128.34, 128.92, 130.88, 132.92, 140.66, 151.61, 155.22, 157.01, 166.63. FTIR (KBr) (cm^{-1}): 3362, 1726, 1605, 1459, 1484, 1429, 1273, 1218, 1152, 1114, 1018, 831, 757, 686, 540. FAB- HRMS $m+1$: 377.13

4-[-(2-Hydroxy-ethoxy)-naphthalen-1-ylazo]-benzoic acid methyl ester (ACE3).

Yield: 1.7 g (76 %) mp: 113 °C. ^1H NMR (CDCl_3) δ ppm: 8.92 (H, d, Ar), 8.28 (H, d, Ar), 8.16 (2H, d, Ar) 7.99 (3H, m, Ar), 7.66 (H, t, Ar) 7.61 (H, t, Ar), 6.88 (H, d, Ar), 4.45 (2H, t, $-\text{OCH}_2\text{-CH}_2-$), 4.21 (2H, t, $-\text{OCH}_2\text{-CH}_2-$) 3.89 (3H, s, $-\text{C}(\text{O})\text{OCH}_3$). ^{13}C NMR (CDCl_3) δ ppm: 52.52, 61.68, 67.01, 105.25, 113.82, 122.41, 122.87, 125.82, 126.21, 126.93, 128.01, 130.97, 131.29, 133.08, 141.95, 156.18, 159.32, 166.73. FTIR (KBr) (cm^{-1}): 3401, 1720, 1599, 1578, 1509, 1465, 1435, 1391, 1322, 1248, 1276, 1248, 1193, 1135, 1039, 1017, 905, 858, 809, 760, 694. FAB- HRMS $m+1$: 351.37

Synthesis of 4-{4-[2-(2-methyl-acryloyloxy)-ethoxy]-phenylazo} benzoic acid methyl ester (M1): Methacryloyl chloride solution (0.69 g, 6.60 mmol) in tetrahydrofuran (2 mL) was added very slowly to a THF (8 mL) solution of

ACE1 (2 g, 6.60 mmol) and triethyl amine (0.66 g, 6.60 mmol) kept at 0 °C. The solution was stirred for 1 h at 0 °C and then at room temperature for 6 h. The salt formed was filtered and removed. The filtrate was then concentrated and the monomer was precipitated in water, filtered and dried. The crude product was further purified by column chromatography using hexane-ethyl acetate mixture (v/v 95/5). Yield: 1.6 g (65 %), mp: 87 °C. ¹H NMR (CDCl₃) δ ppm: 8.14 (2H, d, Ar), 7.90 (4H, m, Ar), 6.98 (2H, d, Ar), 6.09 (1H, s, -C=CH₂), 5.53 (1H, s, -C=CH₂), 4.55 (2H, t, -OCH₂-CH₂), 4.46 (2H, t, -OCH₂-CH₂), 3.88 (3H, s, -C(O)OCH₃), 1.89 (3H, s, CH₃). ¹³C NMR (CDCl₃) δ ppm: 18.61, 51.93, 62.78, 66.18, 114.89, 120.29, 122.33, 125.61, 130.72, 131.35, 135.85, 147.18, 155.24, 161.52, 166.55, 167.23. FTIR (KBr) (cm⁻¹): 3428, 1716, 1599, 1498, 1451, 1405, 1273, 1254, 1163, 1138, 1105, 1026, 861, 837, 773, 694, 540. FAB-HRMS m+1: 369.38

Similarly, (1 g, 2.7 mmol) of **ACE2** and (1 g, 2.9 mmol) of **ACE3** were used to obtain the monomers 4-{4-[2-(2-methyl-acryloyloxy)-ethoxy]-biphenylazo} benzoic acid methyl ester (**M2**) and 4-{4-[2-(2-methyl-acryloyloxy)-ethoxy]-naphthalen-1-ylazo}benzoic acid methyl ester (**M3**) respectively.

4-{4-[2-(2-methyl-acryloyloxy)-ethoxy]-biphenylazo}benzoic acid methyl ester (M2): Yield: 0.7 g (59 %), mp: 99 °C. ¹H NMR (CDCl₃) δ ppm: 8.21(2H, m, Ar), 7.95 (4H, m, Ar), 7.62 (2H, m, Ar), 7.60 (2H, m, Ar), 7.26 (2H, d, Ar), 6.24 (1H, s, -C=CH₂), 5.68 (1H, s, -C=CH₂), 4.41 (2H, t, -OCH₂-CH₂), 4.05 (2H, t, -OCH₂-CH₂), 3.96 (3H, s, -C(O)OCH₃), 1.88 (3H, s, CH₃). ¹³C NMR (CDCl₃) δ ppm: 18.34, 52.32, 63.16, 66.10, 114.89, 115.29, 121.92, 123.53, 126.78, 127.38, 128.25, 128.78, 130.22, 134.26, 136.11, 140.72, 151.63, 156.44, 158.22. 166.01, 167.26 FTIR (KBr) (cm⁻¹): 3291, 1712, 1606, 1487, 1257, 1056, 835 FAB- HRMS m+1: 445.49

4-{4-[2-(2-methyl-acryloyloxy)-ethoxy]-naphthalen-1-ylazo}benzoic acid methyl ester (M3): Yield: 0.7 g (60 %), mp: 105 °C. ¹H NMR (CDCl₃) δ ppm: 8.92 (H, d, Ar), 8.28 (H, d, Ar), 8.16 (2H, d, Ar), 7.98 (3H, m, Ar), 7.63 (H, t, Ar), 7.55 (H, t, Ar), 6.88 (H, d, Ar), 6.10 (H, s, -C=CH₂), 5.54 (H, s, -C=CH₂),

4.55 (2H, t, -OCH₂-CH₂-), 4.45 (2H, t, -OCH₂-CH₂-), 4.04 (3H, s, -C(O)OCH₃), 1.97 (3H, s, CH₃). ¹³C NMR (CDCl₃) δ ppm: 18.27, 55.91, 62.37, 62.83, 103.71, 117.29, 122.16, 123.02, 125.02, 125.95, 126.14, 127.81, 129.33, 130.71, 132.44, 136.16, 143.34, 157.03, 159.21, 166.05, 167.27. FTIR (KBr) (cm⁻¹): 3406, 1720, 1599, 1577, 1509, 1459, 1388, 1317, 1275, 1246, 1163, 1092, 1017, 765. FAB- HRMS m: 418.34

Synthesis of Control Monomer

A control polymer was also synthesized and the synthesis of its monomer is given below. In the first step, 4-phenyl phenol was coupled with 2-chloroethanol to obtain the intermediate **CE** which was then functionalized with methacrylate unit to obtain the corresponding control monomer **CM**. This monomer was then polymerized using free radical polymerization technique to obtain the corresponding control polymer (**CP**).

Synthesis of 2-(biphenyl-4-yloxy)-ethanol (**CE**):

4-Phenyl phenol (2 g, 12 mmol), anhydrous potassium carbonate (2.44 g, 18 mmol), a pinch of KI and 2-chloroethanol (1.14 g, 14 mmol) were dissolved in 10 mL DMF. The mixture was refluxed at 80 °C for 48 h under nitrogen. The resulting solution was cooled to room temperature, poured into water. The product was filtered, washed with water and dried and purified by column chromatography using hexane-ethyl acetate mixture. Yield = 1.7 g (69 %) m.p: 113 °C ¹H NMR (CDCl₃) δ ppm: 7.48 (2H, m, Ar), 7.35-7.30 (4H, m, Ar), 6.92 (2H, m, Ar), 4.06 (2H, t, -OCH₂-CH₂-), 3.92 (2H, t, -OCH₂-CH₂-), 1.63 (1H, s, -OH). ¹³C NMR (CDCl₃) δ ppm: 61.45, 69.16, 114.81, 126.58, 126.72, 128.29, 128.67, 128.71, 134.21, 158.06. FTIR (KBr) (cm⁻¹): 3287, 2929, 1605, 1523, 1487, 1449, 1257, 1199, 1114, 1051, 922, 892, 829, 758, 689. FAB- HRMS m+1: 201.45

Synthesis of 2-Methyl-acrylic acid 2-(biphenyl-4-yloxy)-ethyl ester (**CM**):

Methacryloyl chloride solution (0.73 g, 7 mmol) in tetrahydrofuran (2 mL) was added very slowly to THF (10 mL) solution containing (2-biphenyl-4-yloxy)-ethanol (1 g, 4.70 mmol) and triethyl amine(0.47 g, 4.60 mmol) kept at 0 °C. The

solution was stirred for 1 h at 0 °C and then at room temperature for 6 h. The resulting salt was filtered. The solution was then concentrated and the monomer was precipitated in water, filtered, dried and purified by column chromatography using hexane-ethyl acetate mixture (v/v 95/5).

Yield = 1 g (75 %) m.p: 78 °C ¹H NMR (CDCl₃) δ ppm: 7.48 (2H, m, Ar), 7.41-7.25 (5H, m, Ar), 6.93 (2H, m, Ar), 6.08 (1H, s, -C=C-), 5.52 (1H, s, -C=C-), 4.46 (2H, t, -OCH₂-CH₂), 4.21 (2H, t, -OCH₂-CH₂), 1.88 (3H, s, -CH₃). ¹³C NMR (CDCl₃) δ ppm: 18.22, 65.91, 69.2, 114.91, 126.14, 126.53, 126.64, 126.71, 128.25, 128.63, 134.24, 136.11, 167.45 FTIR (KBr)(cm⁻¹): 3419, 3033, 2928, 2874, 1718, 1632, 1609, 1580, 1520, 1487, 1455, 1409, 1380, 1320, 1294, 1269, 1248, 1167, 1116, 1076, 1051, 1007, 910, 892, 835, 764, 718, 698, 608, 551, 507. FAB- HRMS m+1: 283.23

Free radical Polymerization of Poly 4-{4-[2-(2-methyl-acryloyloxy)-ethoxy]phenylazo}benzoic acid methyl ester P1: Free radical polymerization was carried out in THF using AIBN as initiator at 60 °C. 4-{4-[2-(2-methyl-acryloyloxy)-ethoxy]-phenylazo} benzoic acid methyl ester (**M1**) (0.36 g, 0.98 mmol) and AIBN (0.0184 g, 0.05 mmol) were dissolved in THF (2 mL). The reaction mixture was purged with nitrogen for 10 minutes. The polymerization was carried out by stirring the contents at 60 °C for 24 h. The slightly viscous liquid was cooled and precipitated into methanol. The polymer was purified by filtering and redissolving in tetrahydrofuran followed by repeated reprecipitation into methanol to remove the monomers followed by drying in vacuum at 60 °C for 24 h. Yield: 0.2 g (64 %). ¹H NMR (CDCl₃) δ ppm: 8.05-6.84 (m, Ar), 4.32-3.83 (-OCH₂-CH₂-, OCH₃), 2.25-0.83 (aliphatic). ¹³C NMR (CDCl₃) δ ppm: 17.37, 19.05, 28.85, 29.91, 44.95, 52.47, 55.79, 63.39, 65.68, 114.96, 122.59, 125.42, 130.75, 147.29, 155.28, 161.38, 162.91, 165.78, 166.74, 176.81. FTIR (KBr) (cm⁻¹): 3406, 1722, 1600, 1500, 1436, 1405, 1279, 1254, 1174, 1140, 1111, 1064, 960, 922, 861, 834, 756, 694, 661, 546.

Similarly, (0.20 g, 0.45 mmol) **M2** and (0.25 g, 0.59 mmol) **M3** were subjected to free radical polymerization under identical conditions to obtain the polymers

Poly 4-{4-[2-(2-methyl-acryloyloxy)-ethoxy]-biphenylazo}benzoic acid methyl ester (**P2**) and Poly 4-{4-[2-(2-methyl-acryloyloxy)-ethoxy]-naphthalen-1-ylazo}benzoic acid methyl ester (**P3**) respectively.

Poly 4-{4-[2-(2-methyl-acryloyloxy)-ethoxy]-biphenylazo}benzoic acid methyl ester (P2**):** Yield: 0.1 g (45 %). ^1H NMR (CDCl_3) δ ppm: 7.56-6.96 (m, Ar), 4.36-3.96 ($-\text{OCH}_2-\text{CH}_2-$, OCH_3), 2.07-0.84 (aliphatic). ^{13}C NMR (CDCl_3) δ ppm: 29.69, 52.31, 108.45, 111.37, 115.25, 122.82, 126.74, 128.82, 130.57, 155.17, 166.41. FTIR (KBr) (cm^{-1}): 3434, 1720, 1602, 1514, 1432, 1407, 1276, 1169, 1111, 1018, 862, 820, 760, 697, 464.

Poly 4-{4-[2-(2-methyl-acryloyloxy)-ethoxy]-naphthalen-1-ylazo}benzoic acid methyl ester (P3**):** Yield: 0.2 g (60 %). ^1H NMR (CDCl_3) δ ppm: 8.88-6.62 (m, Ar), 4.23-3.87 ($-\text{OCH}_2-\text{CH}_2-$, OCH_3), 1.91-0.94 (aliphatic). ^{13}C NMR (CDCl_3) δ ppm: 29.91, 55.92, 103.72, 104.23, 108.67, 109.13, 110.26, 111.82, 112.28, 113.59, 114.61, 115.15, 116.91, 119.43, 122.70, 130.58, 167.46, 172.58, 177.65, 179.44. FTIR (KBr) (cm^{-1}): 3412, 1720, 1599, 1578, 1405, 1319, 1273, 1248, 1218, 1095, 1018, 823, 771, 463.

Polymerization of Control Monomer

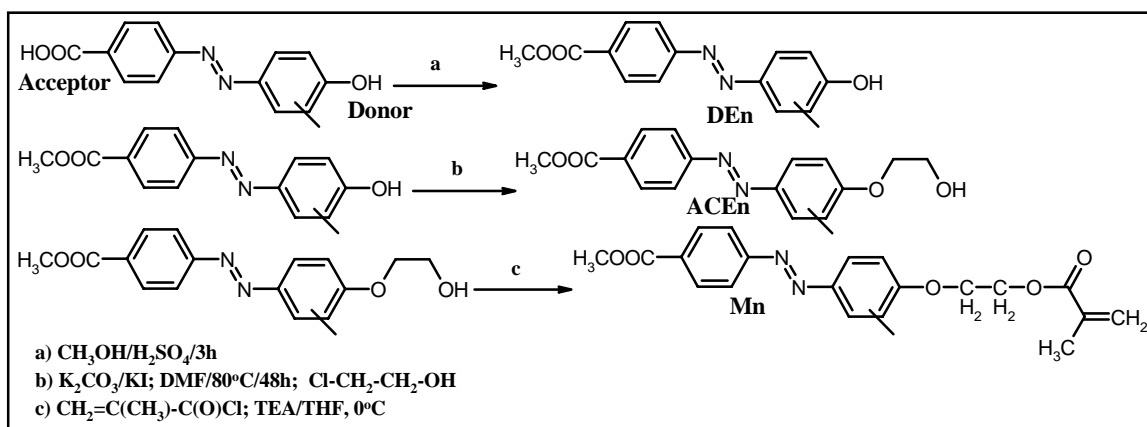
The control polymer was prepared by the same methodology as mentioned for the azo polymers using 0.58 (2 mmol) g of 2-methyl-acrylic acid 2-(biphenyl-4-yloxy)-ethyl ester (**CM**).

Poly 2-Methyl-acrylic acid 2-(biphenyl-4-yloxy)-ethyl ester (CP**):** Yield = 0.4 g (60 %) ^1H NMR (CDCl_3) δ ppm: 7.34-7.23 (m, Ar), 6.72 (m, Ar), 3.97-3.86 ($-\text{OCH}_2-\text{CH}_2-$), 1.76-0.87 (aliphatic). ^{13}C NMR (CDCl_3) δ ppm: 19.32, 34.13, 63.55, 66.24, 114.82, 126.54, 128.74, 132.63, 140.11, 158.55, 177.60. FTIR (KBr) (cm^{-1}): 3423, 2929, 1730, 1608, 1519, 1487, 1454, 1407, 1268, 1244, 1175, 1150, 1117, 1073, 922, 834, 763, 735, 694, 606, 546.

3.4 Results and Discussion

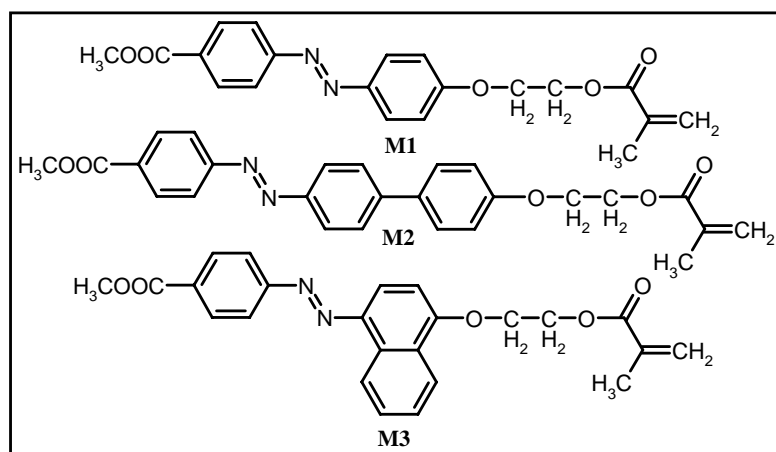
The D-A substituted azo dyes were first converted to the corresponding esters (**DE1-DE3**) by treating the carboxylic acid terminated dye with methanol in presence of sulphuric acid catalyst. The hydroxy group of these dye esters were

then coupled with 2-chloroethanol to obtain **ACE1-ACE3**. The aliphatic hydroxyl group was then converted to the methacrylate by coupling with methacryloyl chloride in presence of triethyl amine. The synthetic scheme is shown in scheme 1 and the structures of monomers are shown in scheme 2.

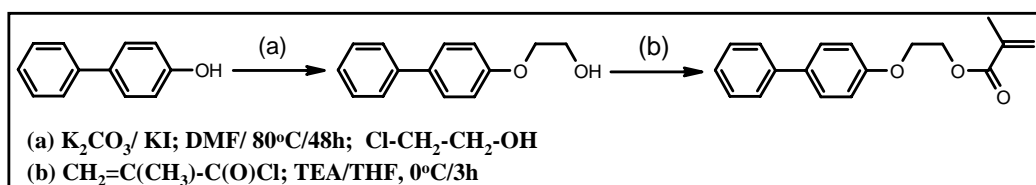


Scheme 1 Synthesis of monomers

In order to compare the properties of the polymers, a control polymer which lacks the azo linkage but containing a phenyl phenol unit was also synthesized. The scheme of synthesis of the control monomer is given in scheme 3.



Scheme 2 Structure of monomers



Scheme 3 Synthesis of control monomer

The structure of dye esters, intermediates and monomers were confirmed by various spectroscopic techniques. The ^1H NMR spectra of dye esters and monomers are given in figure 1 and figure 2 respectively. The various types of protons are labeled by alphabets. The intensity of all the peaks exactly matched with the number of protons, which confirm the formation of the expected molecules. The purity was confirmed by the SEC plots of the molecules which showed a single chromatogram. Figure 3 shows the SEC chromatogram of monomers. As expected, the elution time of the molecules increased with the decrease in the molecular weights.

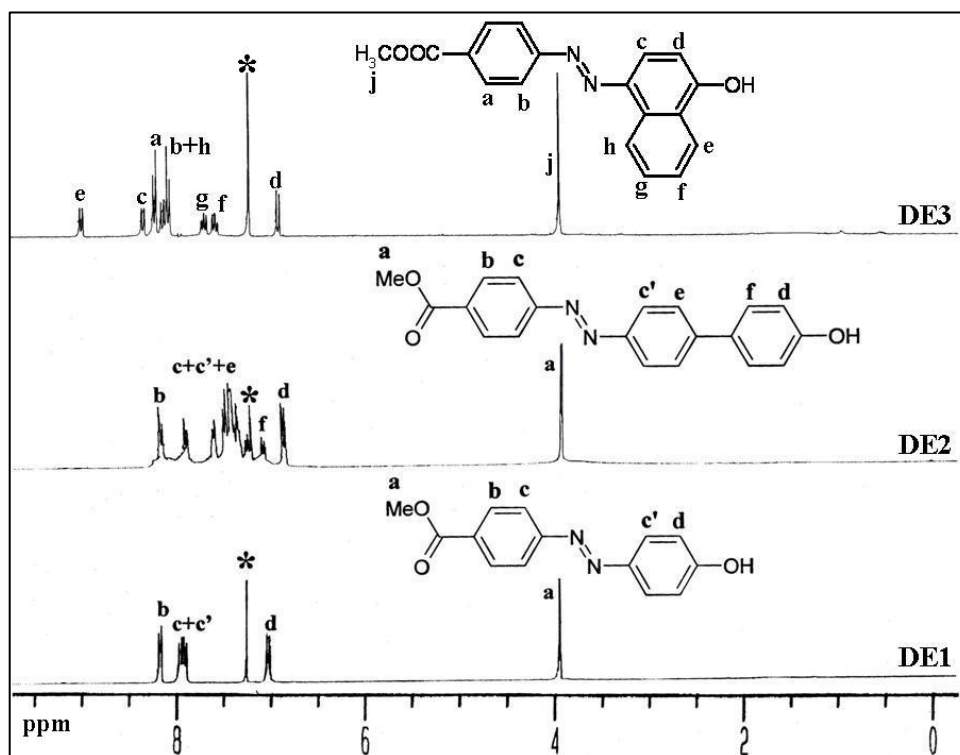


Figure 1 ^1H NMR spectra of dye esters

The samples were subsequently subjected to HRMS analysis and molecular ion peaks were obtained for M or M^{+1} radicals. Figure 4 shows the HR mass spectra of monomers. The NMR, SEC and HRMS data confirmed the structure and high purity of the synthesized molecules.

The normal free radical polymerization of the monomers were carried out by using 5 mol % AIBN as initiator in tetrahydrofuran (THF) as solvent at 60 °C. The viscous polymer solution was cooled and precipitated into methanol.

Scheme 4 shows the synthesis and structure of all the polymers. The molecular weights of azobenzene polymers and control polymer were determined by size exclusion chromatography and structural characterization using ^1H NMR and ^{13}C NMR. Figure 5 shows the SEC chromatograms of all polymers and figure 6 shows the ^1H NMR spectra of the polymers. Figure 7 shows the ^1H NMR spectra of the control monomer and control polymer.

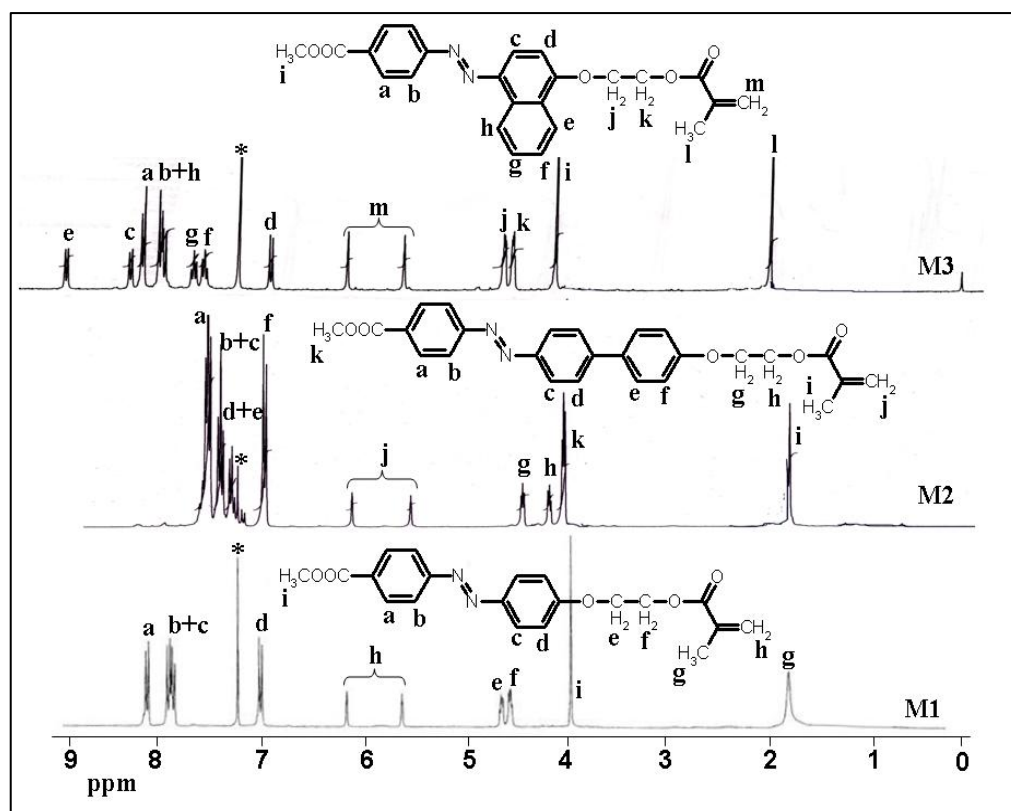


Figure 2 ^1H NMR spectra of monomers

The proton NMR shows the complete disappearance of the methacrylic double bonds upon polymerization. Table 1 gives the sample name, corresponding phenolic component and molecular weight details. The control polymer possessed highest molecular weight among the four polymers. **P2** and **P3** had low molecular weight compared to **P1**. But such low values of molecular weight prepared by free radical polymerization are typical for azobenzene containing polymers.^{15, 16} Additionally, the steric hindrance of the bulky side groups also could result in low degree of polymerization in **P2** and **P3**. The

polymers were soluble in most of the common organic solvents such as chloroform, toluene and THF.

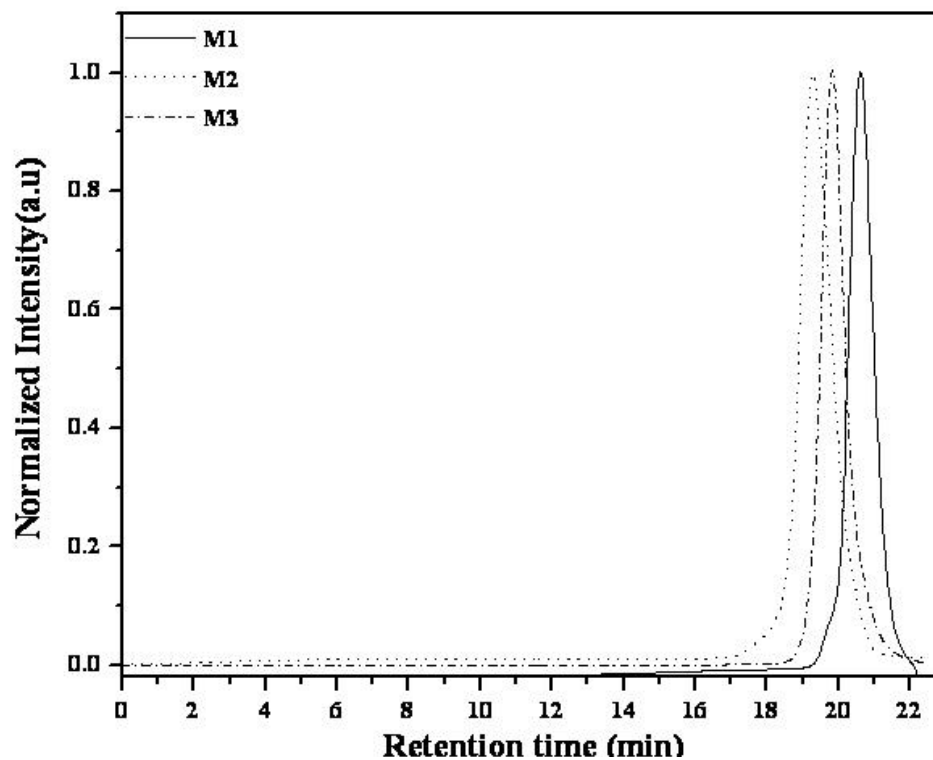


Figure 3 SEC chromatogram of monomers

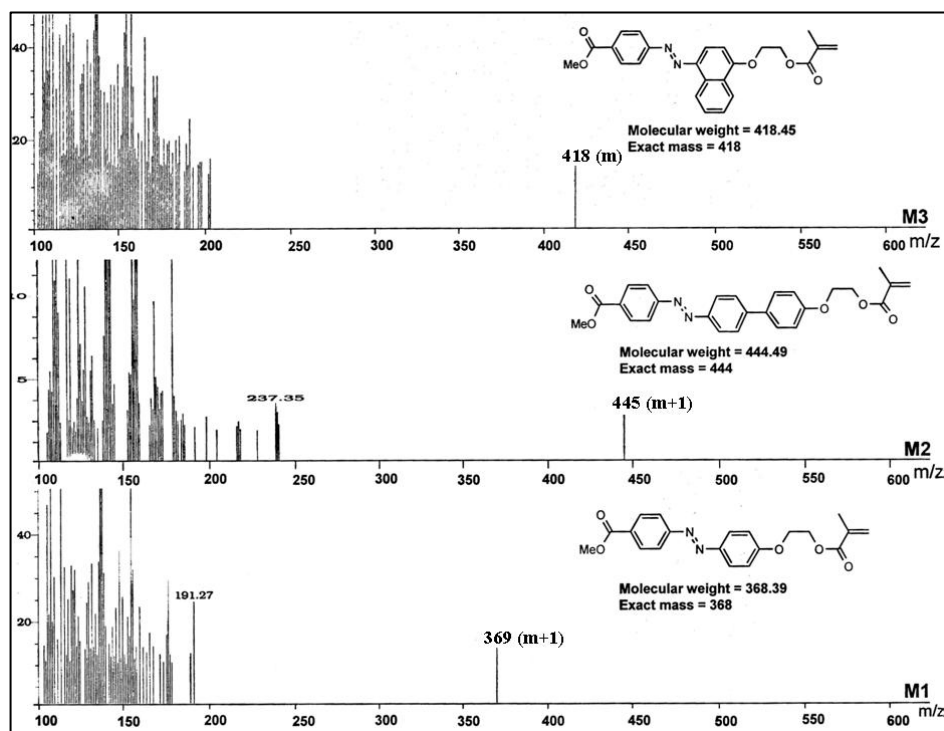
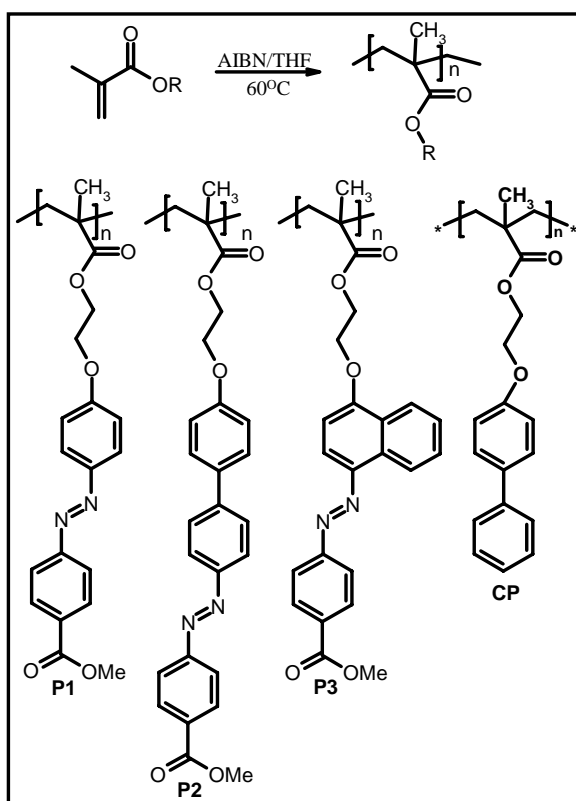


Figure 4 Mass spectra of monomers



Scheme 4 Synthesis and structure of polymers

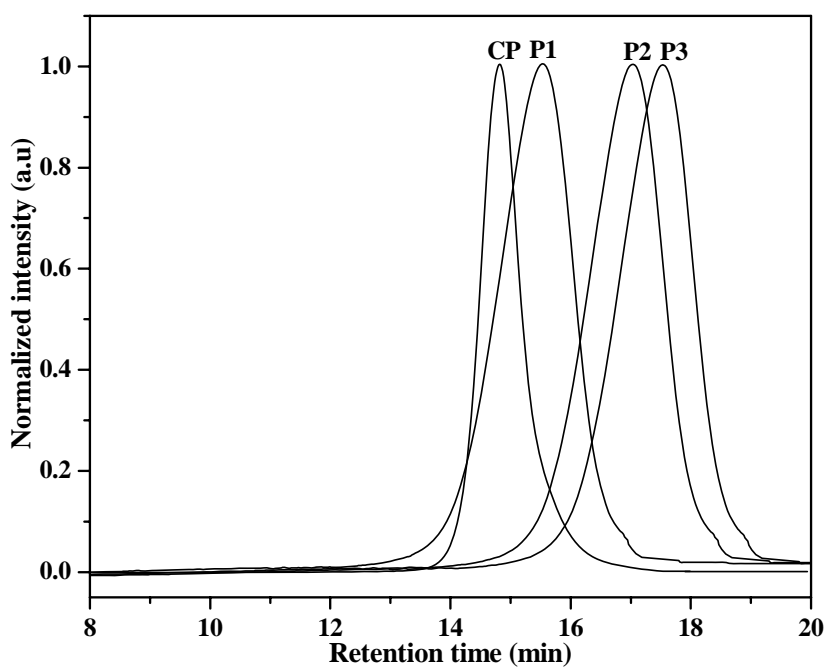


Figure 5 shows the SEC chromatograms of polymers

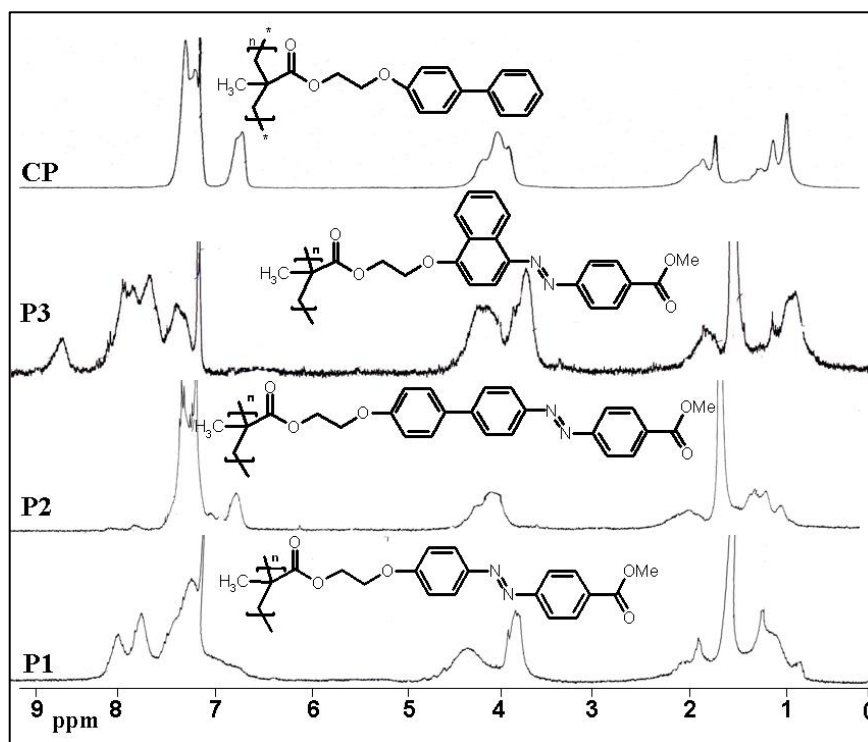


Figure 6 ^1H NMR spectra of the polymers

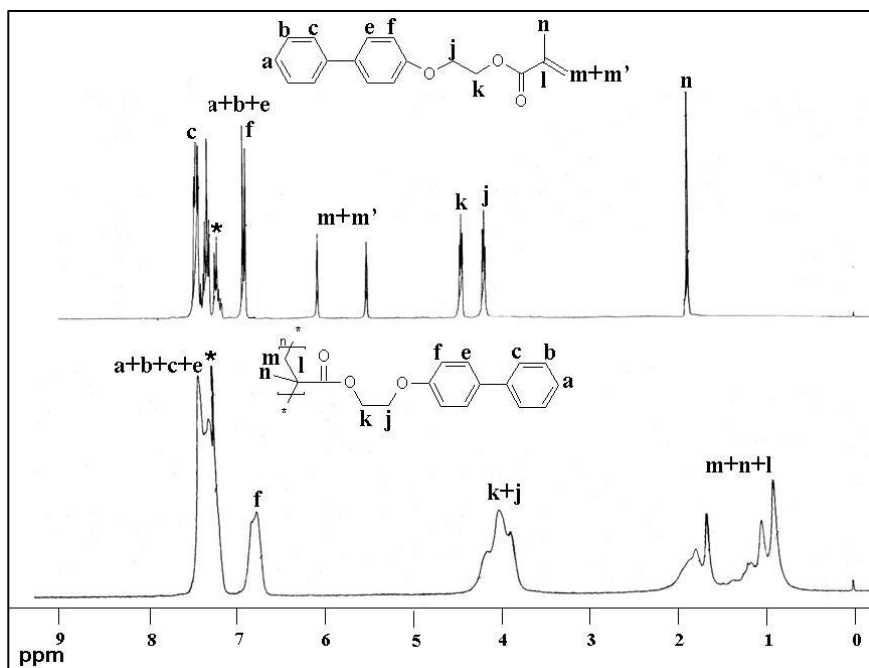


Figure 7 ^1H NMR spectra of the control monomer (CM) and control polymer (CP)

Table 1 Molecular weight data of polymers

Polymer	Phenolic Component	M _w	M _n	No of repeating units	PDI	T _D ^a (°C)
P1	Phenol	11000	6180	17	1.78	259
P2	Phenylphenol	6800	5300	12	1.28	287
P3	Naphthol	3800	2100	5	1.79	306
CP	Phenylphenol	17000	14000	50	1.21	375

a) Temperature represents 10 % weight loss in TGA measurements at heating rate of 10 °C/min under nitrogen.

3.5 Photophysical Properties

The absorption spectra of azobenzene derivatives in solution usually have two featureless absorption bands centered around 350 and 450 nm attributed to π - π^* and n - π^* transitions respectively. The UV-vis spectra of the starting fluorophores i.e. phenol, phenyl phenol and naphthol, the azobenzene ester series (**DE1-DE3**), the monomers (**M1-M3**, **CM**) and polymers (**P1-P3**, **CP**) are shown in figure 8(1), 8(2), 8(3) and 8(4) respectively and the wavelengths of absorption maximum in the UV-Vis spectra in dichloromethane are given in table 2. The absorption spectra of the starting fluorophores except phenyl phenol showed vibronic fine structures which was lost upon coupling with the azobenzene unit in the ester series and polymer. The absorption spectra of azobenzene dye esters, monomers and methacrylate polymers (figure 8) showed a weak band in the visible region and an intense band in the UV spectral region. In the case of the dye esters, the band corresponding to the π - π^* transition of the fluorophore appeared at 254 nm, 260 nm and 280 nm and the band corresponding to π - π^* transition of azo group appeared at 357 nm, 330 nm and 413 nm for **DE1**, **DE2** and **DE3** respectively. For the azobenzene methacrylic

monomers, the peak at 255 nm, 256 nm and 280 nm corresponded to the π - π^* transition of the fluorophore and the peak at 359 nm, 325 nm and 415 nm corresponded to the π - π^* transition of the azo group for **M1**, **M2** and **M3** respectively. For polymers **P1**, **P2** and **P3**, the peak at 256 nm, 259 nm and 280 nm corresponded to the π - π^* transition of the corresponding fluorophores namely phenol, phenyl phenol and naphthol respectively. **P1** showed a weak band with maximum around 440 nm which is attributed to the lowest singlet state of $n\pi^*$ nature and the sharp band with maximum around 356 nm which is attributed to π - π^* transition of the azo group. The intense absorption maxima corresponding to the π - π^* transition were observed at 320 nm for **P2** and 415 nm for **P3**. In **P2** – the phenyl phenol based polymer, the π - π^* band is blue shifted to 320 nm compared to 356 nm in **P1**. Eventhough conjugation is more in **P2**, the two rings are not coplanar, thus effectively decreasing overall conjugation compared to simple phenol based system.^{17, 18} On the other hand, in the naphthol-based polymer **P3**, the π - π^* band is red shifted to 415 nm; the $n\pi^*$ band is almost wholly overlain by the bathochromically and hyperchromically displaced π - π^* band.¹⁹ The main transition at 415 nm could be assigned to the π - π^* band based on their bathochromic shift in solvents of increasing polarity. For the control polymer **CP**, the π - π^* transition band of the fluorophore appeared at 262 nm. The starting fluorophores (phenol, phenyl phenol and naphthol), azobenzene dye esters (**DE1- DE3**), methacrylic monomers (**M1-M3**, **CM**) as well as the polymers (**P1-P3**, **CP**) were excited at the absorption maxima wavelength corresponding to the π - π^* transition of the fluorophore, π - π^* and the $n\pi^*$ transition of the azo group in the respective UV-Vis spectra and their emission were recorded. The emission intensities when excited at the $n\pi^*$ transition of the azo group were negligible for the azobenzene molecules and polymers. Figure 9 also gives a comparison of the emission spectra of 0.1 OD λ_{\max} solutions of the starting fluorophores phenol, phenyl phenol and naphthol (a), azobenzene dye esters (**DE1**, **DE2** and **DE3**) (b) along with the polymers

(P1, P2 and P3) (c), showing their relative intensities. From figure 9a, it can be seen that naphthol has the highest luminescence intensity among the three fluorophores as well as among the whole series of azo dye esters and polymers. Upon coupling with the azobenzene unit, its luminescence intensity was reduced drastically. For phenol, the emission maxima appeared at around 298 nm and for phenyl phenol it was around 330 nm. α -naphthol showed a fine structure with emission maxima at around 341 nm with two weak bands at 327 nm and 356 nm. In the case of dye esters, the phenol based ester **DE1** exhibited negligible emission whereas **DE2** and **DE3** showed fluorescence emission when excited at π - π^* transition of the fluorophore as well as the π - π^* transition of the azo group.

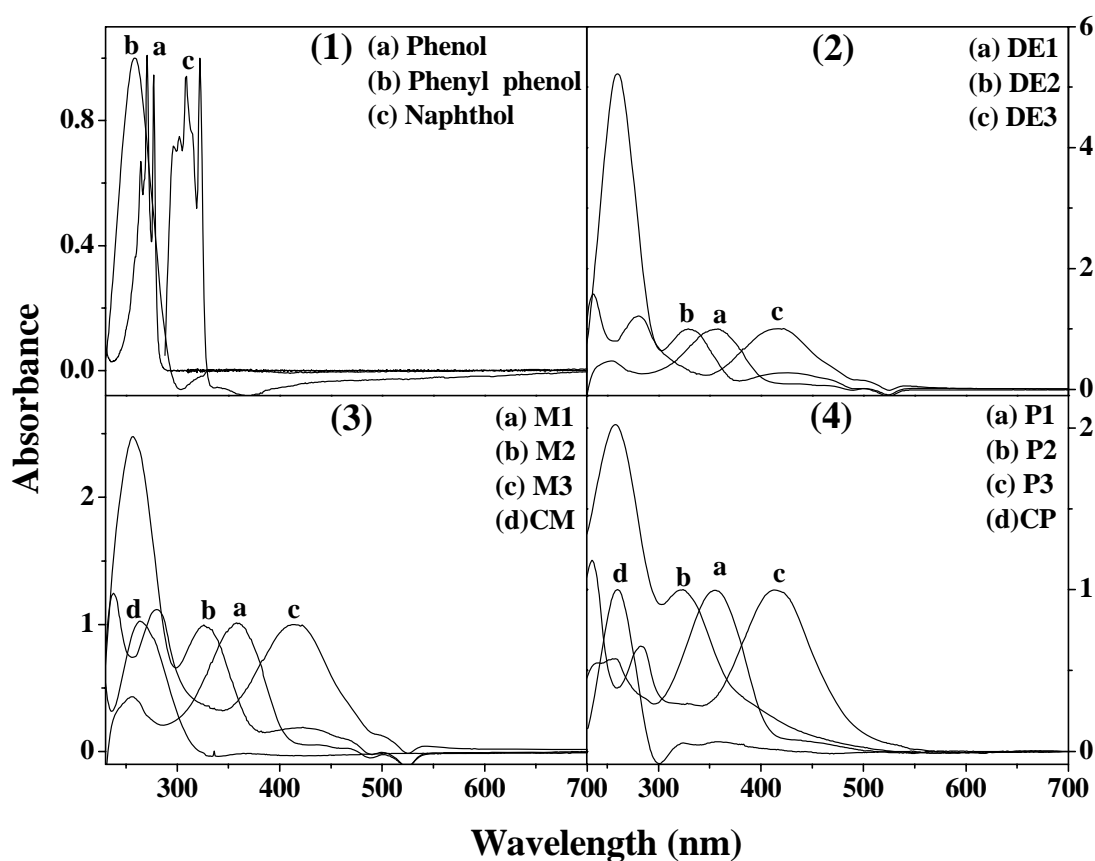


Figure 8 Absorption spectra of (1) fluorophores (2) dye esters (3) monomers (4) polymers

Table 2 Absorption data

Sample	λ_{\max} nm (ϵ , M^{-1} , cm^{-1})		
P1	256 (50820)	355 (18030)	441 (1260)
P2	259 (66180)	320 (48980)	396 (11050)
P3	280 (9070)	415 (10490)	-
CP	262 (47940)	-	-
DE1	254 (8210)	357 (137790)	440 (28610)
DE2	260 (16930)	330 (96700)	427 (28540)
DE3	280 (39750)	413 (18190)	-

DE1 exhibited an emission band at around 440 nm with a shoulder at 407 nm when excited at the wavelength corresponding to the π - π^* transition of the azo group. **DE2** when excited at 260 nm showed emission at 330 nm whereas when excited at 330 nm, the emission appeared at around 400 nm. In the case of **DE3**, when excited at 280 nm, the fine structured emission pattern observed for naphthol was retained even after coupling with the azo group and peaks at around 328 nm, 340 nm and 358 nm which resulted from the azolinkage and additional peaks at 378 nm, 394 nm and 455 nm were observed. But when excited at 415 nm, the emission band appeared at 468 nm for **DE3**. The methacrylic monomers and polymers followed the same pattern of emission as their precursors but with less intensity. Incorporation of the methacrylic functionality quenched the fluorescence intensity drastically but the polymers showed better emission property than their corresponding monomers. The emission quantum yield values at excitation wavelength corresponding to the π - π^* transition of the azobenzene unit were determined in dichloromethane (DCM) for the polymers, monomers and azodye esters using quinine sulphate as standard and are given in table 3. **DE2** had the highest quantum yield ϕ_f of 0.22

upon excitation at the π - π^* transition of the azobenzene unit (330 nm). This quantum yield value is quite high when compared to the normally reported values of quantum yields of azobenzene systems ($10^{-7} - 10^{-5}$)²⁰⁻²² especially when considering that these azo dye esters and polymers are fluorescent at ambient temperature and without any photo irradiation required. Comparing the emission intensities of **DE2** with that of the starting fluorophore phenyl phenol, a four fold *increase* was seen in the fluorescence intensity upon excitation at the π - π^* value of the azobenzene unit (330 nm), whereas the emission at the π - π^* of the fluorophore (260 nm) remained the same. Among the dye ester series **DE3**, the naphthol based ester possessed the second next quantum yield and the phenol based ester **DE1** possessed the least value.

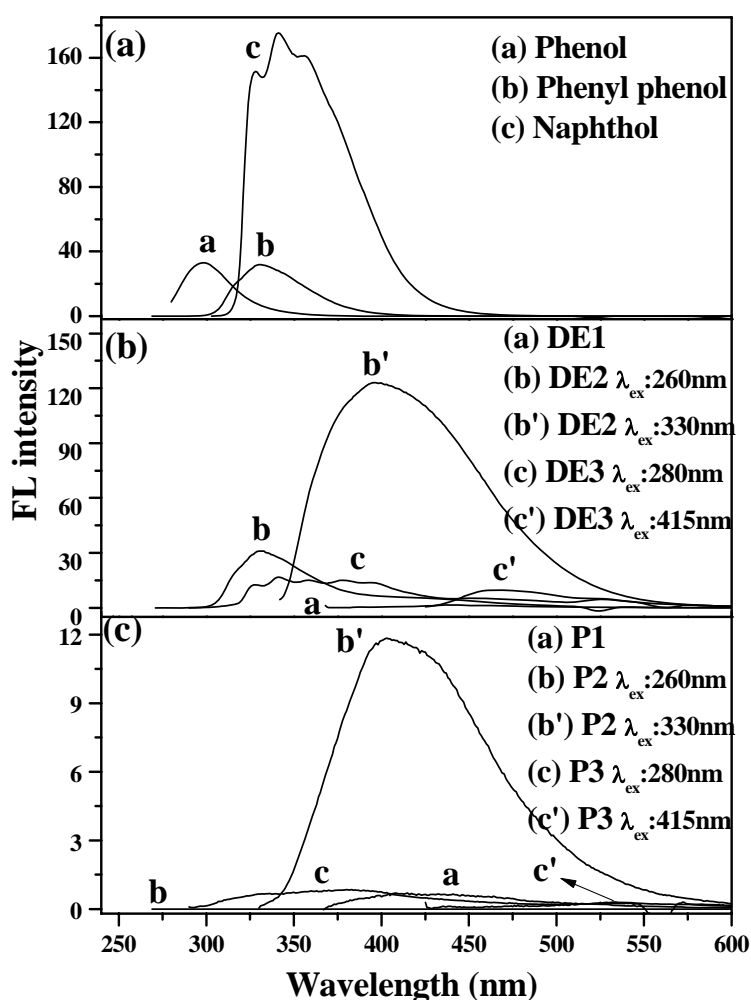


Figure 9 Emission spectra of fluorophores (a), dye esters (b) and polymers (c)

Phenyl phenol has an interesting molecular geometry where the balance between π electron conjugation (which favors the planar structure) and repulsion between ortho hydrogen atoms (which favors the twisted conformation) causes them to adopt a nonplanar and twisted ground state structure. However, upon excitation into the lowest energy singlet excited state the molecule becomes planar in spite of the steric repulsion.^{23,24} Any molecular substitution that helps in increasing the planarity will result in an enhancement of fluorescence emission. Attempts to vary the central torsion angle in biphenyl rings have included introduction of bulky groups at the ortho position or more recently, by building the biphenyl bridge into a macrocyclic polyether of variable size.^{25, 26} These approaches tend to rigidify and thereby prevent the biphenyl chromophore from approaching a planar structure.

Table 3 Emission data

Sample	Emission maxima (λ_{\max} , nm)		Quantum yield (π - π^* transition of the azo unit) Φ_{FL}
	π - π^* transition of the aromatic unit	π - π^* transition of the azo unit	
DE1	-	407	0.002
DE2	330	400	0.221
DE3	378	468	0.018
M1	-	405	0.001
M2	396	434	0.004
M3	397	476	0.004
CM	332	-	0.075
P1	-	408	0.001
P2	398	402	0.024
P3	394	476	0.001
CP	332	-	0.17

In fact, using the latter approach researchers were able to successfully show that the fluorescence quantum yield of the biphenyl macrocyclic polyether bridge was less compared to the parent biphenyl under similar conditions due to the inability of the former to attain a planar structure in the excited singlet state. In **DE2** on the other hand, the incorporation of phenyl phenol as part of an azobenzene unit has enabled it to attain a less twisted structure even in the ground state. The optimized geometry of **DE2** and starting fluorophore phenyl phenol in the gas phase were calculated using AM1 calculations in the Titan Version 1 program from Wavefunction. Figure 10 shows a comparison of the structures in the ground state for phenyl phenol and **DE2**.

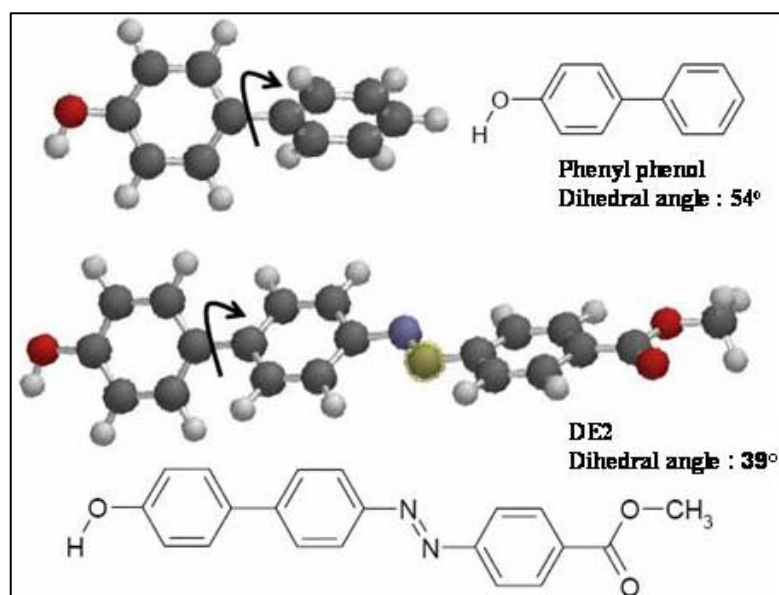


Figure 10 Molecular models of phenyl phenol and **DE2** by AM1 calculations showing the change in the ground state dihedral angle of the biphenyl unit.

The ground state biphenyl in vacuum gave a dihedral angle of 54° whereas under similar conditions the value was 39° for **DE2** clearly showing that the two rings of the phenyl phenol unit have become more planar upon incorporation of one of the ring as part of an azobenzene unit.

Comparing the fluorescence behavior of the polymers, **P1** gave a very weak fluorescence with a quantum yield of 1×10^{-3} , centered at around 408 nm with a shoulder at 432 nm upon excitation at the λ_{max} value of 356 nm. **P2** had

the highest emission among the polymers with maxima centered at 402 nm upon excitation at the λ_{max} value of 320 nm. Its emission at π - π^* of the fluorophore was almost completely quenched, but that at π - π^* of the azobenzene unit remained, though reduced in intensity compared to **DE2**. It had a quantum yield ϕ_{FL} of 0.02. **P3** had very low quantum yield of emission, similar to that shown by **P1** (ϕ_{FL} of 1×10^{-3}) upon excitation at its λ_{max} value of 415 nm. One reason for the higher fluorescence intensity for the ester series compared with the respective polymers lies in the ability of these p-hydroxy azoderivatives to exist in the tautomeric hydrazone form, which is known to exhibit fluorescence behavior.^{22, 27} Figure 11 shows the normalized absorption, excitation and fluorescence spectra of **P2** in dichloromethane at a concentration of 1×10^{-6} M.

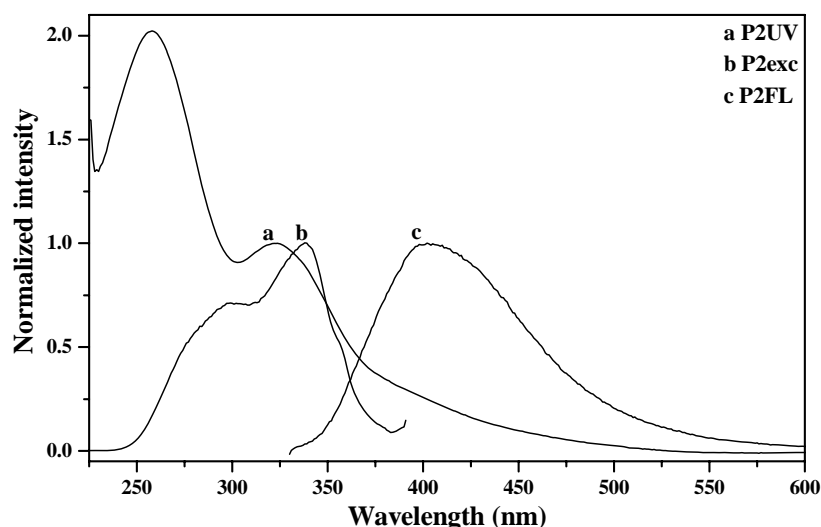


Figure 11 Normalized absorption (a), excitation (b) and fluorescence (c) spectra of **P2** in dichloromethane at a concentration of 1×10^{-6} M

The emission spectra were independent of the excitation wavelength and were collected following excitation at 320 nm corresponding to the $S_0 \rightarrow S_2$ transition. The fluorescence spectra has a reasonable mirror symmetry with the $S_2 (\pi\pi^*) \leftarrow S_0$ absorption band. The excitation spectra were recorded while monitoring the emission intensity at the fluorescence λ_{max} value of 402 nm. The excitation spectra were independent of the emission wavelength and mostly matching the absorption spectra in the $S_0 \rightarrow S_2$ spectral region. This indicates that

the azo unit is the emitting species and the emissions are assignable to the transition from the S_2 to the ground state. The observation of S_2 fluorescence is a direct evidence of violation of Kasha's rule.

3.6 Variable Concentration Fluorescence Measurements

The dye esters and polymers were subjected to variable concentration absorption and fluorescence measurement in dichloromethane at concentrations ranging from 6×10^{-5} to 1×10^{-3} M. The UV-Vis spectra did not show any change in either the wavelengths or the shapes of the absorption signals, except for increased intensity, indicating that no ground state intermolecular aggregates are formed. The phenol based dye ester and polymer did not show any appreciable emission or any significant change in the spectral pattern. Changes were observed in the fluorescence spectra of phenyl phenol based dye ester and polymer when the concentration was increased. Figure 12 a and b shows variable concentration fluorescence measurement carried out for **DE2** and **P2** respectively in dichloromethane at concentrations ranging from 6×10^{-5} to 1×10^{-3} M. From figure 12a, it can be seen that initially, as the concentration increases the fluorescence intensity also increases and further increase results in partial concentration quenching in the case of **DE2**. Also at higher concentration, an additional peak appears at higher wavelength (535 nm). In the case of **P2**, a 1×10^{-6} M solution had fluorescence λ_{\max} centered at 402 nm whereas 6×10^{-5} M solution has the λ_{\max} centered at 420 nm. The fluorescence intensity was proportional to concentration from 1×10^{-6} M to 6×10^{-6} M after which fluorescence self-quenching occurred. Upon further increase of concentration the λ_{\max} value was further red shifted to 498 nm for the highest concentration of 1×10^{-3} M with almost complete quenching of fluorescence. Figure 13a and 13b shows the variation in the total emission area and emission maxima as a function of concentration for **DE2** and **P2** respectively. The integrated intensity gives a more complete measure of the spectra rather than the peak intensity.^{28, 29}

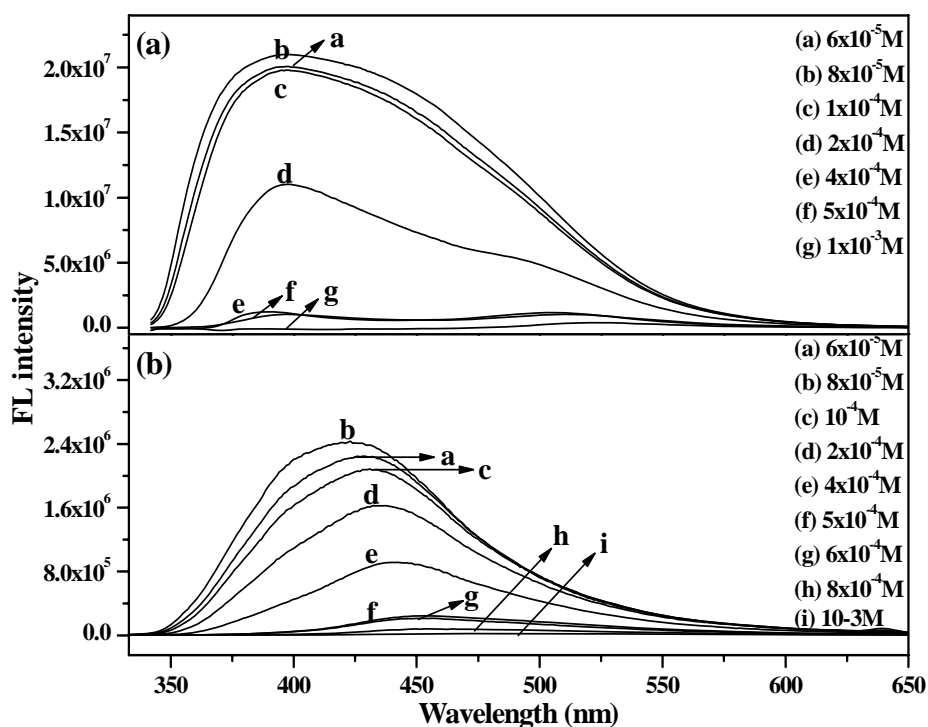


Figure 12 Variable concentration fluorescence spectra (a) DE2 (b) P2

In both cases there is a sudden change in both the area as well as emission maxima value occurring over a small concentration window, with fairly good matching of the point of steep variation. This sudden variation is suggestive of some kind of cooperative effect like aggregation, interchain exciton formation etc.²⁹ The concentration dependant fluorescence measurement was done for the control polymer also. The absorption spectrum showed an increase in intensity with concentration as expected. However no change in emission maxima was observed with increase in concentration. In the emission spectra, the fluorescence was proportional up to a concentration of $5 \times 10^{-5} \text{ M}$ after which partial self quenching occurred. Figure 14 shows a variable concentration fluorescence measurement carried out for control polymer (CP) in dichloromethane at concentrations ranging from 10^{-6} M to 10^{-3} M .

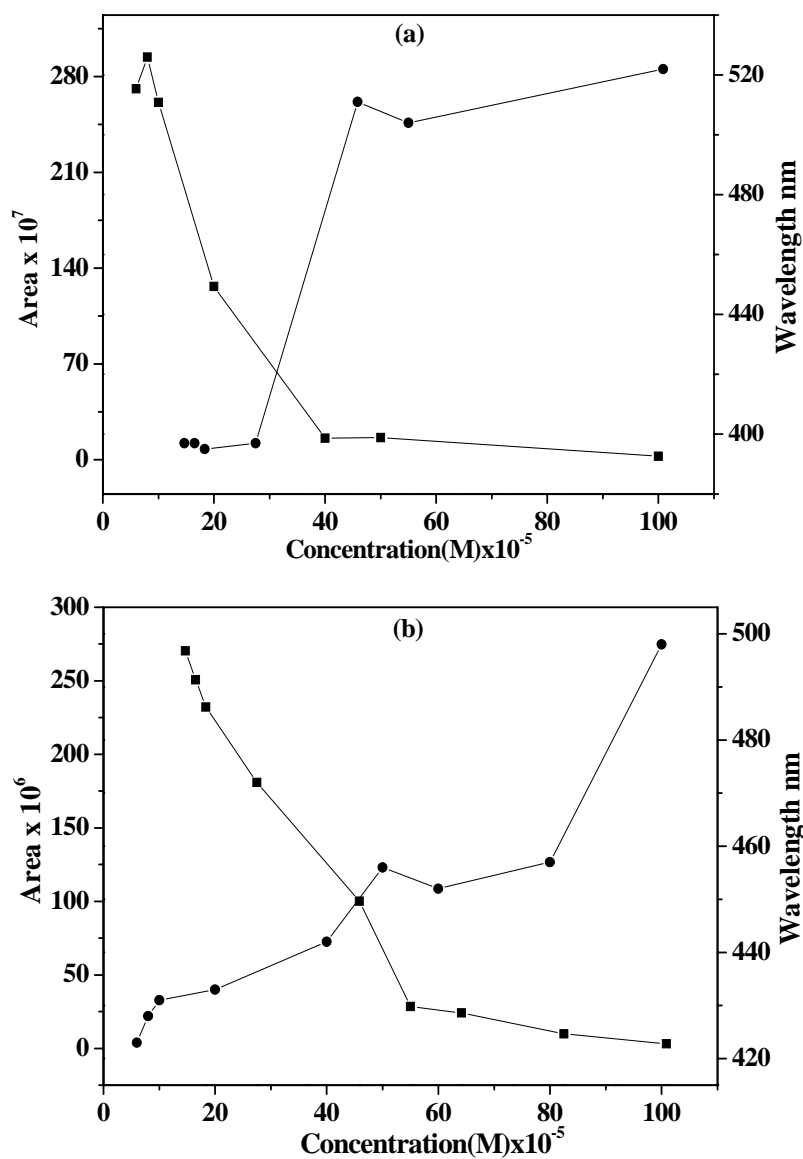


Figure 13 Variation in the total emission area and emission maxima as a function of concentration (a) DE2 (b) P2

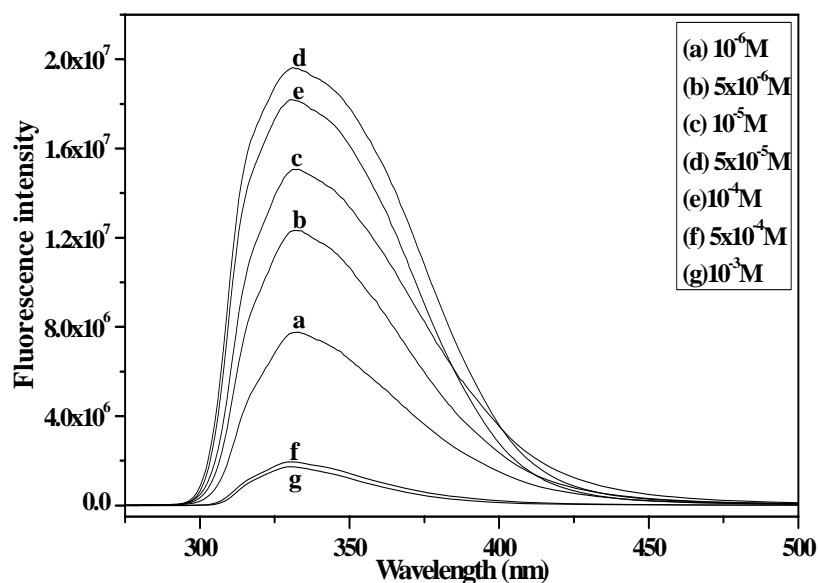


Figure 14 Variable concentration fluorescence spectra for control polymer (CP) in dichloromethane

3.7 Photoisomerization Studies

The polymers were irradiated using the 360 nm band-pass filtered output of a 200 W high-pressure mercury lamp. The dichloromethane solutions of the polymers (concentration- 1×10^{-6} M) were irradiated for a total time period of 150 min and the extent of isomerization was followed by recording the absorption spectra at equal intervals of 30 min. After attaining the photostationary state, samples were subjected to dark incubation. The spectral changes following photochemical conversion of the trans \rightarrow cis on irradiation of **P1**, **P2** and **P3** are shown in figure 15.

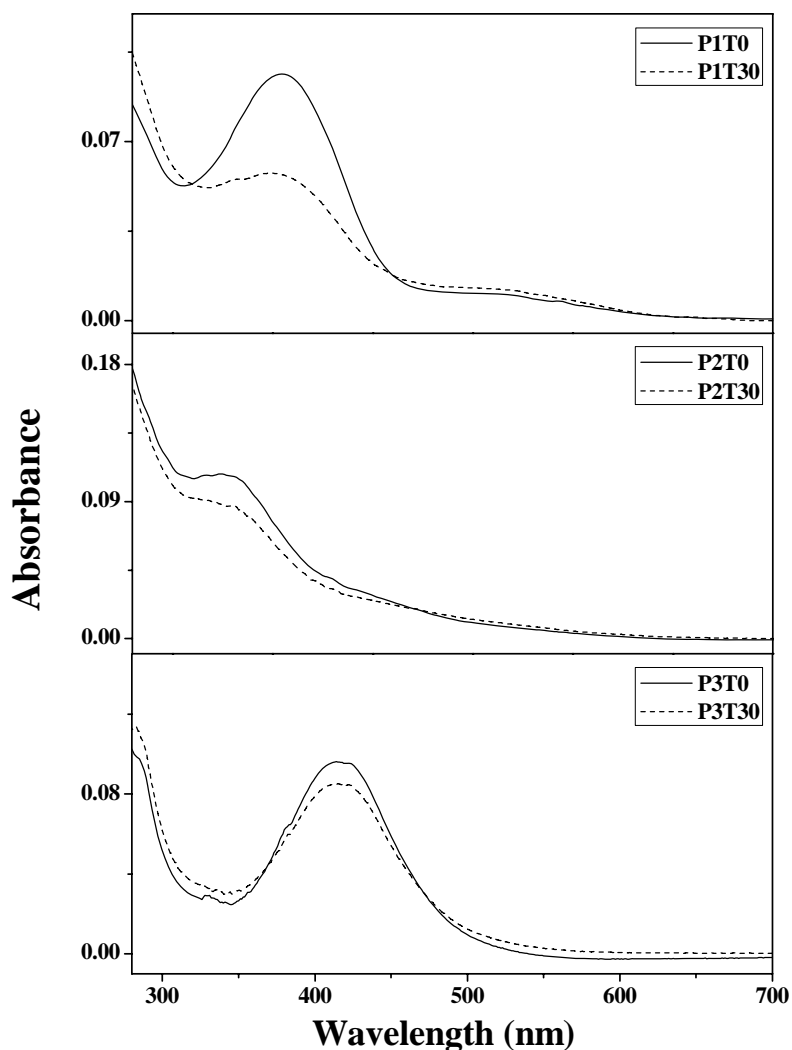


Figure 15 Change in absorption spectra of **P1**, **P2** and **P3** after irradiation for 30 min with light of wavelength 360 nm in dichloromethane solution of concentration $10^{-6}M$

A decrease of the peak at 355 nm followed by increase at 448 nm was observed with two isosbestic points at 309 and 409 nm for **P1**. Similarly the absorbance at 320 nm was decreased with an increase at 440 nm and two isosbestic points at 305 nm and 393 nm for **P2**. In the case of **P3**, the absorbance at 415 nm decreased with increase in the cis band with isosbestic points at 370 nm and 472 nm. Prolonged irradiation (> 30 minutes) led to deviation from the two isosbestic points in the UV-Vis spectra. NMR spectra recorded after 150 minutes of continuous irradiation did not indicate any decomposition and also,

the UV-Vis spectrum of the 150 min irradiated sample taken after 7 days of incubation in the dark, showed almost complete recovery indicating that no other side reactions have taken place. The extent of conversion to the cis isomer after irradiation, calculated based on the decrease in intensity of the $\pi-\pi^*$ peak maxima, was only around 40 % for **P1**, 17 % for **P2** and 11 % for **P3** whereas the highly fluorescent phenyl phenol based dye **DE2** underwent 14 % under identical conditions.

The effect of UV irradiation on emission behavior was also analyzed. The fluorescence spectra showed a two fold enhancement in the intensity without any shift in peak wavelength after UV irradiation for both **DE2** and **P2** in dichloromethane solution of concentration 10^{-6} M. Figure 16 shows the increase in fluorescence intensity for **P2** which became stable after ~ 150 min of irradiation. The fluorescence intensity slowly relaxed back to the original unirradiated value after about 7 days of incubation in the dark. The UV-Vis spectra also relaxed back to the original value after 7 days of dark incubation.

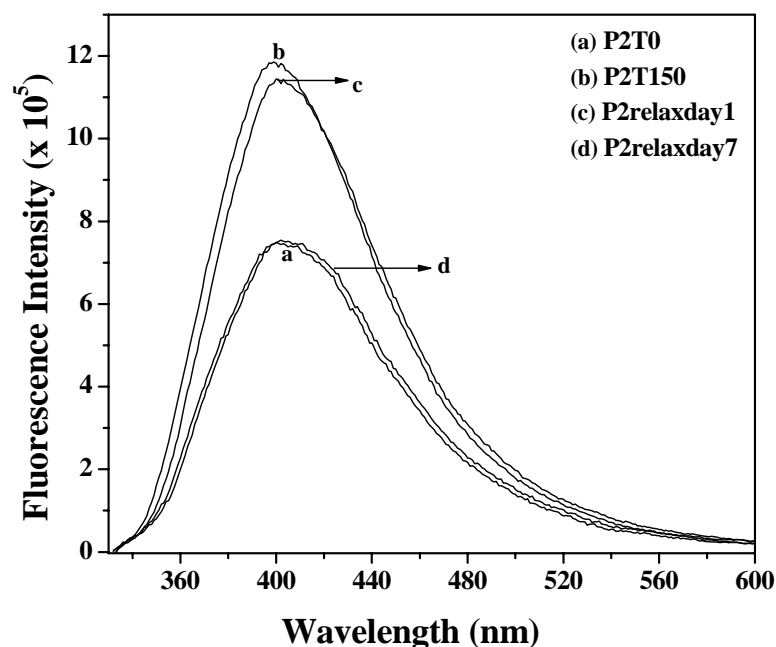


Figure 16 Change in emission spectra of **P2** upon irradiation and dark incubation in dichloromethane solution of concentration 10^{-6} M

A similar trend was observed for **DE2** and **P3** and figure 17 shows the change in emission upon UV irradiation. **DE2** exhibited a 1.3 fold increase in fluorescence intensity after 150 minutes of UV irradiation whereas **P3** showed a 6 fold increase.

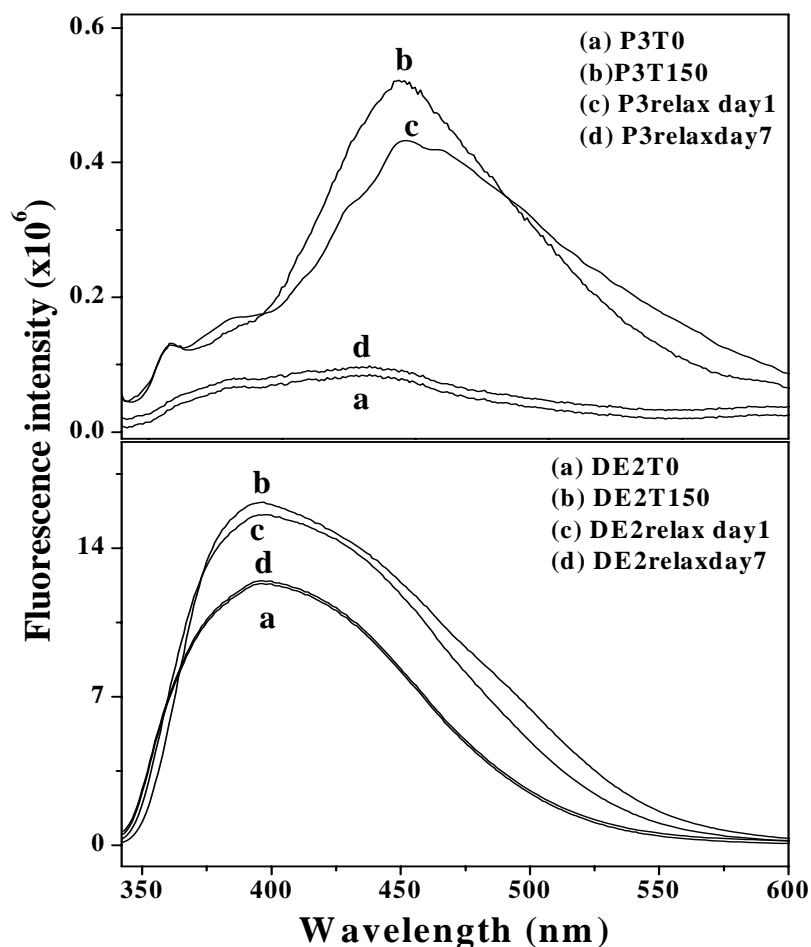


Figure 17 Change in emission spectra of **DE2** and **P3** upon irradiation and dark incubation in dichloromethane solution of concentration $10^{-6}M$

In order to understand the effect of trans-cis isomerization on fluorescence intensity, a blank experiment was done with the control polymer (**CP**) that was structurally analogous to **P2** but without the N=N unit in it. The dichloromethane solution of control polymer of concentration $1 \times 10^{-6} M$ was irradiated with the same wavelength for the same period of time. The emission spectra of the control polymer under similar conditions of irradiation did not show any variation and figure 18 shows the emission spectra of the control

polymer. Therefore, it can be concluded that the fluorescence enhancement of **P2** is associated with the trans to cis isomerization with respect to the N=N bond present in **P2**. In the literature, the fluorescence enhancement upon cis isomerization has been attributed to inhibition of photoinduced electron transfer (PET).¹⁰ The cis isomer that is formed upon photoisomerization has a nonplanar structure for the aromatic rings that are connected directly to the azo nitrogen atoms. This nonplanarity across the N=N reduces the effective conjugation of the lone pair of electrons on the nitrogen with the π electrons of the fluorophore, thereby inhibiting the PET mechanism. Since the extent of conversion to the cis isomer is very low (~17 %) we do not see a very high enhancement in fluorescence upon photoisomerization like those reported by others.

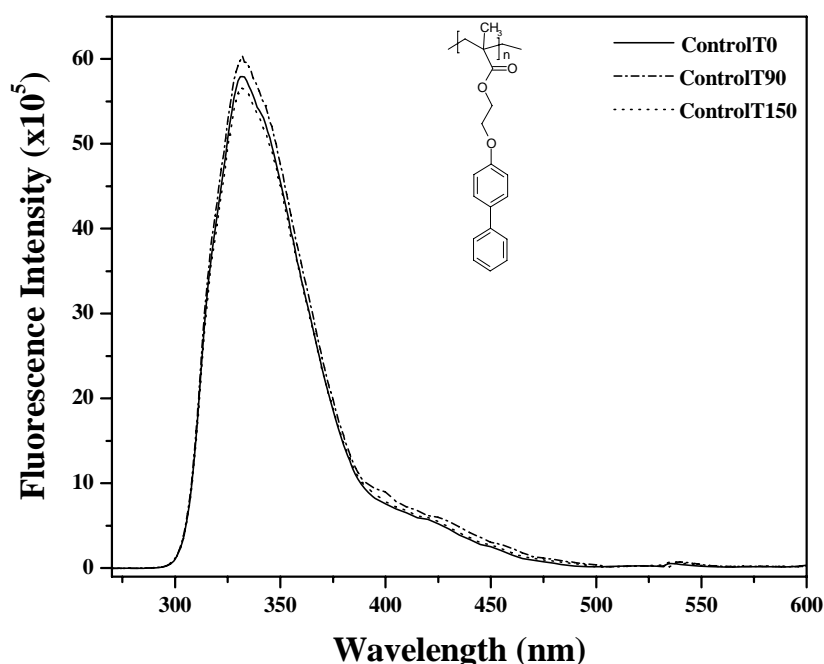


Figure 18 Emission spectra of control polymer (CP) in dichloromethane solution of concentration $10^{-6}M$ at various intervals of irradiation.

The most concentrated solution i.e. $1 \times 10^{-3} M$ of both **P2** and **DE2** in dichloromethane was exposed to continuous UV irradiation at 360 nm and their fluorescence spectra were recorded after varying intervals of time. Figure 19a and 19b shows the irradiation spectra of **P2** and **DE2** respectively. The $1 \times 10^{-3} M$ solution of **P2** which was almost non-fluorescent due to concentration

quenching, started fluorescing again at a much higher wavelength of 532 nm upon irradiation (figure 19a).³⁰ In the case of **DE2**, the fluorescence was not fully quenched for the 1×10^{-3} M sample but had two relatively sharp peaks centered at 390 and 535 nm with a shoulder at 569 nm (figure 19b). Upon continuous irradiation, the aggregation peak at 535 nm started decreasing while the emission from the molecularly dissolved species at 390 nm started increasing in intensity.

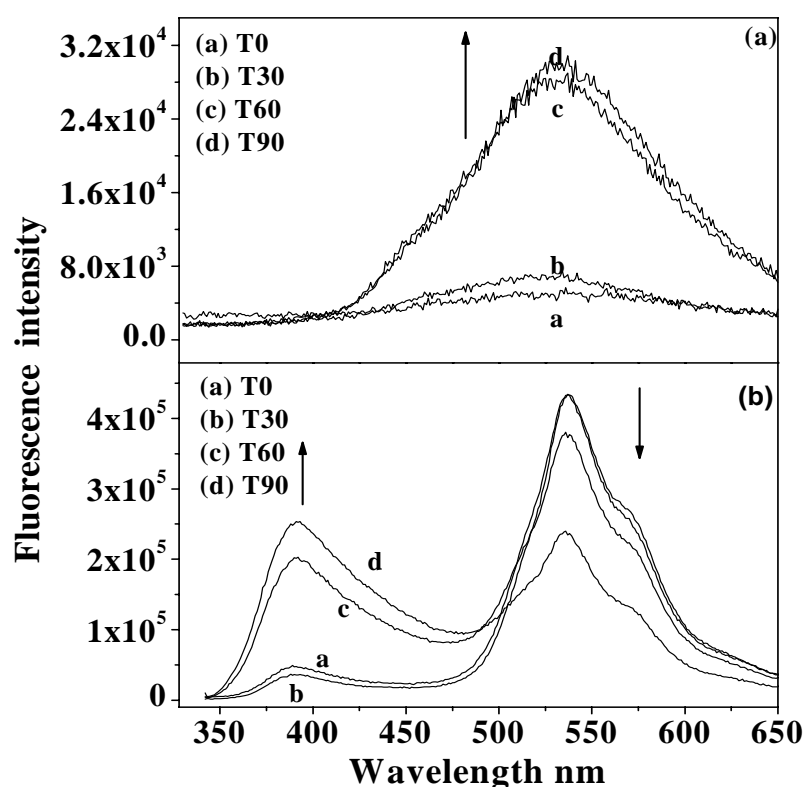


Figure 19 Changes in the fluorescence emission of **P2** (a) and **DE2** (b) (1×10^{-3} M in dichloromethane) upon irradiation

A similar observation was reported by Mina Han et. al for their amphiphilic azobenzene molecule which had a biphenyl fluorophore and long alkyl chain whose highly concentrated non-fluorescent sample exhibited two discrete emission peaks centered at 420 and 546 nm after UV irradiation.³⁰ They showed the existence of aggregates using SEM and TEM as well as fluorescence microscopic images.

3.8 Morphological Studies

In order to understand the aggregation behavior of polymers, SEM and TEM measurements were done by drop casting the samples from tetrahydrofuran (THF) solution. The solution studies ie, the absorption and fluorescence measurements were done in dichloromethane solvent; however dichloromethane has been shown to disintegrate the formvar coating on the TEM grids. Therefore tetrahydrofuran and not dichloromethane was used to prepare samples for drop casting for the SEM and TEM analysis. The polymers had showed similar behavior in tetrahydrofuran and dichloromethane for solution studies. The polymer films for SEM micrograph analysis were prepared by drop casting polymer solution of concentration 10^{-3}M on glass slides and allowing it to evaporate under atmospheric conditions. Spontaneous pore formation was observed for phenol and phenyl phenol based azobenzene side chain polymers **P1** and **P2** respectively. These observations were perfectly reproducible, films of each sample prepared on different occasions under identical conditions gave similar pore dimensions in their SEM micrographs. Observation under the optical microscope also revealed the honeycomb patterns produced by these polymers. Figure 20 shows the microscopic images of polymers **P1** and **P2** and it is clear from the images that these polymers form porous structures. No pattern was observed under the optical microscope for naphthol based polymer **P3** and control polymer **CP**. SEM pictures of polymers **P1**, **P2**, **P3** and **CP** are shown in figure 21. The polymers **P1** and **P2** showed a typical microporous membrane type texture whereas the **P3** and control polymer **CP** appeared more like a phase separation. Also none of the dye esters gave any specific morphology. The average pore size was calculated from SEM. For **P1**, the size varied from 0.75 to 2.16 μm and for **P2**, it was in the range of 0.21 to 0.84 μm .

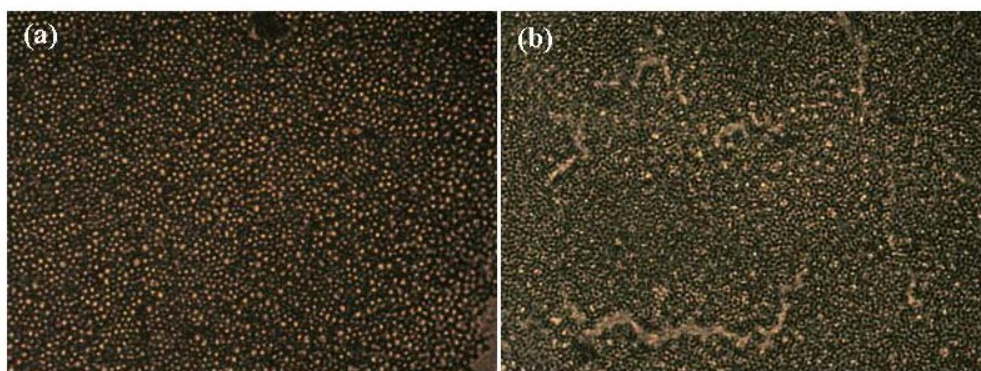


Figure 20 Microscopic images of **P1** (a) and **P2** (b). Samples were prepared by drop casting the polymer solutions of concentration $10^{-3}M$ onto a glass slide.

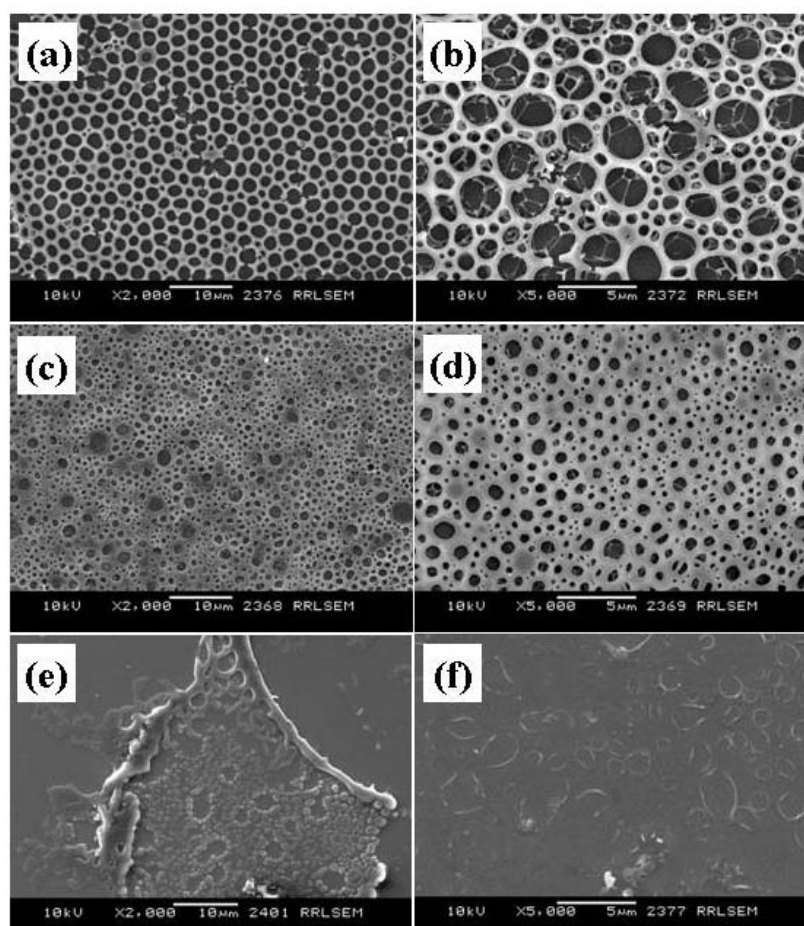


Figure 21 SEM images of **P1** (a & b) **P2** (c & d), **P3** (e) and **CP** (f). Samples were prepared by drop casting the polymer solutions of concentration $10^{-3}M$ onto a glass slide

The porous morphology was found throughout the sample and not confined to any small areas of edges. In the case of **P2**, a straight through pore like morphology with very less three dimensional networking can be observed whereas for **P1**, more uniform and circular, densely packed three dimensional honeycomb patterns was observed. Several groups have reported the formation of 3D microporous films and submicron films by means of the water assisted method.^{36, 37} According to their speculations, the ordered structures are formed by evaporating solutions of a simple coil-like polymer in a volatile solvent, in the presence of moisture with forced air flow across the solution surface. A hexagonally packed array of holes then forms on the surface of the polymer. When the solvent having lower density than water is used, the hexagonal array propagates through the film. Different from this water assisted method, Ishizu et al. reported a new method to construct the ordered microporous films based on solvent induced mechanism by casting PS-block-PBMA (SB) diblock copolymer from hot cyclohexane solution at 20 °C under atmospheric humidity, without any forced air flow.³⁸ A similar strategy was adapted in the present case also, where the films were cast under atmospheric humidity without airflow. The physical process leading to the formation of honeycomb pattern explained by Francois and Maruyama^{39, 40} et al. is as follows: When a droplet of the tetrahydrofuran (THF) solution is placed on the glass substrate, the THF starts to evaporate. This leads to a cooling of the solution and micron sized water droplets condense onto the tetrahydrofuran solution of the polymer. Because of the reduced surface tension between water and THF, the water droplets are stabilized and do not fuse. As the evaporation proceeds, more water droplets get close to the three phase line (solution-air-substrate) and are hexagonally packed due to capillary force generated at the solution front. The three phase line moves over the array of water droplets. The water droplets and some of the polymer between them are left behind and finally the water evaporates to result in the honeycomb structure. Generally honeycomb pattern is formed by those molecules that have an optimum hydrophilic-hydrophobic balance and which form spherical aggregates

upon solvent evaporation. In the azobenzene polymers **P1-P3**, the backbone is poly (methyl methacrylate) which is hydrophobic in nature whereas the ethylene oxy unit is hydrophilic in nature. **P1** with the highest molecular weight has a better balance of hydrophilic-hydrophobic ratio resulting in a very uniform 3-D network honeycomb pattern. At the other extreme, **P3** had the lowest degree of polymerization because of the very bulky naphthyl unit, thus losing out on the hydrophilic-hydrophobic balance and hence failed to exhibit any solvent induced patterns. **P2** is midway between **P1** and **P3**, both in terms of the polymer molecular weight build up as well as bulkiness. Thus porous patterns, though not so regular as in the case of **P1** was observed in the case of **P2**, whereas the control polymer with the phenyl phenol unit (and without the azo unit) did not form any porous morphology.

The variable concentration fluorescence measurement had indicated tendency for aggregate formation for **P2**. In order to further investigate this, TEM measurements were carried out by drop casting the polymer solution (tetrahydrofuran) on a formvar coated copper grid. The solution concentration used for sample preparation was 10^{-6} M. Figure 22 shows the TEM images of **P2** carried out without staining.

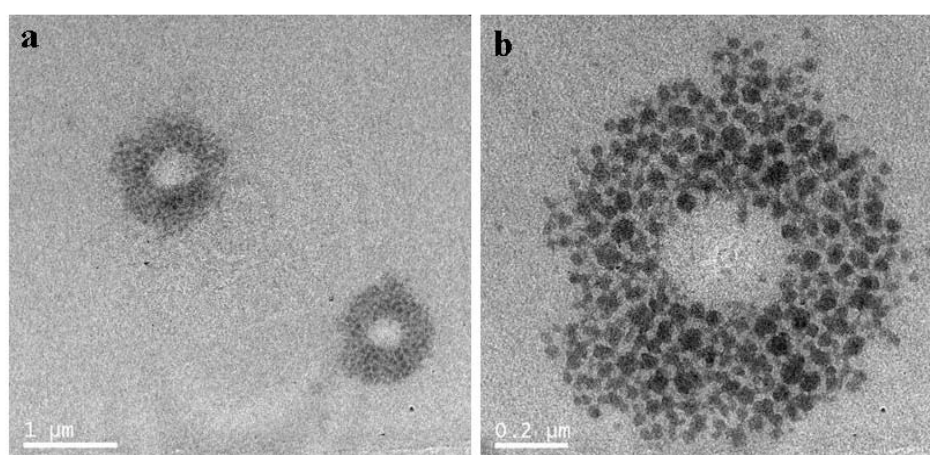


Figure 22 TEM images of P2

TEM images showed circular or toroidal features with an average diameter around $0.98 \mu\text{m}$ and outer diameter around $0.4 \mu\text{m}$. Each toroid

consisted of particles having size $0.05 \pm 0.01 \mu\text{m}$. In the literature, there are a number of reports of polymer architecture that can result in toroid formation.⁴¹⁻⁵¹The mechanism proposed by Kindt and Tlustý et al., for toroid formation suggests the formation of a rather inhomogeneous vesicle initially whose hydrophilic components are distributed inhomogeneously within its center.⁵²⁻⁵⁴ Upon growing to a critical size, this inhomogeneous vesicle breaks at certain points on the surface and this process leads to the redistribution of the block copolymers as a result of the balance of the internal free energy resulting in the formation of toroidal structures. A similar reasoning could be adopted in the case of P1 to explain the toroid formation.

On the basis of these results, it can be assumed that the fluorescence of the phenyl phenol based azobenzene dye ester (**DE2**) and polymer (**P2**) originates from the trans form at room temperature. There is no aggregate formation in the ground state, however in the excited state, J-type aggregates are formed at higher concentration as evidenced by the red shifted emission peak for the highly concentrated samples of both **DE2** and **P2** as well as by the toroid pattern in TEM measurements. However, the mechanism of aggregate formation is not the same in both cases. For instance, **DE2** possessing a hydroxyl group can form aggregates due to hydrogen bonding at higher concentration, as evidenced by room temperature FTIR spectra, which will be discussed later on. The excited state planar conformation of the biphenyl unit can also favor a J-type aggregate formation. Irradiation using 360 nm UV light results in the photoisomerization of the trans to the cis form which has a rather destabilizing effect upon the **DE2** aggregates. The photoisomerization destroyed the organized aggregated phase of **DE2** and the chromophores became isolated. Hence as irradiation time was increased from 30 to 90 minutes, the aggregate peak at 535 nm reduced in intensity and monomeric fluorescence intensity increased as the number of isolated molecules (both cis and trans) increased. In the case of **P2**, association due to hydrogen bonding can be ruled out. Although side chain azobenzene polymers are known to self-organize due to strong π - π interactions leading to

interdigitation of the chromophores, such an organization also can be ruled out for **P2** since the twisted nature of the phenyl phenol unit hinders any close contact. One probable mode of association, occurring especially at higher concentrations is that of a hydrophilic versus hydrophobic interaction, brought about by the ethyleneoxy spacer in **P2** linking the azobenzene chromophore to the ‘all-alkyl chain’ back bone. Figure 23 shows a schematic representation of the changes happening to the aggregates of **P2** and **DE2** upon irradiation. It shows that in contrast to **DE2**, **P2** can form much more stable aggregates, which remains unchanged by irradiation; whereas the hydrogen bonded aggregates of **DE2** disrupted upon formation of the bent cis isomers. The small extent of cis isomers formed (~17 %) is responsible for the slight enhancement of the aggregation peak at 535 nm in the highly concentrated solution upon irradiation.

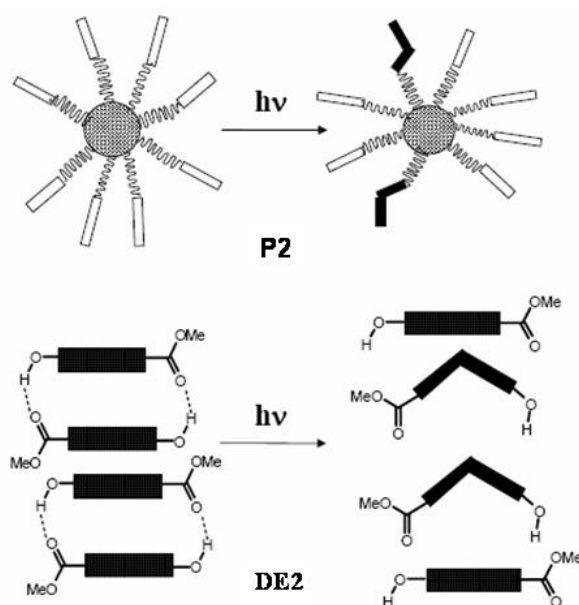


*Figure 23 Schematic representation of the aggregates of **P2** and **DE2** upon photoirradiation*

Proof of the existence of hydrogen bonding in **DE2** was traced using FTIR spectroscopy. Figure 24 shows the infrared spectra of the carbonyl stretching of **DE2** and **P2**. **P2** gives a carbonyl absorption peak at 1722 cm^{-1} whereas **DE2** shows a carbonyl stretching frequency that is split into two bands at 1721 and 1692 cm^{-1} respectively. The peak at higher wavenumber corresponds

to the free carbonyl stretch and the one at lower wavenumber corresponds to hydrogen bonded carbonyl stretching frequency.³¹ In **P2**, there is no possibility of hydrogen bond formation and therefore, the spectrum shows only one carbonyl absorption peak. On the other hand, **DE2** clearly shows the evidence of hydrogen bond formation.

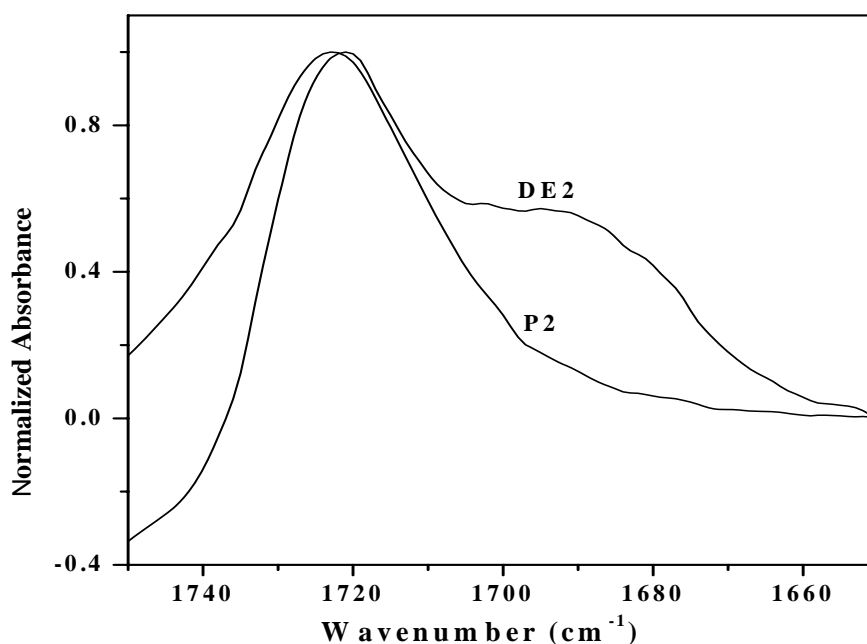


Figure 24 FTIR spectra recorded at room temperature between 1750 and 1650 cm^{-1} for **DE2** and **P2**

3.9 Solid State Luminescence Studies

Additional information regarding the intramolecular conformational changes of the phenyl phenol unit enhancing the fluorescence was obtained from solid state luminescence studies. The general trend of chromophores and polymers that show high fluorescence in solution is to have a completely quenched fluorescence in the solid state due to processes like intermolecular vibronic interactions which induce nonradiative deactivation.³² Thin films of **P2** made by drop casting on glass substrates gave an absorption spectra that was red shifted by ~ 40 nm compared with the solution. Figure 25 compares the fluorescence spectra of **P2** in film and in solution in DCM having ~ 0.1 OD absorption. The emission spectra of **P2** upon excitation at λ_{320} nm shows a > 7 fold enhancement for the film compared with solution. Conformational studies on biphenyl have

revealed that a more planar conformation is favored in the solid state.^{33, 34} This planarization can extend the effective conjugation length thereby enhancing the fluorescence.³⁵

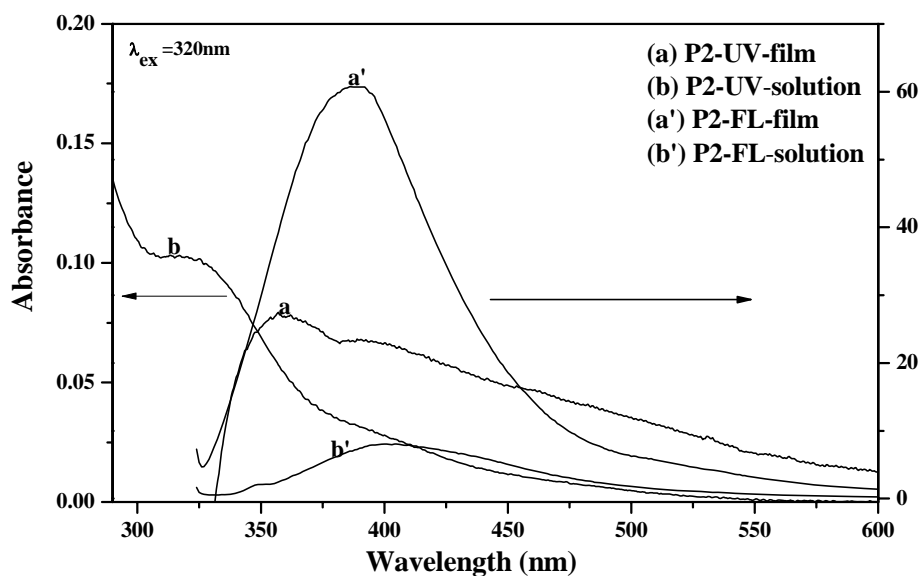


Figure 25 Comparison of UV (a, b) and fluorescence (a', b') of **P2** solution and film

3.10 Thermal Properties

The thermal characterization of the polymers was done using DSC and TGA. Generally azobenzene systems have a thermal stability limit < 250 °C. Figure 26 shows the TGA thermograms of the azo side chain polymers and control polymer. These side chain azobenzene polymers showed good thermal stability and weight loss was not observed at temperatures below 200 °C. All three polymers were completely amorphous and no melting endotherms were observed in the DSC analysis. Generally incorporation of phenyl phenol units are known to induce rigidity and mesogenicity, however, **P2** did not show any liquid crystalline character.

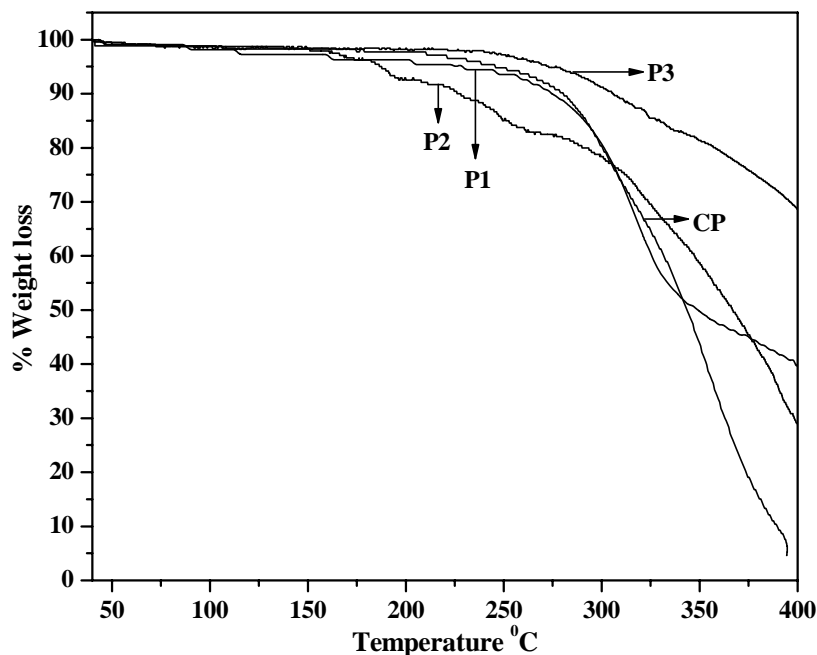


Figure 26 TGA thermograms for the azo side chain polymers and the control polymer

3.11 Conclusion

Fluorescent azobenzene dyes and side chain polymers comprising fluorophores like phenyl phenol and naphthol units have been synthesized. The phenyl phenol based azobenzene dye and polymer showed high fluorescence. The molecular geometry of the phenyl phenol unit which has a twisted ground state structure and more planar excited state is the cause of this fluorescence emission in spite of its incorporation into a normally non-fluorescing azobenzene system. The phenyl phenol azobenzene polymer exhibited photoinduced enhanced emission in solution upon irradiation. The enhancement of fluorescence emission intensity in dilute solution upon photoirradiation can be explained in terms of the inhibition of photoinduced electron transfer mechanism. Highly concentrated solutions of the azobenzene phenyl phenol dye and polymer showed red shifted aggregated fluorescence peak. This aggregated emission increased in intensity following continuous irradiation in the polymer whereas in the dye the intensity of the aggregated emission decreased with simultaneous increase of intensity of molecularly dissolved species. Aggregation

is driven by hydrogen bonding in the hydroxyl azobenzene dye molecule which gets disrupted due to the bent cis molecules upon photoirradiation. On the other hand, the aggregation of the highly concentrated polymer solution is brought about by hydrophilic-hydrophobic interactions and remains stable upon formation of cis isomers during photoirradiation. The toroid structure in the TEM analysis confirms the aggregation tendency of these polymers.

3.12 References

1. Shimomura, M.; Kunitake, T. *J. Am. Chem. Soc.* **1987**, 109, 5175.
2. Constantino, C. J. L.; Aroca, R. F.; Mendonca, C. R.; Mello, S. V.; Balogh, D. T.; Oliveira, O. N. *Spectrochem. Acta. Part: A* **2001**, 57, 281.
3. Tsuda, K.; Dol, G. C.; Gensch, T.; Hofkens, J.; Latterini, L.; Weener, J. W.; Meijer, E. W.; De Schryver, F. C. *J. Am. Chem. Soc.* **2000**, 122, 3445.
4. Nithyanandhan, J.; Jayaraman, N.; Davis, R.; Das, S. *Chem. Eur. J.* **2004**, 10, 689.
5. Anilkumar, P.; Jayakannan, M. *J. Phys. Chem. C* **2007**, 111, 3591
6. Ghedini, M.; Pucci, D.; Calogero, G.; Barigelletti, F. *Chem. Phys. Lett.* **1997**, 267, 341
7. Yoshino, J.; Kano, N.; Kawashima, T. *Chem. Comm.* **2007**, 6, 559.
8. Han, M. R.; Hara, M. *New J. Chem.* **2006**, 30, 223.
9. Han, M. R.; Hirayama, Y.; Hara, M. *Chem. Mater.* **2006**, 18, 2784.
10. Zacharias, P. S.; Ameerunisha, S.; Korupoju, S. R. *J. Chem. Soc. Perkin Trans.* **1998**, 2, 2055.
11. Grimes, A. F.; Call, S. E.; Vicente, D. A.; English, D. S.; Harbron, E. J. *J. Phys. Chem. B* **2006**, 110, 19183.
12. Harbron, E. J.; Vicente, D. A.; Hoyt, M. T. *J. Phys. Chem. B* **2004**, 108, 18789.
13. Izumi, A.; Teraguchi, M.; Nomura, R.; Masuda, T. *Macromolecules* **2000**, 33, 5347.

14. Smitha, P.; Asha, S. K.; Pillai, C. K. S. *J. Polym. Sci. Part A: Polym. Chem.* **2005**, 43, 4455.
15. Cojocariu, C.; Rochon, P. *J. Mater. Chem.* **2004**, 14, 2909.
16. Tsutsumi, O.; Kitsunai, T.; Kanazawa, A.; Shiono, T.; Ikeda, T. *Macromolecules* **1998**, 31, 355.
17. Sarker, A. M.; Ding, L.; Lahti, P. M.; Karasz, F.E. *Macromolecules* **2002**, 35, 223.
18. Bhowmik, P. K.; Han, H.; Cebe, J. J.; Burchett, R. A. *J. Polym. Sci. Part A: Polym. Chem.* **2002**, 40, 141.
19. Zollinger, H. *Azo and Diazo Chemistry. Aliphatic and Aromatic Compounds*; Interscience Publishers, Inc.: New York, **1961**.
20. Fujino, T.; Arzhantsev, S. Yu.; Tahara, T. *J. Phys. Chem. A* **2001**, 105, 8123.
21. Sekkat, Z.; Knoll, W., Eds. *Photoreactive Organic Thin Films*; Academic Press: Elsevier Science, **2002**.
22. Rau. Von H. *Angew. Chem., Int. Ed.* **1973**, 12, 224.
23. Shukla, D.; Wan, P. *J. Am. Chem. Soc.* **1993**, 115, 2990.
24. Shi, Y.; Wan, P. *Chem. Comm.* **1997**, 273.
25. Helms, A.; Heiler, D.; McLendon, G. *J. Am. Chem. Soc.* **1991**, 113, 4325.
26. Benniston, A. C.; Harriman, A.; Patel, P. V.; Sams, C. A. *Eur. J. Org. Chem.* **2005**, 4680.
27. Rau. Von H. *Ber. Bunsen-Ges. Phys. Chem.* **1968**, 72, 637
28. Harbron, E. J.; Vicente, D. A.; Hadley, D. H.; Imm, M. R. *J. Phys. Chem. A* **2005**, 109, 10846.
29. Padmanaban, G.; Ramakrishnan, S. *J. Phys. Chem. B* **2004**, 108, 14933.
30. Han, M. R.; Hara, M. *J. Am. Chem. Soc.* **2005**, 127, 10951.
31. Su, Y. C.; Shiao-Wei, K.; Ding-Ru, Y.; Hongyao, X.; Feng-Chih, C. *Polymer*, **2003**, 44, 2187.
32. Birks, J. B. *Photophysics of Aromatic Molecules*; Wiley: London, **1970**.

33. Trotter, J. *Acta Crystallogr.* **1961**, 14, 1135.
34. Hargreaves, A.; Rizvi, S. H. *Acta Crystallogr.* **1962**, 15, 365.
35. An, B. K.; Kwon, S. K.; Jung, S. D.; Park, S. Y. *J. Am. Chem. Soc.* **2002**, 124, 14410.
36. Srinivasrao, A.; Collings, D.; Philips, A.; Patel, S. *Science* **2001**, 292, 79.
37. Yabu, H.; Shimomura, M. *Chem. Mater.* **2005**, 17, 5231.
38. Ishizu, K.; Tokuno, Y.; Makino, M. *Macromolecules* **2007**, 40, 763.
39. Widawski, G.; Rawiso, M.; Francois, B. *Nature* **1994**, 396, 387.
40. Maruyama, N.; Kioto, T.; Nishida, J.; Sawadaishi, T.; Cieren, X.; Ijio, K.; Karthaus, O.; Shimomura, M. *Thin Solid Films* **1998**, 327-329, 854.
41. Sakaue, T.; Yoshikawa, K. *J. Chem. Phys.* **2002**, 117, 6323.
42. Ishimoto, Y.; Kikuchi, N. *J. Chem. Phys.* **2006**, 125, 074905-1.
43. Cao, Z.; Liu, W.; Liang, D.; Guo, G.; Zhang, J. *Adv. Funct. Mater.* **2007**, 17, 246.
44. Yoshikawa, Y.; Yoshikawa, K.; Kanbe, T. *Langmuir* **1999**, 15, 4085
45. Jain, S.; Bates, F. *Science* **2003**, 300, 460.
46. Pochan, D. J.; Chen, Z. Y.; Cui, H. G.; Hales, K.; Qi, K.; Wooley, K. L. *Science* **2004**, 306, 94.
47. Chen, Z. Y.; Cui, H. G.; Hales, K.; Qi, K.; Li, Z. B.; Pochan, D. J.; Wooley, K. L. *J. Am. Chem. Soc.* **2005**, 127, 8592.
48. Forster, S.; Hermsdorf, N.; Leube, W.; Schnablegger, H.; Regenbrecht, M.; Akari, S.; Lindner, P.; Bottcher, C. *J. Phys. Chem. B* **1999**, 103, 6657.
49. Netz, R. R. *Europhys. Lett.* **1999**, 47, 391.
50. Jiang, Y.; Zhu, J. T.; Jiang, W.; Liang, H. *J. Phys. Chem. B* **2005**, 109, 21549.
51. Choi, J.; Hermans, T. M.; Lohmeijer, B. G. G.; Pratt, R. C.; Dubois, G.; Frommer, J.; Waymouth, R. M.; Hedrick, J. L. *Nano. Lett.* **2006**, 6, 1761
52. Kindt, J. T. *J. Phys. Chem. B* **2002**, 106, 8223.
53. Tlusty, T.; Safran, S. A. *Science* **2000**, 290, 1328.
54. Tlusty, T.; Safran, S. A.; Strey, R. *Phys. Rev. Lett.* **2000**, 84, 1244.

Chapter 4

Synthesis, Characterization and Photophysical Properties of Liquid Crystalline Azobenzene Oligomers

4.1 Abstract

A new series of azobenzene based bichromophoric molecules consisting of two identical chromophores tethered by oligoethyleneoxy spacer has been synthesized. The chromophores were based on two different fluorophores namely: phenyl phenol and naphthol with a simple phenol based molecules as reference compounds. The ethylene oxy spacer length was varied from two, four and six units. Model azodye molecules having a methoxy or ethoxy terminal substitution instead of the oligoethyleneoxy unit were also synthesized to understand the fluorescence characteristics of the phenol, phenyl phenol and naphthol bichromophore series. All the molecules were structurally characterized by using ^1H and ^{13}C NMR spectroscopy and photophysical properties studied using UV-Vis and fluorescence spectroscopies. Emission spectra were recorded by exciting at both the $\pi\text{-}\pi^*$ transition corresponding to the aromatic phenyl unit (260-280 nm for phenyl phenol and naphthol series) as well as at the $\pi\text{-}\pi^*$ transition corresponding to the azodye unit (~320 nm for phenyl phenol series and ~415 nm for the naphthol series). Among the whole series, the model compound **Pp0**, based on phenyl phenol chromophore possessed the highest value of quantum yield ($\phi_{\text{FL}} = 0.35$). The photophysical properties of the naphthol based bichromophores were different from that of the phenyl phenol based azodye bichromophores by the presence of excimer emission peak in the fluorescence spectra of the former. Fluorescence spectra were recorded at various concentrations as well as in various solvents to understand the aggregation behavior of the naphthol series. Thermal characterization using the DSC showed multiple transitions indicating the presence of liquid crystallinity (LC) which was also confirmed by the PLM studies. **P4P**, **P6P**, **Pp4Pp** and **Np6Np** were found to exhibit LC phases. Photoisomerization studies were carried out by irradiation using the 360 and 450 nm band-pass filtered output of a 50 watt short arc mercury vapor lamp and it was found that the photoisomerization efficiency was less for the naphthol and phenyl phenol series when compared with that of the phenol series.

4.2 Introduction

Bichromophoric molecules composed of two identical mesogenic units connected via flexible spacer groups like polyethylene oxide or polyethylene units have attracted much attention recently because they serve as useful models for main chain liquid crystalline polymers. Dimeric liquid crystals, in which two mesogens are linked by a flexible spacer in the sequence mesogen-spacer-mesogen have been known to exhibit an odd-even oscillation of their transition temperatures as a function of the spacer length.¹⁻⁸ Studies reported by Asha et al on the second harmonic generation (SHG) properties of the liquid crystalline azo twin molecules based on 4-nitro-4'-alkoxy azobenzene linked via flexible polymethylene spacers showed the existence of an odd-even oscillation even in their SHG efficiencies as a function of spacer length.⁹ There are a number of reports of liquid crystal dimers composed of two non-identical mesogenic units connected via a flexible central spacer.^{10, 11} Unsymmetrical dimers comprising of a cholesteryl ester as chiral entity and mesogenic moieties like benzoate ester, azobenzene, schiff's base or biphenyl usually exhibit a wide variety of mesomorphic phases.¹²⁻²¹ Tamaoki et al reported cholesterol-azobenzene containing dimesogenic compounds linked via alkyl chain of varying length and most of them exhibited only one cholesteric mesophase.²² Wu et al reported dimesogenic cholesteric liquid crystals containing cholesteryl ester and 4'-nitro azobenzene moieties. The two mesogenic units were linked via dicarboxylic ester bonds and alkylene spacers of varying length.²³

Similar to the liquid crystalline bichromophores, studies have been carried out on fluorescent twin molecules having two fluorophores linked together by flexible spacer groups like polyethylene oxide or polyethylene units.²⁴ Fluorescence has been used in these systems as an effective tool to probe conformational changes and molecular motions around the chromophores. Twin fluorophores based on naphthalene units and poly(ethylene glycol) spacer were reported by Tung et al where the spacer length dependence on inter and intra molecular excimer formation was studied in detail.²⁴ Naphthalene is a unique

fluorescent compound capable of exhibiting excimer fluorescence at longer wavelength region in addition to the monomer fluorescence at shorter wavelength when naphthalene – naphthalene interaction exists.²⁵ The enhanced intensity towards the red and concentration independence in the bichromophoric compounds indicate the intramolecular formation of an excimer. If the excitation spectra for the excimer and monomer are identical and if the maxima correspond to that in the UV spectrum then it is another indication for the formation of intramolecular excimer. There are plenty of examples of excimer emission from naphthalene based molecules, dendrimers and polymers and in most of the cases, the monomer emission from the naphthalene unit appeared at 340-360 nm range and the excimer emission appeared at around 400 nm.^{24, 41, 26, 27}

Formation of excited state dimers as a result of interactions between aromatic chromophores is a well known phenomenon. Although these species have been extensively studied in the condensed phase over the past four decades, the effective merger of the laser and supersonic jet made the characterization of their electronic state and excited state dynamics possible. The aromatic excimer was first discovered by Forster and Kasper who observed the broad, structureless fluorescence from a concentrated solution of pyrene at room temperature.²⁸ The emission which appeared only in concentrated solution was strongly red-shifted with respect to the structured monomer fluorescence of pyrene. Since no new spectral feature other than that of the monomer was evident in the absorption spectra of the concentrated solutions, the anomalous fluorescence was attributed to a dimeric species which is formed by the diffusive association of an electronically excited pyrene with a molecule in the ground electronic state. Both the structureless feature of the excimer fluorescence and its lower energy relative to the monomer fluorescence are consistent with the repulsive character of the ground state potential. A lot of work has been done on this topic and later it was established that the formation of singlet excimers is a rather general property of highly concentrated solutions of aromatic hydrocarbons. The molecular crystals of perylene and pyrene composed of face-to-face arrangement of two molecules

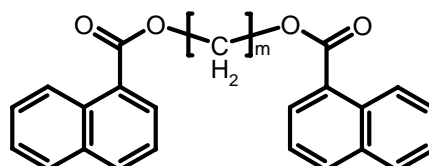
in the crystal lattice also exhibit excimer fluorescence as do the sandwich pairs of naphthalene and anthracene produced by the photolytic dissociation of the corresponding photodimers in a rigid glass. These results as well as the observation of intramolecular excimer formation from dilute solutions of 1,3-diphenylpropane and 1,3-di- α -naphthylpropane led to the conclusion that the preferred conformation of excimers is a symmetrical sandwich structure. This conclusion is supported by semiempirical molecular orbital studies on the naphthalene dimer which indicate that the perfect sandwich pair D_{2h} structure is the most favored conformation of the singlet excimer due to stabilization by exciton resonance ($M^*M \leftrightarrow MM^*$) and to a lesser extent by charge resonance ($M+M \leftrightarrow M^-M^+$).

Excimers are dimeric species which are associated in an excited electronic state and dissociated in their ground state. Stabilizing excited state interaction between two π -systems cause significantly different fluorescent properties of the monomeric chromophore and the excimer for the latter. Based on these differential photophysical properties, several fluorescent chemosensors have been introduced in recent years. Excimer formation between two chromophores requires close contact within a distance defined by their van-der-waals radii. Therefore the efficiency of intramolecular excimer formation is dependant on the ease of chromophore approach, which is dictated by the parameters like temperature, viscosity of the chemical environment as well as by the conformational freedom of the chromophore linking spacer. In this regard, the lipophobic effect of poly(ethylene glycol) (PEG) spacer segments plays an important role since in nonpolar solvents it can adopt various conformations like open or coiled form bringing the two ends of the bichromophore unit in close proximity. These effects can produce very pronounced changes in the fluorescence spectra of the bichromophores. Intramolecular excimers are interesting from the conformational point of view because singlet excimers require the adoption of a specific planar sandwich geometry by the two chromophores. For a given chromophore and spacer, the intensity of excimer

emission in dilute solution depends on the fluorescence lifetime and the Forster radius. The interpretation of the formation of excimer formation is simplest when these two parameters are small.

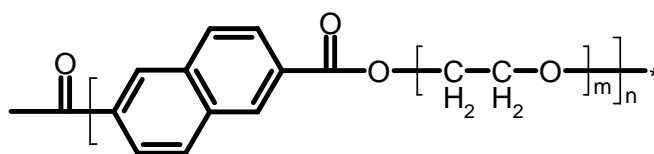
4.3 Excimer Formation in Naphthyl Derivatives

Polycyclic aromatic hydrocarbons are known to easily form excimers which are dictated by their redshifted structureless fluorescence emission which has no corresponding absorption spectrum.²⁹⁻³² Naphthalene based polymers and molecules which can form intramolecular excimers, excited complexes and intramolecular energy transfer were well explored by the group of Mattice et al.³³⁻³⁸ They reported excimer emission from the α , ω - diesters of $\text{HO}(\text{CH}_2)_m\text{OH}$, $m=2-6$ and 1-naphthoic acid in dilute solutions in solvents of different viscosity.³³ They found that the ratio of intensity of the excimer emission with that of the monomer depends upon the value of m and the viscosity of the solvent. They compared these results with those diesters obtained from 2-naphthoic acid. Scheme 1 shows the structure of the molecule investigated.



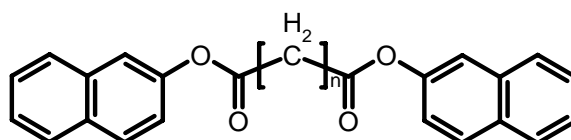
Scheme 1

They also studied the intramolecular excimer emission from the model compounds for polyesters prepared from 2, 6-dicarboxylic acid and different glycols (Scheme 2).³⁴ Studies as the functions of temperature and solvent showed that in contrast to analogous polyesters in which naphthalene moiety is replaced with a benzene ring, there can be a substantial dynamic component to the excimer emission.



Scheme 2

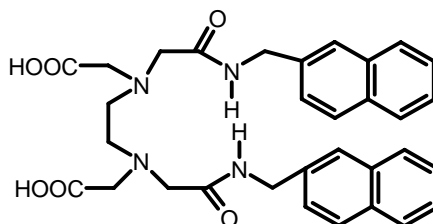
Mattice et al reported intramolecular excimer emission and energy migration in polyesters with 2, 6- naphthalene dicarboxylic acid units separated by spacers of 1-4 ethylene oxide units.³⁵ They also studied the effect of directionality of the ester group on the formation of hairpin like excimers in polyesters containing naphthalene and a flexible spacer using model compounds derived from 2-hydroxy naphthalene and $\text{HOOC}-(\text{CH}_2)_n\text{-COOH}$, $n = 2-6$.³⁶ Scheme 3 shows the structure of the model compound.



Scheme 3

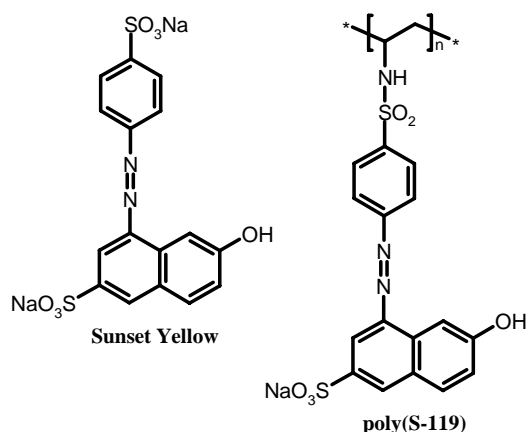
The same group also reported bichromophoric compounds in which two 2-naphthalene carboxylate groups were connected by flexible methylene spacer such as $\text{C}_{10}\text{H}_9\text{-COO}-(\text{CH}_2)_m\text{-OOC-C}_{10}\text{H}_9$.^{37,38} Their studies on the steady state fluorescence and molecular dynamics (MD) trajectories in vacuo at different temperatures showed that the bichromophoric compounds spend a greater fraction of time in a conformation with both chromophores close to an adequate geometry for excimer formation when in vacuo than they might when immersed in a solvent.³⁸ Soutar et al reported intramolecular excimer emission from the copolymers of methyl methacrylate with vinyl naphthalenes and acenaphthalenes.³⁹⁻⁴¹ Lim et al studied the laser-induced transient absorption measurements of intermolecular triplet excimers of naphthalene in fluid solution and they found the transient absorption spectrum is similar to that of dilute solutions of covalently linked dimers of naphthalene.⁴² There are reports of excimer emission of naphthalene when included within cyclodextrin.^{25, 43} Polacka reported delayed and prompt excimer fluorescence from naphthalene in

poly (methyl methacrylate) matrix at higher concentrations and they suggested that molecular pairs of naphthalene are responsible for the excimer fluorescence in the PMMA matrix.⁴⁴ Itoh et al reported the excimer emission from a series of alternating copolymers of 2-naphthylalkyl methacrylates and 2-vinylnaphthalene in tetrahydrofuran solutions.²⁶



Scheme 4

Machi et al reported cadmium sensing naphthalene based bichromophore (Scheme 4) which exhibited excimer emission and they found that upon complexation with the cadmium metal ion the intensity of excimer emission increased whereas when complexed with zinc ion the monomer intensity increased.²⁷ Spies et al reported the excimer emission from dimethyl-2,6-naphthalene dicarboxylate embedded in PMMA matrix.⁴⁵ The excited state dynamics of a water soluble polymeric dye [poly(S-119)] based on Sunset Yellow was investigated using femtosecond time-resolved fluorescence upconversion by Goodson et al.⁴⁶ Multi-exponential relaxation of fluorescence was observed for the polymer in pico second and sub-picosecond range. The difference in excited state dynamics between the polymeric dye and the azo chromophore was explained in terms of intermolecular interactions resulting in intra-chain aggregate formation. Scheme 5 shows the structures of the polymeric dye and Sunset Yellow.



Scheme 5

A chemosensor consisting of a tripodal polyamine receptor bearing naphthalene fluorophores at the terminals has been developed by Pina et al.⁴⁷ This sensor exhibited intense excimer emission and they studied the kinetics of excimer formation in water and ethanol as a function of temperature.

The present study describes the synthesis, photophysical and optical properties of azobenzene based bichromophoric molecules and its model compounds. The bichromophores are dimeric twin molecules designed in the fashion ‘chromophore-spacer-chromophore’ in which the spacer is oligoethyleneoxy units of varying length. The chromophores were azobenzene moieties incorporated with phenol, phenyl phenol or naphthol units. The excimer formation of naphthol based azo bichromophore molecules was analyzed by concentration dependant fluorescence measurements. The morphology of these bichromophores was also analyzed using SEM measurements and the LC property by DSC measurements and PLM studies.

4.4 Experimental Section

Diethylene glycol, tetra ethylene glycol, polyethylene glycol 300, 4-phenyl phenol and p-toluene sulphonyl chloride were purchased from Aldrich Chemical Company Ltd and were used as such. p-Amino benzoic acid, sodium nitrite, phenol, α -naphthol, sodium hydroxide, sulphuric acid, potassium carbonate and potassium iodide were purchased from S.D Fine Chemicals Ltd.

Dimethyl formamide (DMF), tetrahydrofuran and methanol were purchased locally and purified using standard procedures.

^1H and ^{13}C -NMR spectra of all molecules were recorded using 300-MHz Bruker NMR spectrophotometer in deuterated chloroform containing small amount of tetra methyl silane (TMS) as internal standard. For ^{13}C NMR experiments, the carbon atom in CDCl_3 was taken as 77 ppm and all other peaks were assigned with respect to it. The purity of the compounds was determined by JEOL JSM600 fast atom bombardment (FAB) high-resolution mass spectrometry and also by Shimadzu QP-2000 (GC/MS) Micromass Tof Spec 2E instrument using a nitrogen 337 nm laser (4 ns pulse). The matrix used was 2, 5-dihydroxy benzoic acid dissolved in CHCl_3 which was spotted on MALDI target and allowed to dry before introducing into the mass spectrometer. The purity of the bichromophores was further confirmed by SEC in THF using polystyrene standards. Waters 515 Pump connected through three series of Styragel HR columns (HR-3, HR-4E and HR-5E) and Waters Model 2487 Dual Wavelength UV-vis Detector and Waters 2414 Differential Refractometer was used for analyzing the samples. The flow rate of the THF was maintained as 1 mL throughout the experiments and 0.2 wt % of (2 mg in 1 mL) the sample was filtered and injected for recording the GPC chromatograms at 30°C. Infrared spectra of the bichromophores and model compounds were recorded using a Perkin Elmer, Spectrum one spectrophotometer in the range of 4000 to 400 cm^{-1} . UV-Vis spectra were recorded using Perkin Elmer Lambda 35 UV-Vis Spectrometer. The emission studies were performed by a SPEX Fluorolog F112X spectrofluorimeter. The fluorescence quantum yields of the azobenzene bichromophores were determined in DCM using quinine sulfate in 0.1M H_2SO_4 ($\phi = 0.546$) and Rhodamine-6G ($\phi = 0.93$) as the standards.

The optical density at λ_{max} was maintained at 0.1 ± 0.05 to avoid reabsorption artifacts. The quantum yield was calculated using the equation.

$$\phi_s = \phi_r [F_s A_r / F_r A_s] (n_r/n_s)^2$$

where ϕ_s is the fluorescence quantum yield of the sample, F is the area of the emission peak, n is the refractive index of solution, and A is the absorbance of the solution at the exciting wavelength. The subscripts r and s denote reference and sample respectively.

Thermogravimetric analysis (TGA) was performed using a TGA-50 Shimadzu Thermogravimetric Analyzer. Samples were run from 40 to 400 °C with a heating rate of 10 °C/min under nitrogen. The thermal and phase behavior of the polymers were analyzed using a hot stage polarized light microscope (Leitz-1350 heating stage coupled with PLM) as well as a DSC-Perkin Elmer Pyris 6 Differential Scanning Calorimeter (DSC) at a heating rate of 10 °C/min under nitrogen atmosphere. Typically, 2-3 mg of samples was placed in an aluminium pan, sealed properly and scanned from 10-250 °C for the DSC measurements. The instrument was calibrated with indium standards before measurements. For scanning electron microscope (SEM) experiments, polymer samples were provided a thin gold coating using JEOL JFC-1200 fine coater. The probing side was inserted into JEOL JSM-5600 LV scanning electron microscope for taking photographs. The sample preparation method adopted was as follows. The sample solution of concentration 10^{-3} M was prepared and a drop of this solution was placed on a clean glass slide and was allowed to evaporate slowly in air. Dynamic light scattering (DLS) measurements are done by using a Nano ZS Malvern instrument employing a 4mW He-Ne laser ($\lambda=632.8\text{nm}$) and equipped with a thermo stated sample chamber. Irradiation measurements were carried out in dichloromethane with a Dymax light curing device (Blue Wave 50AS model 39370) having a 50 watt short arc mercury vapor lamp with an output wavelength in the range 280-450 nm in combination with 360 and 450 nm Oriel bandpass filters. The intensity of the lamp was measured to be 18 mW/cm^2 using an Omniscan radiometer.

The rate constant for the trans to cis isomerization which is a first order reaction was determined using the following equation:

$$\ln(A_0 - A_{eq}) / (A_t - A_{eq}) = k_t t$$

where A_0 , A_t and A_{eq} are the initial absorbance, the absorbance at time t and the absorbance at the photostationary state at the π - π^* transition of azo part and k_t is the rate constant of the trans-to-cis isomerization. The slope of the plot of $\ln(A_0 - A_{eq}) / A_t - A_{eq}$ vs UV irradiation time gives the rate constant.

Synthesis of Oligoethyleneoxy Ditosylates

Synthesis of ethylene glycol ditosylate

Diethylene glycol (5.0 g, 47 mmol), NaOH (4.7 g, 118 mmol), 50 mL water and 10 mL THF were taken in an RB flask and cooled to 0 °C with magnetic stirring. p-Toluene sulphonyl chloride (22.5 g, 118 mmol) dissolved in 40 mL THF was added dropwise to the above mixture maintaining the temperature at 0 °C. The solution was stirred at the same temperature for 3 h and then poured into water, neutralized with hydrochloric acid and then extracted with chloroform. The organic layer was dried with anhydrous sodium sulphate and solvent was evaporated. The ditosylate was purified by column chromatography using hexane. Yield = 18.3 g (94 %) ^1H NMR (CDCl_3) δ ppm: 7.80 (4H, d, Ar), 7.36 (4H, d, Ar), 4.19 (4H, t, $-\text{SO}_2\text{-O-CH}_2\text{-CH}_2\text{-}$), 3.68 (4H, t, $-\text{O-CH}_2\text{-CH}_2\text{-}$), 2.45 (6H, s, $\text{H}_3\text{C-C}_6\text{H}_4\text{-}$). ^{13}C NMR (CDCl_3) δ ppm: 24.31, 67.43, 69.21, 129.54, 130.02, 138.36, 144.24. FTIR (KBr) (cm^{-1}): 3564, 2925, 1925, 1738, 1495, 1453, 1359, 1246, 1175, 1137, 1096, 1019, 926, 817, 776, 665, 582, 555. HRMS $m+1$: 415.02

Tetra ethylene glycol ditosylate was prepared by the same procedure using tetraethylene glycol (10 g, 52 mmol) and p-toluene sulphonyl chloride (24.7 g, 130 mmol) and polyethylene glycol 300 ditosylate was prepared by using polyethylene glycol 300 (10 g, 33 mmol) and p-toluene sulphonyl chloride (15.6 g, 83 mmol).

Tetraethylene glycol ditosylate: Yield = 18.2 g (70 %) ^1H NMR (CDCl_3) δ ppm: 7.69 (4H, d, Ar), 7.24 (4H, d, Ar), 4.06 (4H, t, $-\text{SO}_2\text{-O-CH}_2\text{-CH}_2\text{-}$), 3.58-

3.45 (12H, m, -O-CH₂-CH₂-), 2.32 (6H, s, H₃C-C₆H₄-). ¹³C NMR (CDCl₃) δ ppm: 21.32, 68.37, 69.07, 70.29, 127.62, 129.63, 132.63, 144.67. FTIR (KBr) (cm⁻¹): 3448, 2870, 1597, 1492, 1452, 1399, 1355, 1292, 1246, 1177, 1097, 1012, 923, 817, 776, 702, 664, 555. HRMS m+1: 503.14

Polyethylene glycol 300 ditosylate: Yield = 10 g (51 %) ¹H NMR (CDCl₃) δ ppm: 7.72 (4H, d, Ar), 7.28 (4H, d, Ar), 4.09 (4H, t, -SO₂-O-CH₂-CH₂-), 3.65-3.51 (20H, m, -CH₂O-), 2.36 (6H, s, H₃C-C₆H₄-). ¹³C NMR (CDCl₃) δ ppm: 21.69, 67.97, 69.54, 69.97, 128.35, 129.32, 140.33, 144.28. FTIR (KBr) (cm⁻¹): 3337, 3066, 2929, 1643, 1599, 1578, 1538, 1487, 1451, 1356, 1293, 1176, 1122, 1097, 1019, 923, 816, 776, 702, 664, 579, 555. HRMS m+1: 591.23

Synthesis of Azo Bichromophores

Synthesis of P4P

4-(4-Hydroxy-phenylazo)-benzoic acid methyl ester (2.5 g, 9.9 mmol), anhydrous potassium carbonate (1.7 g, 12.3 mmol), a pinch of KI and tetra ethylene glycol ditosylate (2.5 g, 4.9 mmol) were dissolved in 20 mL DMF. The mixture was refluxed at 80 °C for 48 h under nitrogen. The resulting solution was cooled to room temperature, poured into water. The product was filtered, washed with water and dried and purified by column chromatography using ethyl acetate-methanol mixture (v/v 95/5).

Yield = 1 g (15 %) ¹H NMR (CDCl₃) δ ppm: 8.10 (4H, d, Ar), 7.87-7.79 (8H, m, Ar), 6.95 (4H, d, Ar), 4.45 (4H, t, -OCH₂-CH₂O-), 3.88 (6H, s, -C(O)OCH₃), 3.83-3.66 (12H, m, -OCH₂-CH₂O-CH₂-). ¹³C NMR (CDCl₃) δ ppm: 52.29, 67.68, 69.57, 70.65, 70.83, 114.86, 122.34, 125.13, 130.55, 132.41, 144.32, 157.14, 159.60 166.22 FTIR (KBr) (cm⁻¹): 3434, 2929, 1717, 1599, 1501, 1432, 1405, 1281, 1191, 1139, 1110, 955, 864, 840, 774, 722, 691. MALDI-TOF m+1: 671.6

All the bichromophores were synthesized by coupling the dye esters with corresponding ditosylates using the same procedure. **P6P** was prepared by coupling 1.7 g (6.8 mmol) of hexaethylene glycol ditosylate with 2 g (3.4 mmol) 4-(4-Hydroxy-phenylazo)-benzoic acid methyl ester. **Pp4Pp** was prepared by

coupling hexaethylene glycol ditosylate (2 g, 3.9 mmol) with 4-(4'-Hydroxy-biphenyl-4-ylazo)-benzoic acid methyl ester (2.6 g, 7.9 mmol) whereas **Pp6Pp** was prepared using 2 g (3.4 mmol) of hexaethylene ditosylate and 4-(4'-Hydroxy-biphenyl-4-ylazo)-benzoic acid methyl ester (2.3 g, 6.8 mmol). The naphthyl based bichromophore **Np2Np** was prepared by using diethylene glycol ditosylate (2 g, 4.8 mmol) and 4-(4-Hydroxy-naphthalen-1-ylazo) benzoic acid methyl ester (2.9 g, 9.6 mmol) whereas **Np6Np** was prepared by coupling 2.1 g (6.8 mmol) of 4-(4-Hydroxy-naphthalen-1-ylazo) benzoic acid methyl ester with 2 g (3.4 mmol) of the hexa ethylene glycol ditosylate.

P6P: Yield = 0.8g (13 %) ^1H NMR (CDCl_3) δ ppm: 8.10 (4H, d, Ar), 7.86 (8H, m, Ar), 6.96 (4H, d, Ar), 4.28 (4H, m, $-\text{OCH}_2-\text{CH}_2\text{O}$), 4.15 (6H, s, $-\text{C}(\text{O})\text{OCH}_3$), 3.87-3.65 (20H, m, $-\text{OCH}_2-\text{CH}_2\text{O}-\text{CH}_2-$). ^{13}C NMR (CDCl_3) δ ppm: 52.24, 69.54, 70.59, 70.85, 114.88, 122.32, 125.11, 130.54, 131.13, 147.01, 157.22, 159.93, 166.58. FTIR (KBr) (cm^{-1}): 3418, 2868, 1717, 1602, 1498, 1435, 1405, 1281, 1254, 1144, 1109, 954, 866, 840, 776, 697, 722. MALDI-TOF $m+\text{Na}$: 781.5

Pp4Pp: Yield = 0.6 g (12 %) ^1H NMR (CDCl_3) δ ppm: 8.11 (4H, d, Ar), 7.88 (6H, m, Ar), 7.60-7.22 (8H, m, Ar), 6.87 (6H, m, Ar), 4.31 (4H, t, $-\text{OCH}_2-\text{CH}_2\text{O}$), 3.90 (6H, s, $-\text{C}(\text{O})\text{OCH}_3$), 3.73-3.53 (12H, t, $-\text{OCH}_2-\text{CH}_2\text{O}-\text{CH}_2-$). ^{13}C NMR (CDCl_3) δ ppm: 52.28, 67.43, 69.69, 70.78, 114.83, 122.77, 126.64, 126.76, 128.03, 128.66, 130.54, 131.59, 133.81, 151.62, 157.01, 158.27, 166.51. FTIR (KBr) (cm^{-1}): 3440, 2918, 1717, 1602, 1517, 1449, 1276, 1248, 1174, 1108, 1062, 954, 834, 763, 694, 606, 549. HRMS $m+1$: 823.11

Pp6Pp: Yield = 0.6 g (11 %) ^1H NMR (CDCl_3) δ ppm: 8.11 (4H, d, Ar), 7.88 (6H, m, Ar), 7.60 (2H, m, Ar), 7.53 (4H, d, Ar), 7.37 (4H, m, Ar), 7.10-6.88 (4H, m, Ar), 4.31 (4H, t, $-\text{OCH}_2-\text{CH}_2\text{O}$), 3.90 (6H, s, $-\text{C}(\text{O})\text{OCH}_3$), 3.72-3.53 (20H, t, $-\text{OCH}_2-\text{CH}_2\text{O}-\text{CH}_2-$). ^{13}C NMR (CDCl_3) δ ppm: 52.27, 69.80, 70.29, 70.63, 115.36, 122.93, 126.79, 128.18, 128.92, 130.82, 131.73, 142.61, 155.66, 156.54, 158.56, 166.65. FTIR (KBr) (cm^{-1}): 3440, 2868, 1722, 1602, 1512, 1481, 1449, 1350, 1278, 1111, 947, 760, 697. HRMS $m+1$: 911.6

Np2Np: Yield = 1.6 g (36 %) ^1H NMR (CDCl_3) δ ppm: 8.98 (2H, d, Ar), 8.34 (2H, d, Ar), 8.22 (4H, d, Ar), 8.04 (6H, m, Ar), 7.72 (2H, t, Ar), 7.61 (2H, t, Ar), 6.93 (2H, d, Ar), 4.55 (4H, t, $-\text{OCH}_2\text{-CH}_2\text{O}$), 4.09 (6H, s, $-\text{C}(\text{O})\text{OCH}_3$), 3.77 (4H, m, $-\text{OCH}_2\text{-CH}_2\text{O-CH}_2-$). ^{13}C NMR (CDCl_3) δ ppm: 51.41, 70.13, 112.46, 116.24, 122.32, 122.84, 125.31, 126.54, 127.62, 129.41, 130.33, 132.54, 143.42, 157.13, 160.99, 166.64. FTIR (KBr) (cm^{-1}): 2928, 2857, 1729, 1602, 1452, 1391, 1267, 1166, 1116, 979, 760. HRMS $m+1$: 683.24

Np6Np: Yield = 0.4 g (7 %) ^1H NMR (CDCl_3) δ ppm: 8.91 (2H, d, Ar), 8.27 (2H, d, Ar), 8.17 (4H, d, Ar), 7.97 (6H, m, Ar), 7.63 (2H, t, Ar), 7.55 (2H, t, Ar), 6.87 (2H, d, Ar), 4.46 (4H, t, $-\text{OCH}_2\text{-CH}_2\text{O}$), 3.90 (6H, s, $-\text{C}(\text{O})\text{OCH}_3$), 3.66-3.57 (20H, m, $-\text{OCH}_2\text{-CH}_2\text{O}$, $\text{OCH}_2\text{-CH}_2\text{O-CH}_2-$). ^{13}C NMR (CDCl_3) δ ppm: 52.26, 69.56, 70.12, 70.42, 104.64, 113.39, 122.58, 123.00, 125.55, 127.78, 130.58, 130.72, 132.84, 141.69, 155.78, 155.85, 166.65. FTIR (KBr) (cm^{-1}): 3440, 2921, 1717, 1575, 1509, 1460, 1391, 1320, 1277, 1248, 1188, 1094, 1037, 949, 859, 795. MALDI-TOF $m+1$: 859.2

Synthesis of Azo Model Compounds

Synthesis of 4-(4'-methoxy-phenylazo)-benzoic acid methyl ester (**P0**):

The model compound methoxy ester (**P0**), was synthesized adopting the same esterification procedure that was used for the preparation of the azo carboxyl dye ester. 4-(4'-hydroxy-phenylazo)-benzoic acid (1 g, 4 mmol), 0.5 mL sulphuric acid and 20 mL dry methanol were refluxed overnight. The reaction mixture was then poured into cold water, neutralized with base and the precipitate was filtered, washed with water and dried. The crude product was purified by column chromatography using hexane-ethyl acetate (v/v 95/5) mixture. Yield = 0.9g (86 %) ^1H NMR (CDCl_3) δ ppm: 8.18 (2H, d, Ar), 7.97 (4H, m, Ar), 7.04 (2H, d, Ar), 3.95 (3H, s, $-\text{C}(\text{O})\text{OCH}_3$), 3.90 (3H, s, OCH_3). ^{13}C NMR (CDCl_3) δ ppm: 52.10, 55.57, 114.37, 122.34, 125.16, 130.55, 131.30, 147.19, 155.49, 162.76, 166.57. FTIR (KBr) (cm^{-1}): 2949, 2857, 1717, 1602, 1449, 1404, 1282, 1254, 1191, 1106, 1026, 9734, 866, 840, 776, 697, 552. HRMS m : 270.29

Synthesis of 4-(4'-ethoxy-biphenyl-4-ylazo)-benzoic acid methyl ester (Pp0)

In the case of the biphenyl derivative, the ether preparation involved two steps as the esterification procedure did not work out. In the first step, the carboxylic acid was converted into methyl ester. For this, 4-(4'-hydroxy-biphenylazo)-benzoic acid (1 g, 3 mmol), 0.5 mL sulphuric acid and 20 mL dry methanol was refluxed overnight. The reaction mixture was then poured into cold water, neutralized with base and the precipitate was filtered, washed with water and dried.

Yield = 0.9 g (89 %) ^1H NMR (CDCl_3) δ ppm: 8.23 (2H, m, Ar), 7.96 (2H, m, Ar), 7.68 (2H, m, Ar), 7.50 (4H, m, Ar), 7.15 (2H, m, Ar), 3.89 (3H, s, $-\text{C}(\text{O})\text{OCH}_3$) ^{13}C NMR (CDCl_3) δ ppm: 52.44, 115.65, 122.09, 126.62, 128.27, 128.89, 129.81, 130.85, 132.88, 140.76, 151.61, 155.34, 157.42, 166.01. FTIR (KBr) (cm^{-1}): 3368, 1720, 1597, 1427, 1273, 1112, 1015, 963, 861, 831, 689, 635, 593, 562. HRMS $m+1$: 321.13

In the second step, the hydroxy group of the dye was converted into ethoxy derivative by using the ester (0.91 g, 2.7 mmol), ethyl iodide (0.63g, 4.05 mmol) and potassium carbonate (0.63 g, 4 mmol) in dry acetone as solvent (15 mL) under reflux condition for 48 h. The reaction mixture was extracted with dichloromethane, dried over anhydrous sodium sulphate and solvent evaporated and then dried. The crude product was purified by column chromatography using hexane-ethyl acetate (v/v 95/5) mixture.

Yield = 0.9 g (90 %) ^1H NMR (CDCl_3) δ ppm: 8.20 (2H, d, Ar), 7.98 (3H, m, Ar), 7.71 (H, m, Ar), 7.62 (2H, m, Ar), 7.46 (2H, m, Ar), 7.35 (H, m, Ar), 7.18 (H, m, Ar), 4.35 (2H, m, OCH_2CH_3), 3.95 (3H, s, $-\text{C}(\text{O})\text{OCH}_3$), 1.58 (3H, t, $-\text{OCH}_2\text{CH}_3$) ^{13}C NMR (CDCl_3) δ ppm: 14.71, 52.25, 55.59, 114.29, 122.33, 125.16, 130.56, 131.13, 146.98, 155.33, 162.64, 166.63. FTIR (KBr) (cm^{-1}): 2978, 1722, 1602, 1512, 1488, 1435, 1394, 1275, 1188, 1174, 1150, 1109, 1038, 1012, 922, 894, 863, 815, 760, 694, 530. HRMS $m+1$: 361.24

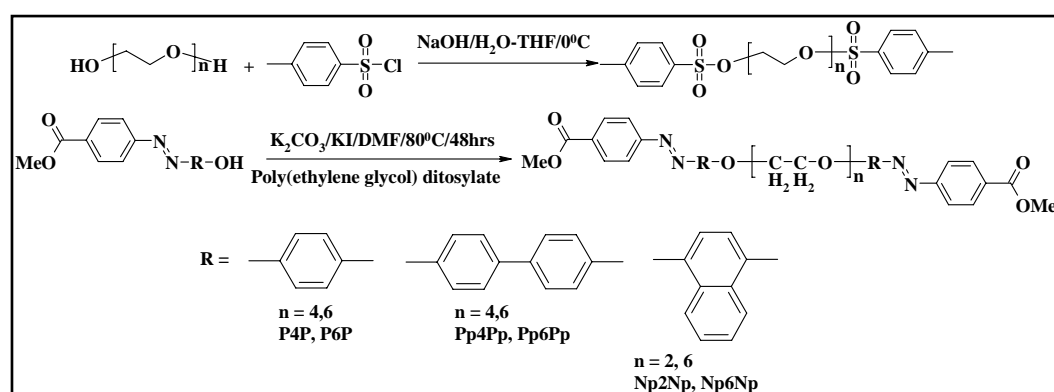
Synthesis of 4-(4'-methoxy-naphthalen-1-ylazo)-benzoic acid methyl ester

(Np0): The model compound **Np0**, was synthesized adopting the same esterification procedure that was used for the preparation of the azo carboxyl dye

ester. 4-(4'-hydroxy-naphthalen-1-ylazo)-benzoic acid (1 g, 3 mmol), 0.5 mL sulphuric acid and 20 mL dry methanol were refluxed overnight. The reaction mixture was then poured into cold water, neutralized with base and the precipitate was filtered, washed with water and dried. The crude product was purified by column chromatography using hexane-ethyl acetate (v/v 95/5) mixture. Yield = 1 g (90 %) ^1H NMR (CDCl_3) δ ppm: 8.99 (1H, d, Ar), 8.34 (1H, d, Ar), 8.23 (2H, m, Ar), 8.05 (3H, m, Ar), 7.72 (1H, d, Ar), 7.62 (1H, d, Ar), 6.95 (1H, d, Ar), 4.11 (3H, s, $-\text{C}(\text{O})\text{OCH}_3$), 3.97 (3H, s, OCH_3) ^{13}C NMR (CDCl_3) δ ppm: 52.08, 55.84, 103.76, 113.67, 122.19, 123.09, 125.73, 125.88, 127.74, 130.57, 131.18, 132.86, 141.89, 155.98, 159.18, 166.57. FTIR (KBr) (cm^{-1}): 2950, 2923, 1720, 1630, 1602, 1322, 1275, 1188, 1063, 1037, 955, 922, 859, 760. HRMS $m+1$: 321.78

4.5 Results and Discussion

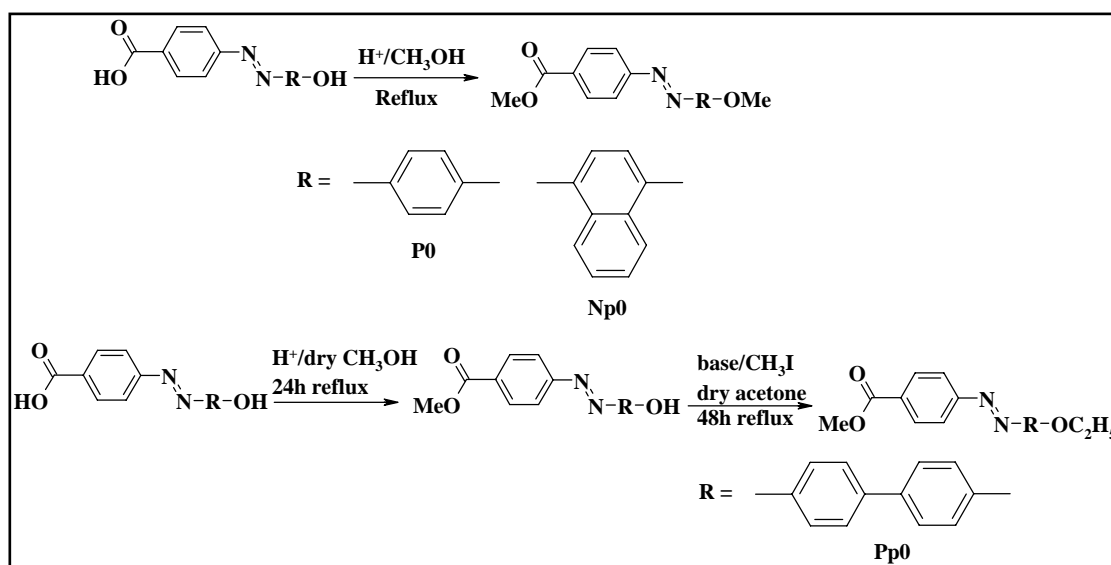
The general scheme of synthesis of the azo bichromophores is shown in scheme 6.



Scheme 6 Synthesis of bichromophores

The ditosylates of polyethylene glycols were prepared by reacting the diol with p-toluene sulphonyl chloride at 0°C in THF solvent. The ditosylates were then coupled with azo dye esters to obtain the corresponding azochromophore-ethylene glycol spacer-azochromophore bichromophores. For the phenol and phenyl phenol series, two bichromophores having four and six ethylene glycol units as the central spacer segment was synthesized. For the naphthol series, a spacer of shorter length – di ethylene glycol and another of longer length – hexa

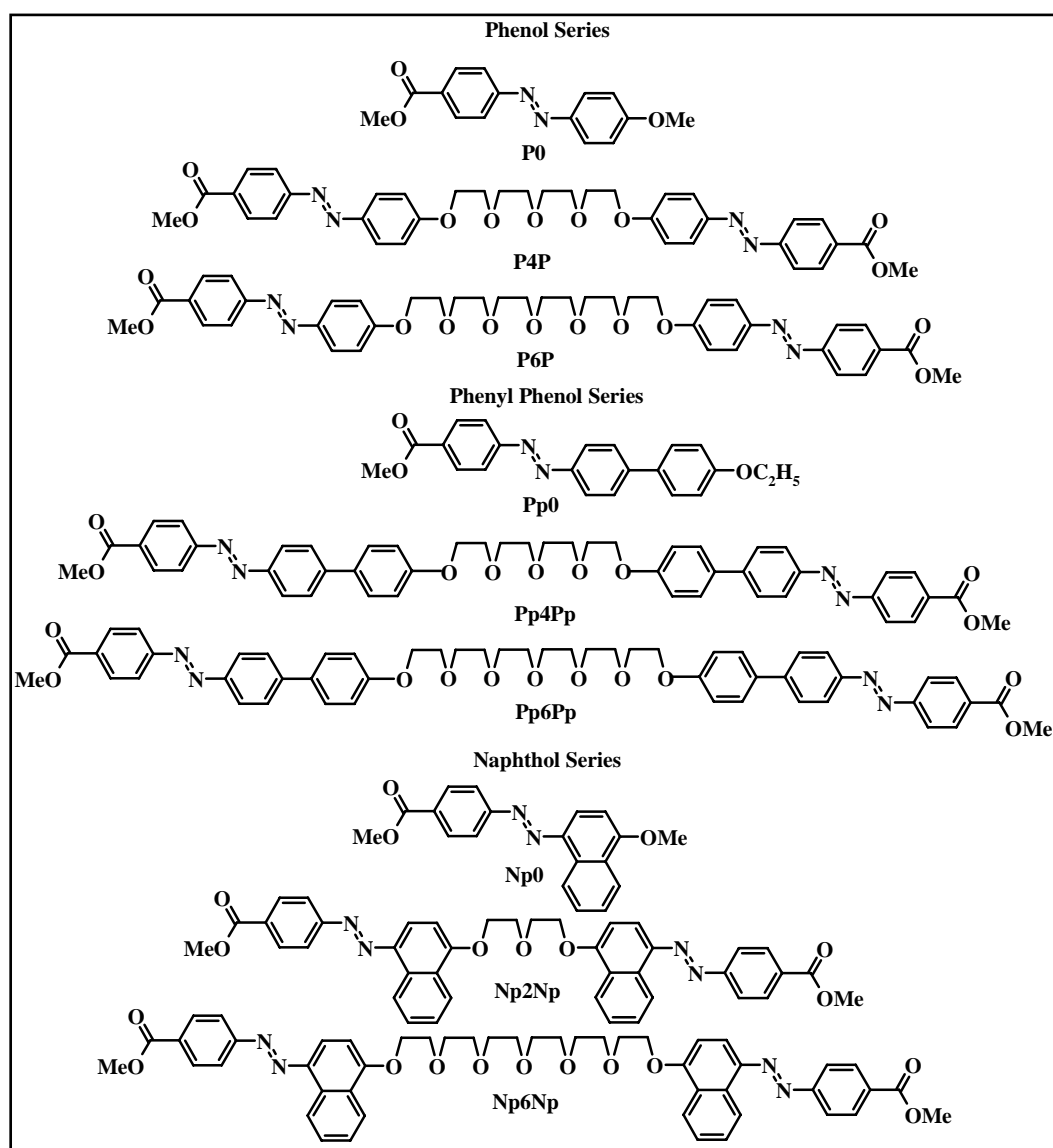
ethylene glycol were chosen for the central spacer segment. The naphthol chromophore has been well studied in the literature for its excimer forming tendency. Therefore, it was expected that the effect of the spacer length on the excimer formation in the naphthol based azo bichromophores would be more discernible using a spacer of shorter length (two ethylene glycol units). Three model compounds corresponding to phenol (**P0**), phenyl phenol (**Pp0**) and naphthol (**Np0**) were also synthesized as given in scheme 7. **P0** and **Np0** were synthesized using the same procedure for esterification i.e reflux in presence of acid in methanol as solvent. Normally introduction of ether linkage at the phenolic position requires reaction of an alkyl halide in presence of base. However, in these push-pull azo systems, carrying out esterification for slightly longer time resulted in esterification of the carboxyl group as well as introduction of ether linkage at the phenolic position. However, the same procedure did not yield the desired product in the case of the phenyl phenol azo molecule (**Pp0**). This could be probably due to the out-of-plane twisting of the two rings of phenyl phenol which reduces the through conjugation in the molecule. The structures of all the molecules are given in scheme 8. The structure of all the molecules was confirmed by ^1H and ^{13}C NMR, UV-Vis and FT-IR spectroscopy. Figure 1 shows the ^1H NMR spectra of the ditosylates and figure 2 (a, b, c) that of the bichromophores and the various types of protons are labeled by alphabets.



Scheme 7 Synthesis of model compounds

The purity of all the molecules was confirmed by size exclusion chromatography (SEC) and high resolution mass spectroscopy (HRMS) or matrix assisted laser desorption ionization-time of flight (MALDI-TOF). Figure 3 shows the SEC plot of the bichromophoric molecules and model compounds and the molecules showed a single chromatogram which confirmed the purity of the samples. As expected, the elution time of the molecules increases with the decrease in the molecular weights. In the HRMS/MALDI-TOF analysis, molecular ion peaks were obtained for m or $m+1$ radical. Figure 4, figure 5 and figure 6 shows HRMS/MALDI-TOF spectrum of the bichromophores and model compounds. In the MALDI-TOF spectra of **P6P**, **Pp6Pp** and **Np6Np**, molecular ion peaks $m+1$ radical, $m + \text{Na}$ and $m + \text{K}$ were obtained. Sodium and potassium salts were used in the synthesis steps of these bichromophoric molecules. In contrast to the MALDI spectra of diethyleneoxy and tetraethyleneoxy spacer tethered twin molecules, hexaethyleneoxy spacer linked twins showed a distribution of molecular mass which is characteristic of oligomers and polymers. For example, in the case of **P6P**, in addition to the peaks $m + \text{Na}$ (peak at 781.5) and $m + \text{K}$ (797.2), peaks corresponding to tetra, penta as well as heptaethyleneoxy tethered twin molecules were also obtained. So the additional peak at 693.3 corresponded to tetraethyleneoxy derivative plus Na, the peak at

737.3 corresponded to pentaethyleneoxy derivative and the peak at 825.6 corresponded to the heptaethyleneoxy spacer derivative plus Na. The same trend was observed in the other two hexaethyleneoxy spacer twin molecules **Pp6Pp** and **Np6Np** also. The NMR, SEC and HRMS/MALDI-TOF data confirmed the structure and high purity of the synthesized molecules.



Scheme 8 Structure of all molecules

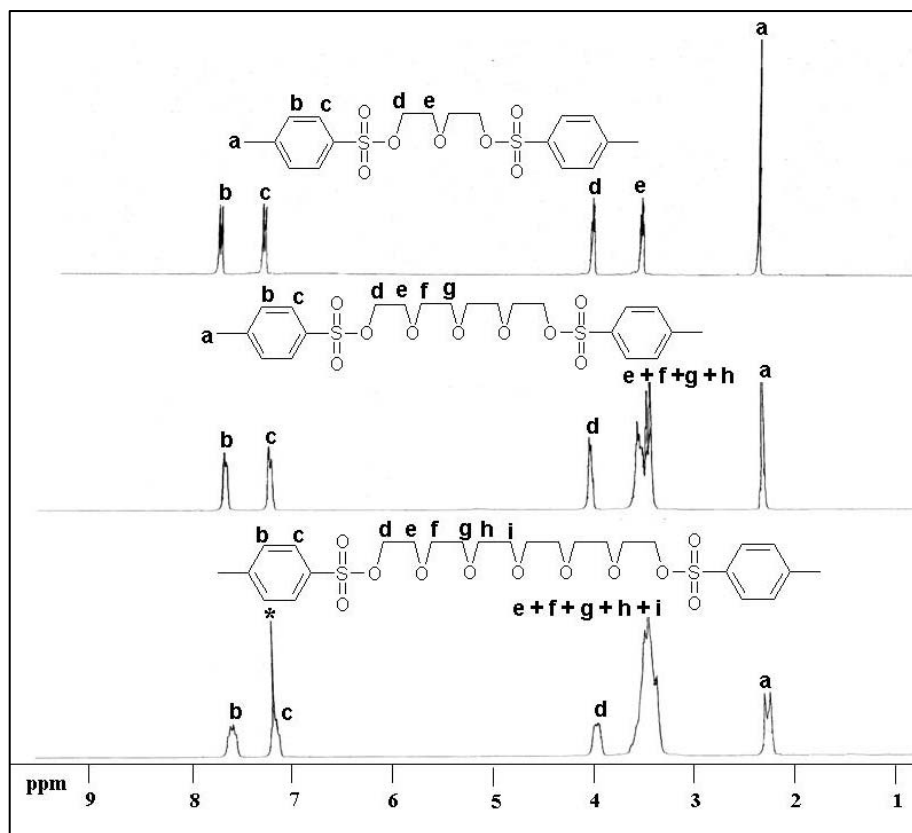


Figure 1 ^1H NMR spectra of polyethyleneoxy ditosylates

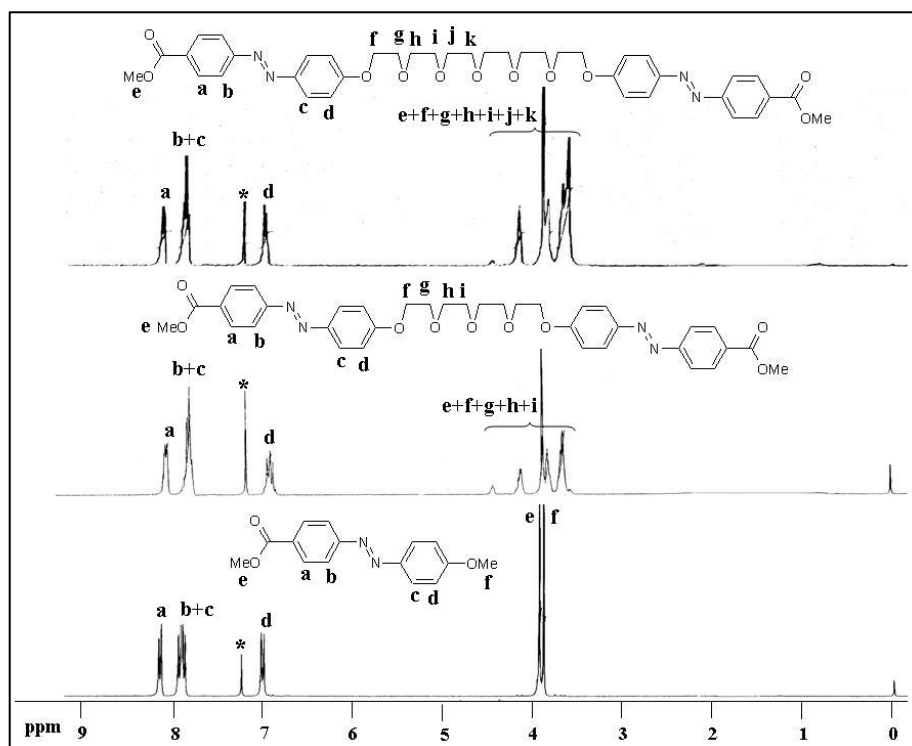


Figure 2a ^1H NMR spectra of phenol series **P0**, **P4P** and **P6P**

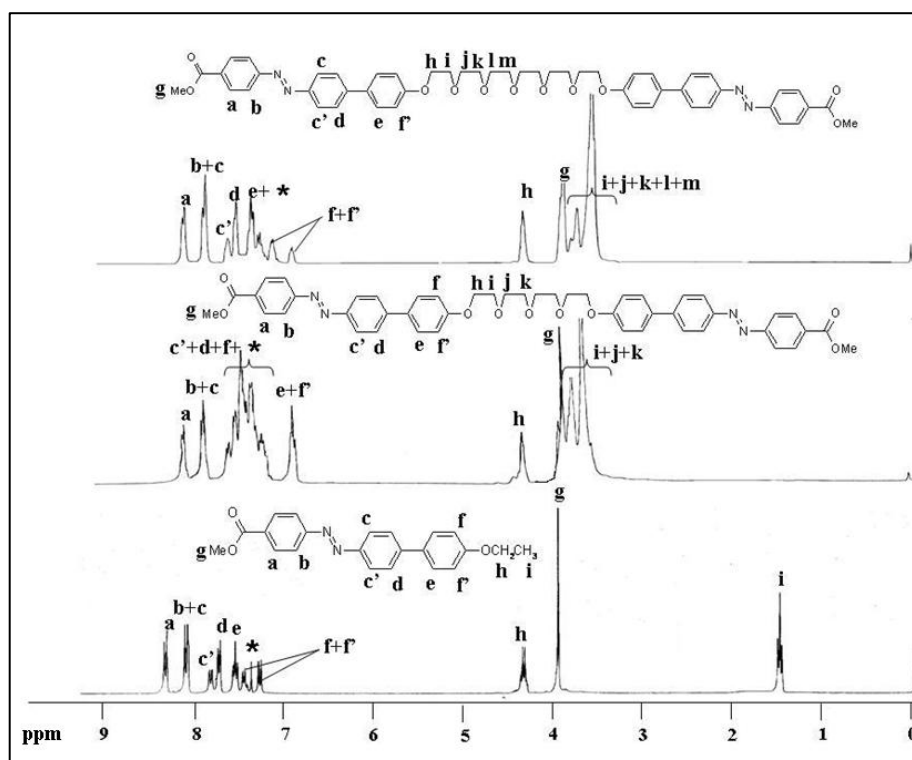


Figure 2b ^1H NMR spectra of phenyl phenol series **Pp0**, **Pp4Pp** and **Pp6Pp**

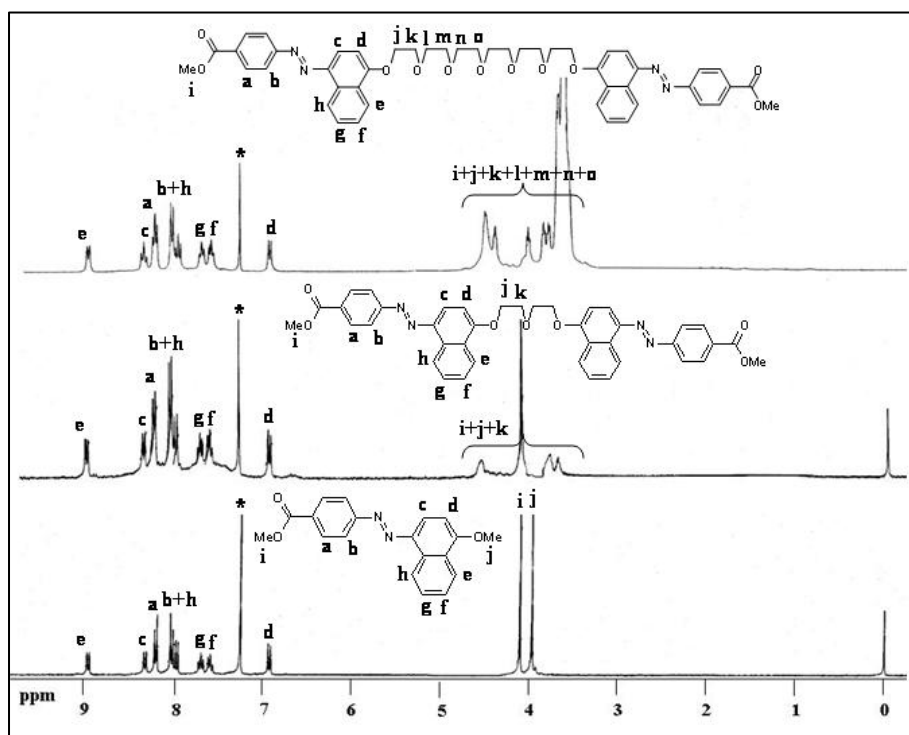


Figure 2c ^1H NMR spectra of **Np0**, **Np2Np** and **Np6Np**

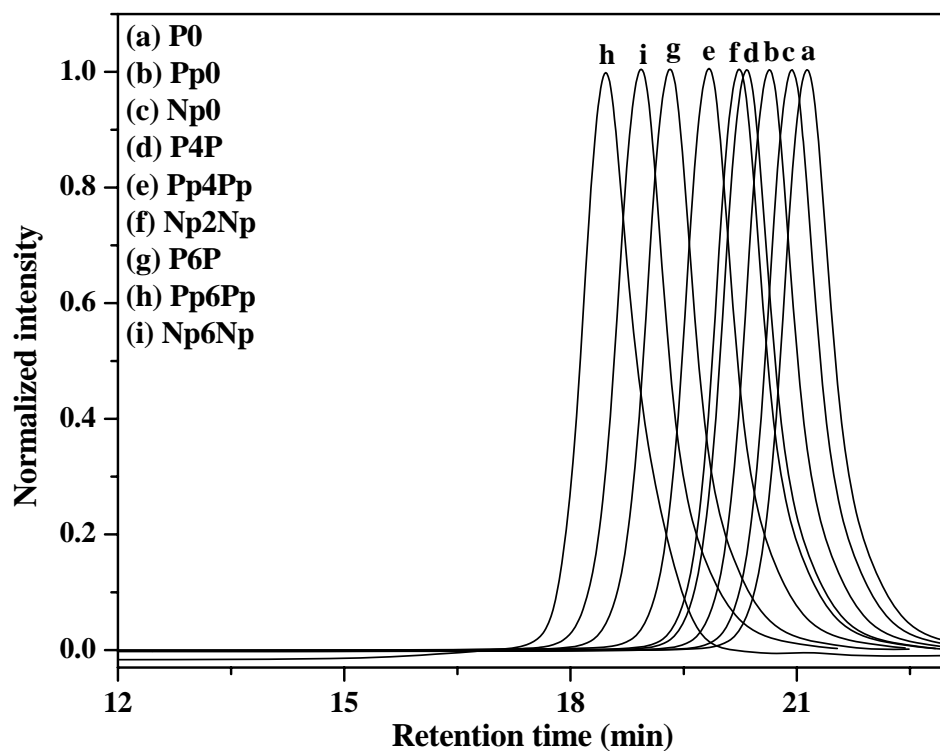


Figure 3 GPC chromatogram of bichromophores and model compounds

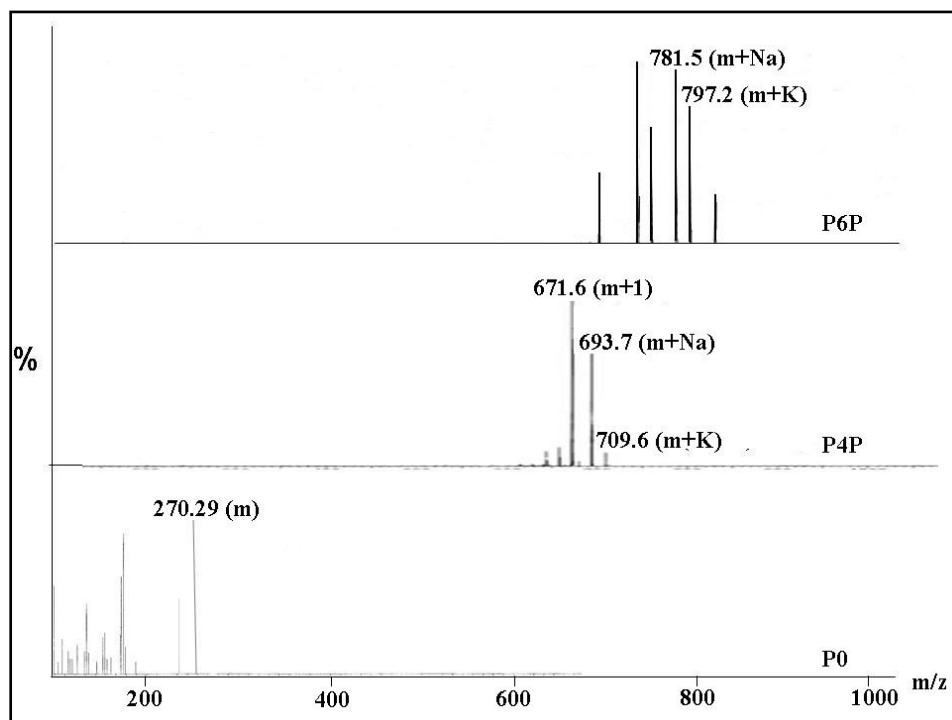


Figure 4 Mass spectra of phenol based azo series

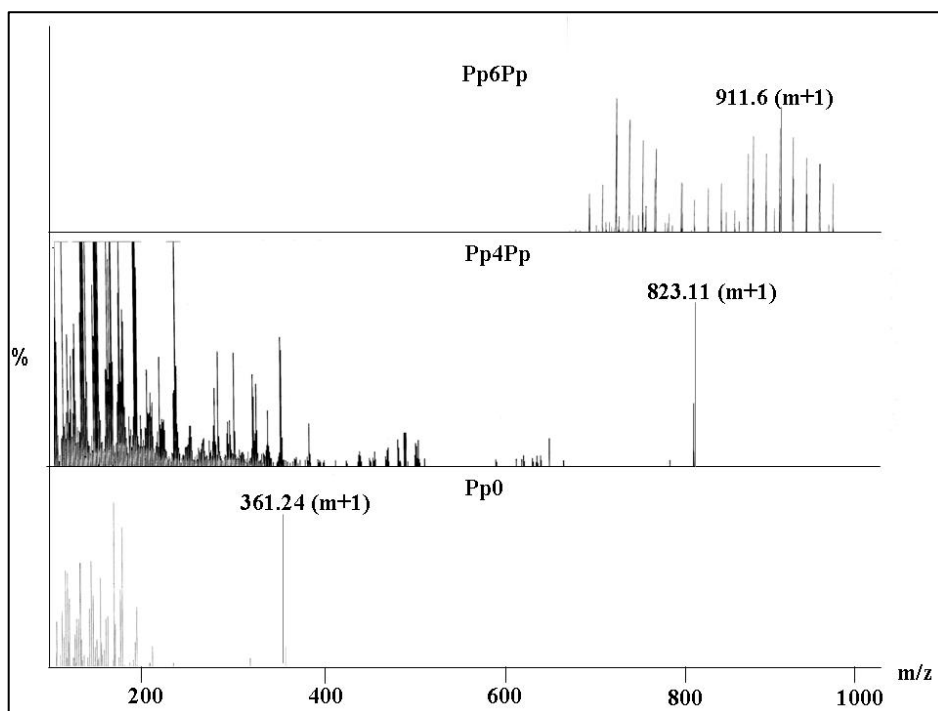


Figure 5 Mass spectra of phenyl phenol based azo series

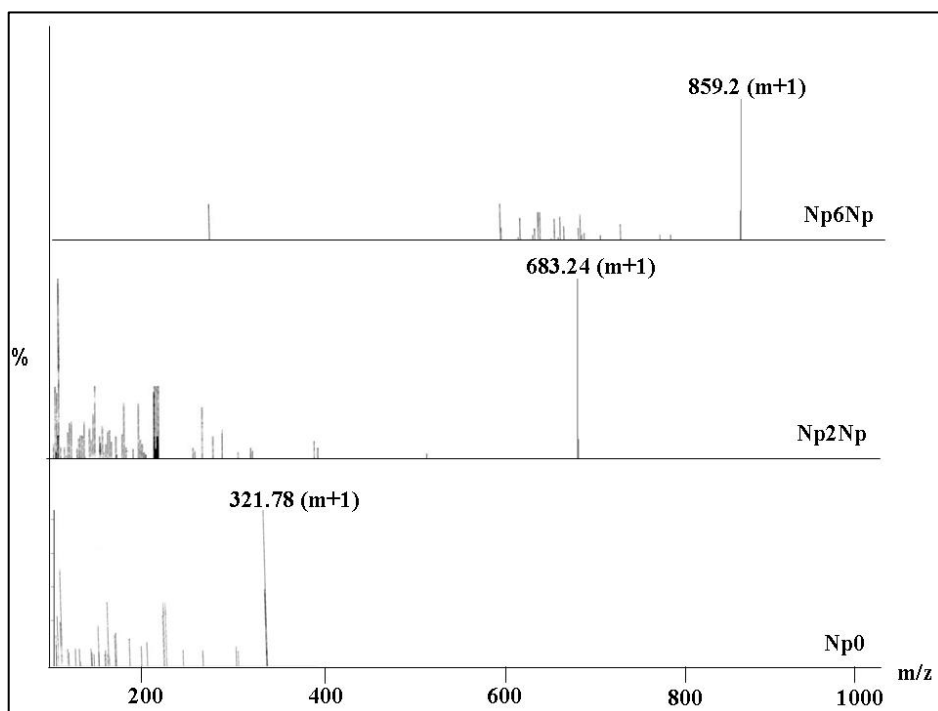


Figure 6 Mass spectra of naphthol based azo series

4.6 Photophysical Properties

The absorption spectra of azobenzenes consist of three absorption bands. The lowest energy transition occurs at approximately 430-440 nm and is assigned to the $n-\pi^*$ transition. The second transition occurs in the UV region around 320 nm and is assigned to the $\pi-\pi^*$ transition for trans azobenzene (for cis azobenzene the $\pi-\pi^*$ band occurs around 280 nm). The peak maximum of this band is sensitive to the polarity and also to the presence of substituents. The third energy transition around 230-240 nm is considered to arise from the $\pi-\pi^*$ transition in the phenyl rings. The absorption spectra of the bichromophores along with the corresponding model compounds are given in figure 7.

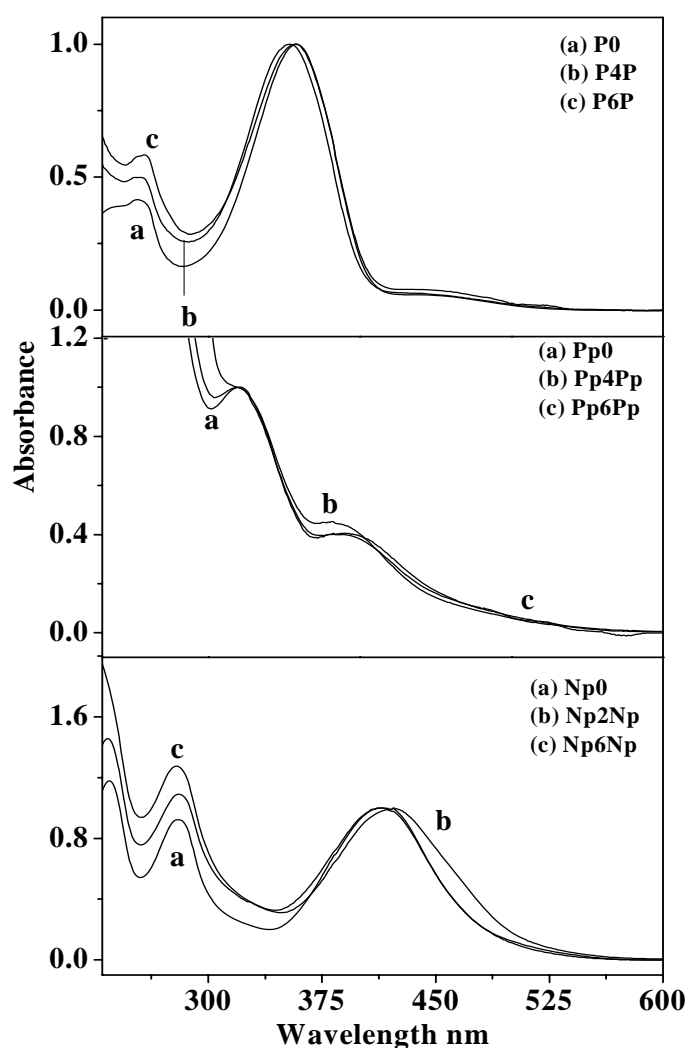


Figure 7 Absorption spectra of bichromophores and model compounds

In push-pull substituted aromatic azobenzene systems, there is an overall red shift of the π - π^* transitions.⁴⁸ Thus, in the simple phenol based azobenzene molecule, for example **P0** with the ester group at one end and methoxy group at the other end, the n - π^* transition occurs at ~436 nm, the π - π^* transition at 358 nm and the aromatic phenyl π - π^* transition at ~250 nm. In the more conjugated naphthol based azobenzene molecule **Np0**, on the other hand, the n - π^* band is almost wholly overlain by the bathochromically shifted π - π^* band which appears at 414 nm. The aromatic phenyl π - π^* transitions are observed at ~280 and 235 nm. The π - π^* transition corresponding to the azo unit was slightly red shifted in the case of the bichromophore with the shortest spacer length (**Np2Np**) and it appeared at 422 nm unlike in **Np0** and **Np6Np** where it occurred at 414 nm. In the phenyl phenol based azomolecule **Pp0**, the n - π^* transition is at ~390 nm, the π - π^* transition is at 320 nm and the aromatic phenyl π - π^* transition is at ~260 nm. This blue shift in the π - π^* and n - π^* transitions is due to the lack of planarity of the two phenyl rings of phenyl phenol. The wavelength of absorption maximum in the UV-Vis spectra recorded in dichloromethane for all the azo molecules are given in table 1.

Concentration dependent UV absorption measurements in dichloromethane (DCM) for the model compounds as well as bichromophores of all the three azobenzene series showed that they followed the Beer Lambert law and their spectral shape remained unchanged indicating the absence of any strong intra or inter molecular interactions between the chromophores in solution in the ground state. All the molecules were subjected to solvatochromic absorption measurements in five different solvents of varying polarity namely toluene, dichloromethane, methanol, acetonitrile and dimethyl formamide. The absence of any significant positive or negative shift in absorption maxima with solvent polarity ruled out the possibility for any charge transfer process occurring in these systems.

Table 1 Absorption data

Sample	Solution (in DCM) λ_{\max} Abs (ϵ , M^{-1} , cm^{-1})
P0	253 (56600), 358 (136050), 436 (5810)
P4P	252 (18700), 355 (42490), 431 (6470)
P6P	258 (17360), 359 (52210), 433 (7840)
Pp0	266 (53590), 320 (23700), 390 (40580)
Pp4Pp	263 (40590), 319 (5180), 382 (34860)
Pp6Pp	263 (61030), 320 (27080), 380 (19780)
Np0	235 (103100), 280 (80550), 414 (87250)
Np2Np	232 (50760), 280 (12960), 422 (10140)
Np6Np	232 (32260), 279 (16290), 414 (12080)

4.7 Emission Properties

Naphthalene exhibits structured fluorescence emission spectra characteristic of the monomer with maxima at 337-375 nm and a broad structureless excimer peak \sim 390 nm. Incorporation of the naphthalene fluorophore into the azobenzene system modifies its emission characteristics. The fluorescence from simple unsubstituted trans azobenzene itself is a peculiar case where Kasha's rule is not followed because the S_2 fluorescence appears with much higher intensity than the S_1 fluorescence. Indeed, most of the fluorescence reported in literature for azobenzene derivatives have been considered to have π - π^* (S_2) character. However, in spite of the fact that azobenzene is one of the most thoroughly studied systems in literature as far as photoisomerization is concerned, there is not much reliable data available for

fluorescence studies especially after photoexcitation of its aromatic phenyl π - π^* transition.

The bichromophores and their corresponding model compounds were excited at both the aromatic phenyl π - π^* transition at 260 nm for the phenol and phenyl phenol series and 280 nm for the naphthol series as well as at the π - π^* transition corresponding to the N=N bond at 356 nm for the former and 320 nm for the phenyl phenol series and \sim 414/422 nm for the naphthol series respectively. Figure 8 shows the emission spectra for the phenol series at a concentration of 1×10^{-5} M recorded in DCM. The phenol series did not show any emission upon excitation at 260 nm but gave a weak emission with very low quantum yield upon excitation at 356 nm corresponding to the π - π^* transition of the N=N bond.

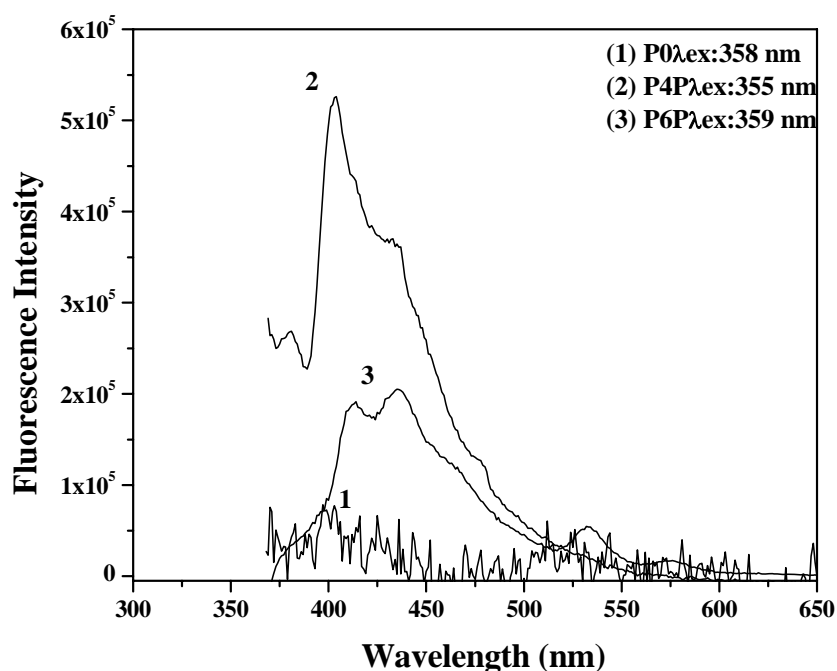


Figure 8 Emission spectra of phenol based azo series

Table 2 gives the emission λ_{\max} values and the quantum yield for the emission for all the molecules. Quinine sulphate was used as the reference compound for the determination of quantum yield of the phenol, phenyl phenol series and naphthol series. It can be seen from table 2 that among the whole series, the

model compound **Pp0** possessed the highest quantum yield with a value of 0.35 whereas among the bichromophores, **Pp4Pp** possessed the highest value of 0.11.

Figure 9 shows the emission spectra for the phenyl phenol series recorded in DCM upon excitation at both the aromatic phenyl π - π^* transition at 260 nm as well as at the π - π^* transition corresponding to the N=N bond 320 nm.

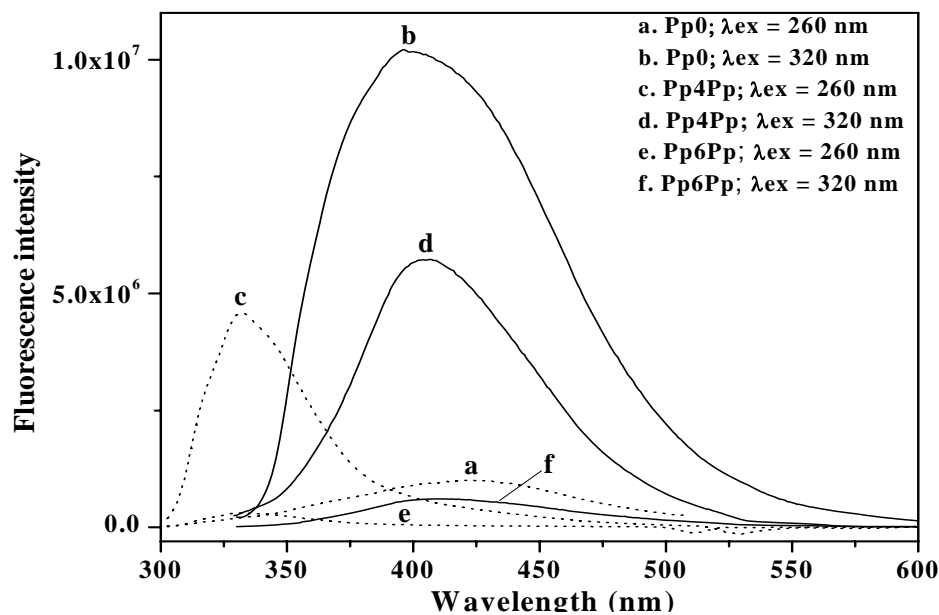


Figure 9 Emission spectra of phenyl phenol based azobenzene series

Table 2 Emission properties of the azobenzene series in dichloromethane

Sample	λ_{\max}^a Em (λ_{exc} : 260/280 nm)	ϕ_{FL}	λ_{\max}^b Em (λ_{exc} : 350/320/415 nm)	ϕ_{FL}
P0	-	-	442	0.004 ^c
P4P	-	-	403, 433	0.006 ^c
P6P	-	-	412, 436	0.001 ^c
Pp0	424	0.14	396	0.35 ^c
Pp4Pp	332	0.15	405	0.11 ^c
Pp6Pp	332	0.009	410	0.012 ^c
Np0	332, 398	0.034	504	0.022
Np2Np	339, 390, 437	0.019	465	0.009
Np6Np	340, 414	0.031	495	0.018

- a. Emission maxima by exciting at the π - π^* transition of the aromatic rings
- b. Emission maxima by exciting at the π - π^* transition of the N=N bond
- c. Quinine sulphate was used as reference for quantum yield calculation

In the phenyl phenol series, when excited at around 260 nm, the model compound **Pp0** exhibited emission maximum at 424 nm whereas **Pp4Pp** and **Pp6Pp** showed emission maxima at 332 nm. When these molecules were excited at the π - π^* transition of the N=N bond (320 nm), the emission maxima appeared at 396, 404 and 412 nm for **Pp0**, **Pp4Pp** and **Pp6Pp** respectively. The emission maxima obtained when excited at both 260 nm and 320 nm matches very well with the n - π^* band of the absorption spectra which clearly indicates that the emission is from the S_1 state in the case of **Pp0**. At the same time, **Pp4Pp** and **Pp6Pp** when excited at 260 nm emits from the S_2 state. This difference in emission behavior may be due to the difference in the planarity of the molecules.

In the case of **Pp0**, when excited using a higher energy (260 nm), the emission occurred at a lower energy (424 nm) than when excited at a lower energy (320 nm). This may be due to the fact that when excited at 260 nm, the molecule reaches a higher vibrational level of first excited state (S_1) from which it undergo vibrational relaxation to a less energy vibrational level before it emits. From figure 9 it can be seen that in the phenyl phenol based azobenzene series, the fluorescence intensity was highest when excited at the π - π^* transition of the N=N bond i.e 320 nm. The shorter tetraethylene glycol tethered bichromophore had higher fluorescence intensity compared to that of the hexaethylene glycol spacer tethered molecule. A similar spacer effect was observed in the phenol series also, where the shorter tetraethylene glycol spacer had higher fluorescence emission and quantum yield compared to the longer hexaethylene glycol spacer.

Figure 10 (a-c) gives the emission spectra of the naphthol based azobenzene molecules in DCM upon excitation at 280 and 414 nm at a concentration of 10^{-7} M. The emission from the model compound **Np0** had peak maxima at 330 nm with a tapering shoulder. The spectra upon deconvolution gave two peaks centered at 334 and 374 nm respectively. The bichromophore **Np2Np** had a

shoulder at 340 nm, maxima at 390 and 437 nm. **Np6Np** had a small shoulder at 240 nm and peak at 395 nm with a broad shoulder. This spectrum upon deconvolution gave three peaks centered at 329, 389 and 472 respectively.

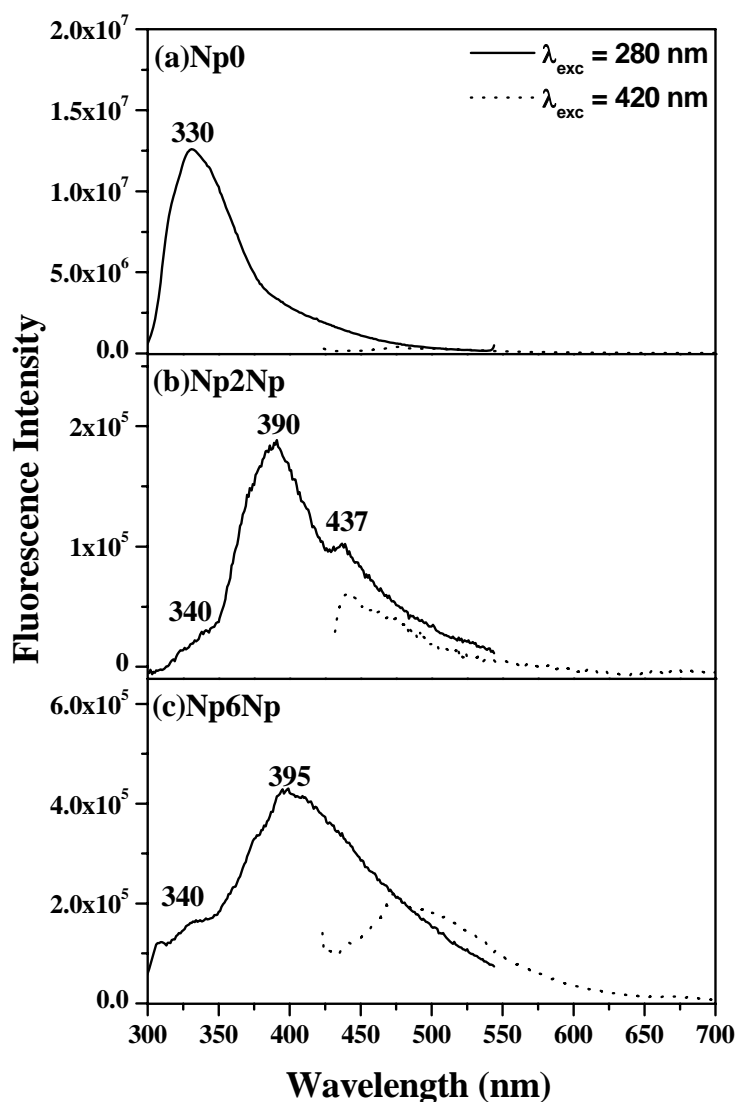


Figure 10 Emission spectra of naphthol based azo series (a) **Np0** (b) **Np2Np** and (c) **Np6Np**

At the very dilute concentration of 1×10^{-7} M all three molecules had very weak emission centered ~ 478 nm upon excitation at 415 nm. Table 2 gives the emission λ_{max} values and the quantum yield for the emission. The strong fluorescence band at ~ 390 nm which was present only in the naphthol azo benzene series and not in the phenol based azo benzene molecule (**P0**) could be assigned to excimer emission. To get a better understanding of the species

responsible for this emission, the excitation spectra were recorded at the monomer and excimer emission.

Figure 11 shows the normalized absorption, excitation and fluorescence spectra of the naphthol series in dichloromethane at a concentration of 1×10^{-7} M. In the figure, plot 'a' corresponds to UV-Vis absorption, 'b' is the emission upon excitation at 280 nm, and 'c' and 'd' are excitation spectra recorded while monitoring the monomer emission at 338 nm and the excimer emission monitored at 390 nm respectively. The S_2 nature of the fluorescence become clearly evident from the figure since the emission λ_{max} is at ~ 390 nm which is energetically higher than the $S_1(n\pi^*) \leftarrow S_0$ transition as well the $S_2(\pi\pi^*) \leftarrow S_0$ transition at 415 nm (the $S_1(n\pi^*) \leftarrow S_0$ peak is in fact overlaid by the $S_2(\pi\pi^*) \leftarrow S_0$ peak). In addition, the fluorescence band also shows a good mirror image of the $S_2(\pi\pi^*) \leftarrow S_0$ absorption band at 280 nm.^{49, 50} These are all clear indication to the fact that the fluorescence corresponds to S_2 and not S_1 . As discussed earlier, the fluorescence in azobenzene systems are an example where violation of Kasha's rule occurs. From the excitation spectra, it can be seen that the excitation spectra for the monomer (monitored at 338 nm, curve 'c') and excimer (monitored at 390 nm, curve 'd') are different for **Np0** and the bichromophores **Np2Np** and **Np6Np**. Since no new peaks were observed in the absorption spectra even at high concentrations indicating the absence of any aggregate formation in the ground state, the emission peak at 390 nm could be assigned to excimer formation.²⁴

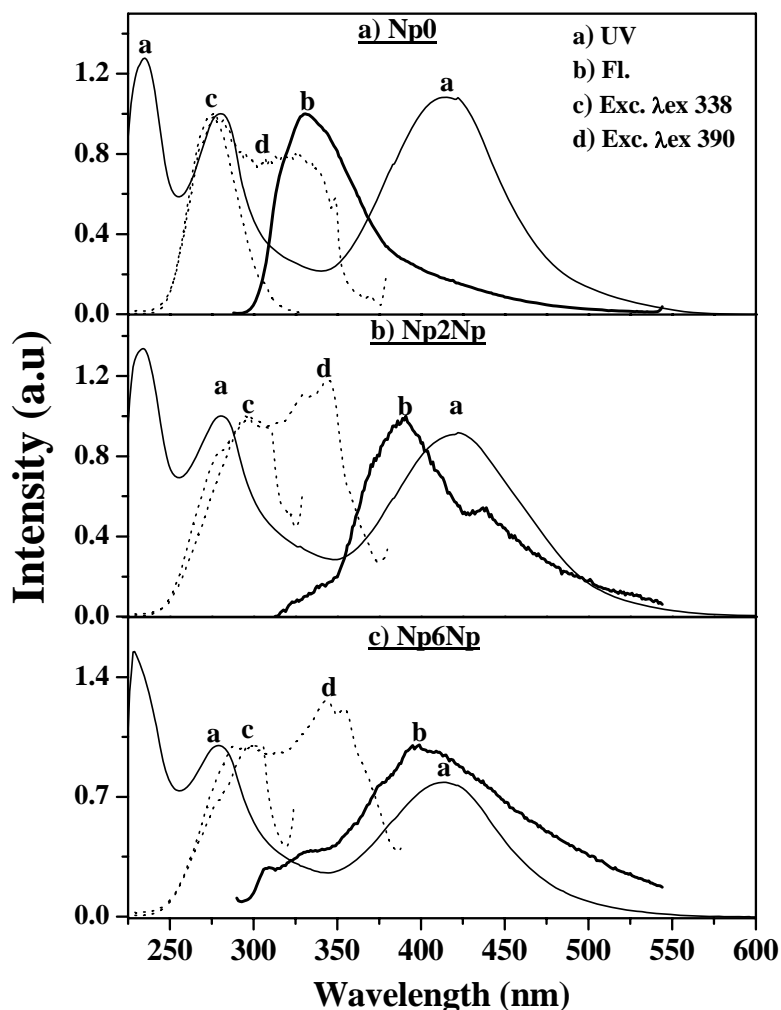


Figure 11 Absorption, emission (λ_{ex} : 280 nm) and excitation spectra of naphthol based azo series

The model compound and the bichromophores have two peaks in the excimer excitation spectra. In **Np0**, one of the peaks overlays exactly with the monomer excitation spectra while the second peak is red shifted by >30 nm. The monomer excitation spectra match exactly with the absorption at 280 nm. In the case of the bichromophores, even the monomer excitation spectra were slightly red shifted from the 280 nm band in the absorption spectra whereas the excimer excitation spectra was considerably redshifted with the redshifted component being the majority fraction. The difference in the excitation spectra of monomer and excimer clearly indicate that the excimer originates from pairs of naphthyl groups which exists prior to excitation ie, a static excimer is formed. From figure

11, it can be seen that the excimer emission is very weak for **Np0** at a concentration of 10^{-7} M whereas at higher concentration, a band corresponding to the excimer originated at ~ 390 nm. The concentration dependence of **Np0** will be discussed later on.

Contrasting the excitation spectra of the naphthol series with that of the phenyl phenol series, the latter is marked by its simplicity. Figure 12 shows the normalized absorption, excitation and fluorescence spectra of the phenyl phenol series in dichloromethane at a concentration of 1×10^{-5} M. In the figure, plot 'a' corresponds to UV-Vis absorption, 'b' and 'c' are the emission upon excitation at 260 nm and 320 nm respectively and 'd' and 'e' are excitation spectra recorded at their corresponding emission maxima. In the case of **Pp0**, the emission spectra obtained by exciting at 260 nm and 320 nm were in the range of 396-424 nm. The fluorescence spectra had good mirror image symmetry with the absorption peak at 320 nm. Also the excitation spectra recorded at 396 and 424 nm were identical and they resembled with π - π^* transition of the N=N bond i.e 320 nm in the absorption spectra. These two factors confirmed the fact that the emitting species is the azo unit of the molecule. Since the emission appeared after 390 nm irrespective of the excitation wavelength it can be concluded that the fluorescence is S_1 in nature for **Pp0**. For the phenyl phenol based bichromophores, **Pp4Pp** and **Pp6Pp**, the nature of spectral pattern was same. The emission spectra obtained by exciting at 260 nm overlapped with the $S_2(n\pi^*) \leftarrow S_0$ peak in the absorption spectrum indicating S_2 fluorescence. The corresponding excitation spectra showed resemblance with the 260 nm band in the absorption spectra and there was a good mirror image relationship between the fluorescence spectra and the 260 nm band. Upon excitation at 320 nm, the emission appeared at higher wavelength with mirror image symmetry with 320 nm band in the absorption spectra.

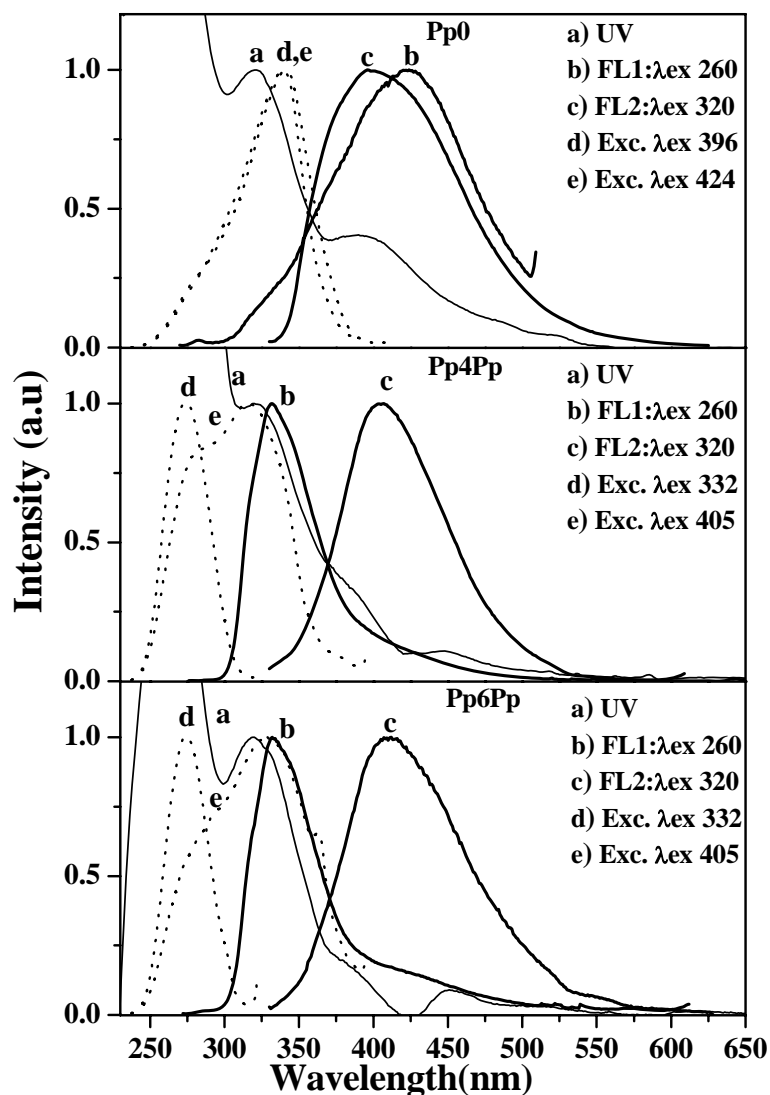


Figure 12 Absorption, emission and excitation spectra of phenyl phenol based azo series

The excitation spectra recorded at 405 nm had two peaks; one peak overlays exactly with the 260 nm band of the absorption spectra while the other overlays with the 320 nm band of the excitation spectra, indicating that the fluorescence has contributions from the phenyl phenol and azo part - in fact the molecule as a whole. The difference in the emission behavior between **Pp0** and the phenyl phenol based bichromophores (**Pp4Pp** and **Pp6Pp**) may be due to the difference in the rotational degree of freedom. When the chromophores are connected via spacer, the flexibility of the spacer renders the freedom of rotation

which effectively reduced the planarity in the case of (**Pp4Pp** and **Pp6Pp**) whereas **Pp0** lacks this freedom which makes it more rigid and planar.

4.8 Variable Solvent Fluorescence Measurements

For a better understanding of the excimer emission in the naphthol series, fluorescence spectra were recorded in solvents of varying polarity.

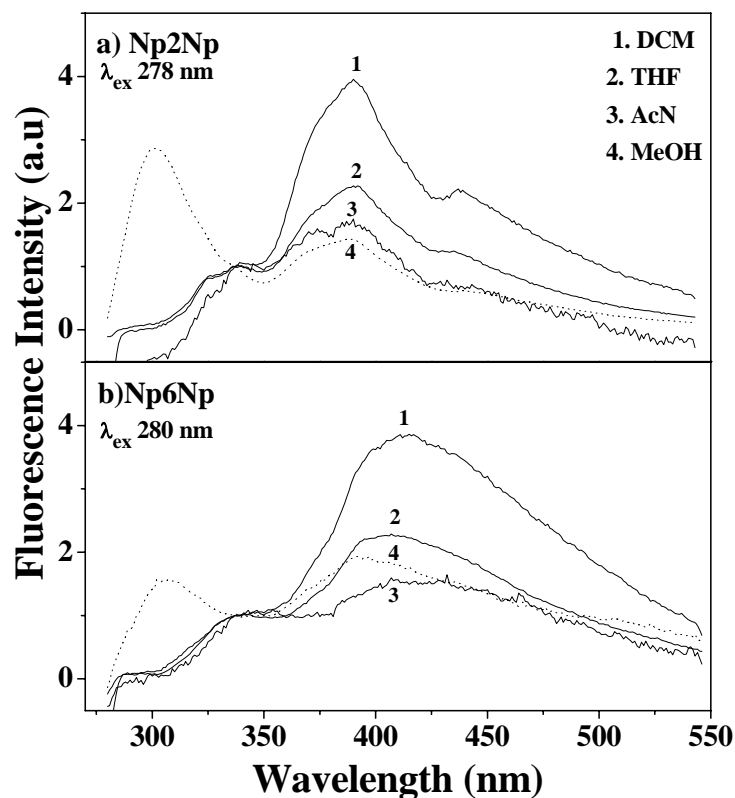


Figure 13 Fluorescence spectra of **Np2Np** and **Np6Np** at a concentration of 1×10^5 M and $\lambda_{ex} \sim 280$ nm in solvents of varying polarity

Figure 13 (a and b) shows the fluorescence spectra of **Np2Np** and **Np6Np** upon excitation at ~ 280 nm in various solvents. The spectra are normalized with respect to the monomer emission at 338 nm. It can be seen from the figure that the band at 390–415 nm does not show any solvatochromic shift with change in solvent polarity; there is no change in the position of λ_{max} with solvent – thereby indicating its non-polar nature.

4.9 Concentration Dependant Fluorescence Measurements

Variable concentration fluorescence measurements were carried out in dichloromethane for the phenyl phenol based bichromophores at concentrations

ranging from 5×10^{-6} to 1×10^{-3} M and for naphthol bichromophores in the range of 1×10^{-7} to 1×10^{-4} M. The UV-Vis spectra did not show any change in either the wavelengths or the shapes of the absorption signals with increase in concentration, except for increased intensity. However, there were changes in the respective fluorescence spectra when the concentration was increased. In the phenyl phenol series, the fluorescence intensity increased with concentration up to a certain level, but further increase in concentration resulted in either partial or complete quenching of the fluorescence. In the case of **Pp4Pp** and **Pp6Pp** upon excitation at 320 nm, the fluorescence increased in intensity initially along with a shift in the emission maxima to the red by 50 nm and 117 nm respectively. Figure 14 a & b shows the shift in emission maxima with concentration for **Pp6Pp** and **Pp4Pp** respectively. This type of red shift in emission maxima is usually attributed to the formation of J-type aggregate in the literature.⁵¹ Excitation at 260 nm, produced an initial increase in fluorescence intensity followed by complete quenching at a concentration of 10^{-3} M without any shift observed in the emission maxima.

Concentration dependant fluorescence measurements can reveal the mode of association of the excited dimeric state ie, inter- or intra. Therefore a concentration dependent fluorescence measurement was carried out for the naphthol bichromophores in DCM. Figure 15 shows a few selected variable concentration fluorescence spectra of (a) **Np0**, (b) **Np2Np** and (c) **Np6Np** upon excitation at 280 nm and 420 nm. For the model compound **Np0**, the solution of concentration of 1×10^{-7} M had an intense emission with peak maxima at 330 nm which had to be scaled by a factor of 5 in order to plot all the spectra in the same range. For the model compound **Np0**, the solution of concentration of 1×10^{-7} M had an intense emission with peak maxima at 330 nm which had to be scaled by a factor of 5 in order to plot all the spectra in the same range.

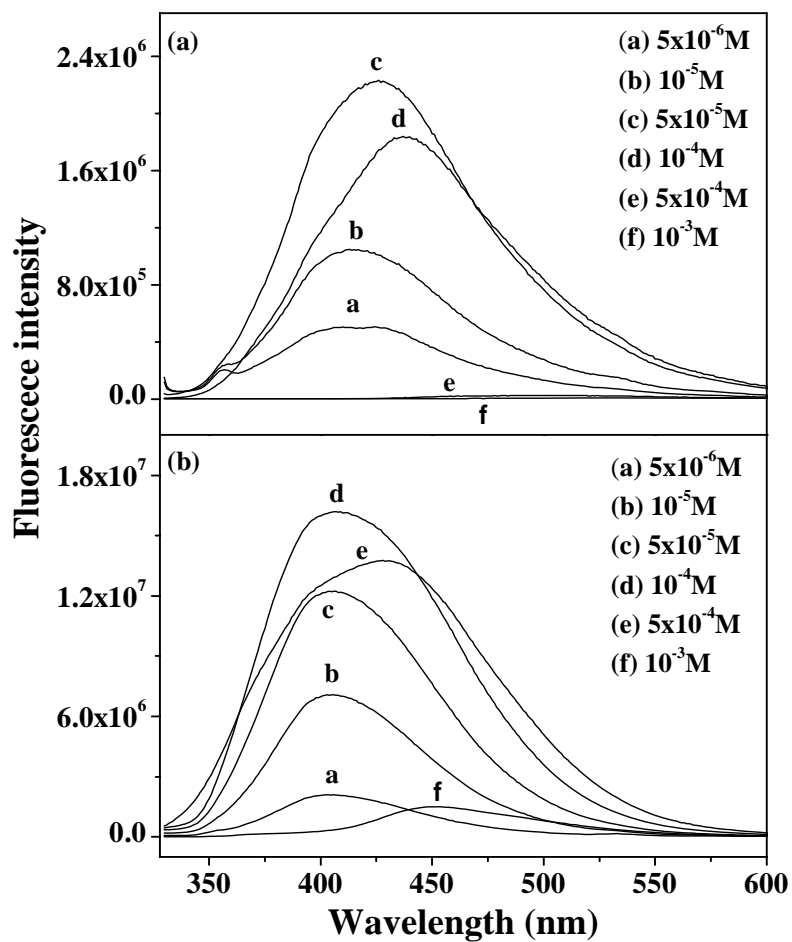


Figure 14 Variable concentration fluorescence spectra of (a) **Pp6Pp** and (b) **Pp4Pp** upon excitation at 320 nm

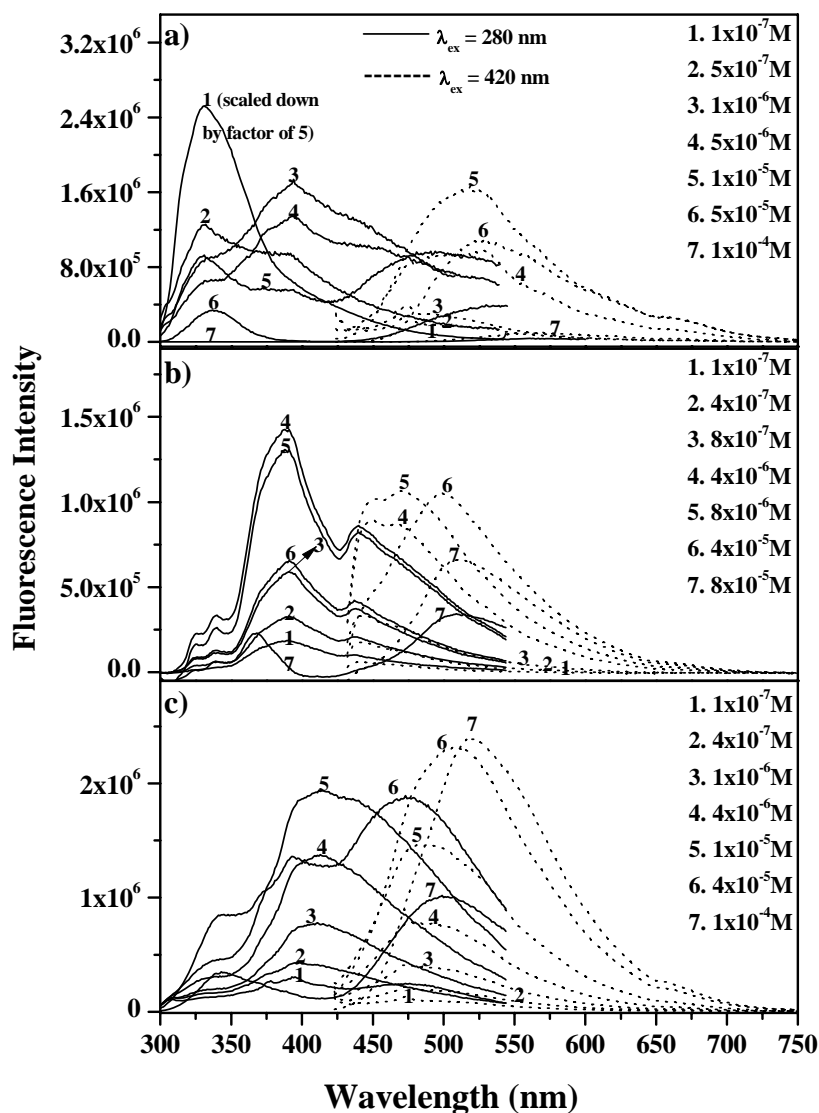


Figure 15 Variable Concentration fluorescence spectra of a) **Np0** b) **Np2Np** and c) **Np6Np** upon excitation at 280 nm and 420 nm.

As the concentration increased a new “excimer” type emission started becoming predominant at 390 nm along with a peak at still higher wavelength of 490 nm. At higher concentration of 5×10^{-5} M the excimer peak at 390 nm was completely quenched and only the peak at 330 and 490 nm remained and at 1×10^{-4} M the entire fluorescence was completely quenched. The bichromophores **Np2Np** and **Np6Np** had very prominent excimer peak at 390 nm at very dilute concentration itself and quenching of this peak occurred only at concentrations as high as 8×10^{-5} and 1×10^{-4} M respectively. The main difference between the

short and long spacer bichromophores was that in **Np6Np** the peak at higher wavelength (~490 nm) also had high intensity even in dilute conditions. The variable concentration emission upon excitation at 420 nm for all the molecules showed a shift in peak maxima from ~490 nm at dilute conditions to > 500 nm at higher concentrations. **Np0** and **Np2Np** showed a quenching of this fluorescence at higher concentrations whereas **Np6Np** continued to show an increasing trend even at the very high concentration of $1 \times 10^{-4} \text{M}$.

The ratio of the area of the excimer (~390 nm) to monomer (~330 nm) – I_E/I_M obtained from the deconvoluted fluorescence spectra of **Np0**, **Np2Np** and **Np6Np** for the 280 nm excitation was plotted as a function of concentration and is shown in figure 16. The inset in the figure shows the deconvoluted spectra of **Np2Np** and **Np6Np** at a concentration of $8 \times 10^{-6} \text{M}$. It can be seen that the ratio of the I_E/I_M is constant over a wide range of concentration (1×10^{-7} to $4 \times 10^{-5} \text{M}$) suggesting that the excimer is intramolecular in the bichromophores whereas in the case of the model compound there was a strong dependence on concentration with a steady rise in the excimer emission upto a certain concentration which then underwent rapid quenching. This concentration dependence as well as the rapid quenching of the fluorescence at higher concentration is an indication of the intermolecular excimer formation in **Np0** which is the only possible mode of association.

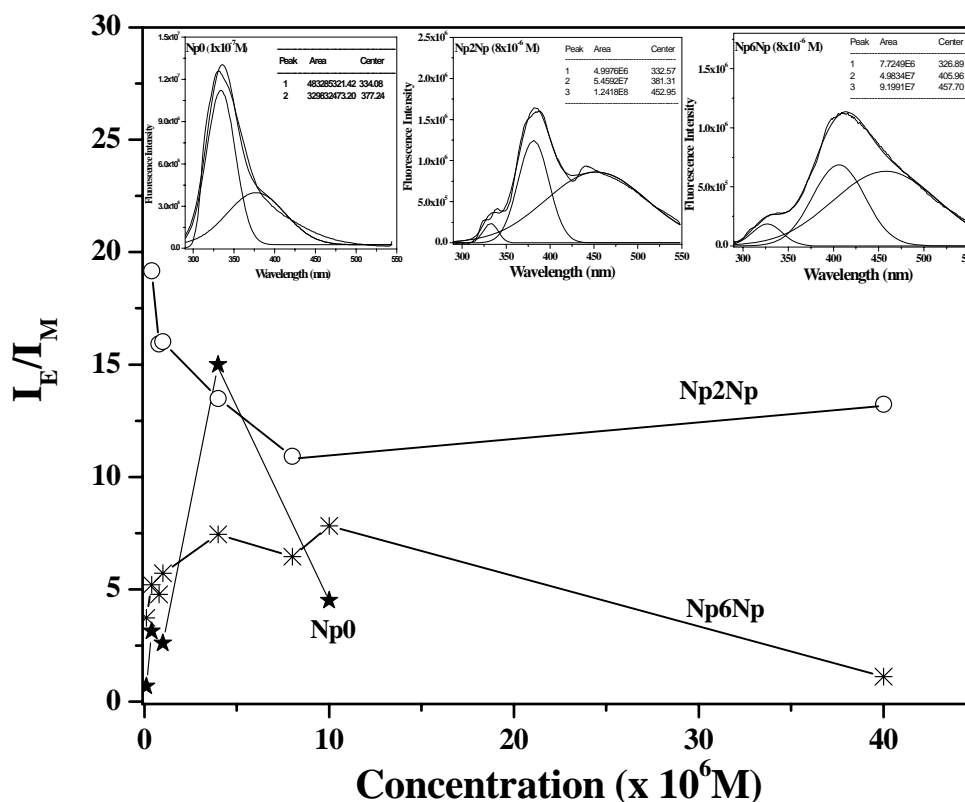


Figure 16 The plot of I_E/I_M of the naphthylazo molecules as a function of concentration.

4.10 Photoisomerization Studies

The azo bichromophores were irradiated with a Dymax light curing device (Blue Wave 50AS model 39370) having a 50 watt short arc mercury vapor lamp with an output wavelength in the range 280-450 nm in combination with 360 and 450 nm Oriel bandpass filters. The intensity of the lamp was measured to be 18 mW/cm² using an Omniscan radiometer. The dichloromethane solutions (1×10^{-6} M) of the samples were irradiated using 360 nm bandpass filter upto a maximum time period of 10-12 min and the absorption was recorded every 30 seconds interval to trace the trans to cis photo isomerization. After attainment of photostationary state, the solution was subjected to 450 nm irradiation and the absorption recorded every 30 seconds interval to trace the reverse isomerization from the cis to the trans form. The change in absorption spectra of phenol, phenyl phenol and naphthol

bichromophoric series upon UV irradiation are given in figures 17, 18 and 19 respectively. The isomerization plot for the model molecules **P0**, **Pp0** and **Np0** are given separately in figure 20. Table 3 shows the % trans to cis conversion and the % recovery in the reverse process as well as the rate constant for these conversions. Within 15 min the molecules reached photostationary state. Generally only the phenol based bichromophores underwent the trans to cis and the reverse isomerization in a proper manner whereas both the phenyl phenol and naphthol series showed a decrease in trans as well as cis absorption band upon UV irradiation. **P4P** underwent 40 % cis conversion in 520 seconds with two isosbestic points at 310 nm and 417 nm whereas its higher homologue **P6P** had a higher conversion of 66 % with isosbestic points at 312 nm and 418 nm in 390 seconds. Upon irradiation with 450 nm, the former molecule attained 86 % recovery in 570 sec and the latter recovered 78 % in 720 seconds. Phenyl phenol derivatives **Pp4Pp** and **Pp6Pp** had 12 % and 19 % trans to cis conversion respectively. Irradiation of these molecules with 450 nm radiation did not result in the reverse conversion in a perfect fashion as in the case of the phenol bichromophores. In the case of **Np2Np**, there was 1 % conversion with a single cross over at 499 nm and for **Np6Np**, there was only 5 % conversion with isosbestic points at 316 and 499 nm. In the case of the model compounds, the conversion efficiencies (trans to cis) were very poor. **P0** underwent only 4 %, **Pp0** 1 % and the **Np0** around 0.2 % trans to cis isomerization. The backward cis to trans conversion was not very effective. The rate constant for first order reaction (trans to cis) was determined using the first order equation: ^{52,53}

$$\ln(A_0 - A_{eq}) / (A_t - A_{eq}) = k_t t$$

The slope of the linear fit of the plot of $\ln(A_0 - A_{eq}) / (A_t - A_{eq})$ vs UV irradiation time gives the rate constant for the trans to cis isomerization. Figure 21 shows the plots for the forward trans to cis conversion for the bichromophores as well as the model compounds.

Table 3 Isomerization data

Sample	% trans to cis conversion	% Recovery	Rate constant (10^{-3}) k_t (sec^{-1})
P0	4	96	1.7
P4P	40	86	5.9
P6P	66	78	6.6
Pp0	1	-	5.0
Pp4Pp	12	88	4.2
Pp6Pp	19	82	2.4
Np0	0.2	-	4.3
Np2Np	1	98	2.6
Np6Np	5	93	6.7

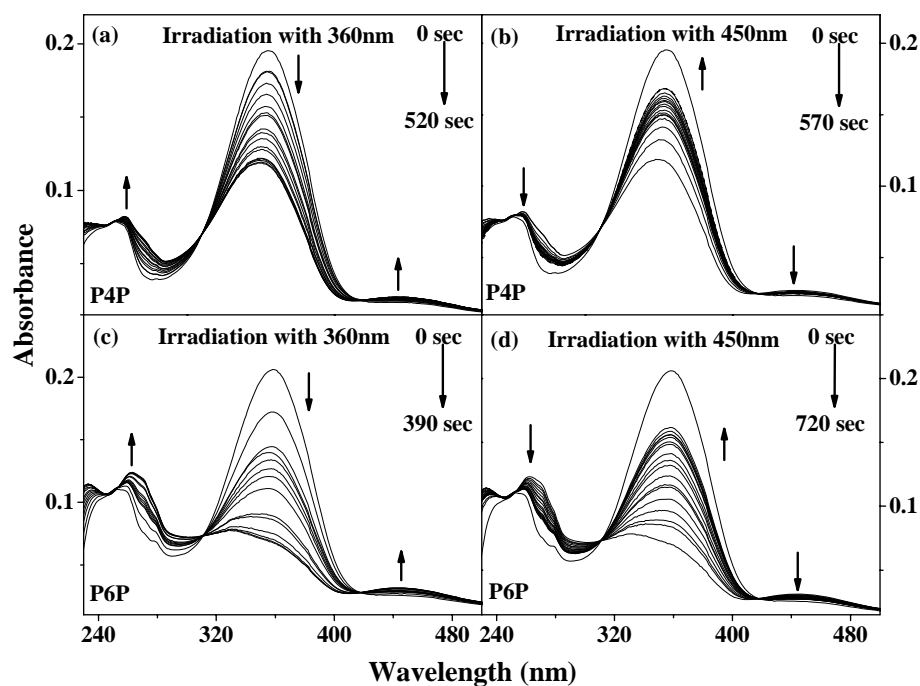


Figure 17 Change in absorption spectra of **P4P** (a & b) and **P6P** (c & d) upon UV irradiation

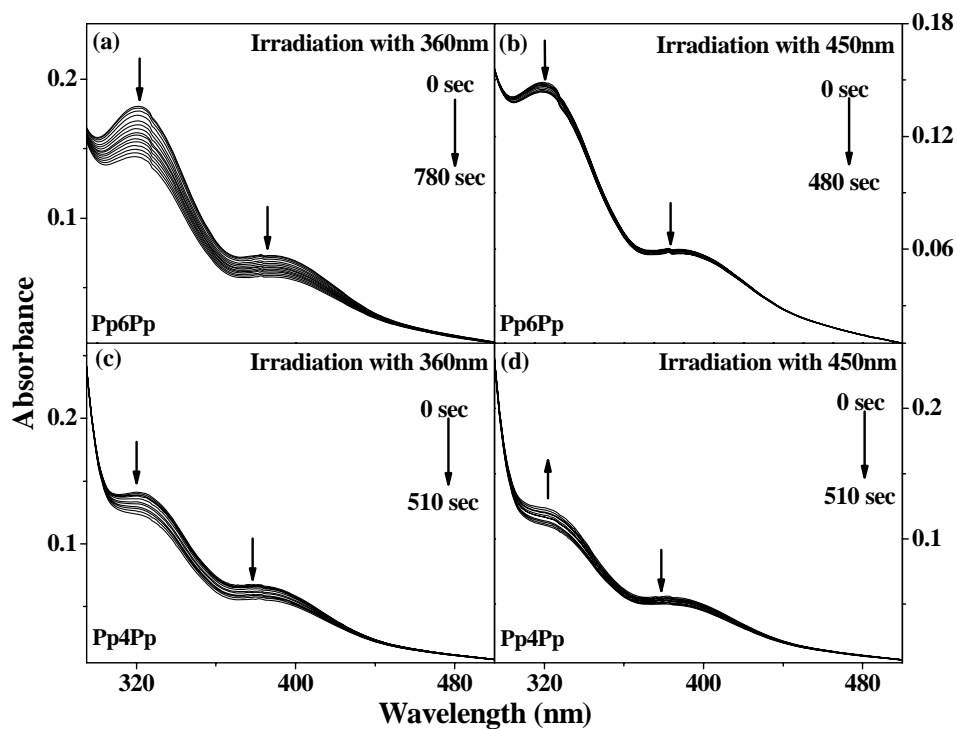


Figure 18 Change in absorption spectra of **Pp6Pp** (a & b) and **Pp4Pp**(c & d) upon UV irradiation

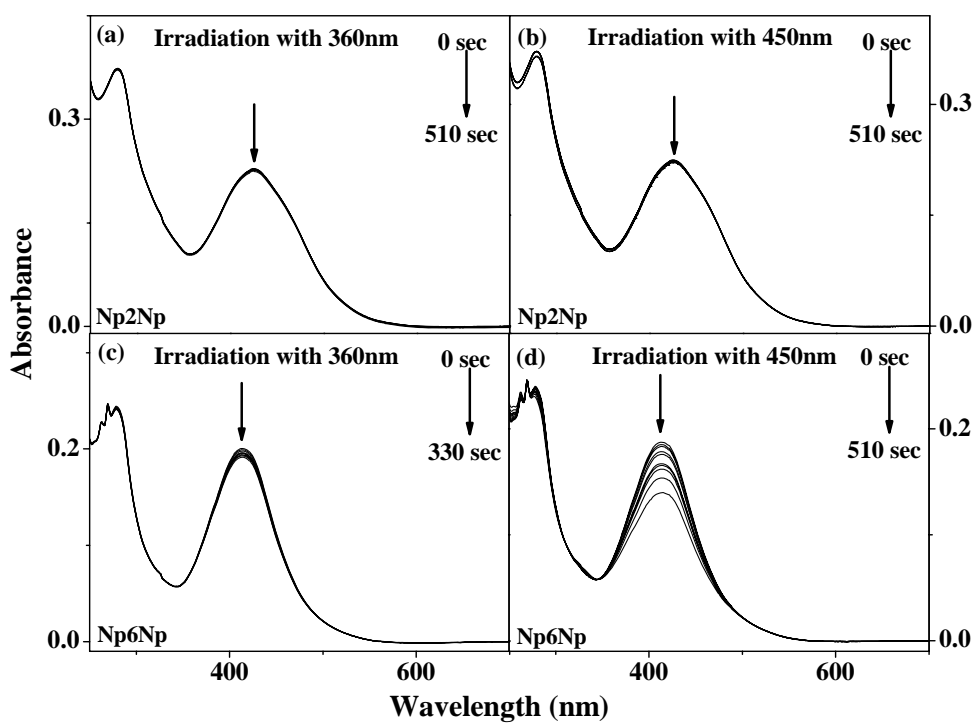


Figure 19 Change in absorption spectra of **Np2Np** (a) & (b) and **Np6Np** (c) & (d)

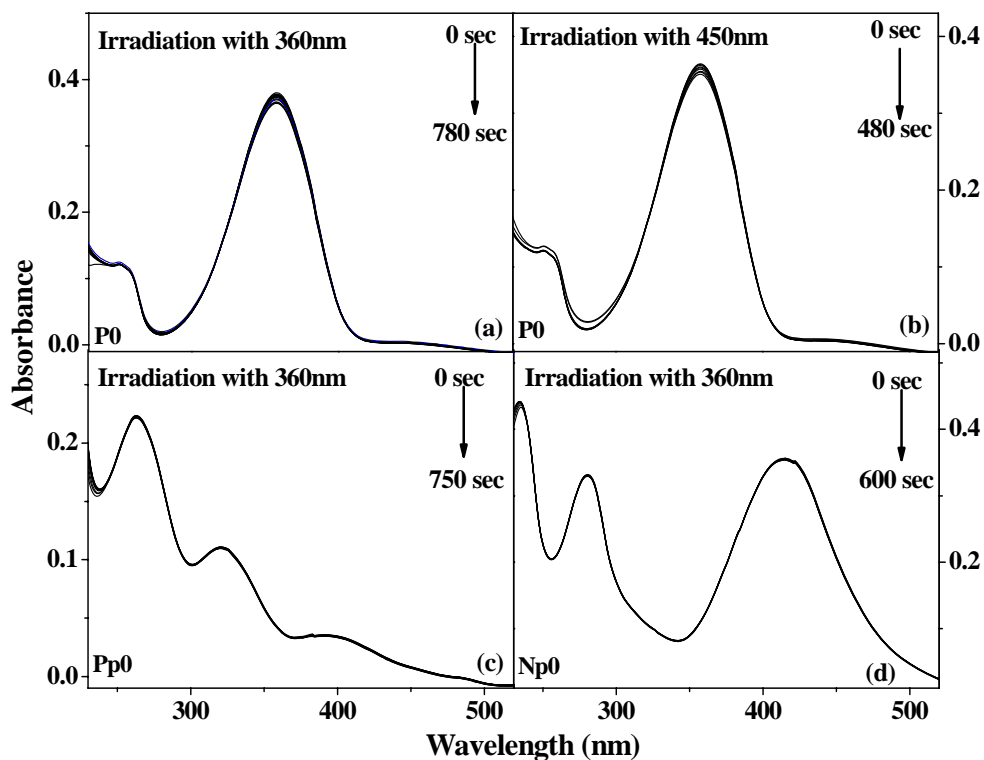


Figure 20 Change in absorption spectra upon irradiation with UV and visible light (a) & (b) **P0**, (c) **Pp0** and (d) **Np0**

From Table 3, it can be seen that among the three series, the phenol based one had the highest trans to cis conversion for the model compound as well as for the bichromophores. This is in accordance with the literature data which shows that the efficiency of trans to cis isomerization decreased upon incorporation of bulky groups into the azobenzene moiety.^{54, 55} Also these values are in agreement with literature reports.^{56, 57}

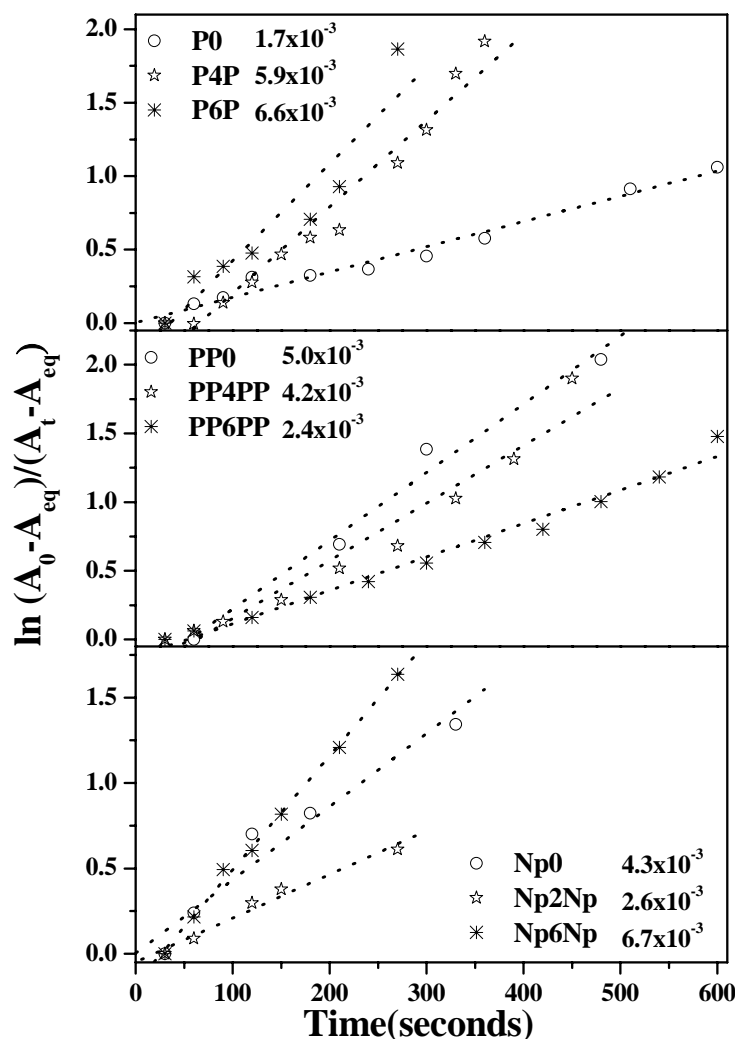


Figure 21 Plots for the forward trans to cis conversion for the bichromophores as well as the model compounds

4.11 Thermal Properties

The thermal stability of the bichromophores was determined by TGA under nitrogen atmosphere. No weight loss was observed until they were heated to 200^oC. TG thermograms of the bichromophores are given in figure 22 and the 10 weight % temperature is given in table 4. It can be seen from the table that the phenyl phenol based bichromophores had the highest thermal stability with their 10 wt % loss temperature well above 300^oC, followed by the phenol based ones whose 10 wt % loss temperature was ~ 250^oC. The naphthol based bichromophore had the lowest values with **Np6Np** having a 10 wt % loss temperature ~ 200^oC. Among the model compounds, **Pp0** possessed highest thermal stability with 10 wt % loss temperature well above 270^oC followed by

Np0 whose 10 wt % loss temperature was ~ 254 °C and then **P0** with 10 wt % loss temperature was ~ 219 °C.

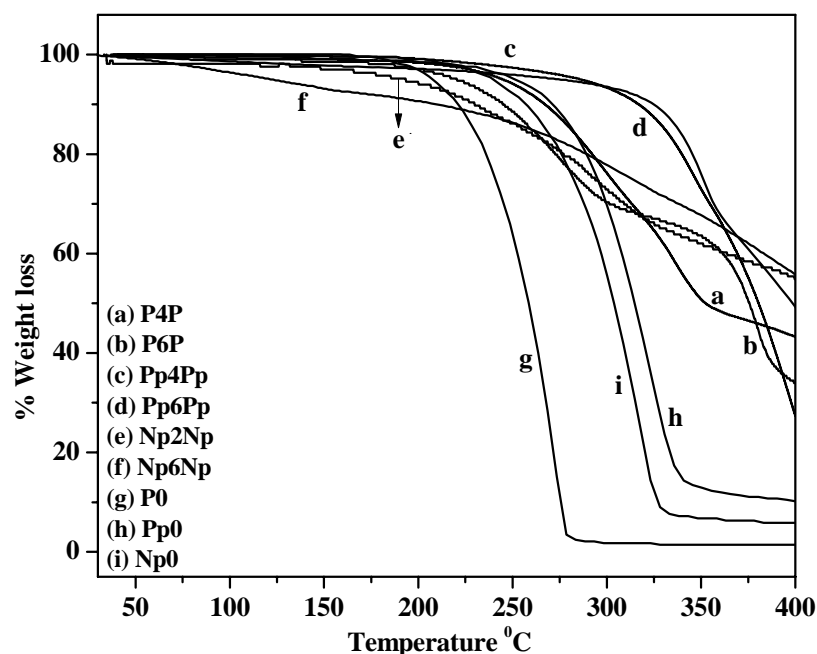


Figure 22 TG thermograms of the bichromophores and model compounds

The phase transitions of the bichromophores were investigated by means of differential scanning calorimetry (DSC) and polarizing light microscopy (PLM). The DSC thermograms of the three series phenol, phenyl phenol and naphthol are shown in figure 23, 24 and 25 respectively and the enthalpy values and phase transition temperature are given in table 4. The samples were heated to melt and subsequently cooled at 10 °C/ min from the melt for their crystallization. Samples **P4P**, **P6P**, **Np2Np**, **P0**, **Pp0** and **Np0** were cooled to 30 °C whereas all other samples were cooled to -50 °C in the cooling cycle. Sample **Pp4Pp** had to be cooled from room temperature (30 °C) to -50 °C after annealing at room temperature for two days and then heated to the melting point to observe the phase transitions in DSC as well as under the PLM. **P0** exhibited a sharp endotherm at 166 °C ($\Delta H = 72.32$ J/g) with a shoulder at 152 °C ($\Delta H = 1.38$ J/g) in the heating cycle. The shoulder peak corresponded to the crystal to LC transition and the sharp endotherm to that of the LC to isotropic transition. In the cooling cycle, it showed an exotherm at 158 °C ($\Delta H = -77.08$ J/g) which

corresponded to isotropic to LC transition and a small one ~ 132 °C ($\Delta H = -1.3$ J/g) corresponding to LC to crystallization.

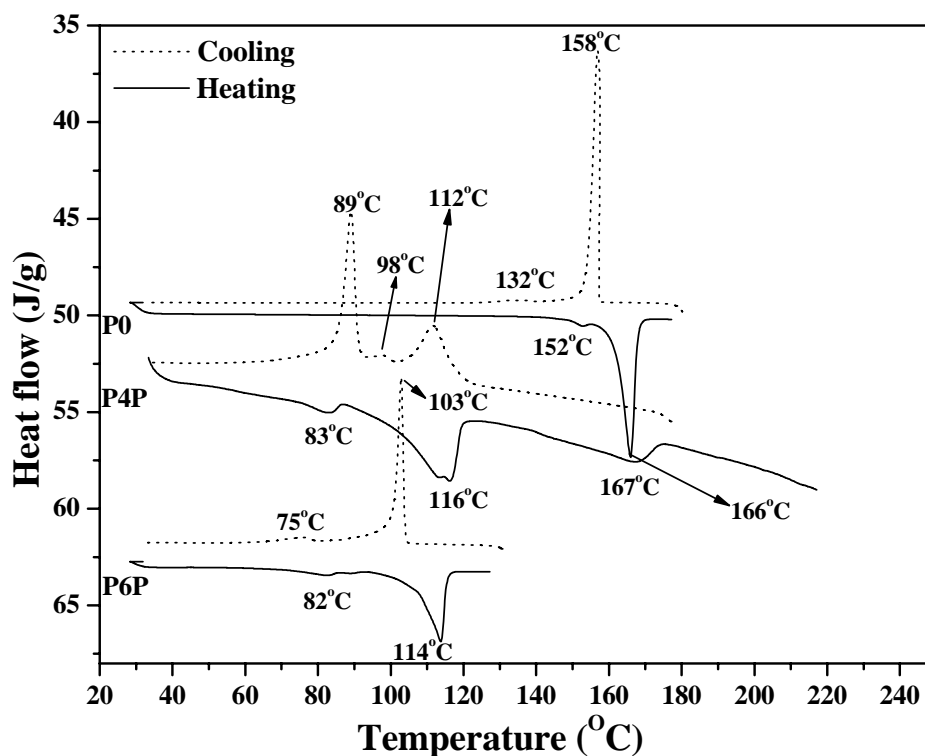


Figure 23 DSC thermogram of samples **P0**, **P4P** and **P6P**

P4P had a small endotherm at 83 °C ($\Delta H = 1.3$ J/g) and two sharp endotherms, one at 116 °C ($\Delta H = 20.2$ J/g) with a shoulder at 113 °C and the other one at 167 °C ($\Delta H = 9.6$ J/g) in the second heating cycle. These multiple peaks corresponded to crystal to LC phases and LC to isotropic state. While cooling from the melt, **P4P** showed two peaks at 112 °C ($\Delta H = -11.59$ J/g) and at 98 °C ($\Delta H = -0.46$ J/g) corresponding to the isotropic to liquid crystalline transition in addition to a peak at 89 °C ($\Delta H = -5.29$ J/g) corresponding to liquid crystalline to crystalline transition.

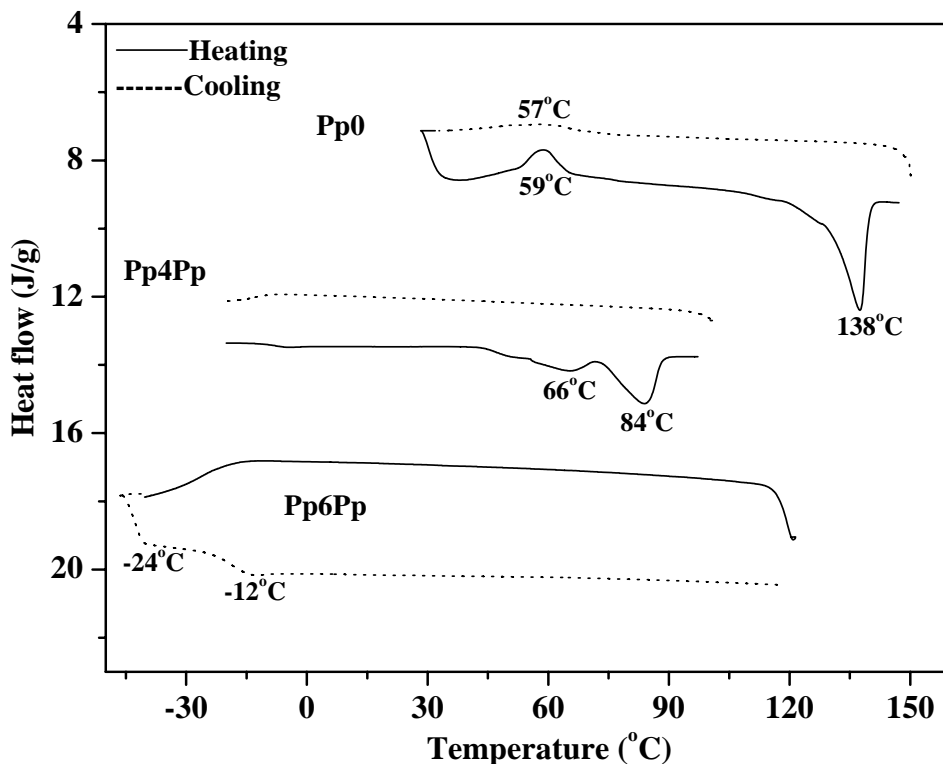


Figure 24 DSC thermogram of Pp0, Pp4Pp and Pp6Pp

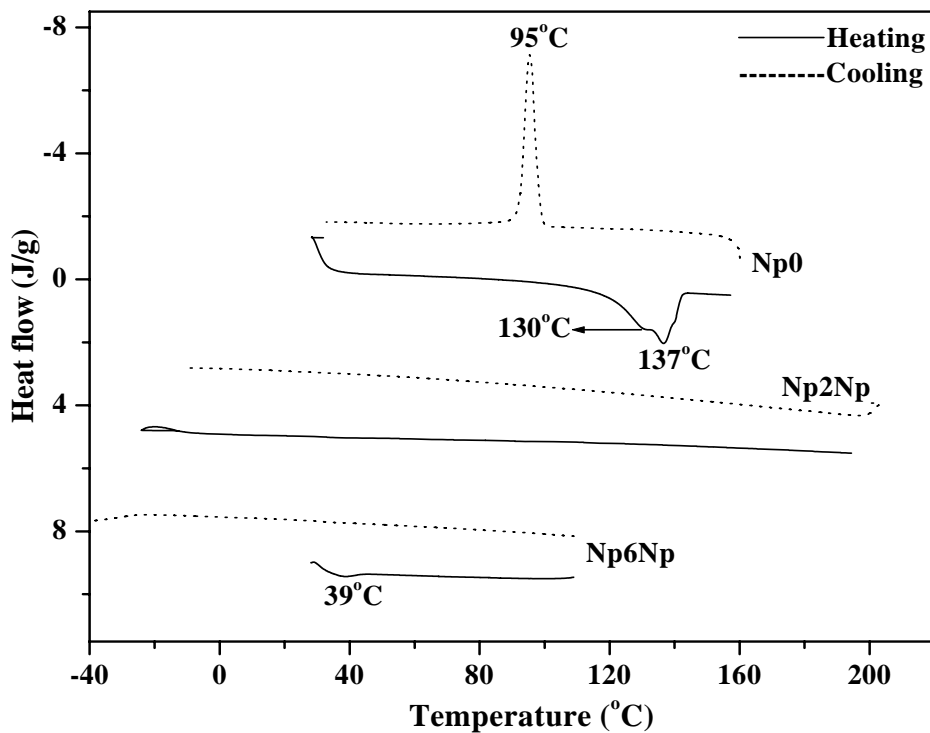


Figure 25 DSC thermogram of Np0, Np2Np and Np6Np

P6P which is structurally similar to **P4P** except for the difference in the spacer length, showed only two transitions in the heating cycle. As expected there was a decrease in T_m from 167 °C (**P4P**) to 114 °C (**P6P**) with increase in spacer length from tetraethyleneoxy unit to hexaethyleneoxy unit. In the cooling cycle, there were 2 exotherms at 103 °C ($\Delta H = -42.81$ J/g) and 75 °C ($\Delta H = -2.53$ J/g) corresponding to the isotropic to LC and LC to crystal transitions for **P6P**. In the heating cycle, there were two endotherms at 82 °C ($\Delta H = 4.37$ J/g) and 114 °C ($\Delta H = 44.14$ J/g) corresponding to the crystal to LC phase and LC to melt. As the chain length increased from four ethyleneoxy unit (**P4P**) to six ethyleneoxy unit (**P6P**), the liquid crystalline window also increased from 4 °C to 25 °C in the respective cooling cycles.

Table 4 Thermal data of bichromophores

Sample	T_m^a (C-N) (°C)	ΔH_m^a (C-N) (J/g)	T_m^a (N-I) (°C)	ΔH_m^a (N-I) (J/g)	T_c^b (I-N) (°C)	ΔH_c^b (I-N) (J/g)	T_c^b (N-C) (°C)	ΔH_c^b (N-C) (J/g)	LC window (cool)	T_D^c (°C)
P0	152	1.4	166	72.3	158	-77.1	132	-1.3	26	219
P4P	116	20.2	167	9.6	112	-11.6	89	-5.3	23	266
P6P	82	4.4	114	44.1	103	-42.8	75	-2.5	27	246
Pp0	-	-	138	36.8	-	-	-	-	-	271
Pp4Pp	66	11.5	84	24.8	-	-	-	-	-	318
Pp6Pp	50	2.1	125	2.0	-	-	-	-	-	322
Np0	-	-	137	55.0	95	-63.2	-	-	-	254
Np2Np	-	-	-	-	-	-	-	-	-	230
Np6Np	37	1.6	122	62.8	-	-	-	-	-	207

a) Measured for heating cycle at 10 °C/min heating rate

b) Measured for the cooling cycle from the melt at 10 °C/min cooling rate

c) Temperature represents 10 % weight loss in TGA measurements at heating rate of 10 °C/min under nitrogen.

In the phenyl phenol series, **Pp0** showed an exotherm corresponding to crystallization at 59 °C ($\Delta H = -18.33$ J/g) and an endotherm at 138 °C ($\Delta H = 36.84$ J/g) with a shoulder at 114 °C in the second heating cycle. Upon cooling, it underwent super cooling at 58 °C but the crystallization was not complete. In the case of **Pp4Pp**, there were 2 sharp endotherms at 66 °C ($\Delta H = 11.48$ J/g) and 84 °C ($\Delta H = 24.82$ J/g) with a shoulder at 56 °C and a weak endotherm at -5 °C in the second heating cycle. The sharp endotherm at 84 °C corresponded to melting transition and the one at 66 °C corresponded to the crystal to LC transition. The multiple endotherms in the DSC thermogram indicate multiple phase transitions. Cooling from the melt, **Pp4Pp** did not show any transition as it solidifies into a glass. **Pp6Pp** and **Np6Np** which are based on phenyl phenol and naphthol with hexaethyleneoxy spacer showed multiple endotherms in the first heating cycle when heated the samples to its melting point and then annealed them at room temperature for 48 h. Figure 26 shows the first heating scan of the DSC thermogram for **Pp6Pp** and **Np6Np**. **Pp6Pp** showed 3 endotherms at 24 °C ($\Delta H = 0.55$ J/g), 50 °C ($\Delta H = 2.06$ J/g) which corresponded to two different phase transitions and one at 125 °C ($\Delta H = 2.01$ J/g) that corresponded to melting transition. Similarly, **Np6Np** showed 3 endotherms at 22 °C ($\Delta H = 3.06$ J/g), 37 °C ($\Delta H = 1.59$ J/g) and at 122 °C ($\Delta H = 62.79$ J/g) in which the first two corresponded to two different phase transitions and the one at 122 °C corresponded to melting transition. Both **Pp6Pp** and **Np6Np** did not show any transition either in their second heating or in the cooling scans. **Np0** exhibited an exotherm at 30 °C in the first heating cycle and a sharp endotherm at 142 °C. In the cooling cycle, it showed an exotherm at 95 °C ($\Delta H = -63.18$ J/g) which corresponded to crystallization. It showed an endotherm at 137 °C ($\Delta H = 55.03$ J/g) corresponding to the crystal to isotropic transition and a shoulder at 130 °C which may be due to some crystal –crystal transition in the second heating cycle. **Np2Np** did not show any transitions in the second heating and cooling cycles.

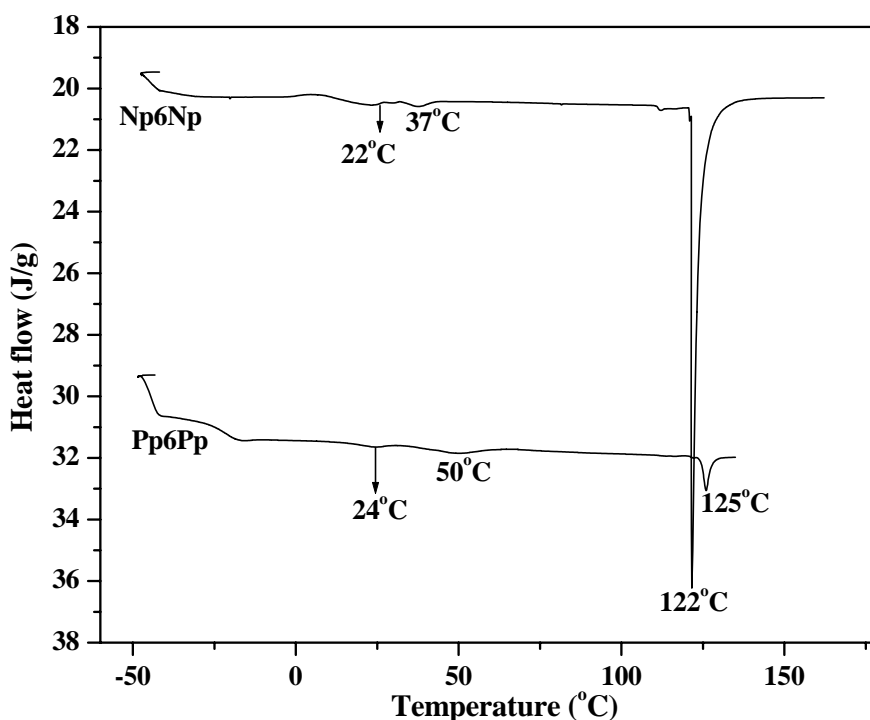


Figure 26 DSC thermogram showing the first heating scan of **Pp6Pp** and **Np6Np**

In order to confirm the LC behavior, all the molecules were subjected to polarizing light microscopy (PLM) analysis equipped with a temperature-controlled hot stage. The samples were heated to melting at 10 °C/min and isothermally maintained for 2min (the melt appeared dark under the polarizer and no crystallites were visible), the melt was subsequently cooled under control at 10 °C/min. Figure 27 shows PLM pictures of **P0**, **P4P** and **P6P** and figure 28 shows that of **Pp4Pp** and figure 29 that of **Np0** and **Np6Np**. **P0** exhibited isotropic phase at 166 °C and upon cooling, threadlike pattern appeared at 158 °C which was stable upto 132 °C. In the case of **P4P** also, a grainy pattern was observed during cooling from the melt and also in the subsequent heating cycle. The observed LC phase was stable even up to room temperature. **P4P** was completely melted at 167 °C and held at this temperature for 2 min. During cooling from the melt, the phase started to appear initially as small nucleation sites at 112 °C, which then flowed and started to form a uniform pattern (figure 27b).

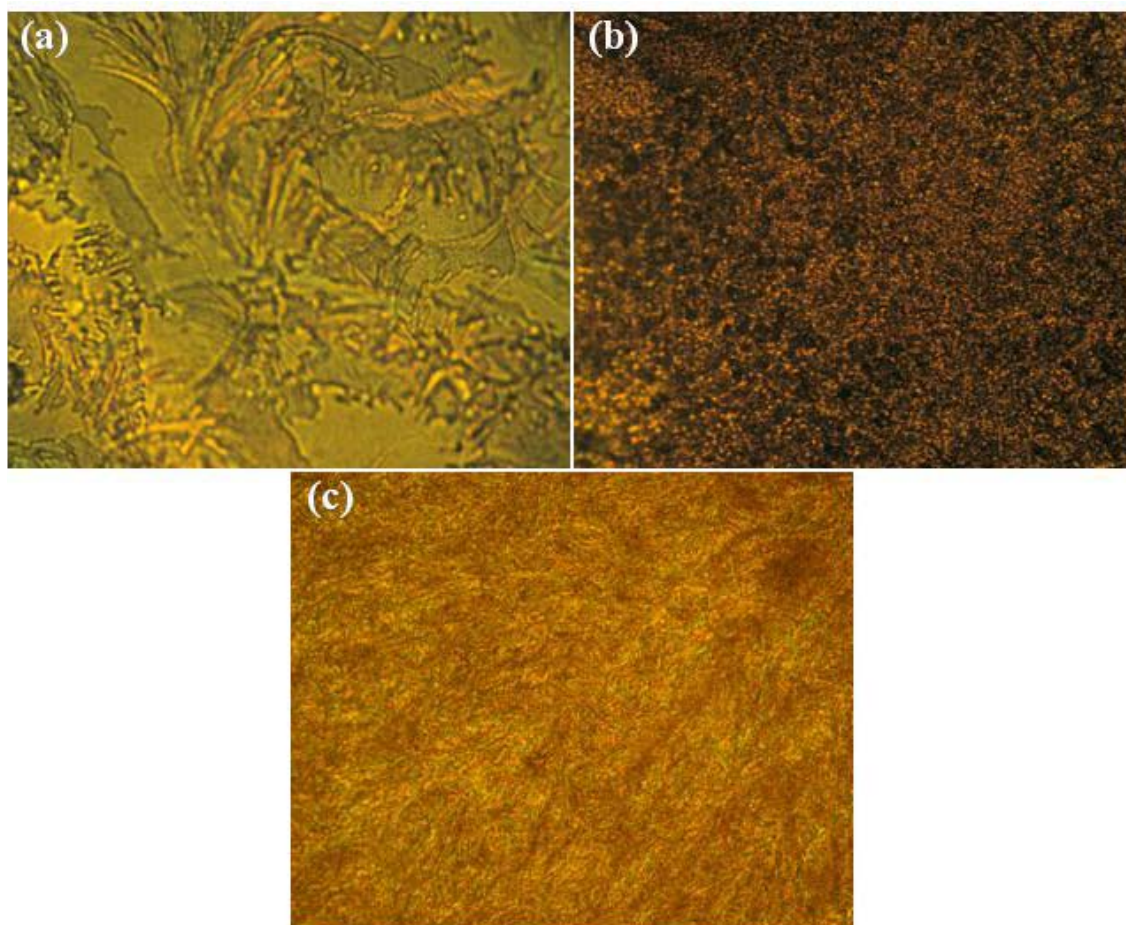


Figure 27 Polarizing light microscopic photographs of (a) **P0** at 130 °C (b) **P4P** at 111 °C (c) **P6P** at 103 °C.

P6P was heated up to 130 °C and held at this temperature for 2min. In the cooling cycle, the LC phase started to appear at 103 °C and then formed a uniform pattern (figure 27c). **Pp0** and **Pp6Pp** exhibited isotropic phase at 138 °C and 125 °C, but did not show any LC phase either in the cooling scan or in the heating scan. **Pp4Pp** was completely melted at 84 °C and was held at that temperature for 2 min. This sample had to be kept at room temperature for two days and then cooled to -50 °C and finally heated for observing LC phase under PLM (figure 28b). Also in DSC no transition was observed in the cooling scan. **Np0**, **Np2Np** and **Np6Np** showed isotropic phases at 137 °C, 203 °C and 122 °C respectively. **Np2Np** and **Np0** did not show any LC phase in both cooling and heating scans even after annealing. On the other hand, **Np6Np** exhibited a threaded pattern when cooled to 30 °C.

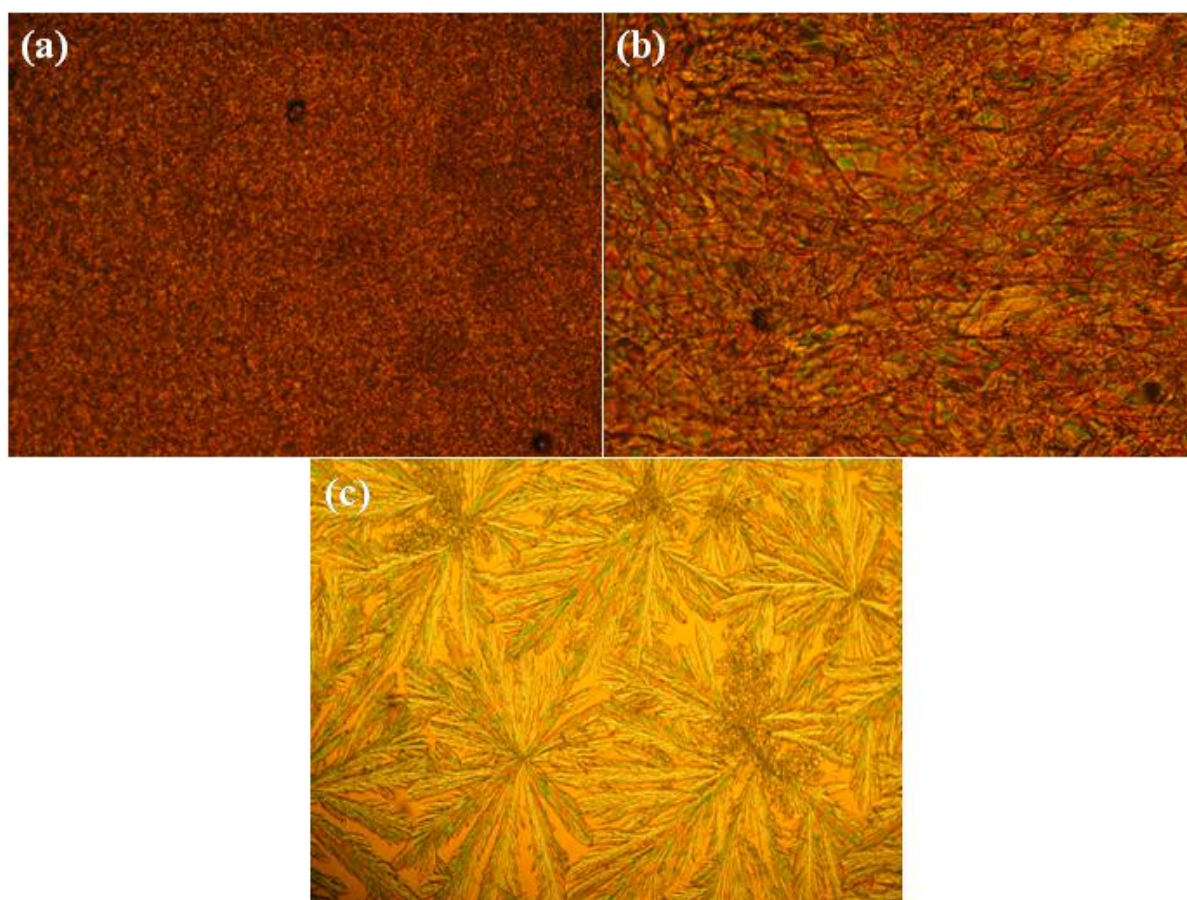


Figure 28 Polarizing light microscopic photographs of **Pp4Pp** at (a) 68 °C (b) 65 °C and (c) 62 °C

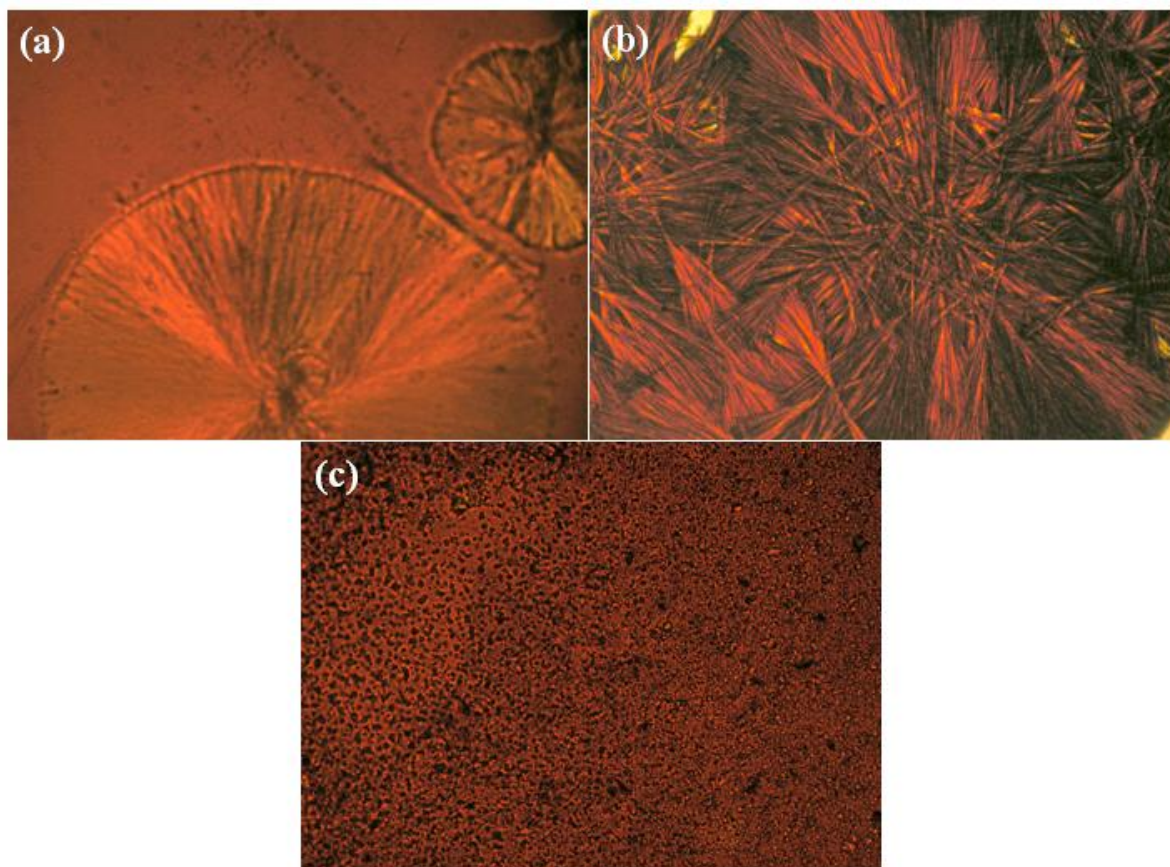


Figure 29 Polarizing light microscopic photographs of **Np0** at (a) 126 °C (b) 90 °C and (c) **Np6Np** at 30 °C

4.12 SEM Analysis

In order to understand the morphology of polymers, SEM measurements were done by drop casting the samples from tetrahydrofuran solution. The samples for analysis were prepared by drop casting polymer solution of concentration 10^{-3} M on glass slides and allowing evaporation under atmospheric conditions. All the samples were subjected to SEM analysis, but only two of them gave interesting patterns. Figure 30 shows the SEM micrographs of **P4P** and **Np6Np** and this gives the indication of aggregate formation of these bichromophores. In the case of **P4P**, the particles had a deformed spherical geometry with average size $1.4 \pm 0.3 \mu\text{m}$. **Np6Np** showed belt like structure which are associated to form rods along with well separated belt-like structures. These aggregates possessed a width of $7.6 \pm 1.8 \mu\text{m}$ whereas the individual belt had a width of $0.7 \pm 0.2 \mu\text{m}$. The SEM image of highly ordered aggregates of

Np6Np is in conformation with the data obtained from variable concentration fluorescence studies which showed the formation of a new red shifted peak at higher concentration.

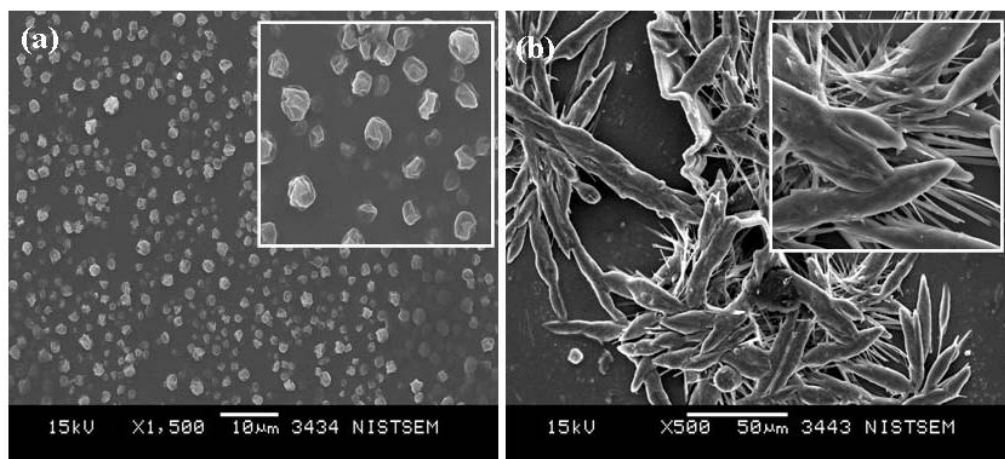


Figure 30 SEM images of (a) **P4P** and (b) **Np6Np**

4.13 DLS Measurement

Dynamic light scattering (DLS) is a well established technique for measuring particle size over the size range from few nanometer to microns. The technique measures particle diffusion due to Brownian motion and relates this to the size of the particle ie, DLS measures time-dependant fluctuation in the intensity of scattered light. The increase in scattered intensity with increase in particle size is used for the qualitative and quantitative detection of aggregates. To confirm the aggregate formation tendency of the bichromophores and to determine the size and size distribution of these aggregates, DLS measurement was performed for the bichromophores in THF solvent. Measurements were performed at same concentration (10^{-3} M) and same solvent (THF) as that used for SEM. Figure 31 shows the DLS measurement for all the bichromophores. The phenol as well as naphthol bichromophores showed broad peaks corresponding to aggregates in the 500-600 nm range. The phenyl phenol bichromophores showed comparatively sharp peaks in much more smaller dimensions of ~250-300 nm range. The dimensions of the aggregates observed by DLS measurements are much smaller compared to the micrometer sized

particles in the SEM images of the phenol and naphthol bichromophores. This could be attributed to concentration dependent aggregation during sample preparation for SEM measurements. The drop cast samples on glass plates collapse to form bigger aggregates upon solvent evaporation followed by application of vacuum.

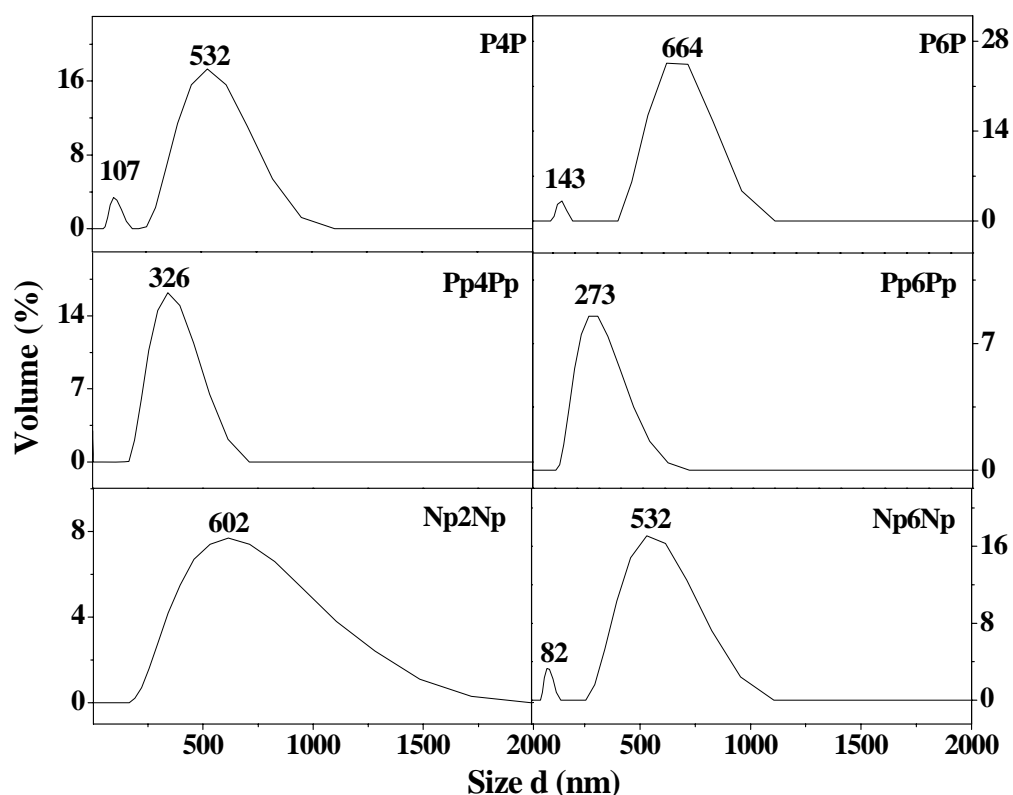


Figure 31 Dynamic light scattering measurements for the bichromophores recorded in THF

4.14 Conclusion

A new series of azobenzene based bichromophores with different fluorophores and spacer length have been synthesized. A corresponding set of model compounds which do not have any spacer were also synthesized. Among the whole series, phenyl phenol based molecules showed high fluorescence. Even though phenyl phenol is having a twisted geometry in the ground state, the more planar excited state is responsible for the high fluorescence observed. The naphthol based systems also exhibited reasonable quantum yield. Majority of the

molecules violated Kasha's rule and exhibited S_2 fluorescence. But the model compound based on phenyl phenol fluorophore exhibited S_1 fluorescence and followed Kasha's rule. The naphthol derivatives were found to form excited state dimers. The naphthol based model compound formed intermolecular excimer whereas the bichromophores formed intramolecular excimer. The monomer excitation spectra and excimer excitation spectra were different which confirmed the static nature of excimer. The excimer formation was confirmed by concentration dependant fluorescence measurements. Photoisomerization studies revealed that the phenol based bichromophores undergo better conversion than the other two fluorophoric systems. The conversion efficiency of the model compounds was very poor which can be accounted on the basis of the rigidity of the molecules. Most of bichromophores showed liquid crystalline phases.

4.15 Reference

1. Ferrarini, A.; Luckhurst, G. R.; Nordio, P. L.; Roskilly, S.J. *Chem. Phys. Lett.* **1993**, 214, 409.
2. Griffin, A. C.; Havens, S. J. *J Polym. Sci. Polym. Phys. Ed.* **1981**, 19, 951.
3. Koide, N.; Iimura, K. *Mol. Cryst. Liq. Cryst.* **1987**, 153, 73.
4. Griffin, A. C.; Vaidya, S. R.; Hung, R. S. L.; Gorman, S. *Mol. Cryst. Liq. Cryst. Lett.* **1985**, 1 (5), 131.
5. Asha, S. K.; Kavitha, K.; Das, P. K.; Ramakrishnan, S. *Chem. Mater.* **1999**, 11, 3352.
6. Abraham, S.; Mallia, A.; Ratheesh, V.; Tamaoki, N.; Das, S. *J. Am. Chem. Soc.* **2006**, 128, 7692.
7. Abe, A.; Furuya, H.; Shimizu, R. N.; Nam, S. Y. *Macromolecules* **1995**, 28, 96.
8. So, B. K.; Kim, H. J.; Lee, S. M.; Song, H. H.; Park, J.H. *Dyes and pigments* **2006**, 70, 38.
9. Asha, S. K.; Ray, P. C.; Ramakrishnan, S. *Polym. Bull.* **1997**, 39, 481.
10. So, B. K.; Jang, M. C.; Park, J. H.; Song, H. H.; Lee, K. S.; Lee, S.M. *Opt. Mater.* **2002**, 21, 685.

11. Imrie, C. T.; Iuckhurst, G. R.; Demus, D.; Goodby, J.; Gray, H.W.; Spiess, H.W.; Vill, V. (Eds) *Hand Book of Liquid Crystals*, Volume 2B, Wiley-VCH, Weinheim, **1998**, p801.
12. Jin, J. I.; Kim, H. S.; Shin, J. W.; Chung, B. Y.; Jo, B. W. *Bull. Korean. Chem. Soc.* **1990**, 11, 209.
13. Yelamaggad, C.V.; Nagamani, S.A.; Hiemath, U. S.; Nair, G. G. *Liq. Cryst.* **2001**, 28, 1009.
14. Yelamaggad, C. V.; Srikrishna, A.; Shankar Rao, D. S.; Prasad, S. K. *Liq. Cryst.* **1999**, 26, 1547.
15. Yelamaggad, C. V.; Mathews, M.; Fujita, T.; Iyi, N. *Liq. Cryst.* **2003**, 30, 1079.
16. Cha, S.W.; Jin, J. I.; Laguerre, M.; Achard, M. F.; Hardouin, F. *Liq. Cryst.* **1999**, 26, 1325.
17. Cha, S. W.; Jin, J. I.; Achard, M. F.; Hardouin, F. *Liq. Cryst.* **2002**, 29, 755.
18. Hardouin, F.; Achard, M. F.; Jin, J. I.; Shin, J. W.; Yun, Y.K. *J. Phys, II Fr.4.* **1994**, 627.
19. Marcelis, A. T. M.; Koudijs, A.; Karczmarzyk, Z.; SudhOlter, E. J. R. *Liq. Cryst.* **2003**, 30, 1357.
20. Marcelis, A. T. M.; Koudijs, A.; SudhOlter, E. J. R. *Liq. Cryst.* **2004**, 411, 1235.
21. Marcelis, A. T. M.; Koudijs, A.; SudhOlter, E. J. R. *Liq. Cryst.* **2000**, 27, 1515.
22. Mallia, V.A.; Tamaoki, N. *J. Mater. Chem.* **2003**, 13, 219.
23. Wu, C. *Mat. Let.* **2007**, 61, 1380.
24. Tung, C. H.; Wang, Y. M. *J. Am. Chem. Soc.* **1990**, 112, 6322.
25. Yana, D.; Shimizu, T.; Hamasaki, K.; Mihara, H.; Ueno, A. *Macromol. Rapid. Commun.* **2002**, 23, 11.
26. Inoue, M.; Itoh, Y.; Kusano, S.; Shirai, H.; Suzuki, S. *Pure. Appl. Chem.*, **2000**, A37, 81.
27. Machi, L. Santacruz, H.; Sanchez, M.; Inoue. *Inorg. Chem. Commun.* **2007**,

- 10, 547.
28. Forster, T.; Kasper, K. Z. *Phys. Chem. (N.F.)*, **1954**, 1, 275.
29. Forster, T. *Angew. Chem., Int. Ed. Engl.*, **1969**, 8, 333.
30. Birks, J. B. *Photophysics of Aromatic Molecules*, Wiley-Interscience, New York, **1970**, ch. 7.
31. Birks, J. B. *Rep. Prog. Phys.*, **1975**, 38, 903.
32. Rettig, W.; Paepflow, B.; Herbst, H.; Mullen, K.; Desvergne, J. P.; Laurent, H. B. *New. J. Chem.* **1999**, 23, 453.
33. Mendicuti, F.; Patel, B.; Mattice, W. L. *Polymer* **1990**, 31, 1877.
34. Mendicuti, F.; Patel, B.; Mattice, W. L. *Polymer* **1990**, 31, 453.
35. Gallego, J.; Mendicuti, F.; Saiz, E.; Mattice, W. L. *Polymer* **1993**, 34, 2475.
36. Martin, O.; Sanchez-Camacho, A.; Mendicuti, F.; Mattice, W. L. *J. Polym. Sci. Part B: Polym. Phys.* **1997**, 35, 1127.
37. Gallego, J.; Mendicuti, F.; Mattice, W. L.. *Comp. Polym. Sci.* **1994**, 4, 7.
38. Martin, O.; Mendicuti, F.; Saiz, E.; Mattice, W. L. *J. Polym. Sci: Part B: Polym. Phys*, **1996**, 34, 2623.
39. Reid, R. F.; Soutar, I. *J. Polym. Sci. Polym. Lett. Ed.* **1977**, 15, 153.
40. Reid, R. F.; Soutar, I. *J. Polym. Sci. Polym. Phys. Ed.* **1978**, 16, 231.
41. Anderson, R. A.; Reid, R. F.; Soutar, I. *Eur. Polym. J.* **1979**, 15, 925.
42. Wang, X.; Kofron, W.G.; Kong, S.; Rajesh, C. S.; Modarelli, D. A.; Lim, E. *C. J. Phys. Chem. A* **2000**, 104, 1461.
43. Mohanambe, L.; Vasudevan, S. *J. Phys. Chem. B* **2005**, 109, 22523.
44. Polacka, B. *J. Photochem.* **1987**, 36, 205.
45. Spies, C.; Gehrke, R. *J. Phys. Chem. A.* **2002**, 106, 5348.
46. Varnavski, O.; Goodson III, T. *Chem. Phys. Lett.* **2000**, 320, 688.
47. Albelda, M. T.; Garcia-Espana, E.; Gil, L.; Lima, J. C.; Lodeiro, C.; de Melo, J. S.; Melo, M. J.; Parola, A. J.; Pina, F.; Soriano, C. *J. Phys. Chem. B.* **2003**, 107, 6573.
48. Zollinger, H. *Azo and Diazo Chemistry. Aliphatic and Aromatic Compounds*. Interscience Publishers, Inc: New York, **1961**.

49. Azuma, J.; Shishido, A.; Ikeda, T.; Tamai, N. *Mol. Cryst. Liq. Cryst.* **1998**, 314, 83.
50. Fujino, T.; Arzhansev, S. Y.; Tahara, T.; *J. Phys. Chem. A.* **2001**, 105, 8123.
51. a) Nithyanandhan, J.; Jayaraman, N.; Davis.; Das, S. *Chem. Eur. J.* **2004**, 10, 689.
- (b) Shimomura, M.; Kunitake, T. *J. Am. Chem. Soc.* **1987**, 109, 5175.
52. Borshch, A.; Brodyn, M.; Lyakhovetsky, V.; Volkov, V.; Kutsenko, A.; Maloletov, S. *Materials Science* **2002**, 20, 29.
53. van Delden, R. A.; Mecca, T.; Rosini, C.; Feringa, B. L. *Chem. Eur. J.* **2004**, 10, 61.
54. Bo, Q.; Zhao, Y. *Langmuir* **2007**, 23, 5746.
55. Ma, N.; Wang, Y.; Wang, Z.; Zhang, X. *Langmuir* **2006**, 22, 3906.
56. Winnik, F. M. *Chem. Rev.* **1993**, 93, 587.

Chapter 5

Summary and Conclusion

The thesis entitled **“Nonlinear Optical, Fluorescence and Liquid Crystalline Properties of Novel Azobenzene Polymers and Their Oligomers”** describes the synthesis of a series of azobenzene molecules and polymers with interesting optical and electronic properties. The major concepts explored in this thesis are the photophysical properties especially nonlinear optical activity, the fluorescence emission and liquid crystallinity. A series of donor-acceptor substituted AB type azobenzene monomers has been synthesized where the donor part is kept constant and the acceptor part as variable. The NLO measurements of these monomers by Hyper Rayleigh scattering technique revealed the effect of conjugation length and substituents on SHG value. The second order NLO activity could be modulated by increasing the conjugation length. These monomers have been polymerized to obtain their corresponding main chain polymers. Unfortunately the very high rigidity of the backbone made them insoluble in common organic solvents. As the NLO property of a compound depends on the conjugation length and the donor-acceptor strength, the latter parameter can be varied by substituting strong electron withdrawing (like nitro, cyano etc) as well as strong electron releasing groups to obtain systems with better NLO property.

The azobenzene monomers with good NLO activity have been selected for the preparation of oligomers and polymers with diverse properties. The side chain approach was selected for the preparation of soluble polymers. The side chain polymers were found to exhibit fluorescence emission. The azobenzene systems are generally nonfluorescent because of the efficient photoisomerization reaction. Based on the available data it has been proposed that the emission behavior is due the more planar excited state of the chromophore. Also the quantum yield is found to have a direct correlation with the isomerization efficiency which in turn is structure dependant. Inhibition of photoinduced electron transfer mechanism explains the enhanced emission upon UV irradiation. Hydrogen bonding serves as the driving force for aggregate formation in the case of the starting dye esters whereas the hydrophilic-hydrophobic interactions facilitate aggregation in polymers. As the polymers were found to exhibit enhanced emission upon

aggregation, introduction of more hydrophilic oligoethyleneoxy spacers can promote the formation of aggregates and thereby an increase in fluorescence emission. The aggregation behavior can be followed by SEM as well as the fluorescence microscopic measurements.

The role of spacer length in controlling the emission property and liquid crystallinity of azobenzene oligomers has been established by the detailed studies of bichromophores prepared by using the azobenzene chromophore and ethyleneoxy spacers of varying length in the fashion chromophore-spacer-chromophore. The formation of excited state dimers by naphthyl derivatives was confirmed by the steady state as well as the concentration dependant fluorescence measurements. It was found that the photoisomerization efficiency is related to the rigidity of the chromophore. Concentration dependant fluorescence measurement and morphological studies revealed aggregation tendency of the bichromophores. The liquid crystalline property of the bichromophores is clear from the multiple phase transitions in the differential scanning calorimetry thermogram and the polarizing light microscopic studies. In summary, the present study is systematic and detailed effort towards the designing of azobenzene molecules, oligomers and polymers with multiple properties like NLO, fluorescence emission and liquid crystallinity and investigation on structure-property relationship.

Oligomers of the type 'chromophore-spacer-chromophore' can undergo complexation through the oxygen atoms of the ethyleneoxy spacer with metal ions like Li^+ , Ca^{2+} , K^+ , Cu^{2+} , Hg^{2+} etc which are of biological importance. Upon binding, these molecules may have the tendency to form foldamer or podant like structures in solution which modulates the ground state as well as the excited state properties and nonlinear optical behavior. The trans-cis isomerization can be used for conformational switching of the bichromophores that can lead to the design of novel molecular switching devices. And most importantly, these bichromophores can serve as model compounds for main chain polymers. Experiments in this direction can result in main chain polymers with enhanced optical and photophysical properties.